



NOAA Atlas NESDIS 16

CLIMATOLOGICAL AND INTERANNUAL VARIABILITY OF TEMPERATURE, HEAT STORAGE, AND RATE OF HEAT STORAGE IN THE UPPER OCEAN

Washington, D.C.
August 1997

U.S. DEPARTMENT OF COMMERCE
National Oceanic and Atmospheric Administration
National Environmental Satellite, Data, and Information Service



NOAA Atlas NESDIS 16

CLIMATOLOGICAL AND INTERANNUAL VARIABILITY OF TEMPERATURE, HEAT STORAGE, AND RATE OF HEAT STORAGE IN THE UPPER OCEAN

Sydney Levitus and John Antonov
National Oceanographic Data Center
Ocean Climate Laboratory
Silver Spring, Maryland 20910

Washington, D.C.
August 1997

U.S. DEPARTMENT OF COMMERCE
William M. Daley, Secretary

National Oceanic and Atmospheric Administration
D. James Baker, Under Secretary

National Environmental Satellite, Data, and Information Service
Robert S. Winokur, Assistant Administrator

National Oceanographic Data Center USER SERVICES

Additional copies of this publication, as well as information about NODC data holdings, products, and services, are available on request directly from the NODC. NODC information and data are also available over the Internet through the NODC World Wide Web and Gopher sites.

National Oceanographic Data Center
User Services Branch
NOAA/NESDIS E/OC1
SSMC3, 4th Floor
1315 East-West Highway
Silver Spring, MD 20910-3282

Telephone: (301) 713-3277
Fax: (301) 713-3302
E-mail: services@nodc.noaa.gov
NODC World Wide Web site: <http://www.nodc.noaa.gov/>
NODC Gopher site: [gopher.nodc.noaa.gov](gopher://gopher.nodc.noaa.gov)

Contents

Acknowledgments	xi
Abstract	1
1. Introduction	1
2. Climatological annual cycle of upper ocean temperature	2
2.1 Zonally averaged climatological annual mean and monthly anomaly temperature	2
2.2 Fourier analysis of global, climatological monthly temperature fields at standard level depths from the surface to 400 meters depth	2
2.3 Zonal averages of fourier parameters of global, climatological monthly temperature	2
3. Climatological seasonal cycle of heat storage in the upper 275 meters of the world ocean	2
3.1 Climatological monthly mean ocean heat storage	2
3.2 Fourier analysis of climatological monthly mean ocean heat storage	2
3.3 Seasonal cycle of zonally integrated monthly mean ocean heat storage for Atlantic, Pacific and Indian oceans	2
4. Climatological seasonal cycle of the rate of heat storage in the oceans	3
4.1 Climatological monthly mean rate of ocean heat storage	3
4.2 Fourier analysis of climatological monthly mean rate of ocean heat storage	3
4.3 Seasonal cycle of zonally averaged rate of heat storage for Atlantic, Pacific and Indian oceans	3
5. Climatological annual cycle of heat storage and the rate of heat storage averaged over the world ocean and individual hemispheres	3
6. Interannual variability of integrated heat storage and rate of heat storage	3
6.1 Zonally integrated heat storage as a function of year (1960-1990) and latitude for the world ocean and individual ocean basins	3
6.2 Basin integrals of heat storage as a function of year (1960-1990)	4
6.3 Zonally averaged rate of heat storage as a function of year (1961-1990) and latitude for the world ocean and individual ocean basins	4
6.4 Basin averages of the rate of heat storage as a function of year (1961-1990)	4
7. Yearly (1960-90) temperature anomaly estimates for the world ocean, individual ocean basins, and selected 10° latitude belts	4
7.1 Yearly basin-mean temperature anomaly as a function of depth	4
7.2 Yearly basin-mean temperature anomaly at selected individual depths	4
7.3 Yearly basin-mean temperature anomaly at 125 m depth for selected 10° latitude belts	5
8. Future Work	5
9. References	6
10. Appendix A: Zonally averaged deviation (°C) of the monthly mean temperature from the annual mean for individual oceans from the sea surface to 400 meters depth	

11. Appendix B: Fields of annual and semiannual harmonics of the temperature annual cycle from the sea surface to 400 meters depth
12. Appendix C: Zonally averaged parameters of annual and semiannual harmonics of the temperature annual cycle
13. Appendix D: Monthly mean fields and zonal integrals of heat storage integrated through 275 m depth
14. Appendix E: Monthly mean fields and zonal averages of rate of heat storage integrated through 275 m depth
15. Appendix F: Monthly mean heat storage and rate of heat storage for individual oceans, Southern and Northern hemispheres, and the World Ocean
16. Appendix G: Annual mean anomalies of heat storage and rate of heat storage for the upper 275m layer for individual oceans, Southern and Northern hemispheres, and the World ocean
17. Appendix H: Annual mean temperature anomaly ($^{\circ}\text{C}$) from the sea surface to 400 m depth for individual oceans, Southern, and Northern hemispheres, and the World ocean

LIST OF FIGURES

APPENDIX A

- Fig. A1 Zonally averaged annual mean temperature ($^{\circ}\text{C}$) for the Pacific, Atlantic, and Indian oceans from top to bottom respectively.
- Fig. A2 Deviation ($^{\circ}\text{C}$) of the monthly mean temperature from the annual mean for the Pacific Ocean (from top to bottom are January, February, and March).
- Fig. A3 Deviation ($^{\circ}\text{C}$) of the monthly mean temperature from the annual mean for the Pacific Ocean (from top to bottom are April, May, and June).
- Fig. A4 Deviation ($^{\circ}\text{C}$) of the monthly mean temperature from the annual mean for the Pacific Ocean (from top to bottom are July, August, and September).
- Fig. A5 Deviation ($^{\circ}\text{C}$) of the monthly mean temperature from the annual mean for the Pacific Ocean (from top to bottom are October, November, and December).
- Fig. A6 Deviation ($^{\circ}\text{C}$) of the monthly mean temperature from the annual mean for the Atlantic Ocean (from top to bottom are January, February, and March).
- Fig. A7 Deviation ($^{\circ}\text{C}$) of the monthly mean temperature from the annual mean for the Atlantic Ocean (from top to bottom are April, May, and June).
- Fig. A8 Deviation ($^{\circ}\text{C}$) of the monthly mean temperature from the annual mean for the Atlantic Ocean (from top to bottom are July, August, and September).
- Fig. A9 Deviation ($^{\circ}\text{C}$) of the monthly mean temperature from the annual mean for the Atlantic Ocean (from top to bottom are October, November, and December).
- Fig. A10 Deviation ($^{\circ}\text{C}$) of the monthly mean temperature from the annual mean for the Indian Ocean (from top to bottom are January, February, and March).
- Fig. A11 Deviation ($^{\circ}\text{C}$) of the monthly mean temperature from the annual mean for the Indian Ocean (from top to bottom are April, May, and June).
- Fig. A12 Deviation ($^{\circ}\text{C}$) of the monthly mean temperature from the annual mean for the Indian Ocean (from top to bottom are July, August, and September).
- Fig. A13 Deviation ($^{\circ}\text{C}$) of the monthly mean temperature from the annual mean for the Indian Ocean (from top to bottom are October, November, and December).

APPENDIX B

- Fig. B1 Amplitude ($^{\circ}\text{C}$) of the 1st harmonic of the annual temperature cycle at the sea surface.
- Fig. B2 Amplitude ($^{\circ}\text{C}$) of the 1st harmonic of the annual temperature cycle at 10 m depth.
- Fig. B3 Amplitude ($^{\circ}\text{C}$) of the 1st harmonic of the annual temperature cycle at 20 m depth.
- Fig. B4 Amplitude ($^{\circ}\text{C}$) of the 1st harmonic of the annual temperature cycle at 30 m depth.
- Fig. B5 Amplitude ($^{\circ}\text{C}$) of the 1st harmonic of the annual temperature cycle at 50 m depth.
- Fig. B6 Amplitude ($^{\circ}\text{C}$) of the 1st harmonic of the annual temperature cycle at 75 m depth.
- Fig. B7 Amplitude ($^{\circ}\text{C}$) of the 1st harmonic of the annual temperature cycle at 100 m depth.
- Fig. B8 Amplitude ($^{\circ}\text{C}$) of the 1st harmonic of the annual temperature cycle at 125 m depth.
- Fig. B9 Amplitude ($^{\circ}\text{C}$) of the 1st harmonic of the annual temperature cycle at 150 m depth.
- Fig. B10 Amplitude ($^{\circ}\text{C}$) of the 1st harmonic of the annual temperature cycle at 200 m depth.
- Fig. B11 Amplitude ($^{\circ}\text{C}$) of the 1st harmonic of the annual temperature cycle at 250 m depth.
- Fig. B12 Amplitude ($^{\circ}\text{C}$) of the 1st harmonic of the annual temperature cycle at 300 m depth.
- Fig. B13 Amplitude ($^{\circ}\text{C}$) of the 1st harmonic of the annual temperature cycle at 400 m depth.
- Fig. B14 Percent variance explained by the 1st harmonic of the annual temperature cycle at the sea surface.
- Fig. B15 Percent variance explained by the 1st harmonic of the annual temperature cycle at 10 m depth.
- Fig. B16 Percent variance explained by the 1st harmonic of the annual temperature cycle at 20 m depth.
- Fig. B17 Percent variance explained by the 1st harmonic of the annual temperature cycle at 30 m depth.

- Fig. B66 Phase (months) of the 2nd harmonic of the annual temperature cycle at the sea surface.
 Fig. B67 Phase (months) of the 2nd harmonic of the annual temperature cycle at 10 m depth.
 Fig. B68 Phase (months) of the 2nd harmonic of the annual temperature cycle at 20 m depth.
 Fig. B69 Phase (months) of the 2nd harmonic of the annual temperature cycle at 30 m depth.
 Fig. B70 Phase (months) of the 2nd harmonic of the annual temperature cycle at 50 m depth.
 Fig. B71 Phase (months) of the 2nd harmonic of the annual temperature cycle at 75 m depth.
 Fig. B72 Phase (months) of the 2nd harmonic of the annual temperature cycle at 100 m depth.
 Fig. B73 Phase (months) of the 2nd harmonic of the annual temperature cycle at 125 m depth.
 Fig. B74 Phase (months) of the 2nd harmonic of the annual temperature cycle at 150 m depth.
 Fig. B75 Phase (months) of the 2nd harmonic of the annual temperature cycle at 200 m depth.
 Fig. B76 Phase (months) of the 2nd harmonic of the annual temperature cycle at 250 m depth.
 Fig. B77 Phase (months) of the 2nd harmonic of the annual temperature cycle at 300 m depth.
 Fig. B78 Phase (months) of the 2nd harmonic of the annual temperature cycle at 400 m depth.

APPENDIX C

- Fig. C1 Zonally averaged parameters of the 1st harmonic of the annual temperature cycle for the World Ocean.
 Top panel is the amplitude (°C), middle panel is the percent variance explained by this harmonic, and
 bottom panel is the phase (months).
 Fig. C2 Zonally averaged parameters of the 2nd harmonic of the annual temperature cycle for the World Ocean.
 Top panel is the amplitude (°C), middle panel is the percent variance explained by this harmonic, and
 bottom panel is the phase (months).
 Fig. C3 Zonally averaged parameters of the 1st harmonic of the annual temperature cycle for the Pacific Ocean.
 Top panel is the amplitude (°C), middle panel is the percent variance explained by this harmonic, and
 bottom panel is the phase (months).
 Fig. C4 Zonally averaged parameters of the 2nd harmonic of the annual temperature cycle for the Pacific Ocean.
 Top panel is the amplitude (°C), middle panel is the percent variance explained by this harmonic, and
 bottom panel is the phase (months).
 Fig. C5 Zonally averaged parameters of the 1st harmonic of the annual temperature cycle for the Atlantic Ocean.
 Top panel is the amplitude (°C), middle panel is the percent variance explained by this harmonic, and
 bottom panel is the phase (months).
 Fig. C6 Zonally averaged parameters of the 2nd harmonic of the annual temperature cycle for the Atlantic Ocean.
 Top panel is the amplitude (°C), middle panel is the percent variance explained by this harmonic, and
 bottom panel is the phase (months).
 Fig. C7 Zonally averaged parameters of the 1st harmonic of the annual temperature cycle for the Indian Ocean.
 Top panel is the amplitude (°C), middle panel is the percent variance explained by this harmonic, and
 bottom panel is the phase (months).
 Fig. C8 Zonally averaged parameters of the 2nd harmonic of the annual temperature cycle for the Indian Ocean.
 Top panel is the amplitude (°C), middle panel is the percent variance explained by this harmonic, and
 bottom panel is the phase (months).

APPENDIX D

- Fig. D1 January heat storage (10^{18} J) integrated through 275 m depth.
 Fig. D2 February heat storage (10^{18} J) integrated through 275 m depth.
 Fig. D3 March heat storage (10^{18} J) integrated through 275 m depth.
 Fig. D4 April heat storage (10^{18} J) integrated through 275 m depth.
 Fig. D5 May heat storage (10^{18} J) integrated through 275 m depth.
 Fig. D6 June heat storage (10^{18} J) integrated through 275 m depth.
 Fig. D7 July heat storage (10^{18} J) integrated through 275 m depth.
 Fig. D8 August heat storage (10^{18} J) integrated through 275 m depth.
 Fig. D9 September heat storage (10^{18} J) integrated through 275 m depth.

Fig. D10 October heat storage (10^{18} J) integrated through 275 m depth.

Fig. D11 November heat storage (10^{18} J) integrated through 275 m depth.

Fig. D12 December heat storage (10^{18} J) integrated through 275 m depth.

Fig. D13 Amplitude (10^{18} J) of 1st harmonic of the annual cycle of heat storage for the 0-275 m layer.

Fig. D14 Percent variance explained by 1st harmonic of the annual cycle of heat storage for the 0-275 m layer.

Fig. D15 Phase (months) of 1st harmonic of the annual cycle of heat storage for the 0-275 m layer.

Fig. D16 Amplitude (10^{18} J) of 2nd harmonic of the the annual cycle heat storage for the 0-275 m layer.

Fig. D17 Percent variance explained by 2nd harmonic of the the annual cycle of heat storage for the 0-275 m layer.

Fig. D18 Phase (months) of 2nd harmonic of the annual cycle of heat storage for the 0-275 m layer.

Fig. D19 Zonally integrated heat storage (10^{20} J) vertically integrated through 275 m depth for the World Ocean.

Fig. D20 Zonally integrated heat storage (10^{20} J) vertically integrated through 275 m depth for the Pacific Ocean.

Fig. D21 Zonally integrated heat storage (10^{20} J) vertically integrated through 275 m depth for the Atlantic Ocean.

Fig. D22 Zonally integrated heat storage (10^{20} J) vertically integrated through 275 m depth for the Indian Ocean.

APPENDIX E

Fig. E1 Rate of heat storage (W/M^2) integrated through 275 m depth for January.

Fig. E2 Rate of heat storage (W/M^2) integrated through 275 m depth for February.

Fig. E3 Rate of heat storage (W/M^2) integrated through 275 m depth for March.

Fig. E4 Rate of heat storage (W/M^2) integrated through 275 m depth for April.

Fig. E5 Rate of heat storage (W/M^2) integrated through 275 m depth for May.

Fig. E6 Rate of heat storage (W/M^2) integrated through 275 m depth for June.

Fig. E7 Rate of heat storage (W/M^2) integrated through 275 m depth for July.

Fig. E8 Rate of heat storage (W/M^2) integrated through 275 m depth for August.

Fig. E9 Rate of heat storage (W/M^2) integrated through 275 m depth for September.

Fig. E10 Rate of heat storage (W/M^2) integrated through 275 m depth for October.

Fig. E11 Rate of heat storage (W/M^2) integrated through 275 m depth for November.

Fig. E12 Rate of heat storage (W/M^2) integrated through 275 m depth for December.

Fig. E13 Amplitude (W/M^2) of 1st harmonic of the annual cycle of the rate of heat storage for the 0-275 m layer.

Fig. E14 Percent variance explained by 1st harmonic of the annual cycle of the rate of heat storage for the 0-275 m layer.

Fig. E15 Phase (months) of 1st harmonic of the annual cycle of the rate of heat storage for the 0-275 m layer.

Fig. E16 Amplitude (W/M^2) of 2nd harmonic of the annual cycle of the rate of heat storage for the 0-275 m layer.

Fig. E17 Percent variance explained by 2nd harmonic of the annual cycle of the rate of heat storage for the 0-275 m layer.

Fig. E18 Phase (months) of 2nd harmonic of the annual cycle of the rate of heat storage for the 0-275 m layer.

Fig. E19 Zonally averaged rate of heat storage (W/M^2) vertically integrated through 275 m depth for the World Ocean.

Fig. E20 Zonally averaged rate of heat storage (W/M^2) vertically integrated through 275 m depth for the Pacific Ocean.

Fig. E21 Zonally averaged rate of heat storage (W/M^2) vertically integrated through 275 m depth for the Atlantic Ocean.

Fig. E22 Zonally averaged rate of heat storage (W/M^2) vertically integrated through 275 m depth for the Indian Ocean.

APPENDIX F

Fig. F1 Heat storage ($10^8 J/M^2$ and 10^{22} J) integrated through 275 m depth for (a) the Southern and (b) the Northern Hemispheres, and (c) the World Ocean.

- Fig. F2 Heat storage (10^8J/M^2 and 10^{22} J) integrated through 275 m depth for (a) the South Pacific, (b) the North Pacific, and (c) the Pacific Ocean.
- Fig. F3 Heat storage (10^8J/M^2 and 10^{22} J) integrated through 275 m depth for (a) the South Atlantic, (b) the North Atlantic, and (c) the Atlantic Ocean.
- Fig. F4 Heat storage (10^8J/M^2 and 10^{22} J) integrated through 275 m depth for (a) the South Indian, (b) the North Indian, and (c) the Indian Ocean.
- Fig. F5 Rate of heat storage (W/M^2) integrated through 275 m depth for (a) the Southern and (b) the Northern Hemispheres, and (c) the World Ocean.
- Fig. F6 Rate of heat storage (W/M^2) integrated through 275 m depth for (a) the South Pacific, (b) the North Pacific, and (c) the Pacific Ocean.
- Fig. F7 Rate of heat storage (W/M^2) integrated through 275 m depth for (a) the South Atlantic, (b) the North Atlantic, and (c) the Atlantic Ocean.
- Fig. F8 Rate of heat storage (W/M^2) integrated through 275 m depth for (a) the South Indian, (b) the North Indian, and (c) the Indian Ocean.

APPENDIX G

- Fig. G1 Zonally integrated heat storage (10^{22}J) integrated through 275 m depth for the World Ocean.
- Fig. G2 Zonally integrated heat storage (10^{22}J) integrated through 275 m depth for the Pacific Ocean.
- Fig. G3 Zonally integrated heat storage (10^{22}J) integrated through 275 m depth for the Atlantic Ocean.
- Fig. G4 Zonally integrated heat storage (10^{22}J) integrated through 275 m depth for the Indian Ocean.
- Fig. G5 Heat storage (10^{22}J) integrated through 275 m depth for (a) the Southern and (b) the Northern Hemispheres, and (c) the World Ocean.
- Fig. G6 Heat storage (10^{22}J) integrated through 275 m depth for (a) the South Pacific, (b) the North Pacific, and (c) the Pacific Ocean.
- Fig. G7 Heat storage (10^{22}J) integrated through 275 m depth for (a) the South Atlantic, (b) the North Atlantic, and (c) the Atlantic Ocean.
- Fig. G8 Heat storage (10^{22}J) integrated through 275 m depth for (a) the South Indian, (b) the North Indian, and (c) the Indian Ocean.
- Fig. G9 Zonally averaged rate of heat storage (W/M^2) integrated through 275 m depth for the World Ocean.
- Fig. G10 Zonally averaged rate of heat storage (W/M^2) integrated through 275 m depth for the Pacific Ocean.
- Fig. G11 Zonally averaged rate of heat storage (W/M^2) integrated through 275 m depth for the Atlantic Ocean.
- Fig. G12 Zonally averaged rate of heat storage (W/M^2) integrated through 275 m depth for the Indian Ocean.
- Fig. G13 Rate of heat storage (W/M^2) integrated through 275 m depth for (a) the Southern and (b) the Northern Hemispheres, and (c) the World Ocean.
- Fig. G14 Rate of heat storage (W/M^2) integrated through 275 m depth for (a) the South Pacific, (b) the North Pacific, and (c) the Pacific Ocean.
- Fig. G15 Rate of heat storage (W/M^2) integrated through 275 m depth for (a) the South Atlantic, (b) the North Atlantic, and (c) the Atlantic Ocean.
- Fig. G16 Rate of heat storage (W/M^2) integrated through 275 m depth for (a) the South Indian, (b) the North Indian, and (c) the Indian Ocean.

APPENDIX H

- Fig. H1 Annual mean temperature anomaly ($^{\circ}\text{C}$) as a function of depth for the Southern (top) and the Northern (middle) Hemispheres, and the World Ocean (bottom).
- Fig. H2 Annual mean temperature anomaly ($^{\circ}\text{C}$) as a function of depth for the South Pacific (top), the North Pacific (middle), and the Pacific Ocean (bottom).
- Fig. H3 Annual mean temperature anomaly ($^{\circ}\text{C}$) as a function of depth for the South Atlantic (top), the North Atlantic (middle), and the Atlantic Ocean (bottom).
- Fig. H4 Annual mean temperature anomaly ($^{\circ}\text{C}$) as a function of depth for the South Indian (top), the North Indian (middle), and the Indian Ocean (bottom).
- Fig. H5 Annual mean temperature deviations ($^{\circ}\text{C}$) from the 1960-90 mean for the World Ocean at (a) the surface, (b) 150 m depth, and (c) 250 m depth.
- Fig. H6 Annual mean temperature deviations ($^{\circ}\text{C}$) from the 1960-90 mean for the Northern Hemisphere at (a) the surface, (b) 150 m depth, and (c) 250 m depth.
- Fig. H7 Annual mean temperature deviations ($^{\circ}\text{C}$) from the 1960-90 mean for the Southern Hemisphere at (a) the surface, (b) 150 m depth, and (c) 250 m depth.
- Fig. H8 Annual mean temperature deviations ($^{\circ}\text{C}$) from the 1960-90 mean for the Pacific Ocean at (a) the surface, (b) 150 m depth, and (c) 250 m depth.
- Fig. H9 Annual mean temperature deviations ($^{\circ}\text{C}$) from the 1960-90 mean for the North Pacific at (a) the surface, (b) 150 m depth, and (c) 250 m depth.
- Fig. H10 Annual mean temperature deviations ($^{\circ}\text{C}$) from the 1960-90 mean for the South Pacific at (a) the surface, (b) 150 m depth, and (c) 250 m depth.
- Fig. H11 Annual mean temperature deviations ($^{\circ}\text{C}$) from the 1960-90 mean for the Atlantic Ocean at (a) the surface, (b) 150 m depth, and (c) 250 m depth.
- Fig. H12 Annual mean temperature deviations ($^{\circ}\text{C}$) from the 1960-90 mean for the North Atlantic at (a) the surface, (b) 150 m depth, and (c) 250 m depth.
- Fig. H13 Annual mean temperature deviations ($^{\circ}\text{C}$) from the 1960-90 mean for the South Atlantic at (a) the surface, (b) 150 m depth, and (c) 250 m depth.
- Fig. H14 Annual mean temperature deviations ($^{\circ}\text{C}$) from the 1960-90 mean for the Indian Ocean at (a) the surface, (b) 150 m depth, and (c) 250 m depth.
- Fig. H15 Annual mean temperature deviations ($^{\circ}\text{C}$) from the 1960-90 mean for the North Indian at (a) the surface, (b) 150 m depth, and (c) 250 m depth.
- Fig. H16 Annual mean temperature deviations ($^{\circ}\text{C}$) from the 1960-90 mean for the South Indian at (a) the surface, (b) 150 m depth, and (c) 250 m depth.
- Fig. H17 Zonally averaged annual mean temperature deviations ($^{\circ}\text{C}$) from the 1960-90 mean in the North Pacific at 125 m depth: (a) 40°N - 50°N , (b) 30°N - 40°N , and (c) 20°N - 30°N .
- Fig. H18 Zonally averaged annual mean temperature deviations ($^{\circ}\text{C}$) from the 1960-90 mean in the North Atlantic at 125 m depth: (a) 50°N - 60°N , (b) 40°N - 50°N , and (c) 30°N - 40°N .

Fig. H19 Division of the World Ocean into individual basins.

Acknowledgments

The work described in this atlas was made possible by the efforts of scientists, technicians, ships' crew, data managers, and science administrators from the international scientific community. This atlas represents the results of several different research/data management projects of the NODC Ocean Climate Laboratory at the National Oceanographic Data Center (NODC) and World Data Center-A (WDC-A) for Oceanography. The products in this atlas are all based on the master oceanographic data archives maintained by NODC/WDC-A as well as data acquired as a result of the IOC/IODE Global Oceanographic Data Archaeology and Rescue (GODAR) project. Funding from the NOAA Climate and Global Change Program and the NOAA Environmental Services Data and Information Management Program have been instrumental in support of the GODAR project.

Oceanographic data archives exist because scientists and data managers of the international scientific community have submitted data to national and regional data centers. In turn, these centers have submitted data to the World Data Center system, established by the International Council of Scientific Unions (ICSU) and now under the auspices of both ICSU and the Intergovernmental Oceanographic Commission (IOC). This atlas and similar works would not exist without these international efforts. In particular, we would like to thank data managers at these centers and the administrators and staff at all of these organizations.

The archiving of oceanographic data at international data centers means that the substantial expenditures in human and capital resources devoted to oceanographic measurement programs will be fully exploited, both for present and future scientific studies. Many of the data have been collected for diverse purposes but when combined in a uniform database provide most of our knowledge of property distributions in the world ocean, for both climatological averaging periods as well as for the temporal variability of these properties.

The data sets and products represented by this atlas are being distributed internationally without restriction in accordance with ICSU/IOC data management policies and U.S. Climate and Global Change policy in support of Global Change Research.

We thank the staff of the Ocean Climate Laboratory for their assistance in this project. Tim Boyer receives particular thanks. This study was completed while John Antonov was an UCAR visiting scientist at the Ocean Climate Laboratory.

Dave Adamec and Igor Belkin provided valuable comments about the original version of this manuscript.

CLIMATOLOGICAL AND INTERANNUAL VARIABILITY OF TEMPERATURE, HEAT STORAGE, AND RATE OF HEAT STORAGE IN THE UPPER OCEAN

Sydney Levitus and John Antonov

Ocean Climate Laboratory

National Oceanographic Data Center / NOAA

Silver Spring, Maryland

ABSTRACT

This atlas presents climatological fields of temperature, heat storage, and rate of heat storage in the upper 400 meters of the world ocean as well as yearly estimates of these quantities for the 1960-1990 period. The results of fourier analyses of the climatological monthly fields are presented. Decadal variability of upper ocean temperature fields in each hemisphere of all three major ocean basins is observed. The decades 1960-70 and 1980-90 are relatively cool compared to the 1970-80 decade. Basin-mean temperature anomalies at individual standard levels are characterized by absolute values of the order 0.05-0.15 °C.

1. INTRODUCTION

This atlas represents an effort to describe systematically the climatological seasonal cycles of temperature, heat storage, and the rate of heat storage in the upper 400 m of the world ocean as well as the interannual variability of these quantities. Our purpose is to present a comprehensive visual description of the seasonal cycle and interannual variability of the these quantities for the upper ocean. It is now possible to do this because of increases in the amount of data available as part of the archives of historical ocean profile data. The IOC/GODAR (Intergovernmental Oceanographic Commission/Global Oceanographic Data Archaeology and Rescue) project (Levitus *et al.* 1994a) has increased the global ocean temperature archives by more than 1.2 million temperature profiles.

Results presented in this atlas are based on the World

Ocean Atlas 1994 (WOA94) database and analyses (Levitus and Boyer, 1994; Levitus *et al.*, 1994b). We use a revised version of the monthly climatological monthly temperature fields that have been subjected to additional quality control compared to the original version of these fields made available as part of the WOA94 CD-ROM series. These revised fields are available via the Internet. Instructions on transferring these data are available from the NODC World Wide Web home page (www.nodc.noaa.gov).

We will only present brief, or in many cases, no descriptions of many features that appear in the figures presented in this atlas, particularly for the climatological annual cycle. We believe much of the information to be self-explanatory. We will present brief descriptions of some of our results that describe

decadal variability but we will not attempt to give a physical interpretation of these changes. Objectively analyzed fields of surface marine data that are analyzed with nearly identical methods as our fields are available on CD-ROM and are shown in atlas form (Da Silva 1994a,b,c,d,e). These fields should prove useful in attempts to understand the causes of the upper ocean temperature variability described in this atlas.

2. CLIMATOLOGICAL ANNUAL CYCLE OF UPPER OCEAN TEMPERATURE

2.1 Zonally averaged climatological annual mean and monthly anomaly temperature

Fig. A1 shows the zonally averaged annual mean temperature fields for the upper 400 m of the Pacific, Atlantic, and Indian Oceans. (Fig. H19 shows the division of the World Ocean that we have used). Figs. A2-A5 show zonally averaged monthly mean minus annual mean difference fields for the Pacific Ocean. Figs. A6-A9 and Figs. A10-13 show similar fields for the Atlantic and Indian Oceans respectively.

2.2 Fourier analysis of global, climatological monthly temperature fields at standard level depths from the surface to 400 meters depth

To further describe the annual cycle of temperature we present the results of fourier analyses of the climatological seasonal cycle of temperature at each of the fourteen standard levels from the sea surface through 400 m depth. Figs. B1-B13 show the amplitude of the first harmonic at each of the upper ocean standard levels. Figs. B14-B26 show the percent variance accounted for by the first harmonic of temperature at each standard level. Figs. B27-B39 show the phase of the first harmonic at each standard level. We repeat this style of presentation for the second harmonic of temperature at each standard level presented in Figs. B40 - B78.

2.3 Zonal averages of fourier parameters of global, climatological monthly temperature

Zonal averages of the fourier parameters presented in Figs. B1 through B78 are shown in Appendix C. Figs C1 shows the zonal averages of the amplitude of

the first harmonic, percent variance accounted by the first harmonic, and the phase of the first harmonic for the World Ocean. Fig. C2 shows the same quantities for the second harmonic. Figs. C3-C8 show similar fields for the Pacific, Atlantic, and Indian Oceans.

3. CLIMATOLOGICAL SEASONAL CYCLE OF HEAT STORAGE IN THE UPPER 275 METERS OF THE WORLD OCEAN

For a vertical column of water, and using spherical coordinates, we define climatological monthly heat storage (H) (Levitus, 1984;1987) as

$$H = \int_{\lambda_1 \varphi_1 0}^{\lambda_2 \varphi_2 z} \rho_0 c_p (T_{\text{month}} - T_{\text{annual}}) a^2 \cos \varphi dz d\varphi d\lambda \quad (1)$$

in which $c_p = 4.187 \text{ J g}^{-1} \text{ K}^{-1}$ is the specific heat of seawater, T_{month} is a climatological monthly mean temperature field, T_{annual} is the climatological annual mean temperature field, ρ_0 is the density of seawater (1.02 g cm^{-3}), and z represents depth. The upper and lower limits of integration are the sea surface and 275 m depth in our computation. The radius of the earth is denoted by 'a'.

3.1 Climatological monthly mean ocean heat storage

Figs. D1-D12 show the global, monthly, climatological heat storage fields in units of 10^{18} J .

3.2 Fourier analysis of climatological monthly mean ocean heat storage

Figs. D13-D18 show the results of fourier analyses of the monthly climatological fields that are shown in Figs. D1-D12. We present the amplitude, phase, and percent variance for each of the first two harmonics.

3.3 Seasonal cycle of zonally integrated monthly mean ocean heat storage for the Atlantic, Pacific, and Indian Oceans

Figs. D19-D22 present the zonally integrated heat storage for the World Ocean and the Pacific, Atlantic,

and Indian Oceans. For the world ocean the range in heat storage occurs at about 38°N and 40°S, the ranges being about 40×10^{20} J and 55×10^{20} J respectively. The smaller range of the northern hemisphere is due to the presence of land. It is well known and we document in Figs. E19-E22 that when we plot heat storage quantities or fluxes per unit area, the northern hemisphere values are always larger than southern hemisphere counterparts. In the tropics of the North Atlantic and North Pacific the annual cycle of heat storage is out of phase with the midlatitude annual cycle.

4. CLIMATOLOGICAL SEASONAL CYCLE OF THE RATE OF HEAT STORAGE IN THE OCEANS

The climatological annual cycle of the rate of heat storage is defined as the time derivative of the heat storage in the same manner as Levitus (1987). A time increment of two months is used so that the January rate of heat storage is defined as the February minus December heat storage (H), divided by the number of seconds in two months. The units of the rate of heat storage are Wm^{-2} .

4.1 Climatological monthly mean rate of ocean heat storage

Figs. E1-E12 show the global, monthly, climatological rate of heat storage fields for the world ocean .

4.2 Fourier analysis of climatological monthly mean rate of ocean heat storage

Figs. E13-E18 show the results of a fourier analysis (first two harmonics) of the climatological monthly fields shown in Figs. E1-E12. We present the amplitude, phase, and percent variance for each of the first two harmonics.

4.3 Seasonal cycle of zonally averaged rate of heat storage for Atlantic, Pacific, and Indian oceans

E19-E22 present the zonally integrated rate of heat storage for the World Ocean and the Pacific, Atlantic, and Indian Oceans. The climatological annual range at 40°N is about 400 Wm^{-2} whereas the maximum range in the southern hemisphere is about 350 Wm^{-2} near 34°S.

5. CLIMATOLOGICAL ANNUAL CYCLE OF HEAT STORAGE AND THE RATE OF HEAT STORAGE AVERAGED OVER THE WORLD OCEAN AND INDIVIDUAL HEMISPHERES

Figs. F1a-c shows the monthly climatological heat storage (per square meter) averaged for the southern hemisphere, northern hemisphere, and the World Ocean respectively. Figs. F2-F4 show similar quantities for the Pacific, Atlantic, and Indian oceans respectively. Figs. F5-F8 show similar averages for the rate of heat storage.

6. INTERANNUAL VARIABILITY OF INTEGRATED HEAT STORAGE AND RATE OF HEAT STORAGE

6.1 Zonally integrated heat storage as a function of year (1960-90) and latitude for the World Ocean and individual ocean basins

Figs. G1-G4 show estimates of yearly zonally integrated upper ocean heat storage (0-275 m depth) as a function of latitude for the period 1960-90 for the World Ocean and for individual ocean basins. Fig. G2 indicates that the tropics and equatorial regions of the Pacific display higher frequency variability of relatively large magnitude (plus or minus 4×10^{20} J) as compared to the extratropical regions. This variability appears to be related to El Nino events. For example Kiladis and Diaz (1989) have noted that during the period 1960-1990, the years 1963, 1965, 1969, 1972, 1976, 1982, 1986 are years when El Nino occurred. During three of these years (1963, 1972, 1976) the zonally integrated heat storage at the equator is a relative positive extremum. Two El Nino events (1969, 1986) occurred one year after relative extrema in zonally integrated heat storage. The 1982 El Nino event occurred when heat storage was zero and the 1965 El Nino occurred during a period of negative heat storage. High frequency variability is also observed along 15°N latitude. The observed variability of heat storage in the equatorial and northern tropics may reflect the “delayed oscillator” El Nino theory described by Schopf and Suarez (1988). Recently, Zhang and Levitus (1996, 1997a,b) have presented evidence for the existence of this mechanism based on a more detailed analysis of the same data we use in the present work. The tropical Atlantic does not exhibit variability in heat storage as

observed in the Pacific. The Indian Ocean exhibits high frequency variability in the equatorial region and also along 14°S. The Pacific Ocean was in a cool state during 1981-1986 whereas the other two oceans do not exhibit a clear signal change.

Figs. G2-G4 indicate that all three oceans were in a relatively cool state until the early 1970's when a warming period began (also see next section). In the Pacific Ocean it appears that the warming occurred at all latitudes. This indicates that the changes in northern hemisphere climate described by Trenberth (1991) may in fact be part of a global phenomenon. In the Atlantic and Indian Oceans, the patterns are disjointed which may reflect a real pattern or may be due to variations of observations with time. Substantial amounts of data are becoming available for the tropics and southern hemisphere which will allow improved estimates in future work.

6.2 Basin integrals of heat storage as function of year 1960-90

Fig. G5 shows estimates of yearly heat storage integrated over the World Ocean and the southern and northern hemispheres for the period 1960-90. Figs. G6-G8 show the results of similar computations for the Pacific, Atlantic, and Indian oceans respectively. These figures clearly document the change in heat storage that occurred in the early 1970s in all three oceans. The changes were more distinct in the North as compared to the South Atlantic and clearer in the South Indian Ocean compared to the North Indian Ocean, perhaps due in part to the smaller volume of water that comprises the North Indian Ocean. For the basin-hemispheric integrals of heat storage, the switch from negative to positive heat storage occurred during 1973 for the Indian and Atlantic Oceans, and during 1972 for the Pacific Ocean. The range in heat storage during the 1960-90 period for the Pacific, Atlantic, and Indian Oceans respectively is approximately the same, the value being, $4 \times 10^{22} \text{ J}$.

6.3 Zonally averaged rate of heat storage as a function of year (1960-90) and latitude for the World Ocean and Individual Ocean basins

Figs. G9-G12 show estimates of yearly zonally averaged upper ocean rate of heat storage for the period 1961-89 for the World Ocean and for individual ocean

basins. Since this quantity is a derivative of the heat storage it is a relatively noisier field.

6.4 Basin averages of rate of heat storage as function of year 1960-90

Fig. G13 shows the rate of heat storage integrated over the World Ocean and the southern and northern hemispheres for the period 1961-89. Figs. G14-G16 show the results of similar computations for the Pacific, Atlantic, and Indian oceans respectively. The interannual range of the rate of heat storage exceeds 10 W m^{-2} for the North Indian Ocean but is typically 4-5 W m^{-2} for the hemispheric averages of the other basins.

7. YEARLY (1960-90) TEMPERATURE ANOMALY ESTIMATES FOR THE WORLD OCEAN, INDIVIDUAL OCEAN BASINS, AND SELECTED 10° LATITUDE BELTS

7.1 Yearly basin-mean temperature anomaly as a function of depth

Fig. H1 shows yearly mean temperature anomaly averaged over the entire World Ocean as a function of depth. Figs. H2-H4 show similar estimates for the northern hemisphere, southern hemisphere, Pacific, Atlantic, and Indian Ocean basins individually. The most interesting feature is the observation that there is phase propagation upward for the North Pacific and North Atlantic Oceans. A typical basin-mean temperature anomaly at any depth level is of the order 0.05-0.10°C. Since average anomalies for smaller regions are commonly observed to be an order of magnitude larger than this value as we document in a later section, it is clear that cancellations of anomalies of opposite sign is occurring.

7.2 Yearly basin-mean temperature anomaly at selected individual depths

Fig. H5 shows yearly mean temperature anomaly averaged over the entire World Ocean for the sea surface, 150 m, and 250 m depth levels. Figs. H6-H16 show similar curves for individual hemispheres and for individual ocean basins and the hemispheric averages within each ocean basin.

7.3 Yearly basin-mean temperature anomaly at 125 m depth for selected 10° latitude belts

Fig. H17 shows the zonally averaged temperature anomaly at 125 m depth for three ten-degree latitude belts in the North Pacific Ocean (40-50° N, 30-40°N, 20-30°N). Fig. H18 shows the zonally averaged temperature anomaly at 125 m depth for three ten-degree latitude belts in the North Atlantic Ocean (50-60°N, 40-50°N, 30-40°N). There are clear latitudinal differences in the magnitude and even the sign of the yearly anomaly fields within different latitude belts of the same ocean basins. The interannual range of the mean temperature anomalies in these particular belt is of the order 0.5°C and is less than 0.8°C.

the historical record back in time and improving representativeness of the yearly anomaly fields. Fields with greater temporal resolution (three or six-month seasonal composites) may be prepared and analyzed in order to provide more insight into the physics responsible for these variations in upper ocean temperature fields. For selected periods the analyses may be extended to greater depths (as data permit). Progressively earlier generations of BTs had shallower penetration depths so analyses are limited by this fact.

Future work will also include producing semi-monthly climatological fields and perhaps increasing spatial resolution for these fields as represented by the work of Boyer and Levitus (1997).

8. FUTURE WORK

Substantial amounts of historical temperature data are being added to the digital archives of NODC/WDC-A. Future work describing the interannual variability of upper ocean thermal structure will focus on extending

9. REFERENCES

- Boyer, T.P., and S. Levitus, 1997: Objective Analyses of temperature and salinity for the world ocean on a 1/4 grid. NOAA/NESDIS Atlas Series. U.S. Government Printing Office, Washington, D.C., 62 pp.
- Da Silva, A., C. Young, and S. Levitus, 1994a: *Atlas of Surface Marine Data 1994, Vol. 1: Algorithms and Procedures. NOAA Atlas NESDIS 6*. U.S. Gov. Printing Office, Washington, D.C., 83 pp.
- _____, C. Young, and S. Levitus, 1994b: *Atlas of Surface Marine Data 1994, Vol. 2: Anomalies of Directly Observed Quantities. NOAA Atlas NESDIS 7*, U.S. Gov. Printing Office, Washington, D.C., 416. Pp.
- _____, C. Young, and S. Levitus, 1994c: *Atlas of Surface Marine Data 1994 Vol. 3: Anomalies of Fluxes of Heat and Momentum. NOAA Atlas NESDIS 8*. U.S. Gov. Printing Office, Washington, D.C., 413. pp.
- _____, C. Young, and S. Levitus, 1994d: *Atlas of Surface Marine Data 1994 Vol. 4: Anomalies of Fresh Water Fluxes. NOAA Atlas NESDIS 9*. U.S. Gov. Printing Office, Washington, D.C., 308. Pp.
- _____, C. Young, and S. Levitus, 1994e: *Atlas of Surface Marine Data Vol. 5: Miscellaneous Derived Quantities. NOAA Atlas NESDIS 10*. U.S. Gov. Printing Office, Washington, D.C., 416. pp.
- Kiladis, G.N. and H. F. Diaz, 1989: Global climatic anomalies associated with extremes of the Southern Oscillation. *J. Climate*, 2, 1069-1090.
- Levitus, S., 1984: Annual cycle of temperature and heat storage in the World Ocean. *J. Phys. Oceanogr.*, 14, 727-746.
- _____, 1987: Rate of change of heat storage in the World Ocean. *J. Phys. Oceanogr.*, 17, 518-528.
- _____, R. Gelfeld, T. Boyer, and D. Johnson, 1994a: *Results of the NODC and IOC Data Archaeology and Rescue projects. Key to Oceanographic Records Documentation No. 19*, National Oceanogr. Data Center, Wash., D.C., 67 pp.
- _____, T. Boyer, and J. Antonov, 1994b: *World Ocean Atlas 1994, Vol. 5: Interannual variability of upper ocean thermal structure. NOAA Atlas NESDIS 5*. U.S. Gov. Printing Office, Washington, D.C., 176 pp.
- _____, and T. Boyer, 1994: *World Ocean Atlas 1994c, Vol. 4: Temperature. NOAA Atlas NESDIS 4*, U.S. Gov. Printing Office, Washington, D.C., 117 pp.
- Schopf, P.S. and M.J. Suarez, 1988: Vacillations in a coupled ocean-atmosphere model. *J. Atm. Sci.*, 45, 549-566.
- Trenberth, K.E., 1991: Recent climatic changes in the northern hemisphere. In "Greenhouse-Gas-Induced Climatic Change: A Critical Appraisal of Simulations and Observations, ed. M.E. Schlesinger, Elsevier, Amsterdam, 377-390.
- Zhang, R-H. and S. Levitus, 1996: Structure and evolution of interannual variability of the tropical Pacific upper ocean temperature. *J. Geophys. Res.-Oceans*, 101, 20501-20524.
- _____, and S. Levitus, 1997a: Structure and cycle of decadal variability of upper ocean temperature in the North Pacific. *J. Climate*, 10, 710-727.
- _____, and S. Levitus, 1997b: Interannual variability of the coupled tropical Pacific ocean-atmosphere system associated with the El Nino-Southern Oscillation, *J. Climate*, 10, 1312-1330.

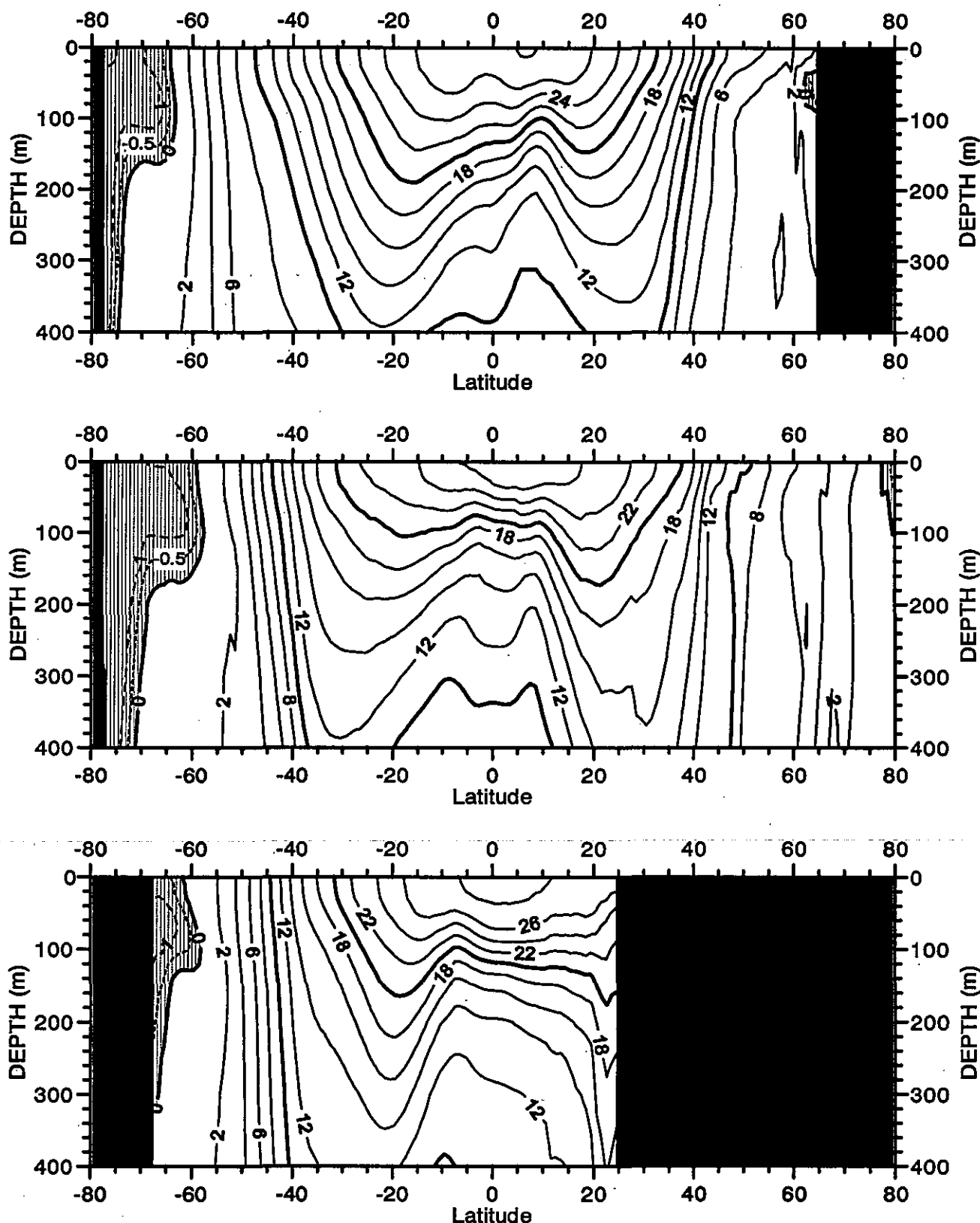


Fig. A1 Zonally averaged annual mean temperature ($^{\circ}\text{C}$) for the Pacific, Atlantic and Indian oceans

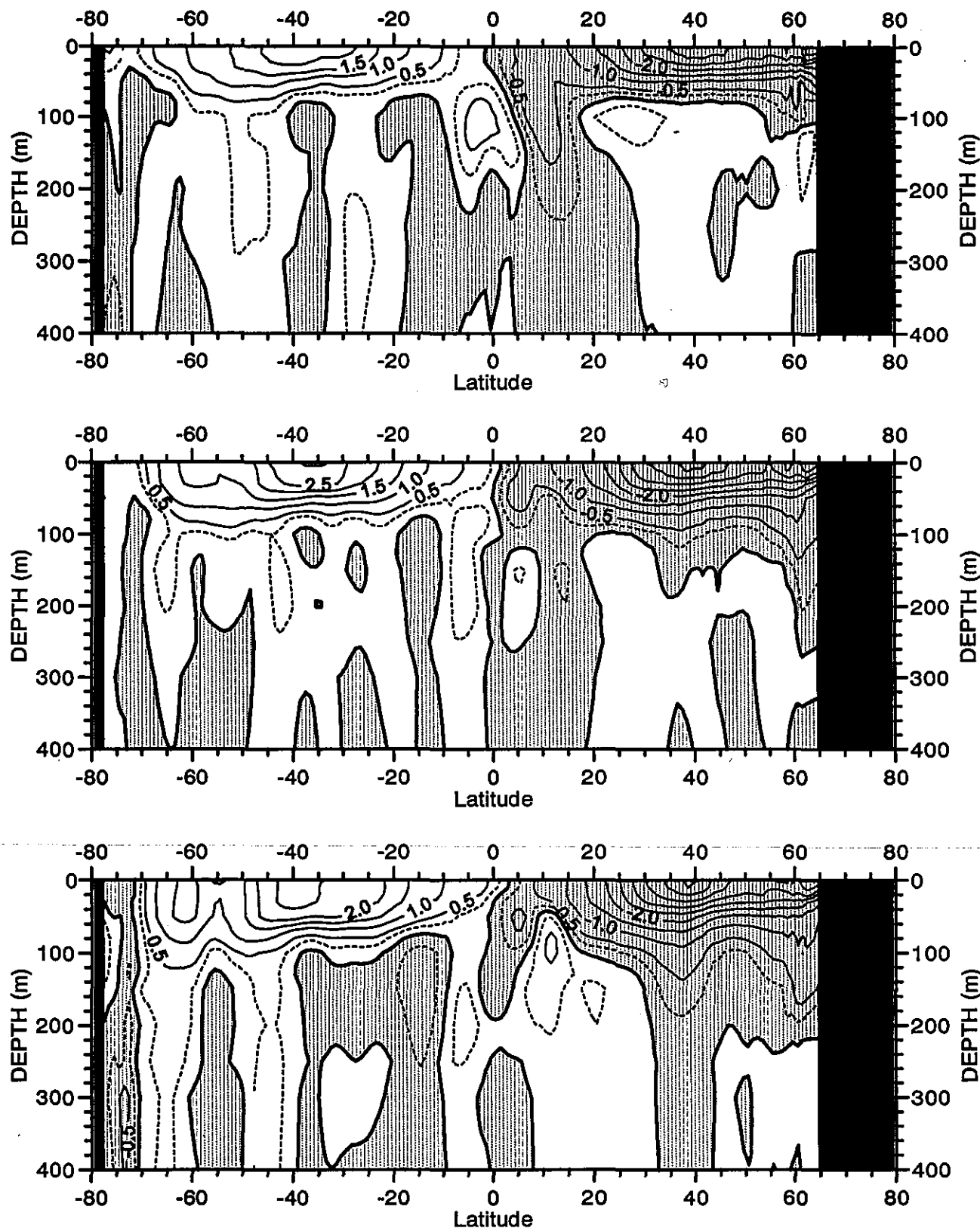


Fig. A2 Deviation ($^{\circ}\text{C}$) of the monthly mean temperature from the annual mean
for the Pacific Ocean (from top to bottom are JANUARY, FEBRUARY, and MARCH)

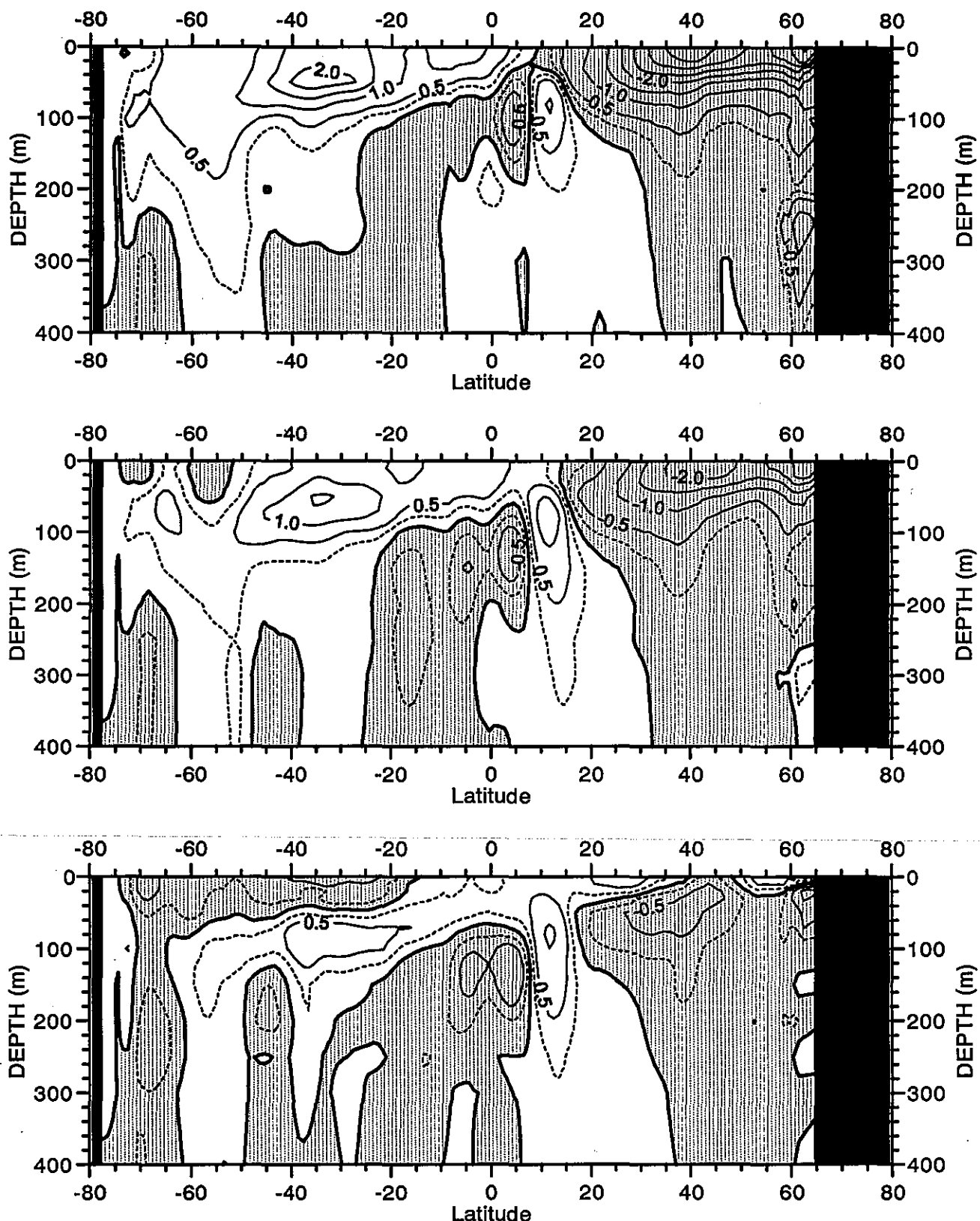


Fig. A3 Deviation ($^{\circ}\text{C}$) of the monthly mean temperature from the annual mean for the Pacific Ocean (from top to bottom are APRIL, MAY, and JUNE)

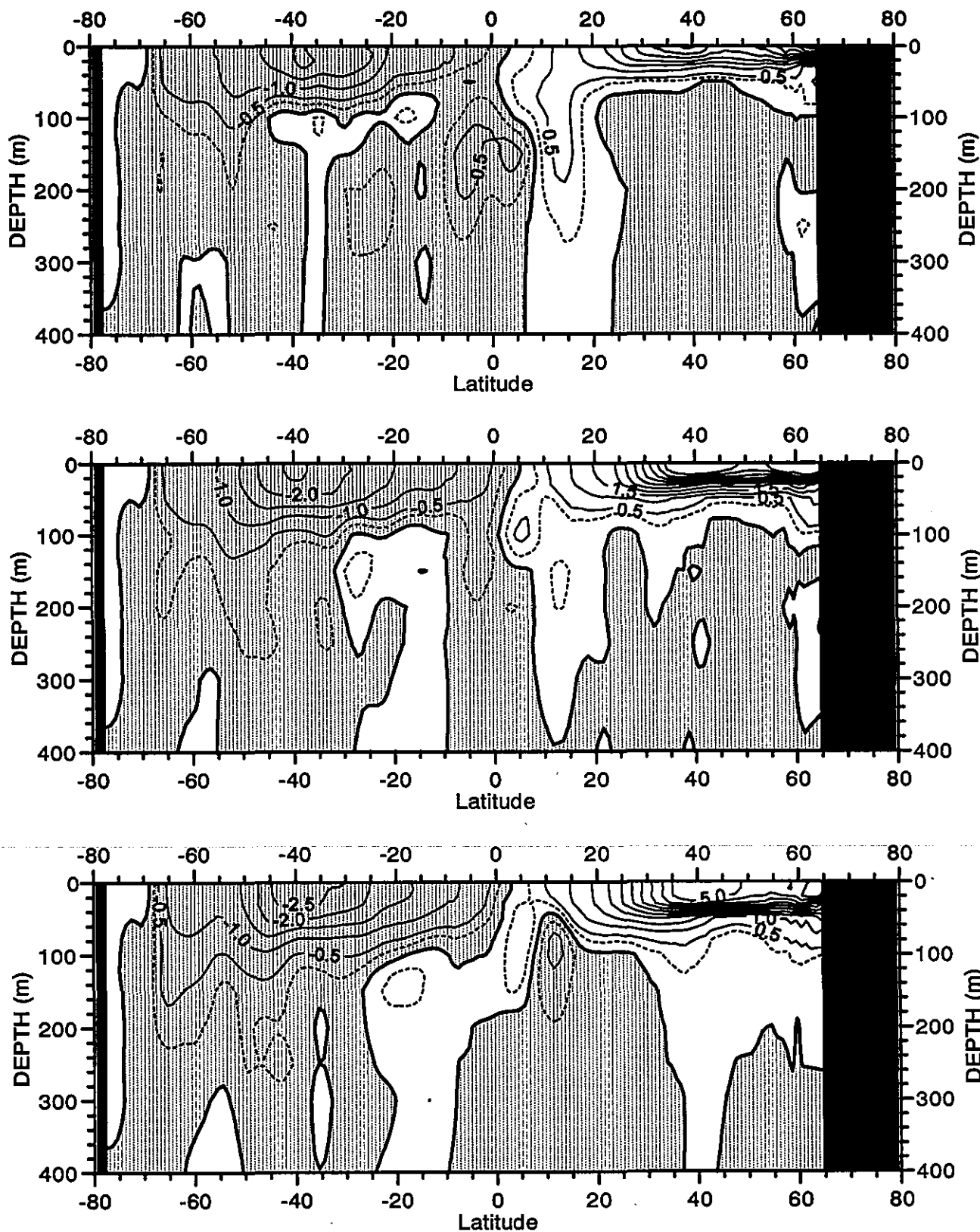


Fig. A4 Deviation ($^{\circ}\text{C}$) of the monthly mean temperature from the annual mean for the Pacific Ocean (from top to bottom are JULY, AUGUST, and SEPTEMBER)

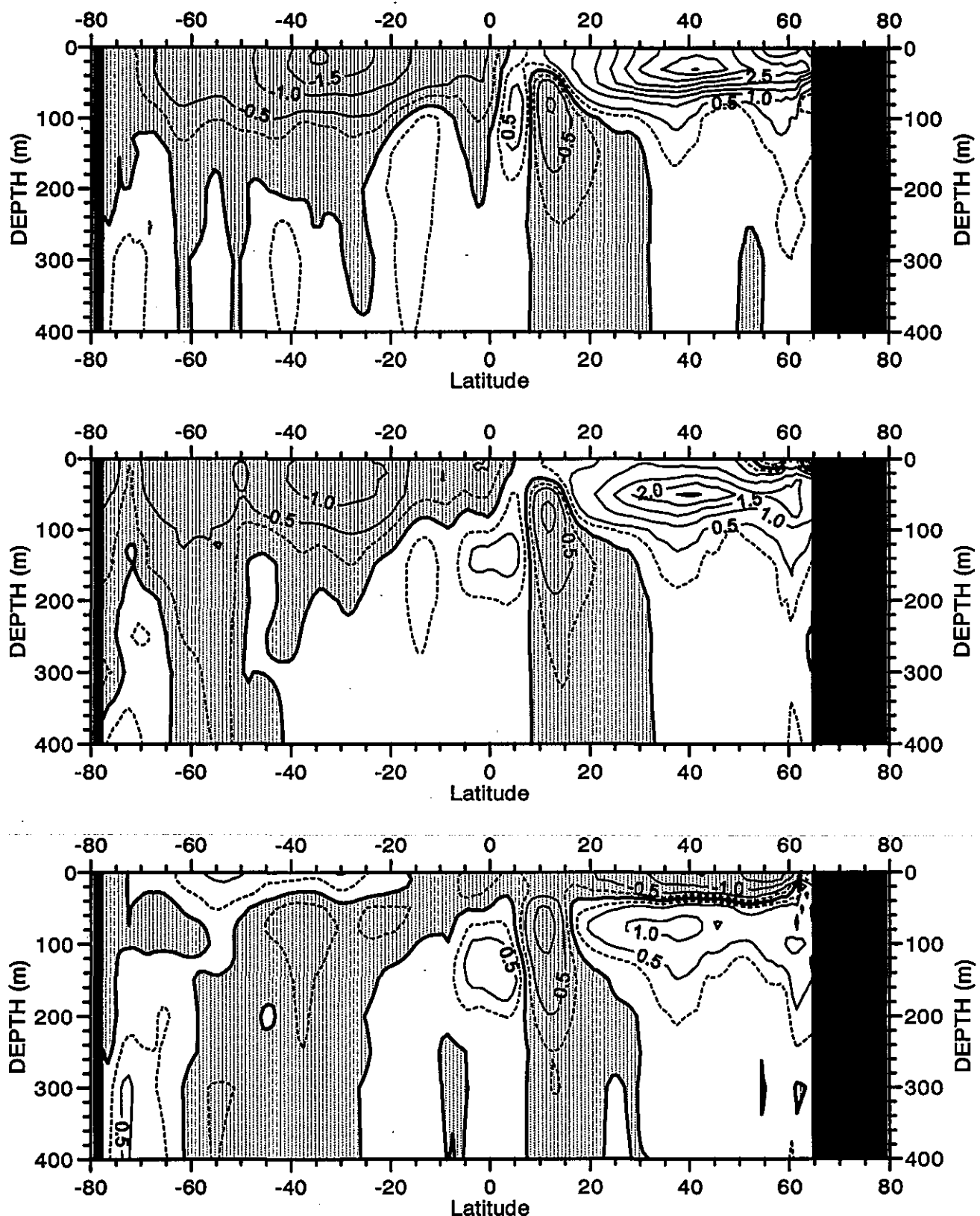


Fig. A5 Deviation ($^{\circ}\text{C}$) of the monthly mean temperature from the annual mean
for the Pacific Ocean (from top to bottom are OCTOBER, NOVEMBER, and DECEMBER)

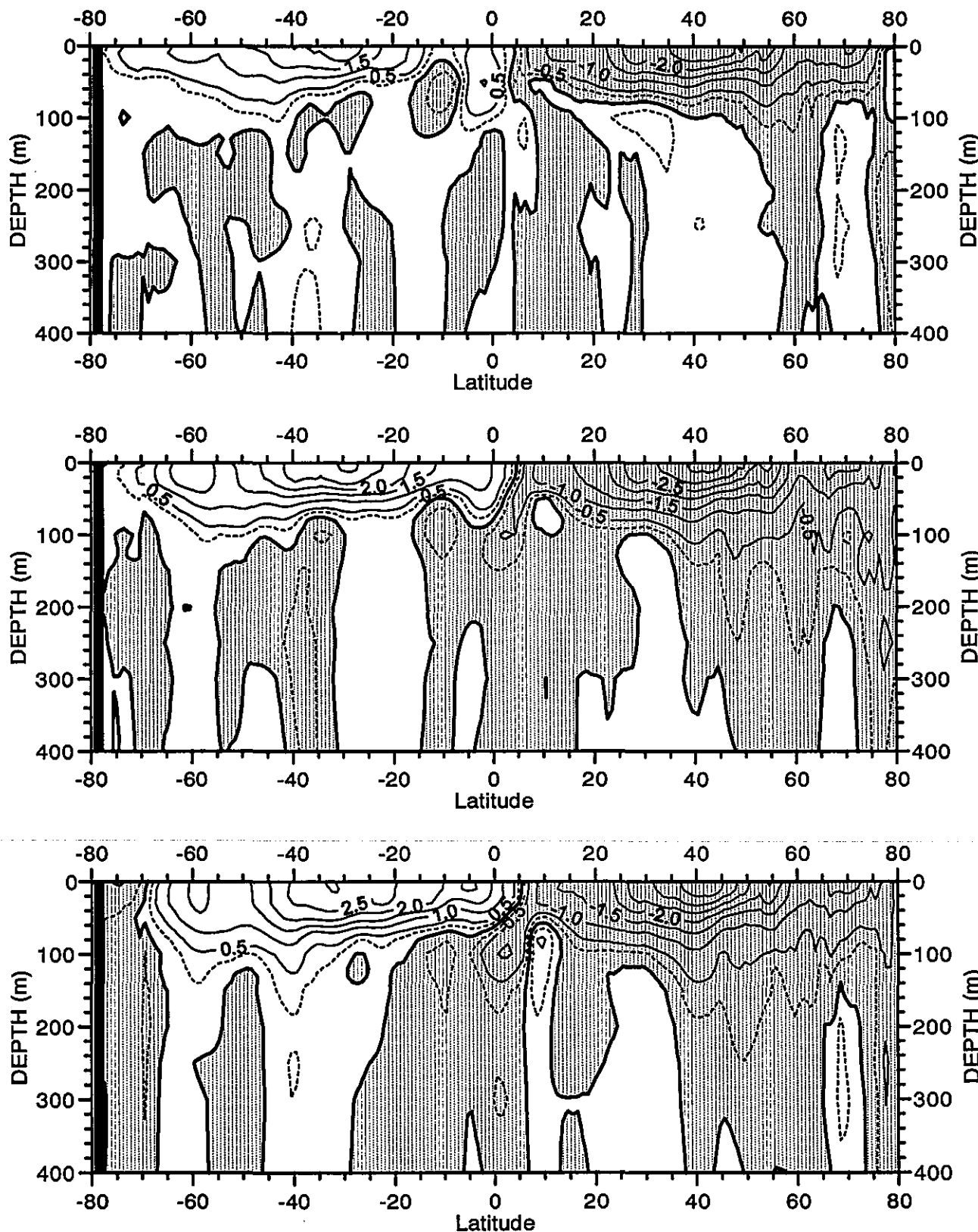


Fig. A6 Deviation ($^{\circ}\text{C}$) of the monthly mean temperature from the annual mean for the Atlantic Ocean (from top to bottom are JANUARY, FEBRUARY, and MARCH)

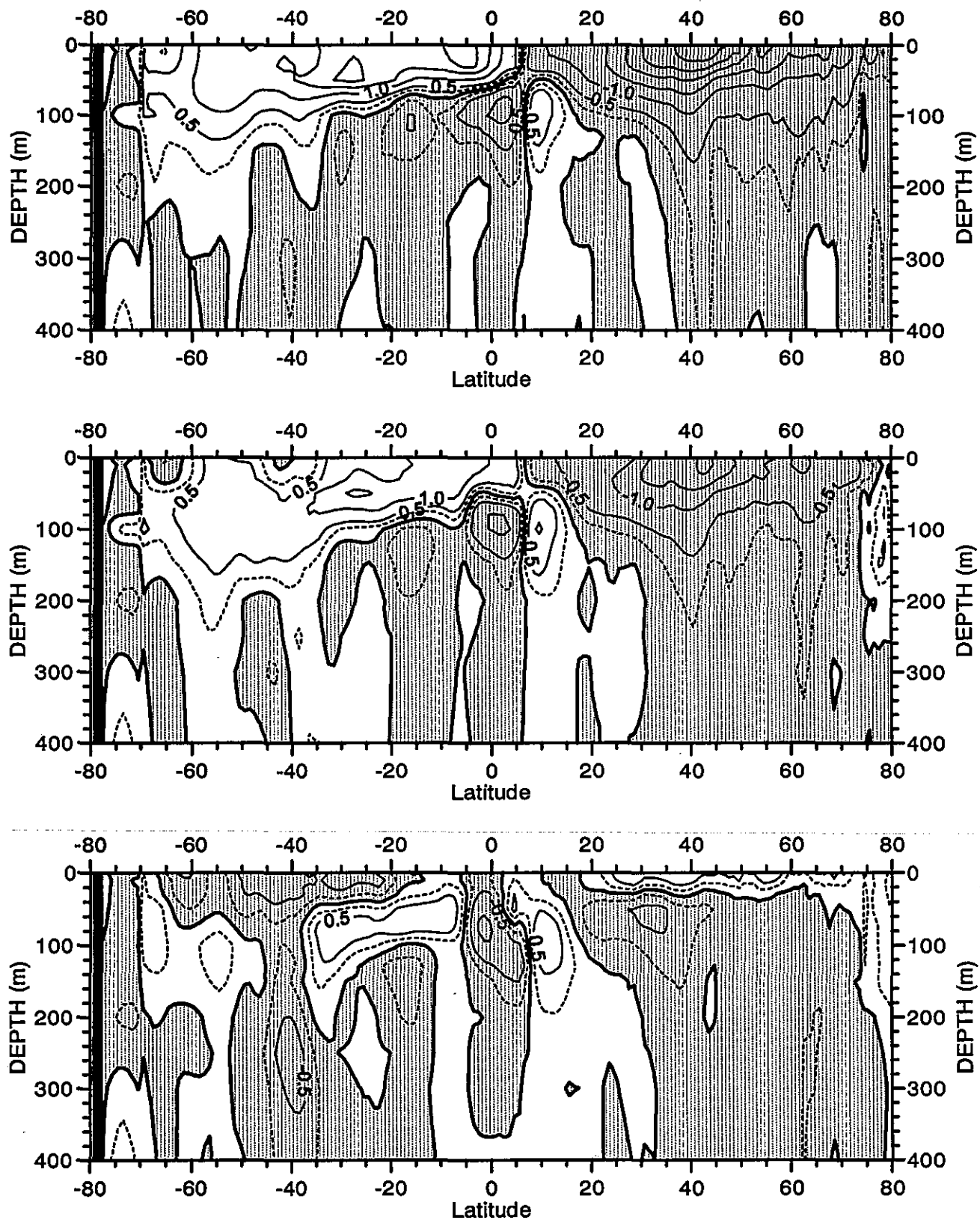


Fig. A7 Deviation ($^{\circ}\text{C}$) of the monthly mean temperature from the annual mean for the Atlantic Ocean (from top to bottom are APRIL, MAY, and JUNE)

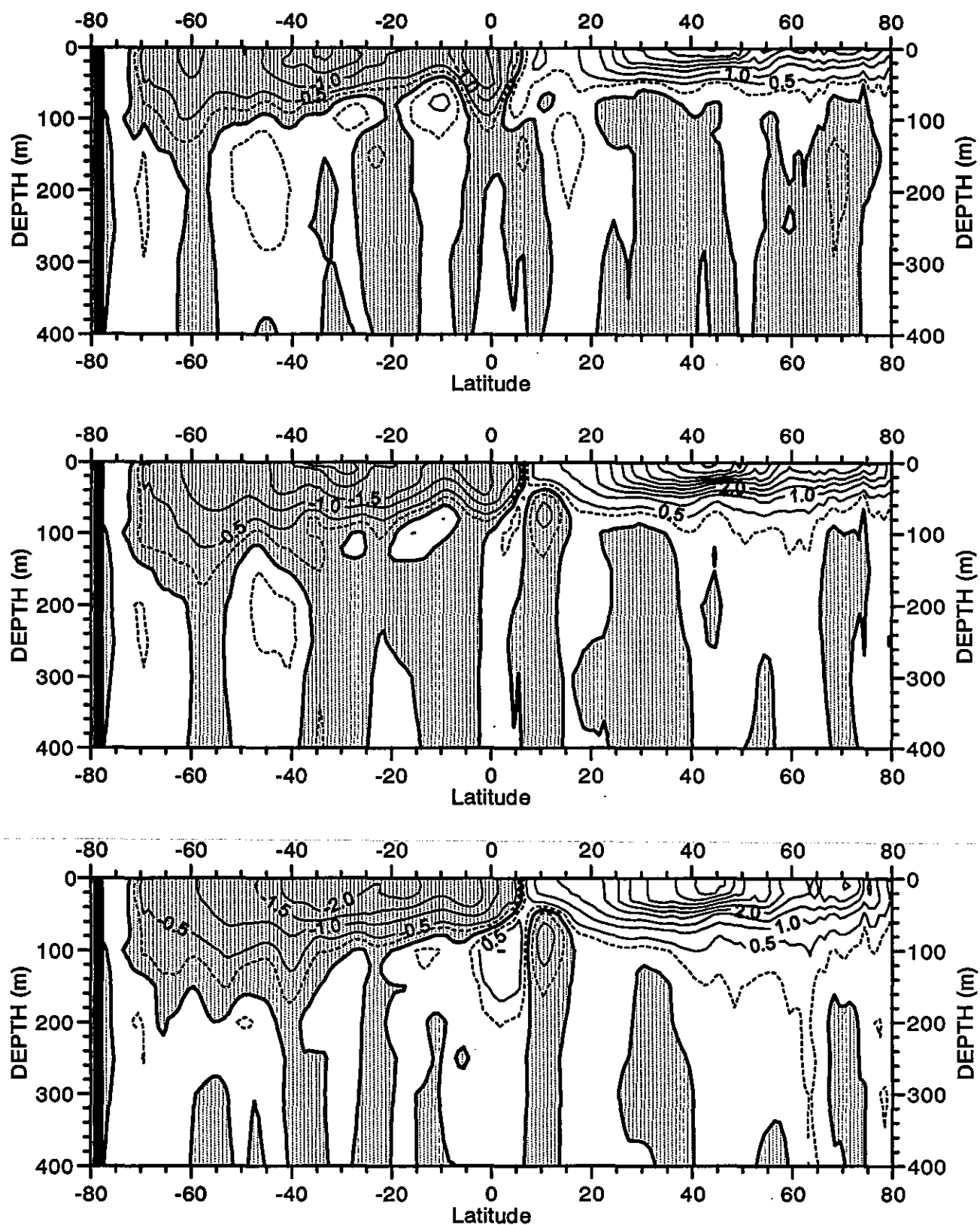


Fig. A8 Deviation ($^{\circ}\text{C}$) of the monthly mean temperature from the annual mean for the Atlantic Ocean (from top to bottom are JULY, AUGUST, and SEPTEMBER)

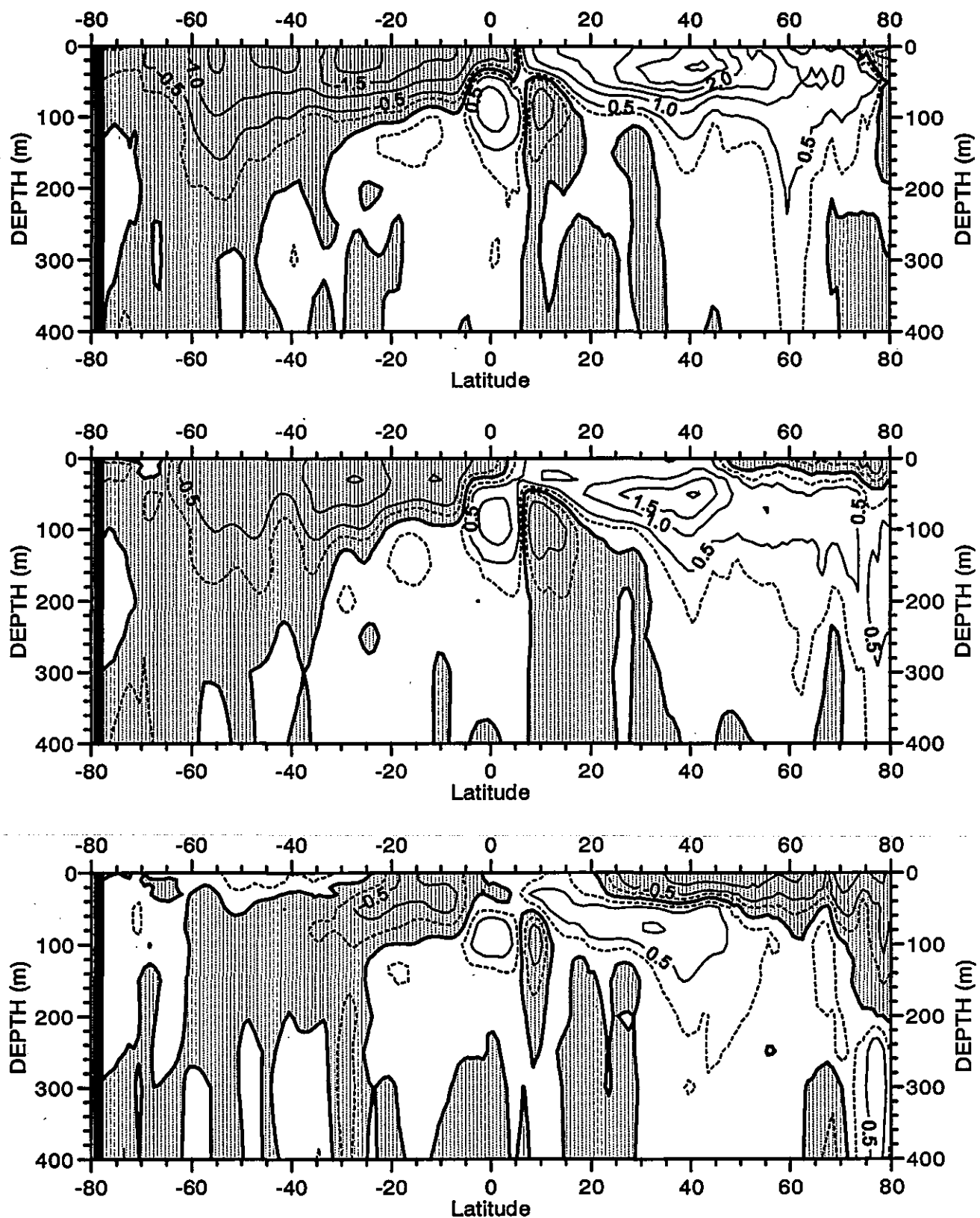


Fig. A9 Deviation ($^{\circ}\text{C}$) of the monthly mean temperature from the annual mean for the Atlantic Ocean (from top to bottom are OCTOBER, NOVEMBER, and DECEMBER)

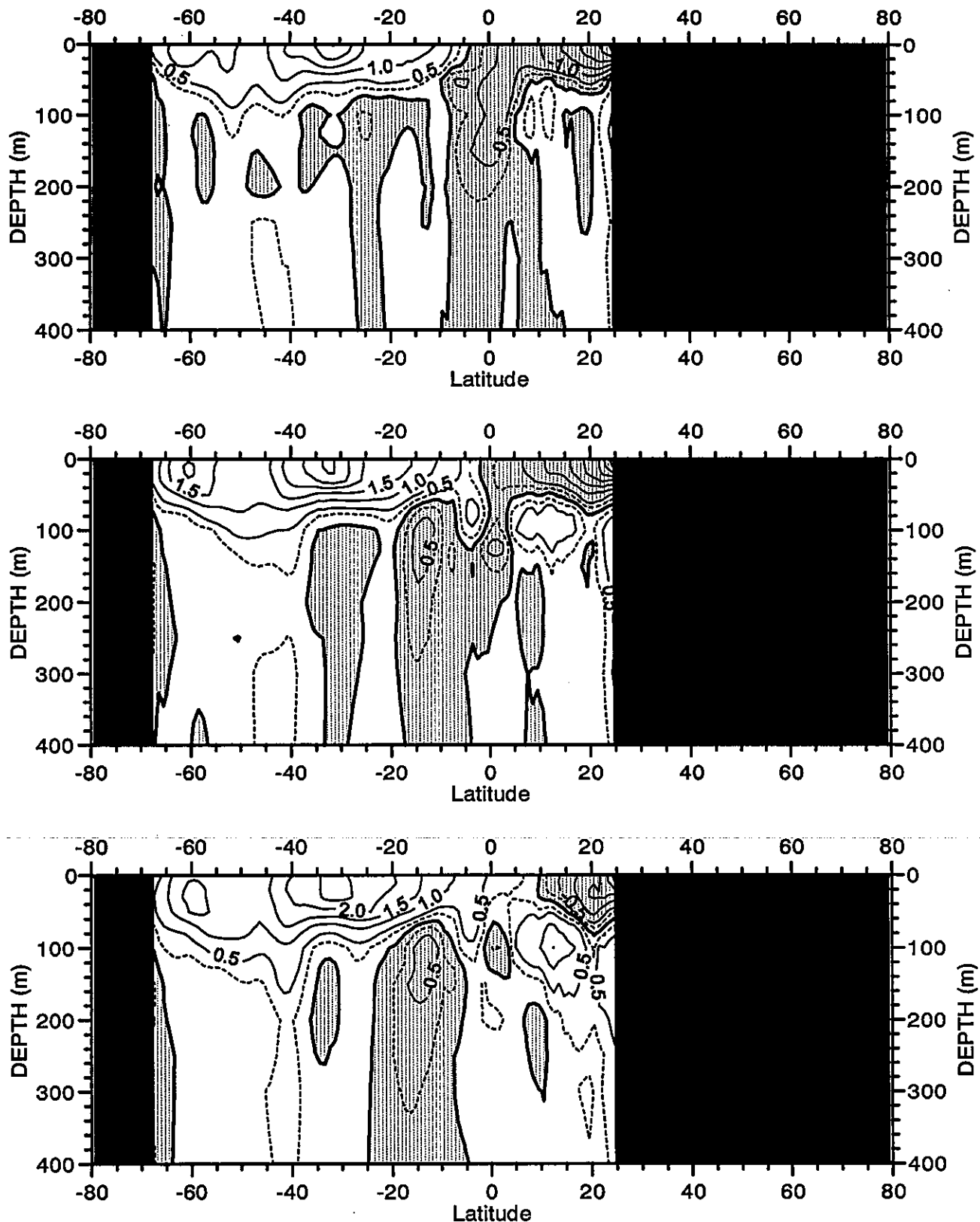


Fig. A10 Deviation ($^{\circ}\text{C}$) of the monthly mean temperature from the annual mean for the Indian Ocean (from top to bottom are JANUARY, FEBRUARY, and MARCH)

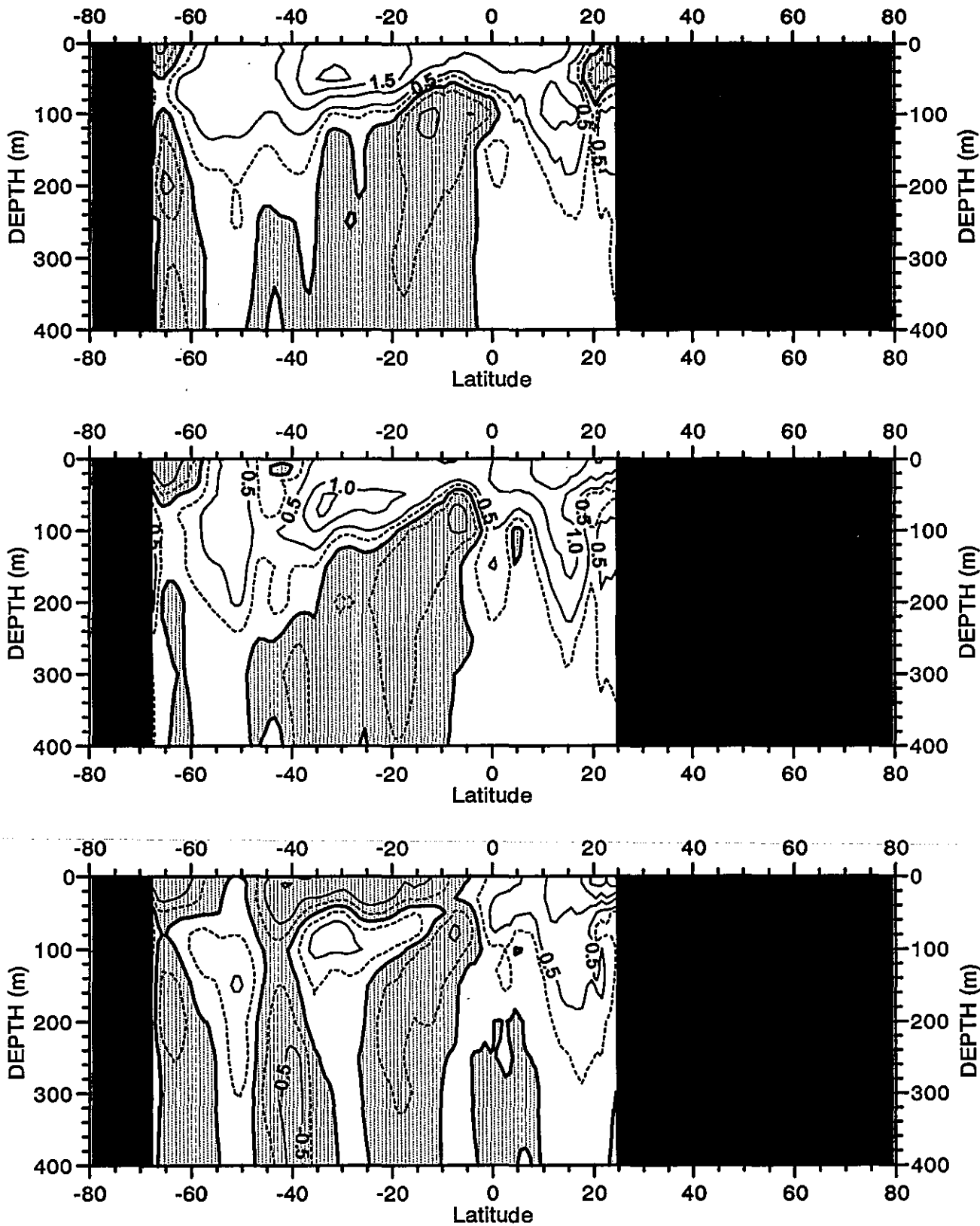


Fig. A11 Deviation ($^{\circ}\text{C}$) of the monthly mean temperature from the annual mean for the Indian Ocean (from top to bottom are APRIL, MAY, and JUNE)

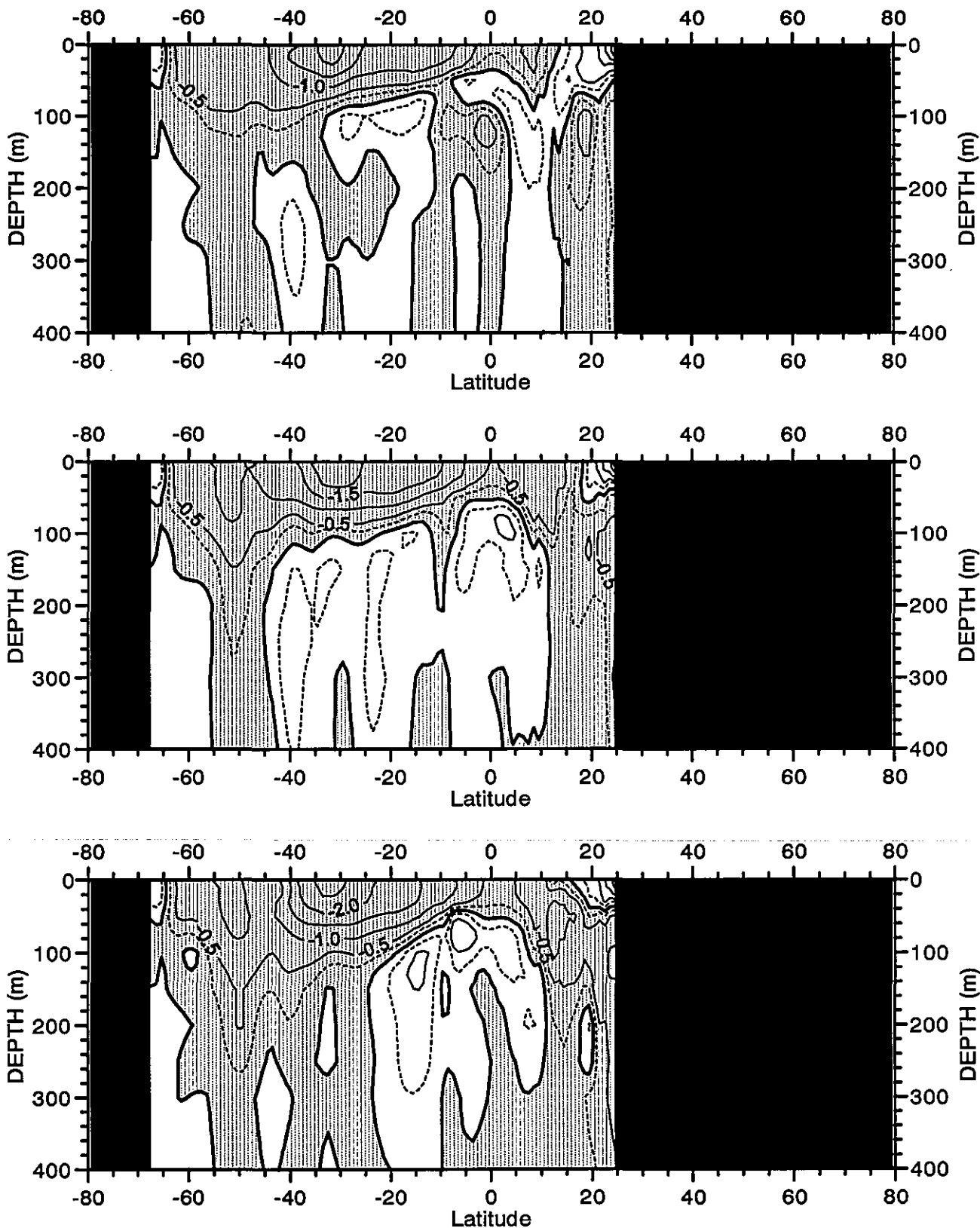


Fig. A12 Deviation ($^{\circ}\text{C}$) of the monthly mean temperature from the annual mean for the Indian Ocean (from top to bottom are JULY, AUGUST, and SEPTEMBER)

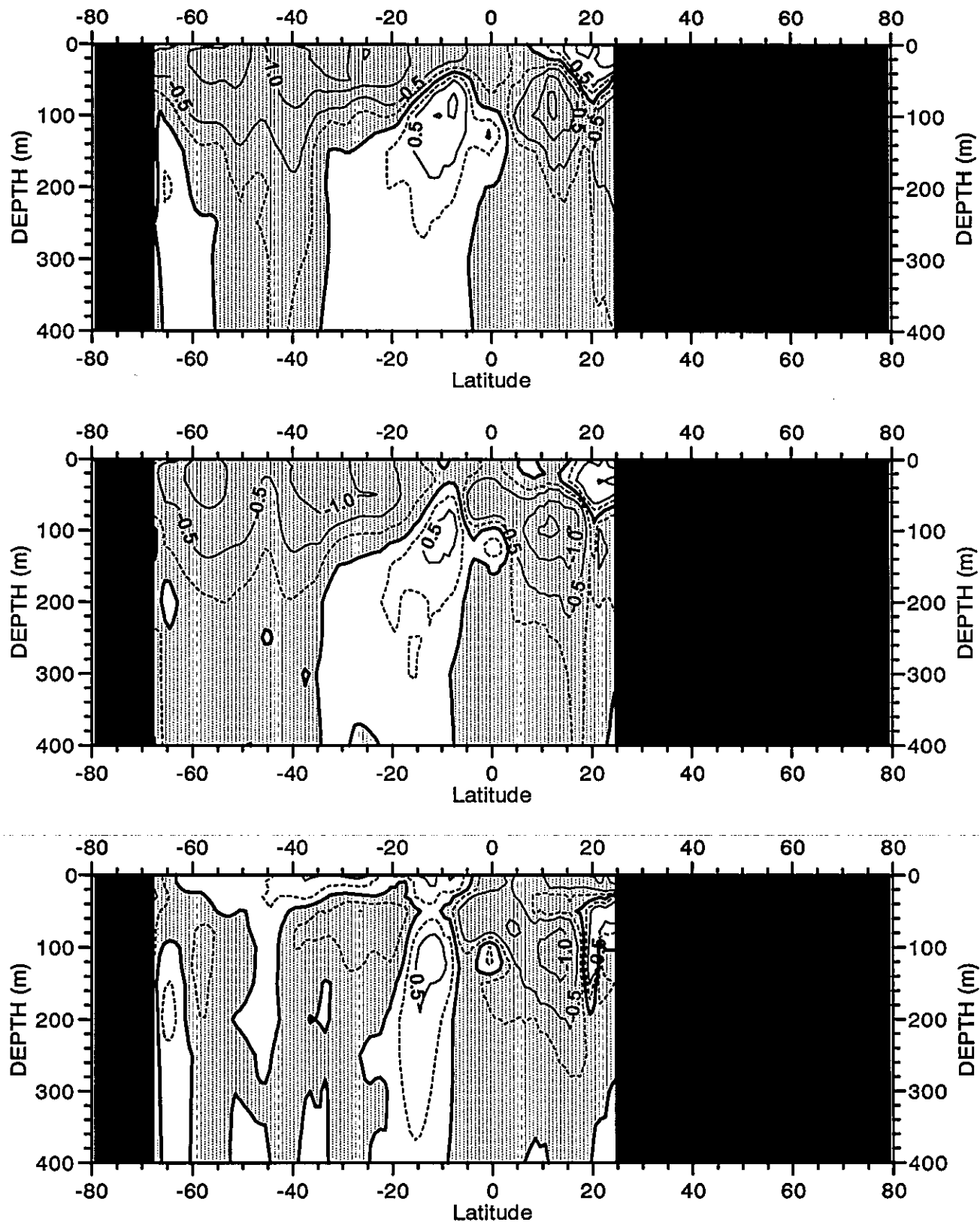


Fig. A13 Deviation ($^{\circ}\text{C}$) of the monthly mean temperature from the annual mean
for the Indian Ocean (from top to bottom are OCTOBER, NOVEMBER, and DECEMBER)

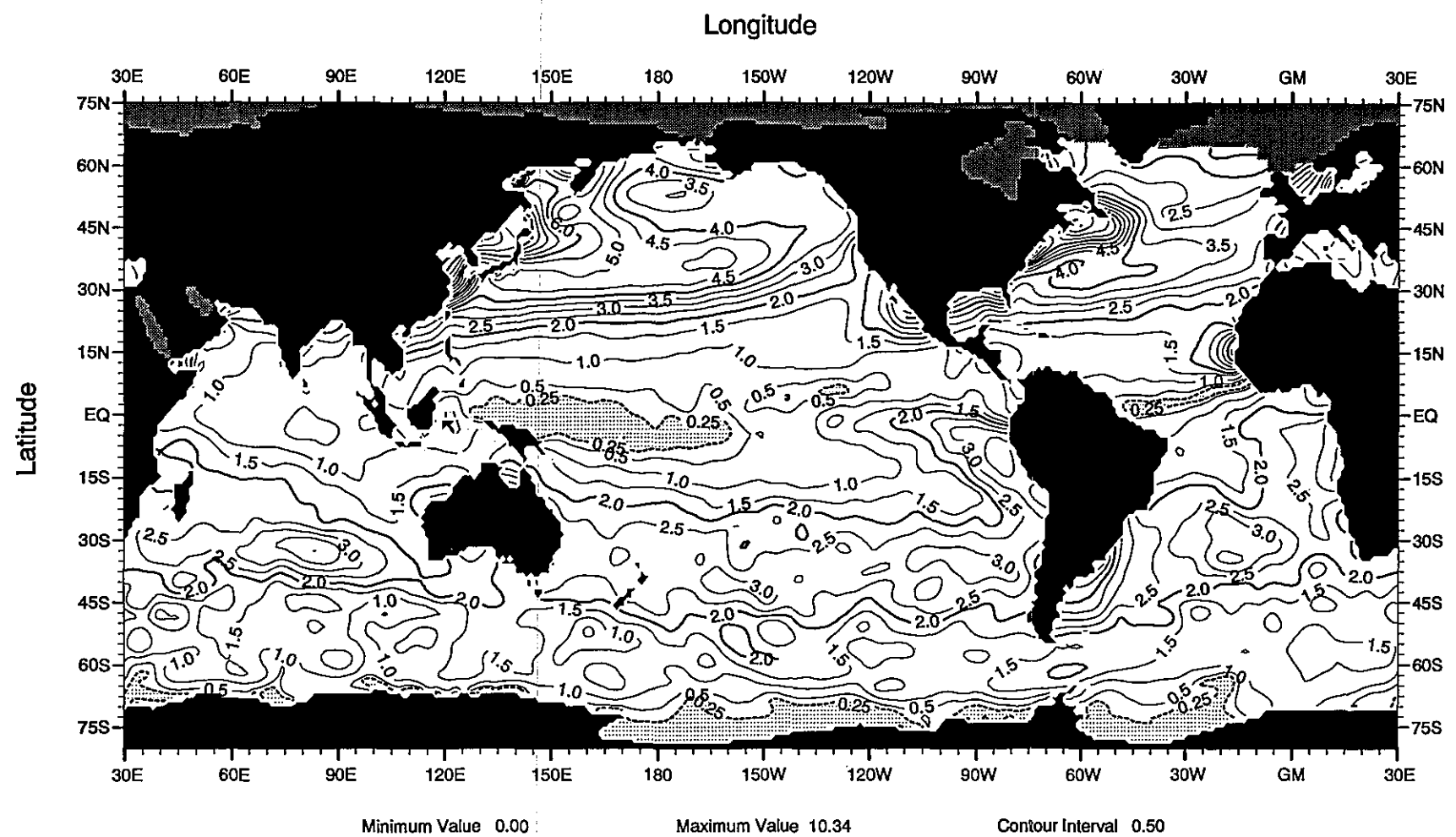


Fig. B1 Amplitude (°C) of the 1st harmonic of the annual temperature cycle at the sea surface

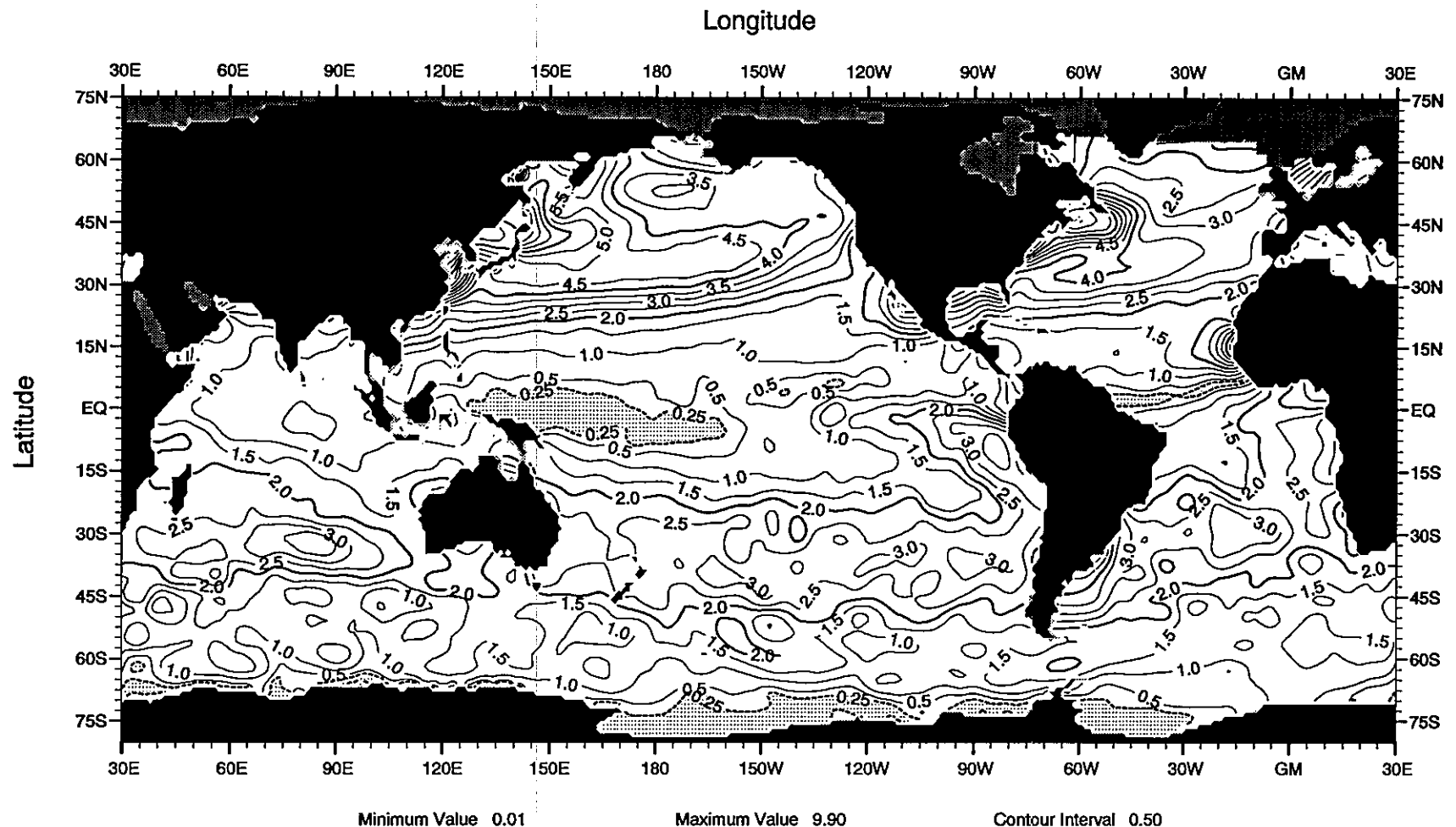


Fig. B2 Amplitude (°C) of the 1st harmonic of the annual temperature cycle at 10 m depth

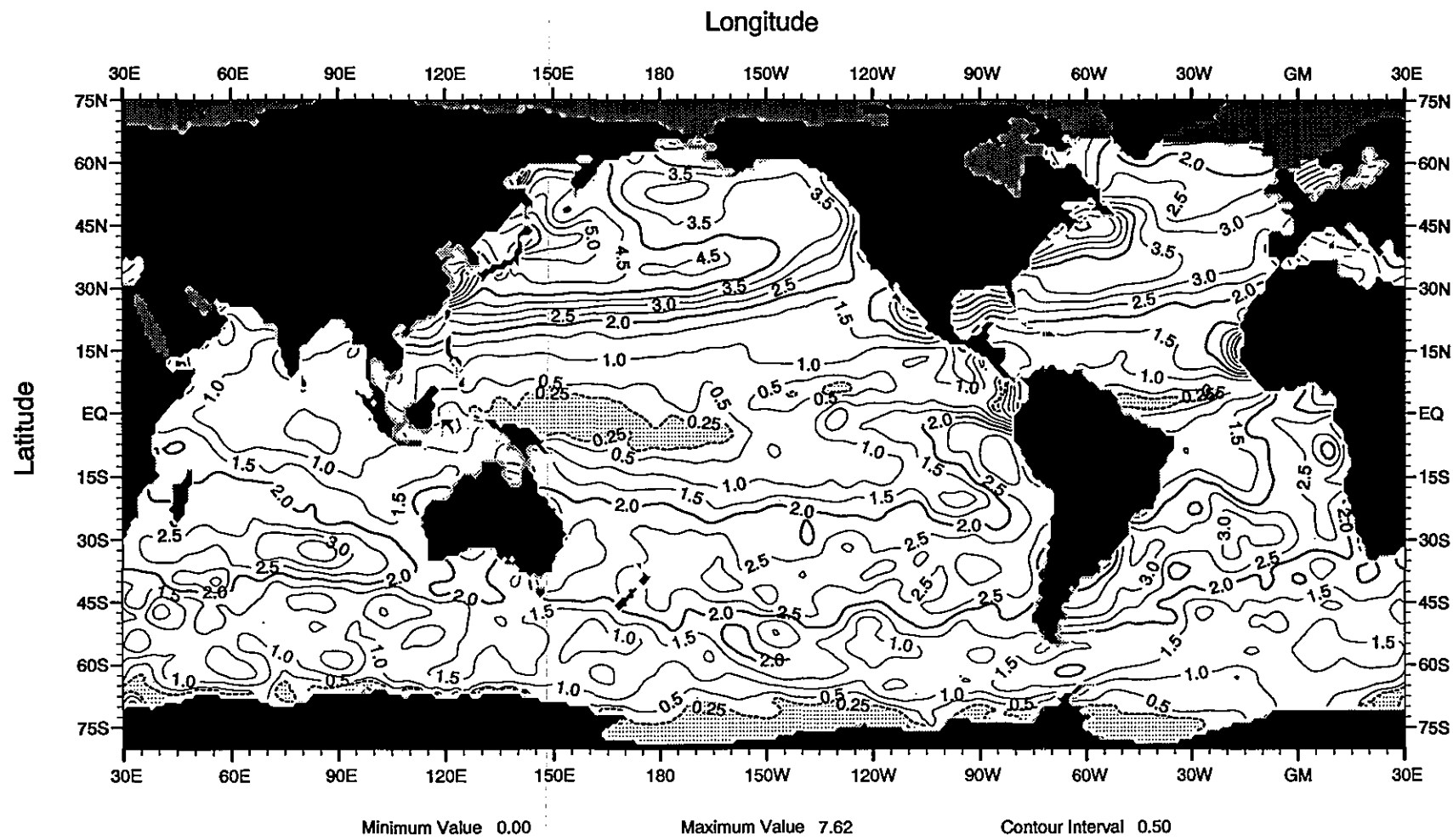


Fig. B3 Amplitude (°C) of the 1st harmonic of the annual temperature cycle at 20 m depth

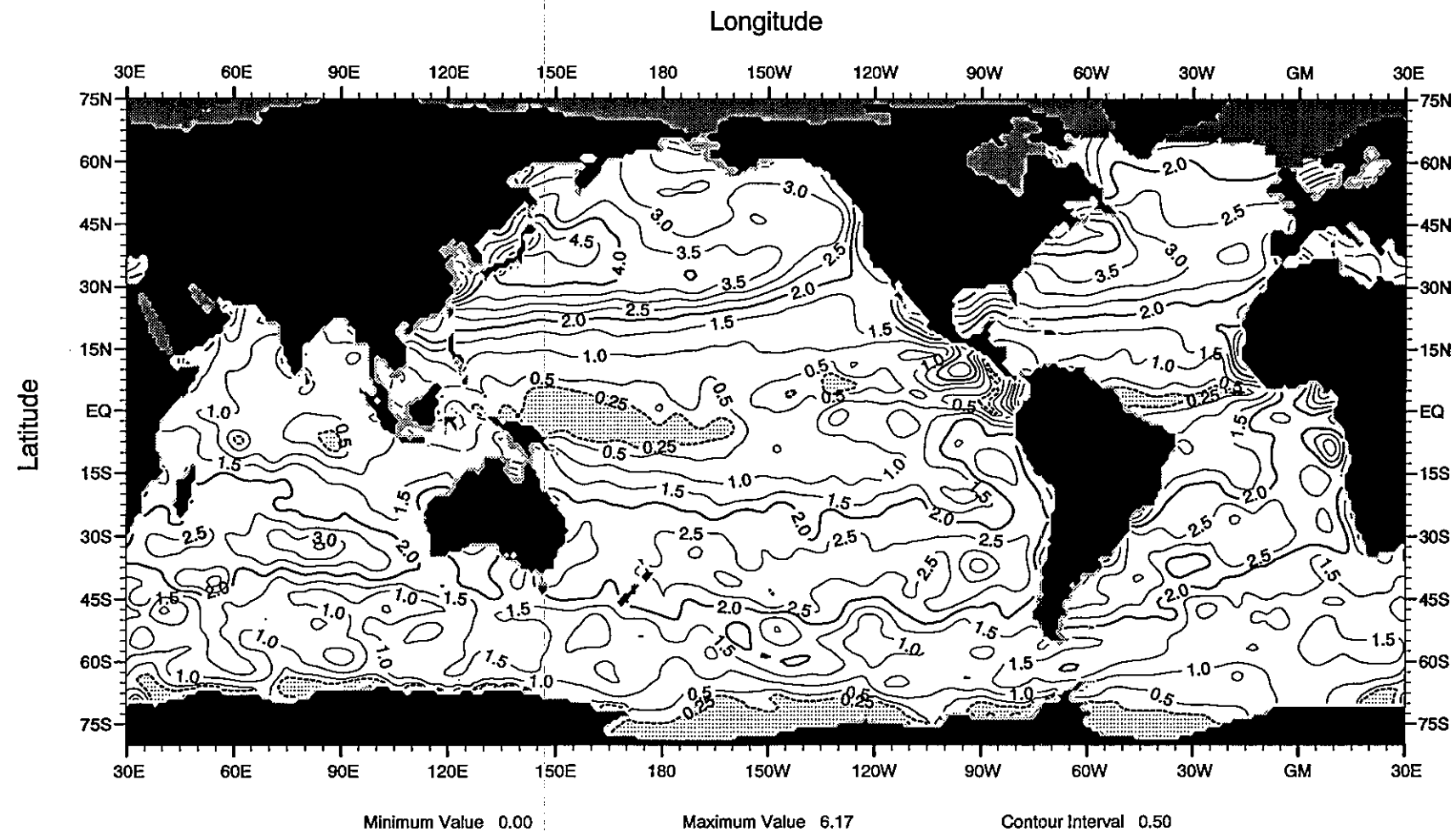


Fig. B4 Amplitude (°C) of the 1st harmonic of the annual temperature cycle at 30 m depth

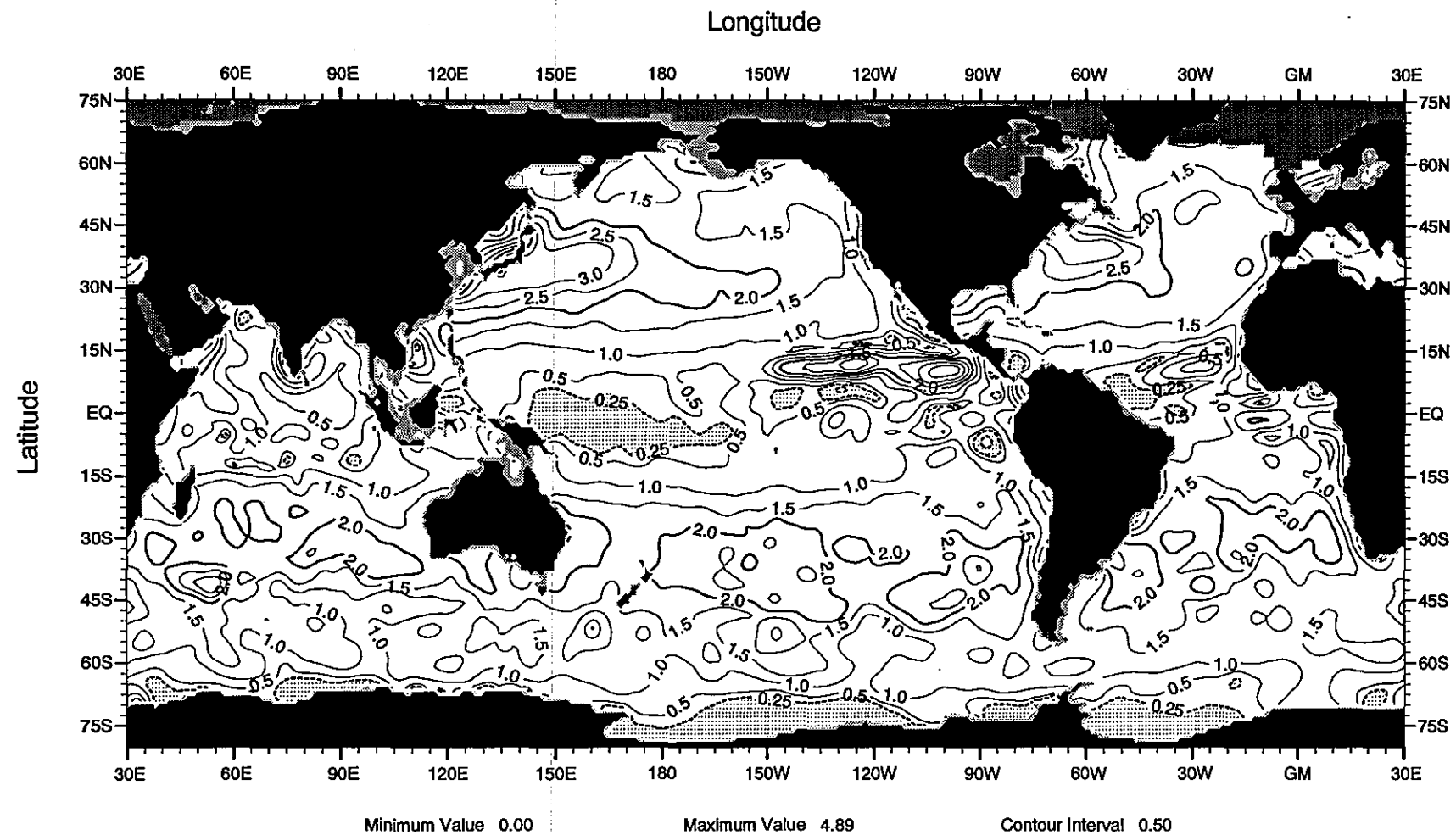


Fig. B5 Amplitude (°C) of the 1st harmonic of the annual temperature cycle at 50 m depth

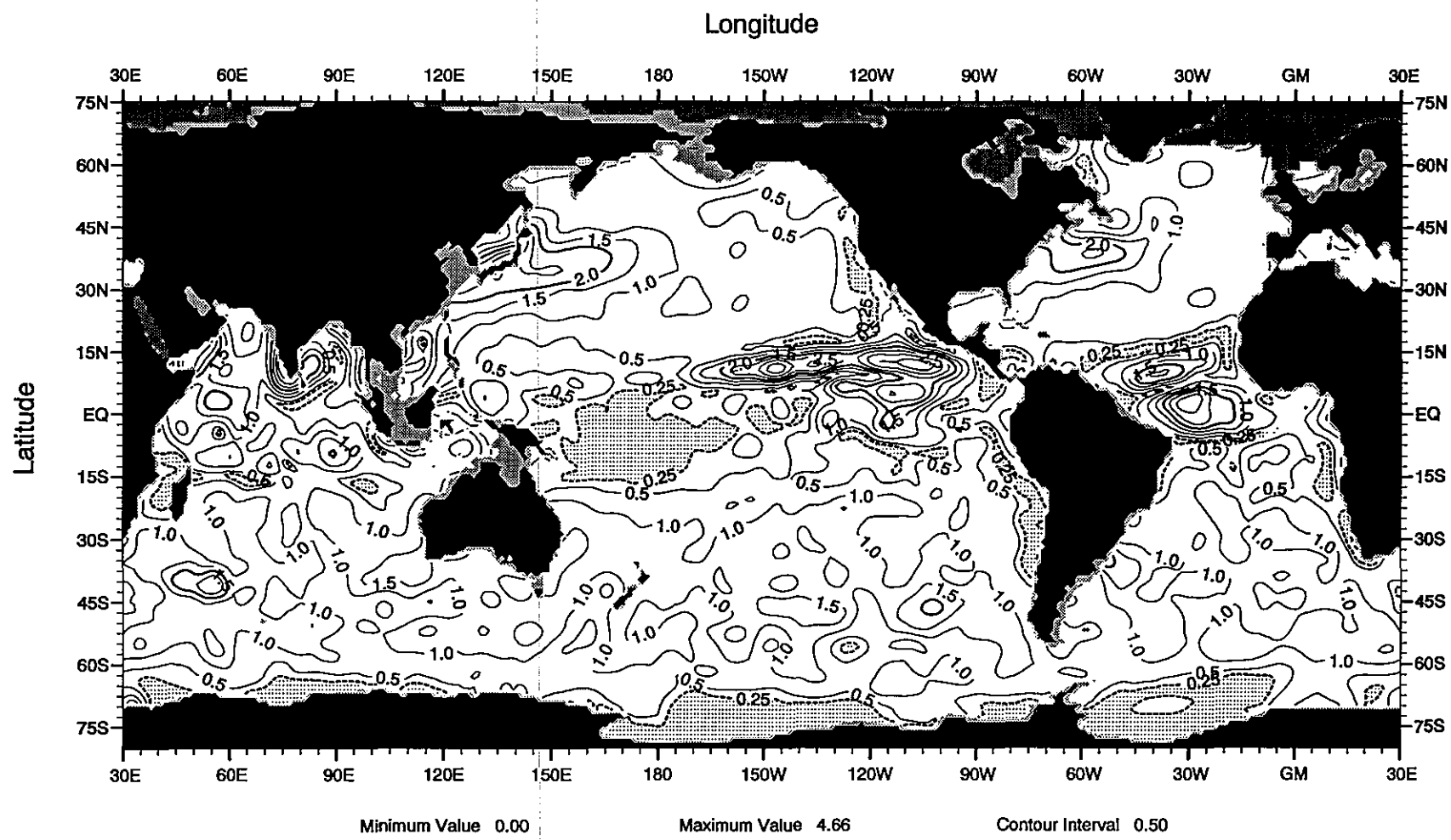


Fig. B6 Amplitude (°C) of the 1st harmonic of the annual temperature cycle at 75 m depth

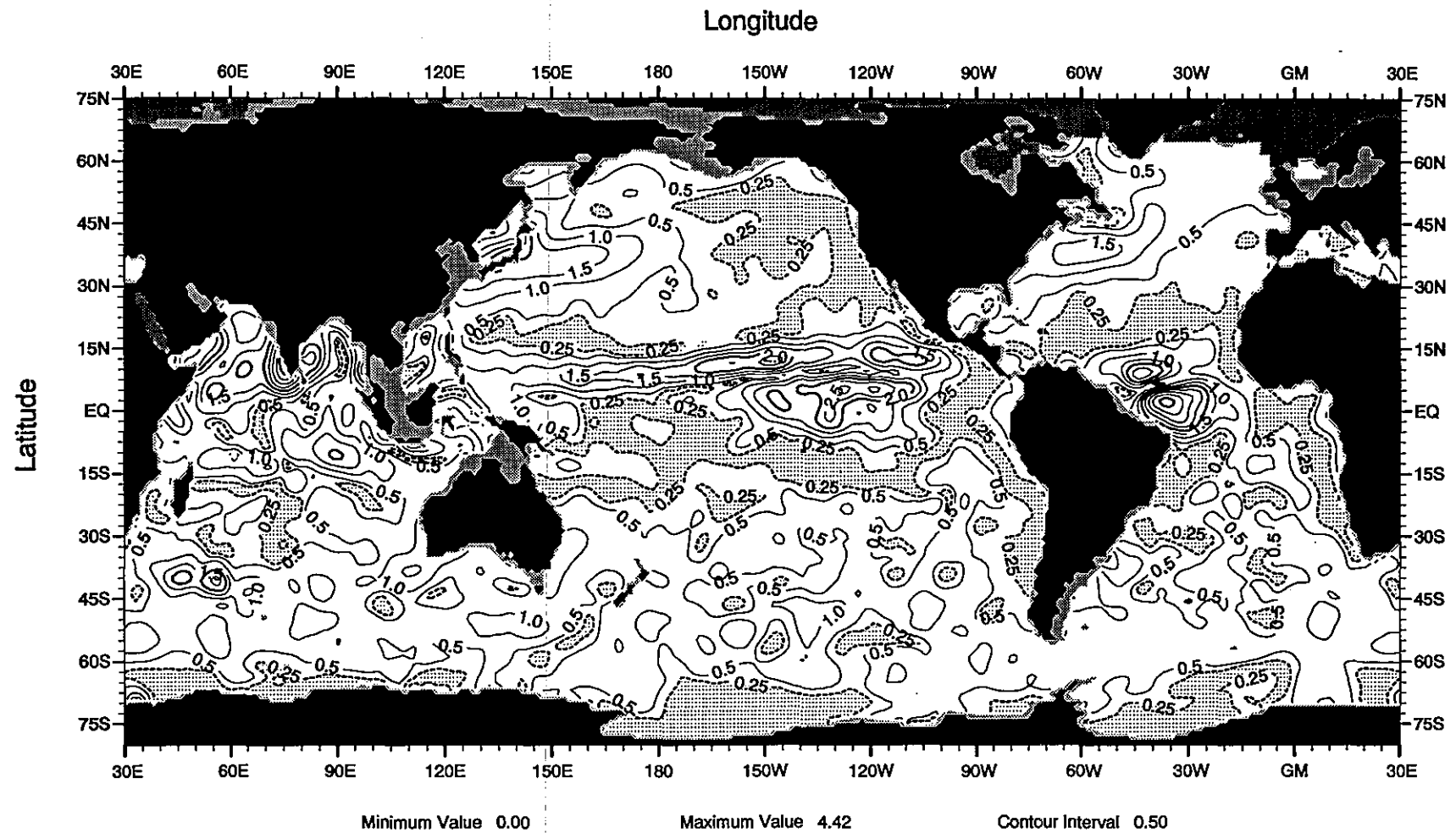


Fig. B7 Amplitude (°C) of the 1st harmonic of the annual temperature cycle at 100 m depth

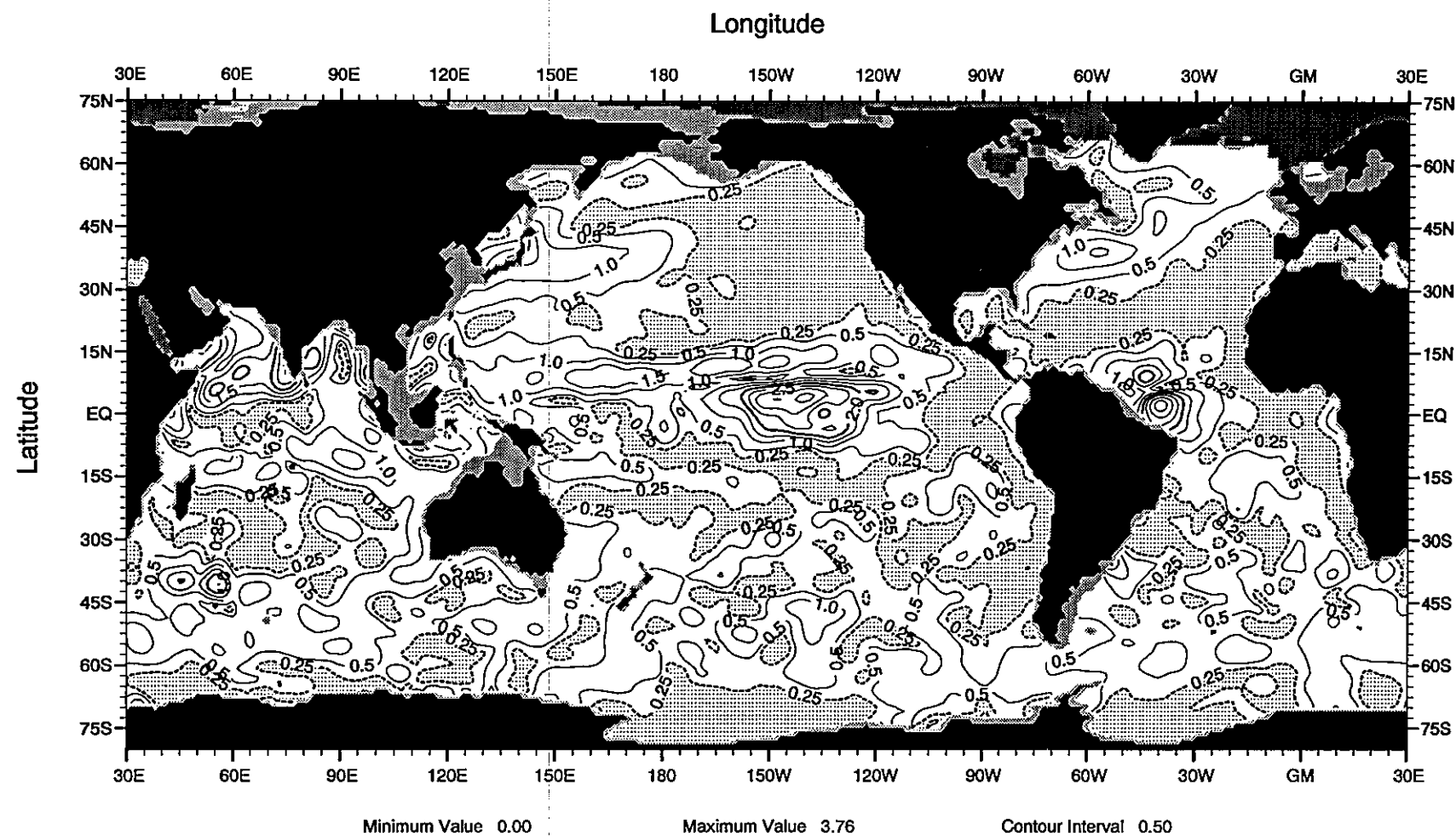


Fig. B8 Amplitude (°C) of the 1st harmonic of the annual temperature cycle at 125 m depth

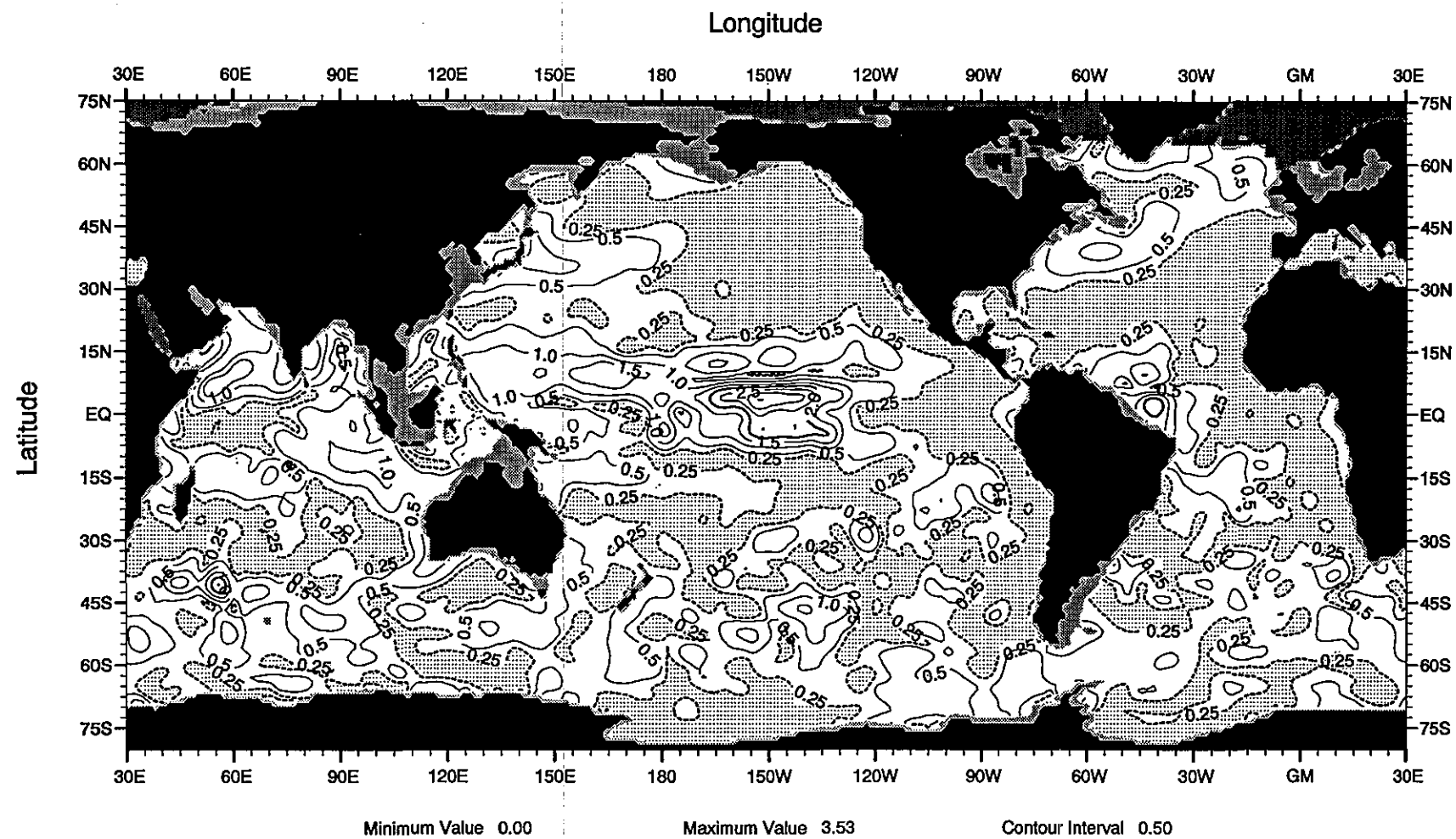


Fig. B9 Amplitude (°C) of the 1st harmonic of the annual temperature cycle at 150 m depth

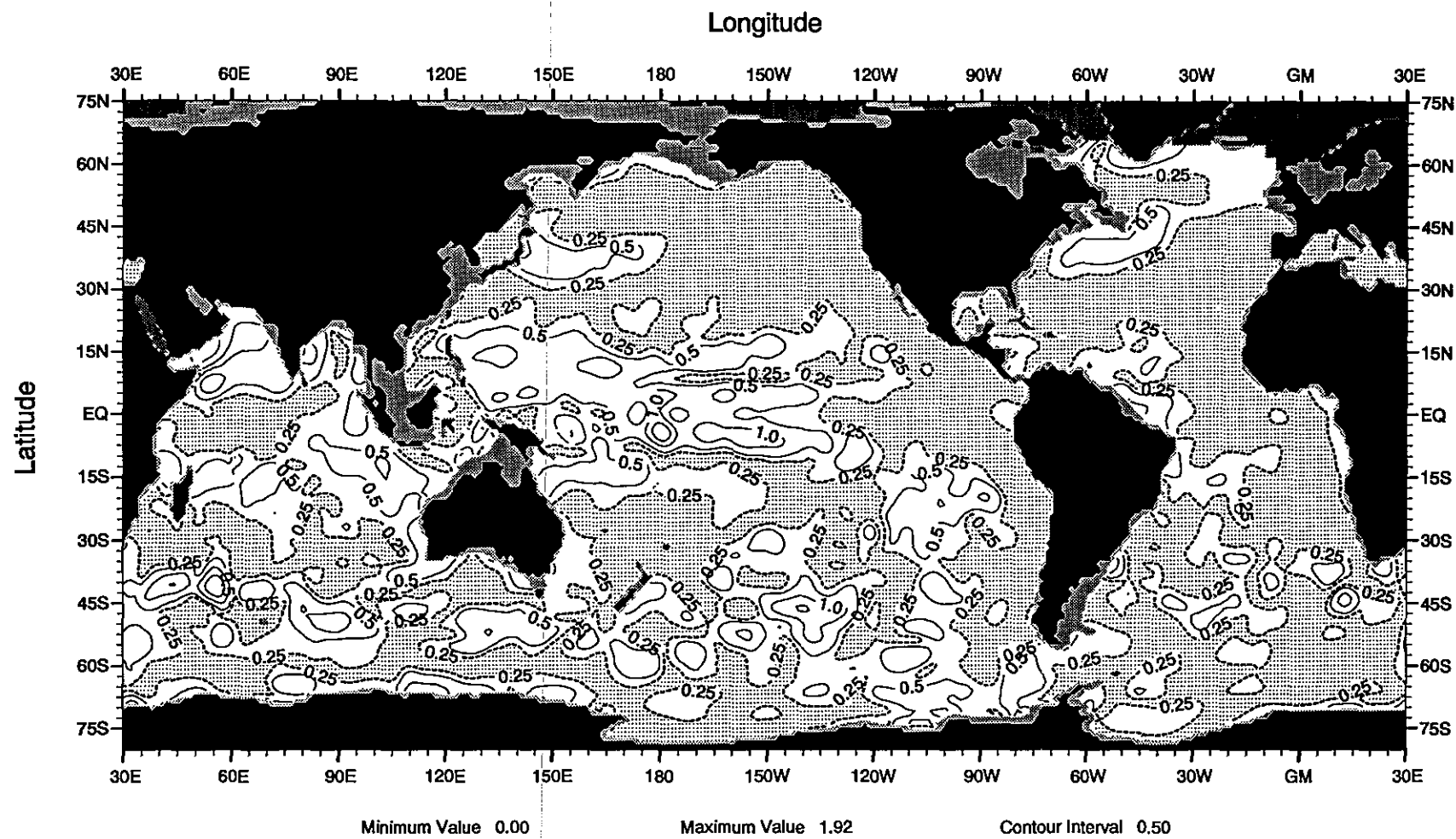


Fig. B10 Amplitude (°C) of the 1st harmonic of the annual temperature cycle at 200 m depth

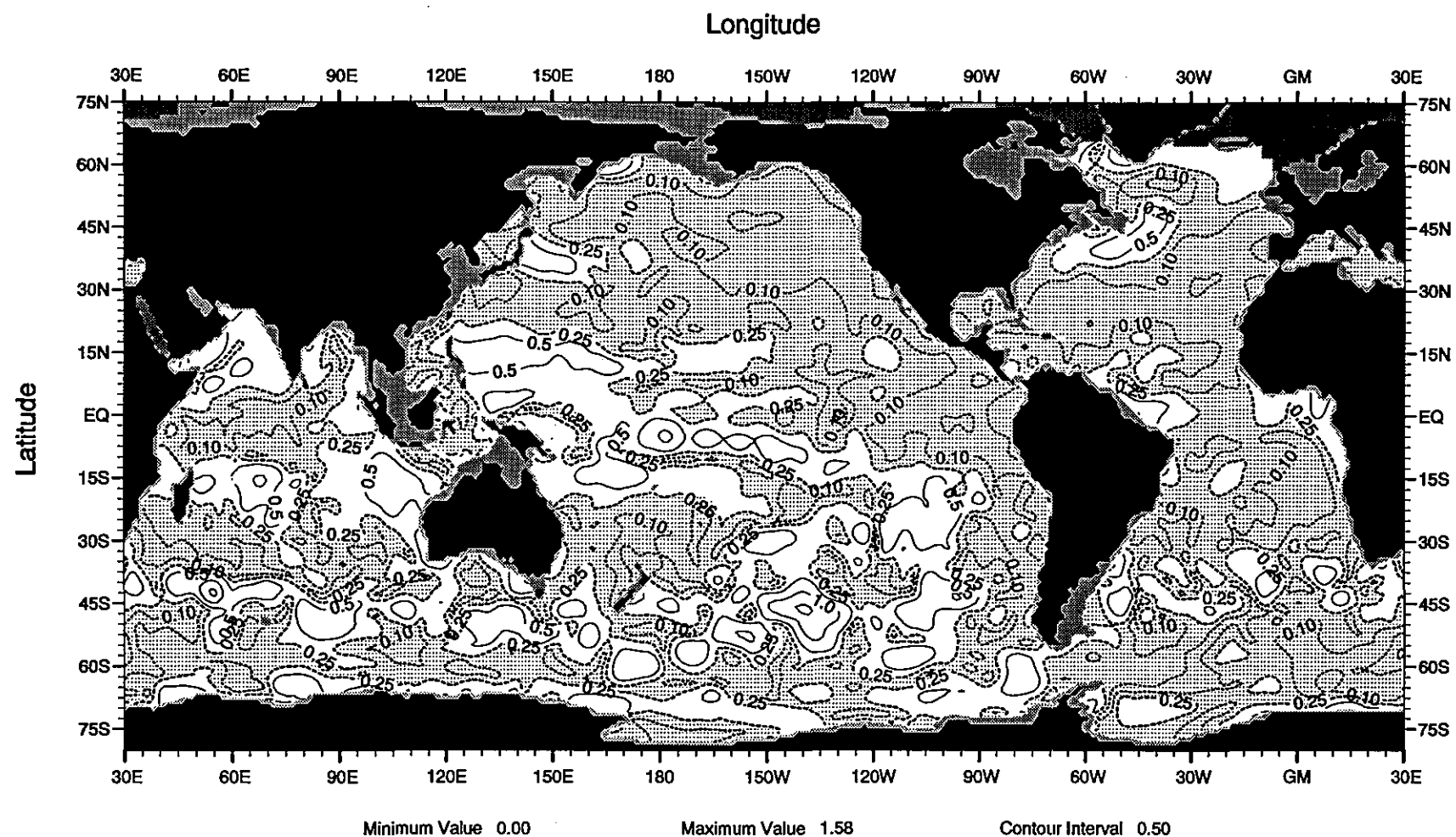


Fig. B11 Amplitude (°C) of the 1st harmonic of the annual temperature cycle at 250 m depth

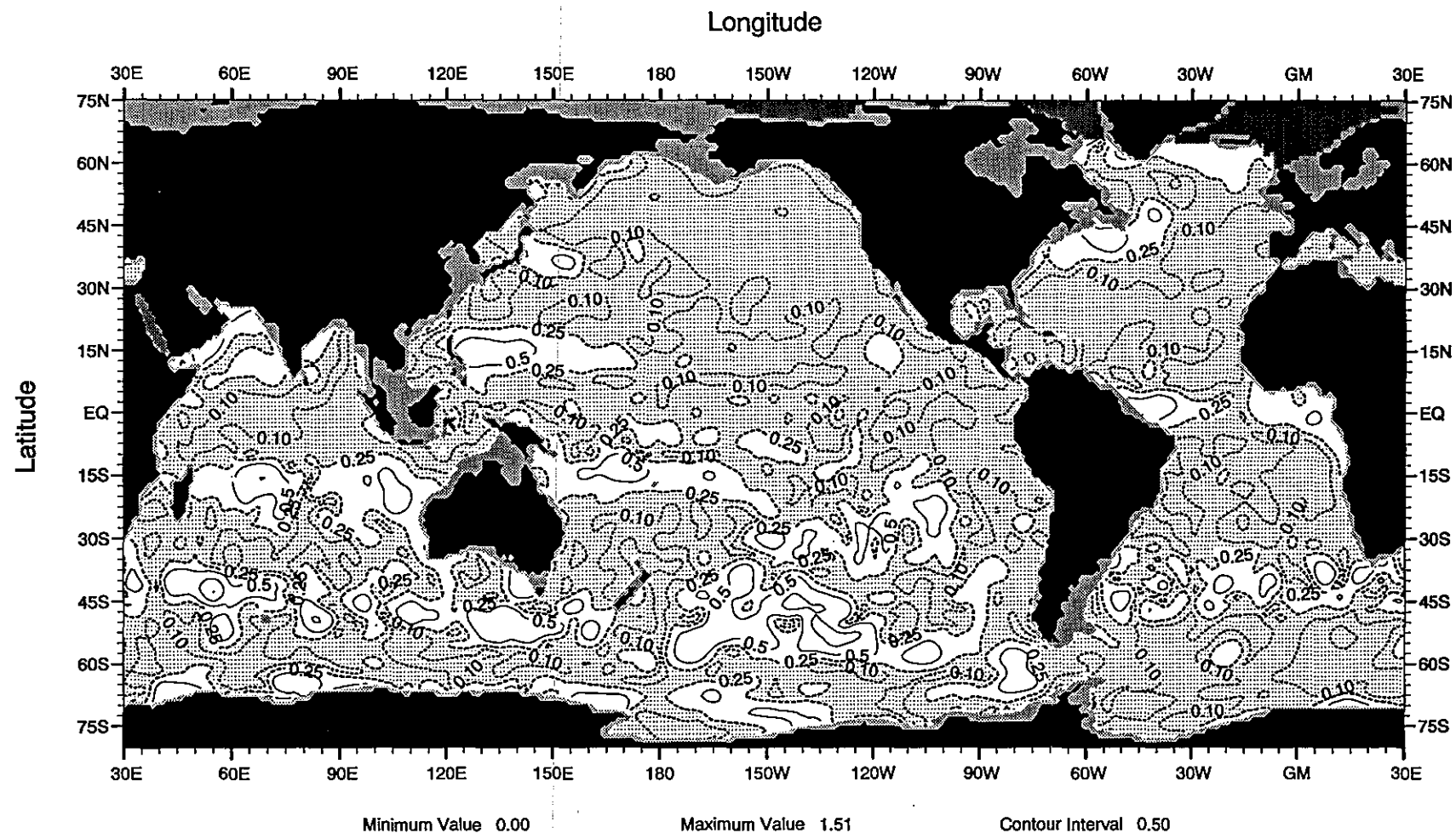


Fig. B12 Amplitude (°C) of the 1st harmonic of the annual temperature cycle at 300 m depth

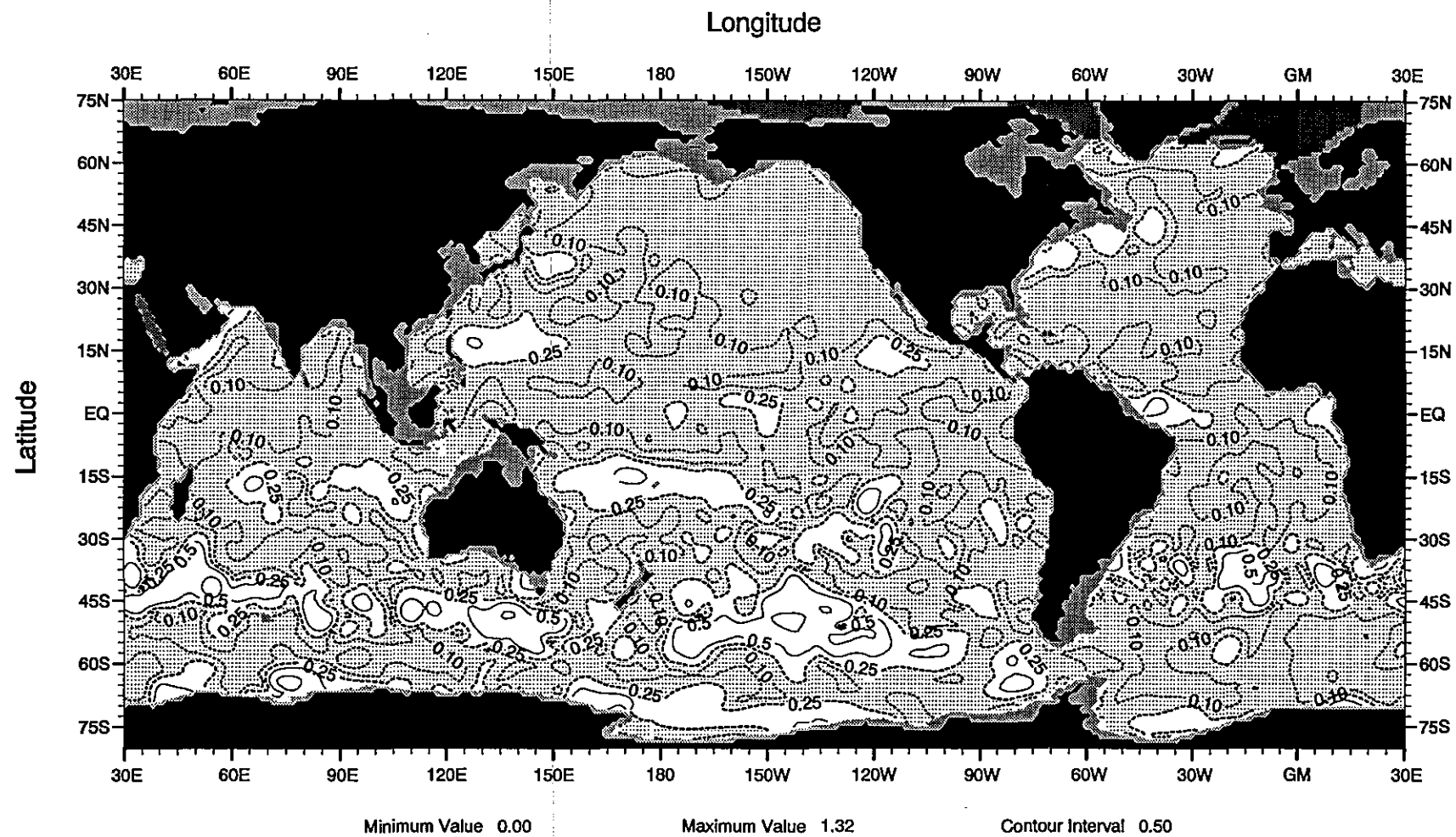


Fig. B13 Amplitude (°C) of the 1st harmonic of the annual temperature cycle at 400 m depth

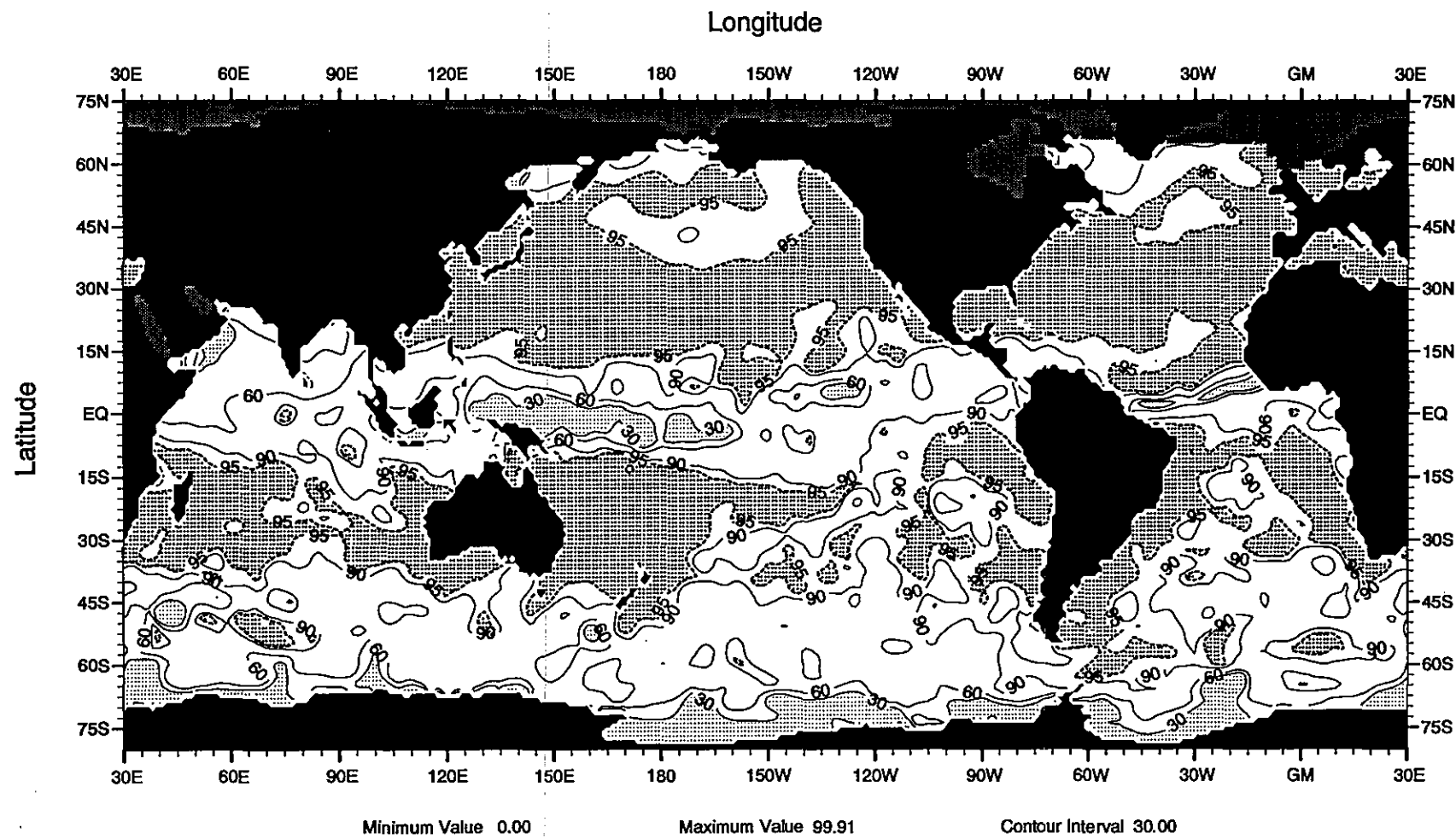


Fig. B14 Percent variance explained by 1st harmonic of the annual temperature cycle at the surface

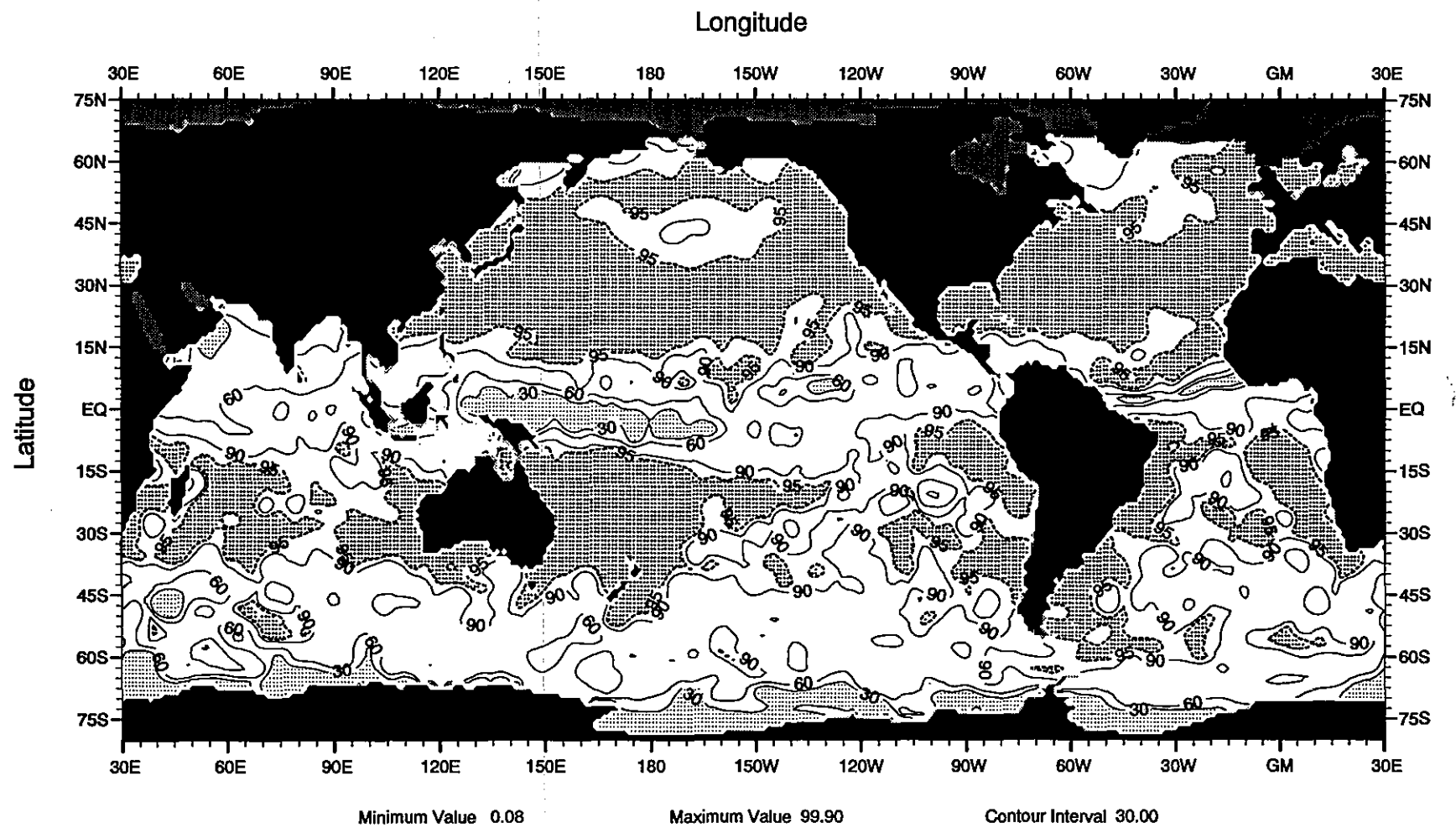


Fig. B15 Percent variance explained by 1st harmonic of the annual temperature cycle at 10 m depth

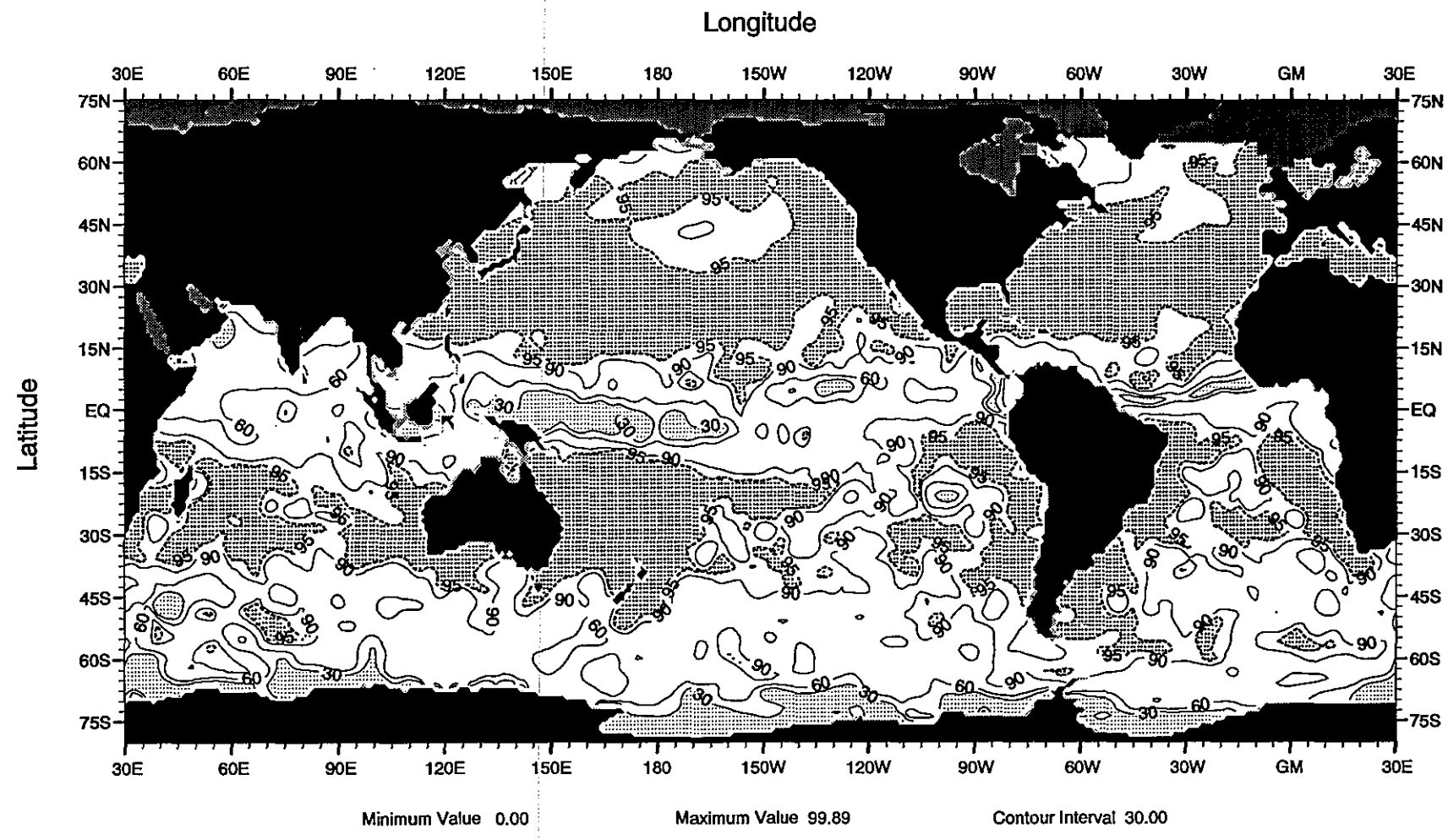


Fig. B16 Percent variance explained by 1st harmonic of the annual temperature cycle at 20 m depth

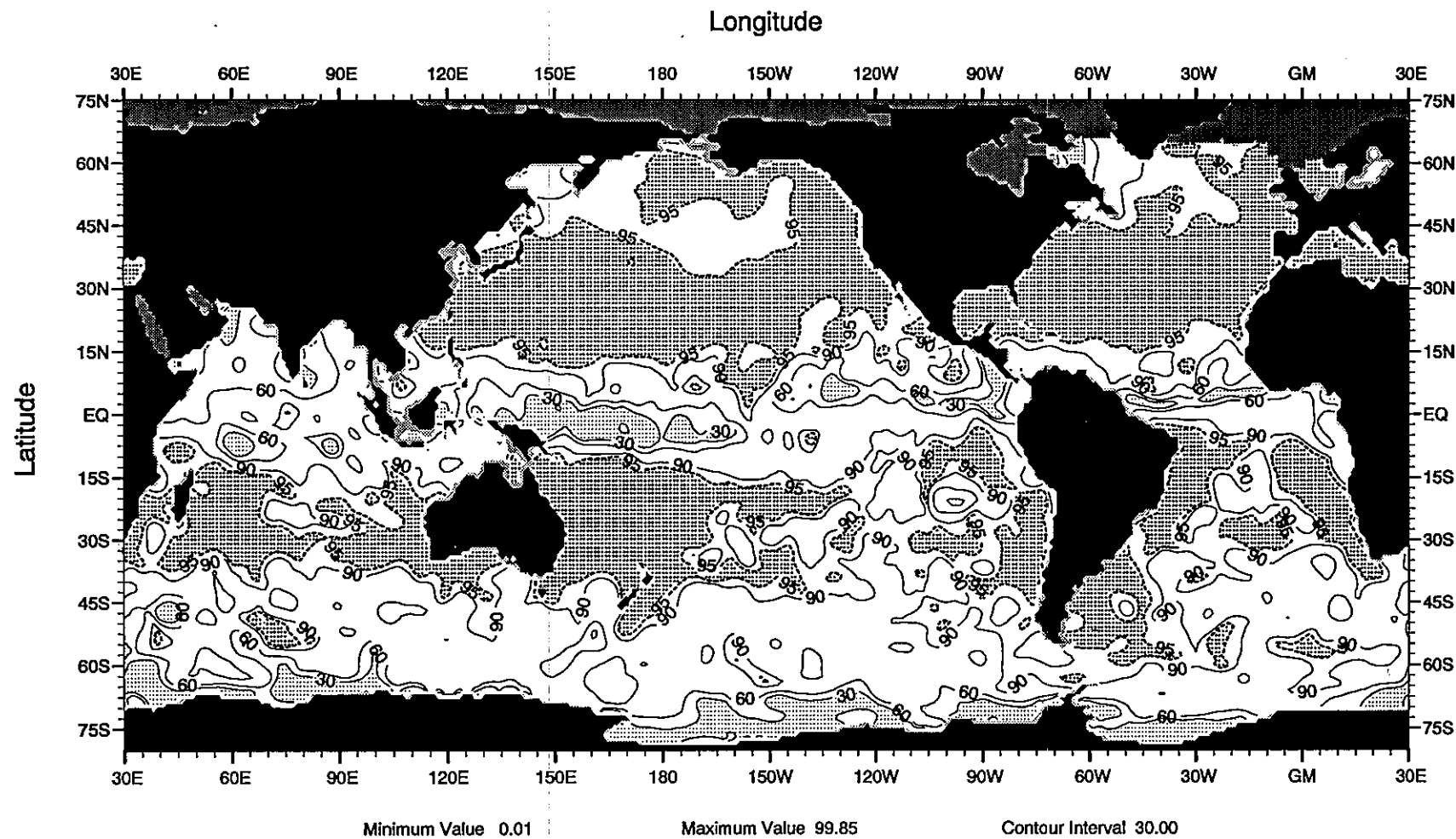


Fig. B17 Percent variance explained by 1st harmonic of the annual temperature cycle at 30 m depth

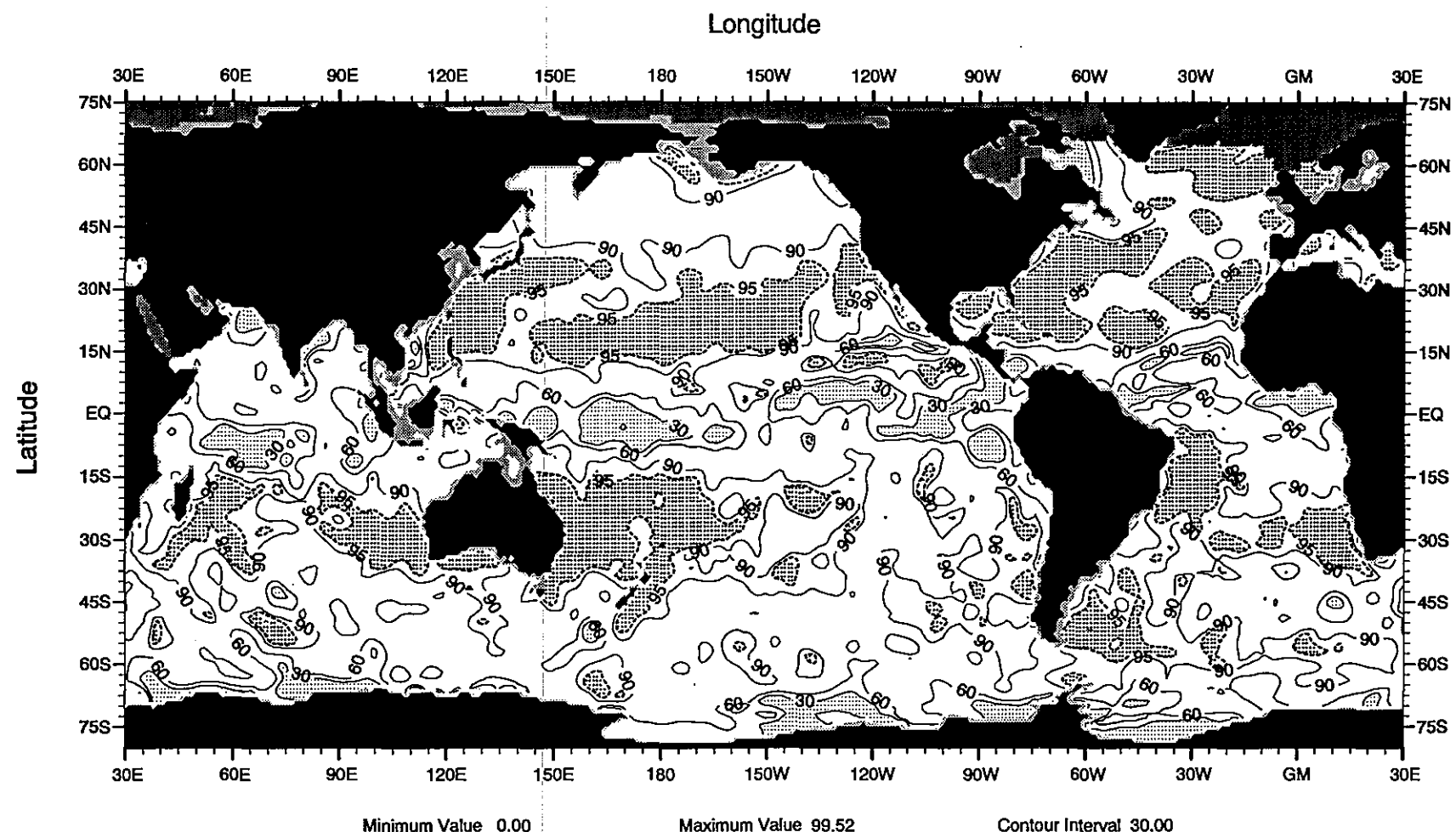


Fig. B18 Percent variance explained by 1st harmonic of the annual temperature cycle at 50 m depth

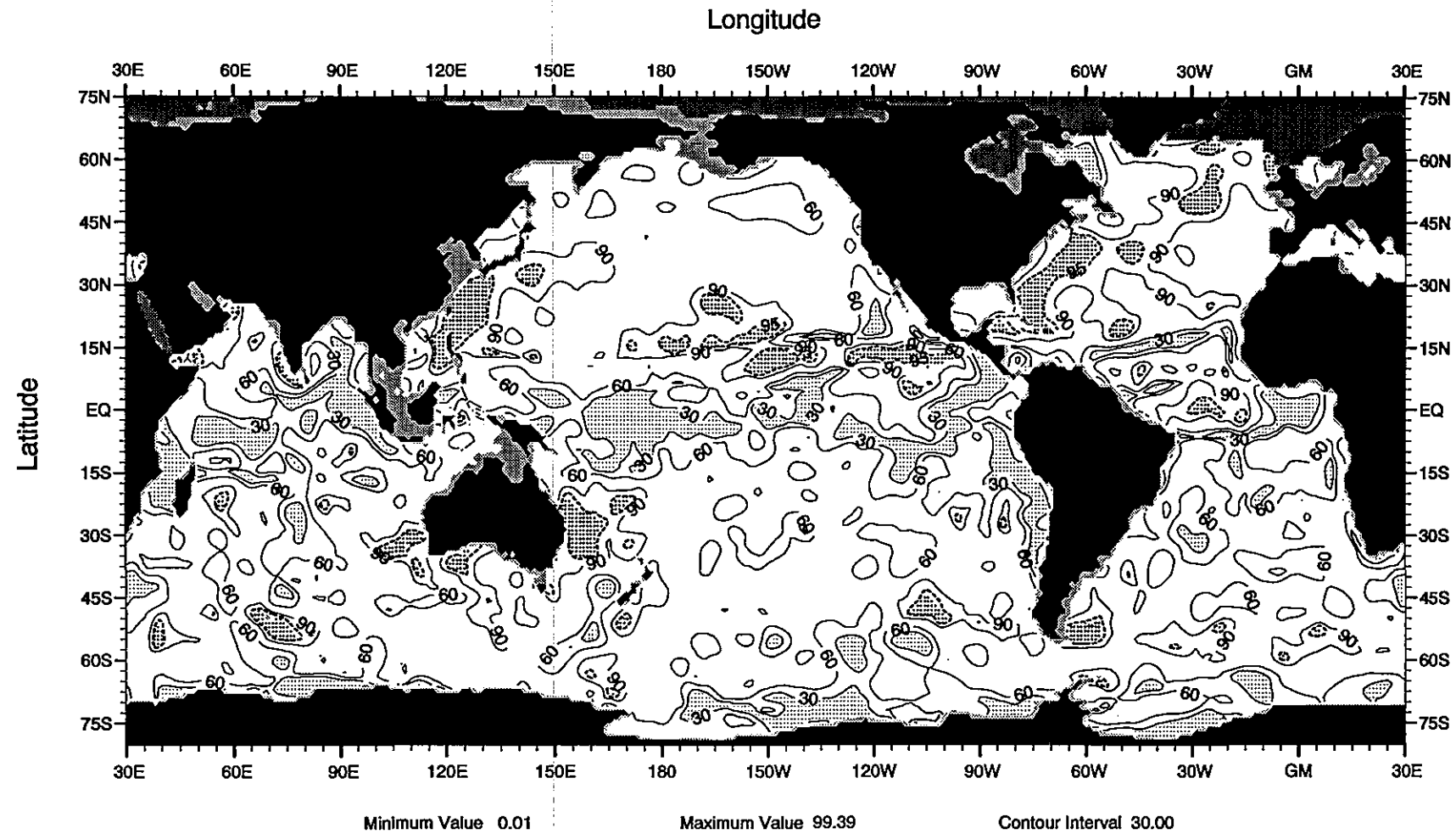


Fig. B19 Percent variance explained by 1st harmonic of the annual temperature cycle at 75 m depth

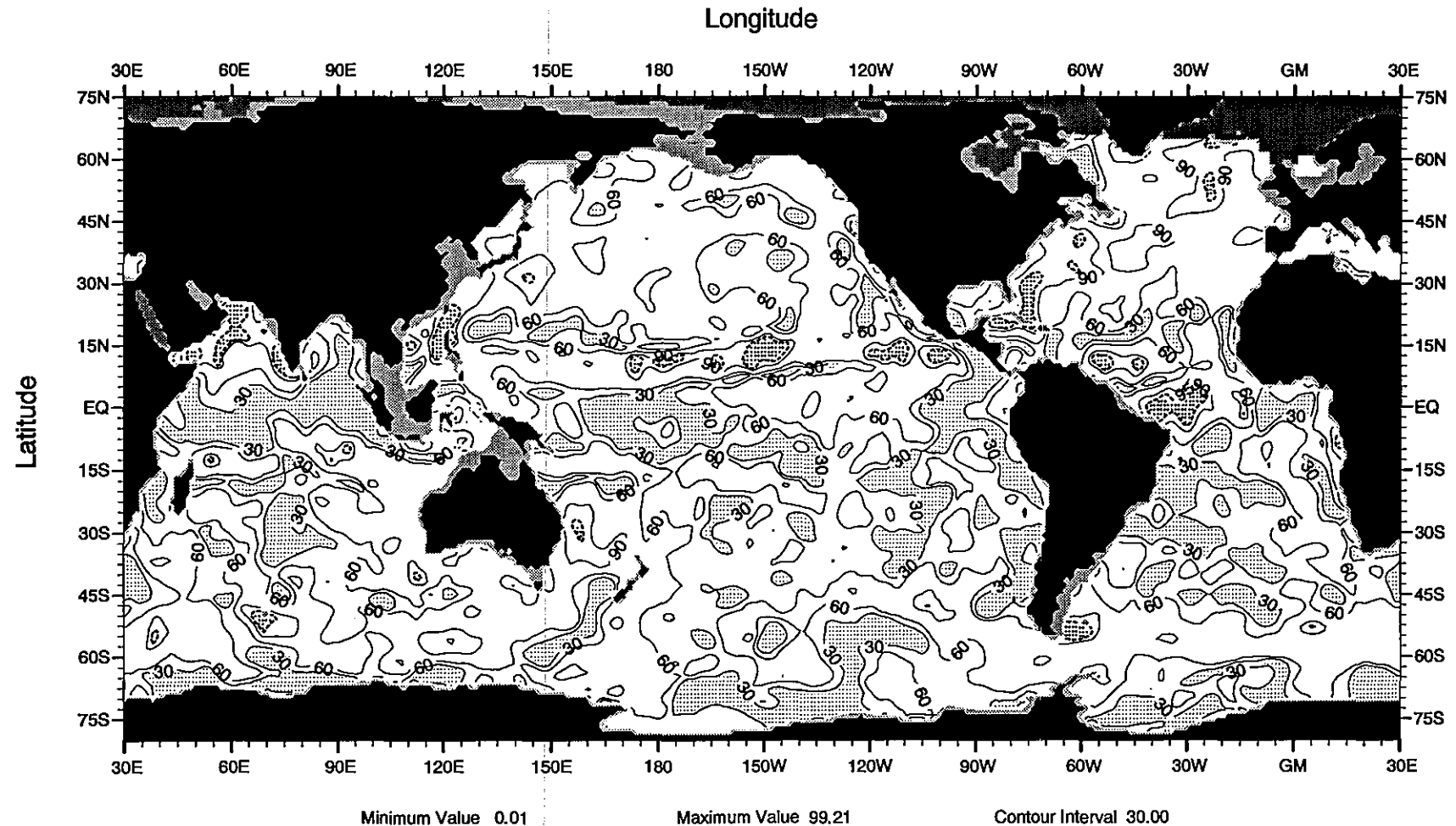


Fig. B20 Percent variance explained by 1st harmonic of the annual temperature cycle at 100 m depth

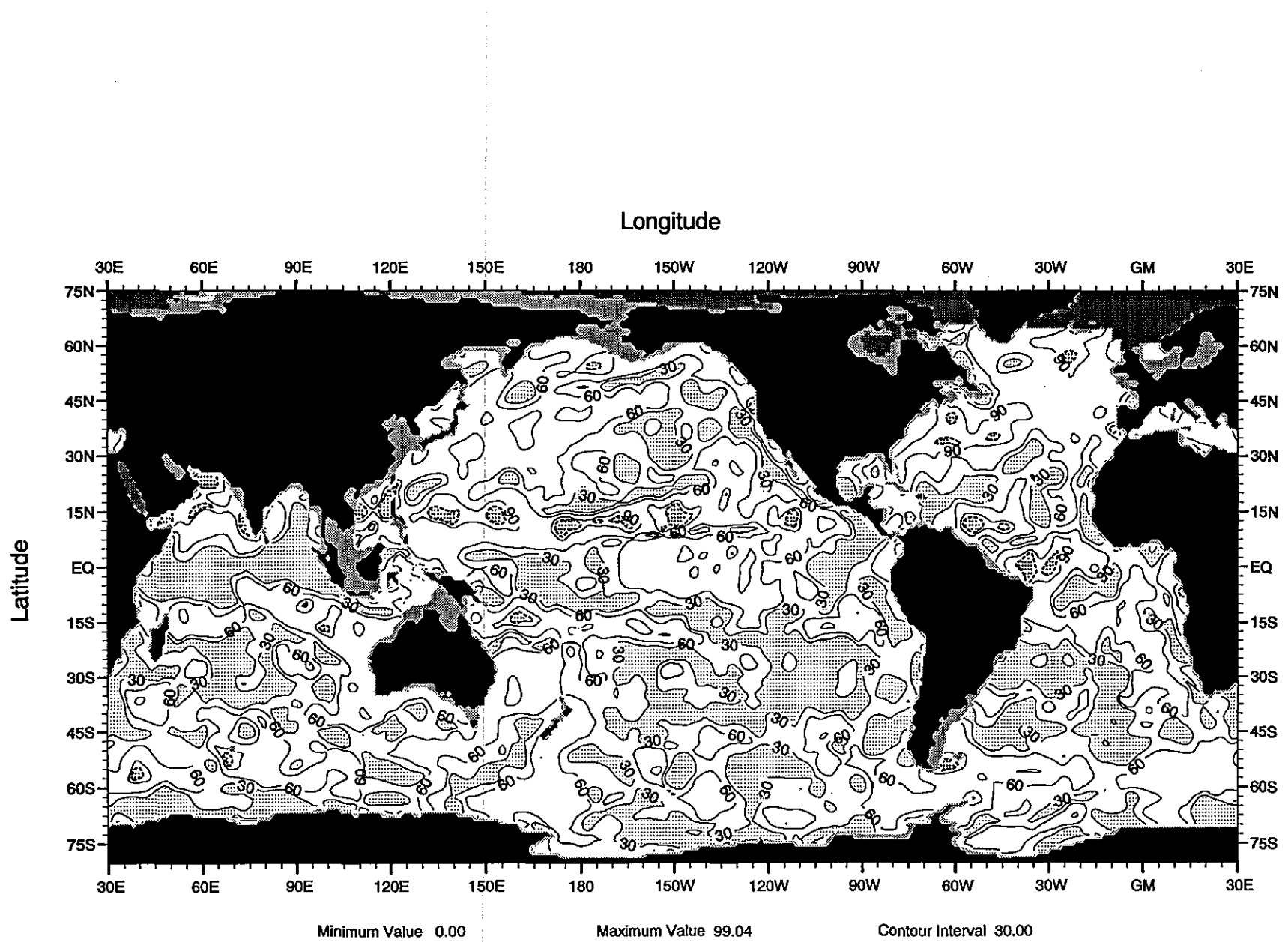


Fig. B21 Percent variance explained by 1st harmonic of the annual temperature cycle at 125 m depth

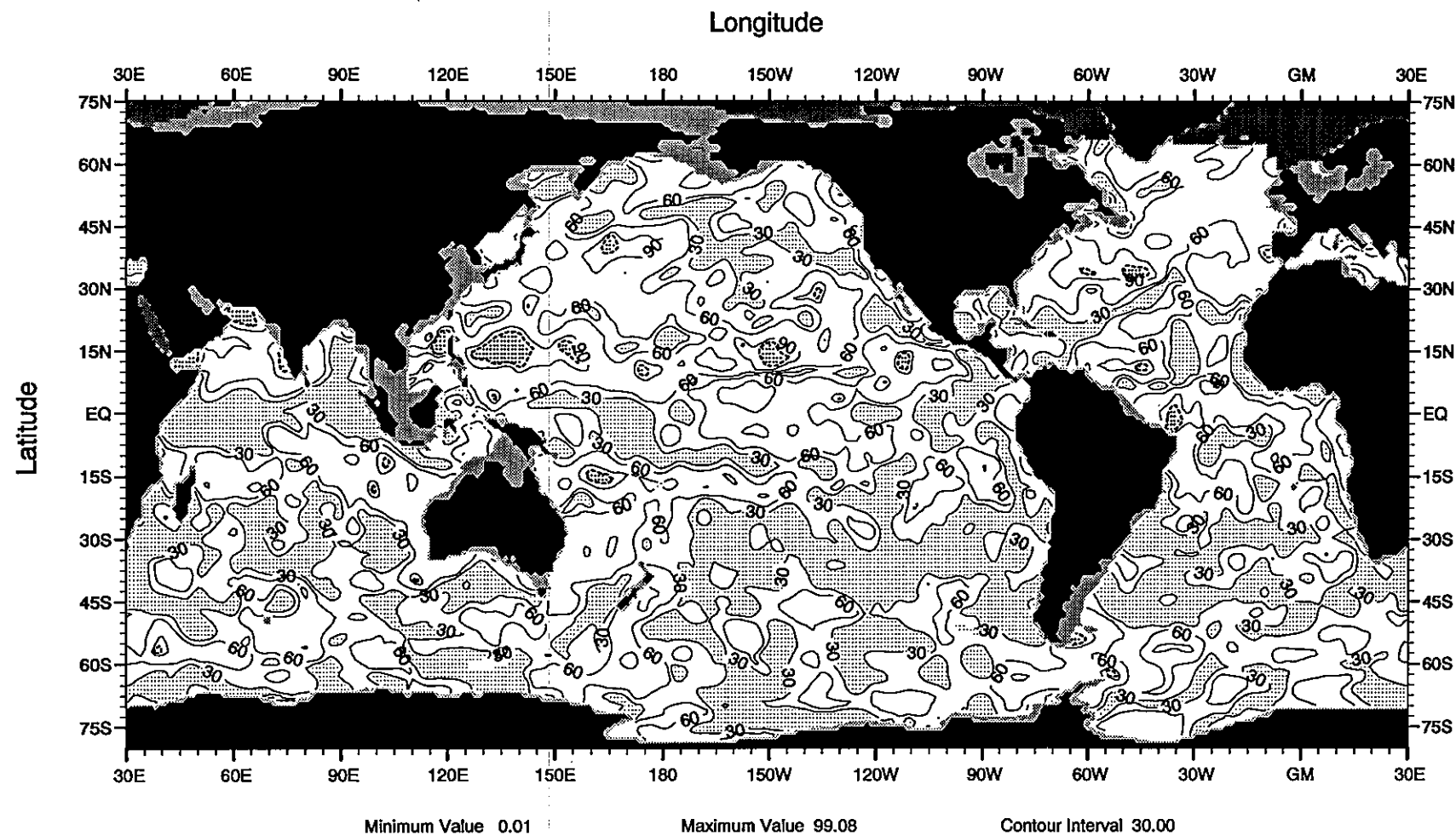


Fig. B22 Percent variance explained by 1st harmonic of the annual temperature cycle at 150 m depth

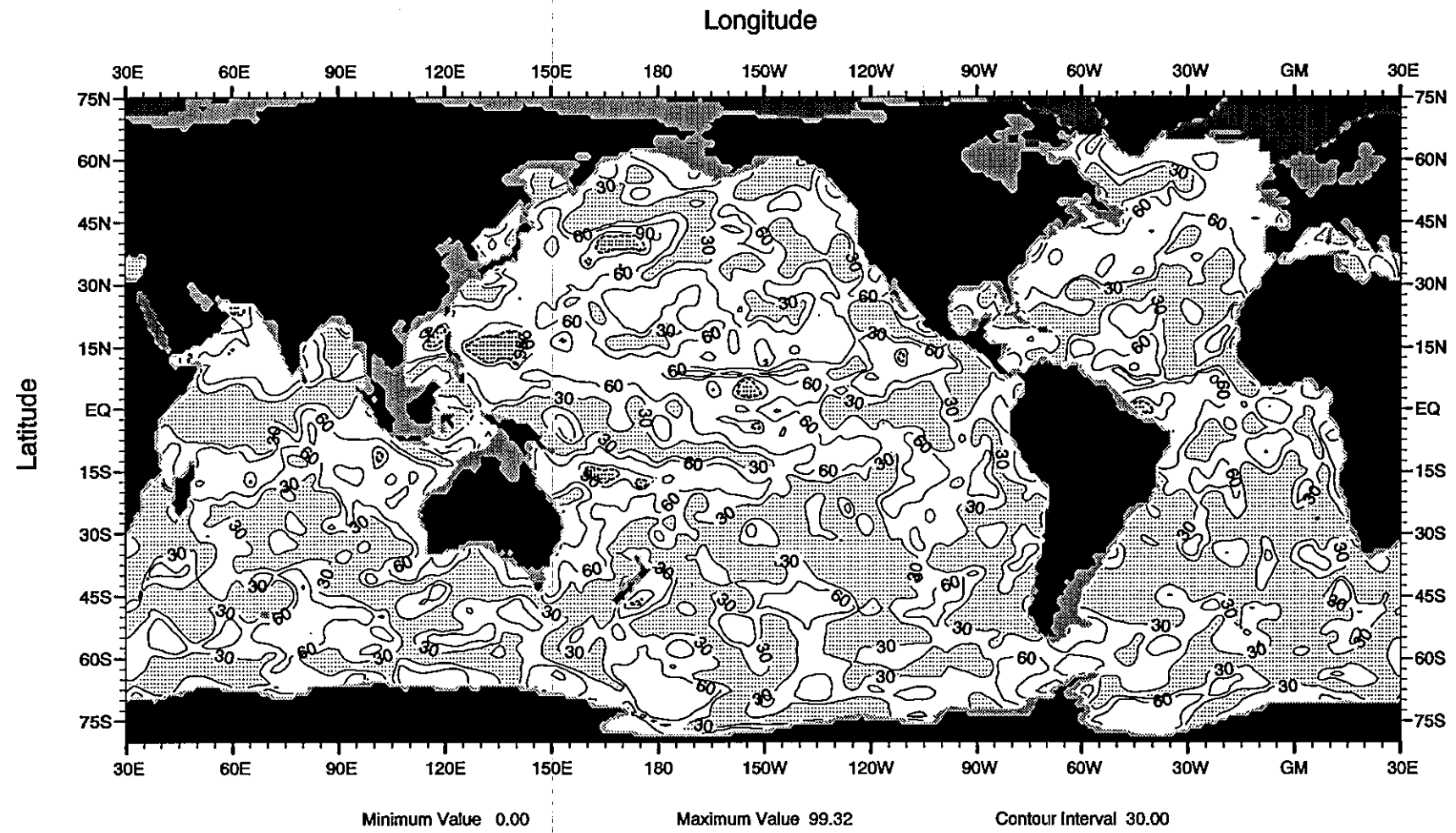


Fig. B23 Percent variance explained by 1st harmonic of the annual temperature cycle at 200 m depth

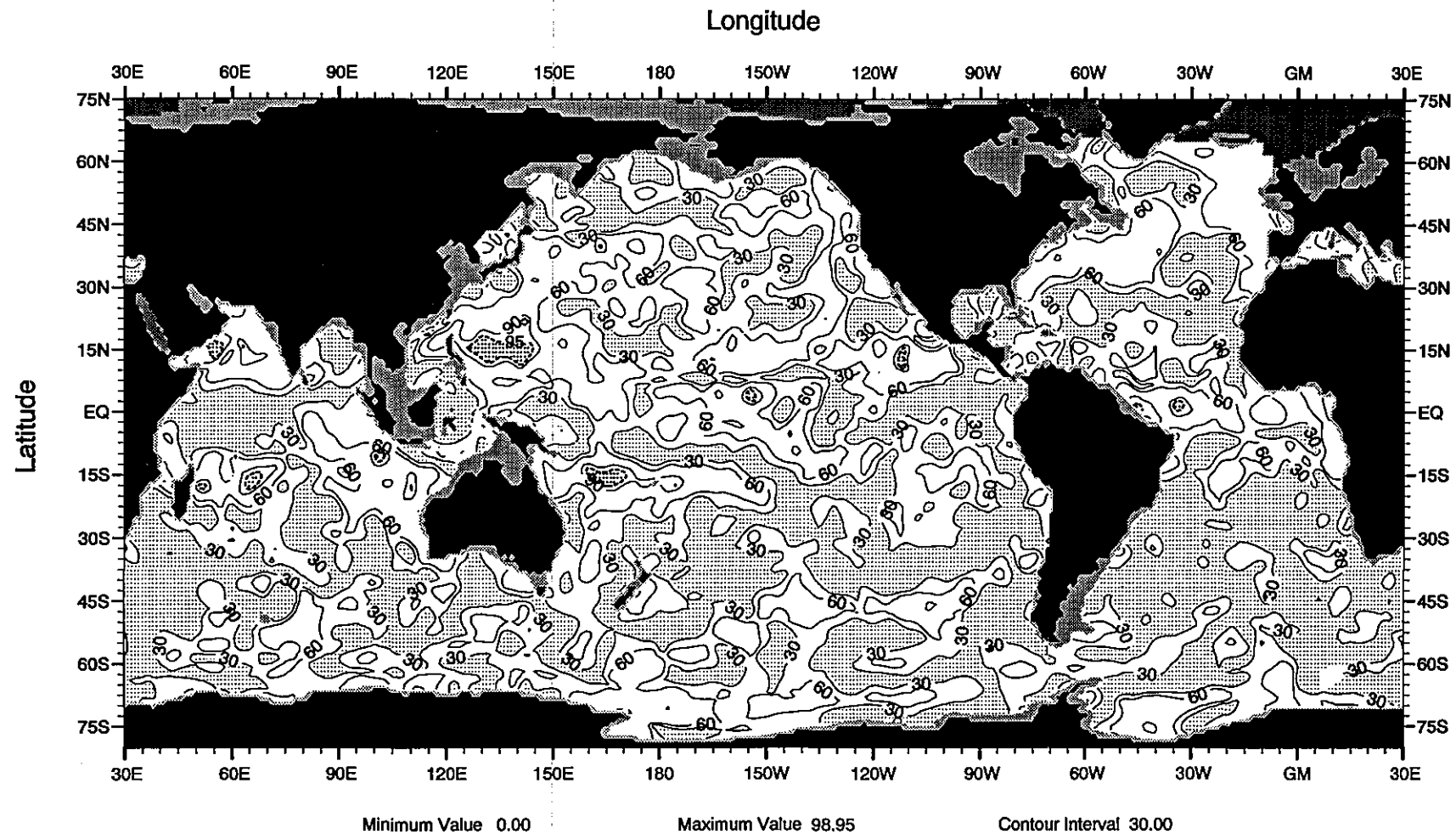


Fig. B24 Percent variance explained by 1st harmonic of the annual temperature cycle at 250 m depth

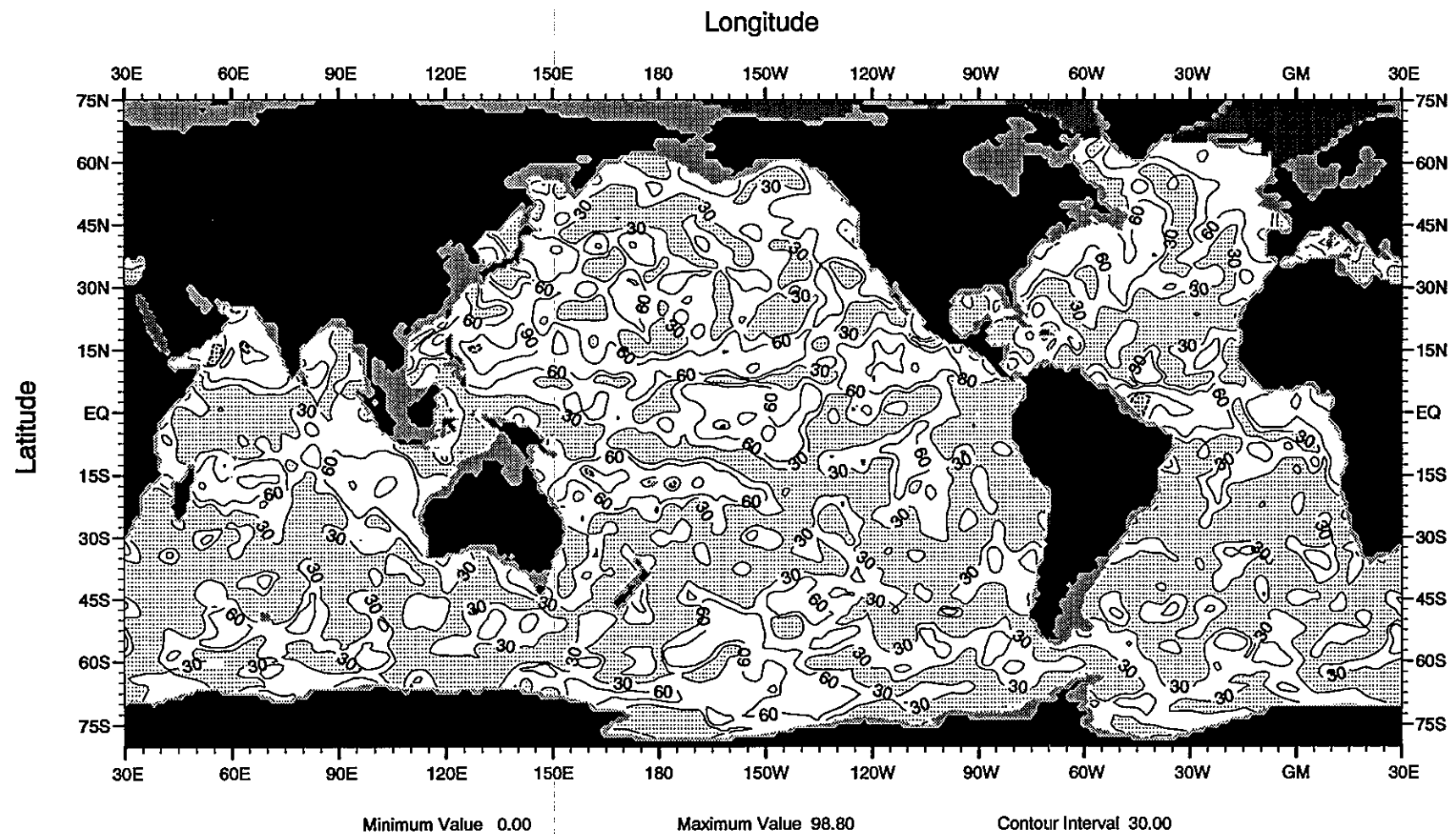


Fig. B25 Percent variance explained by 1st harmonic of the annual temperature cycle at 300 m depth

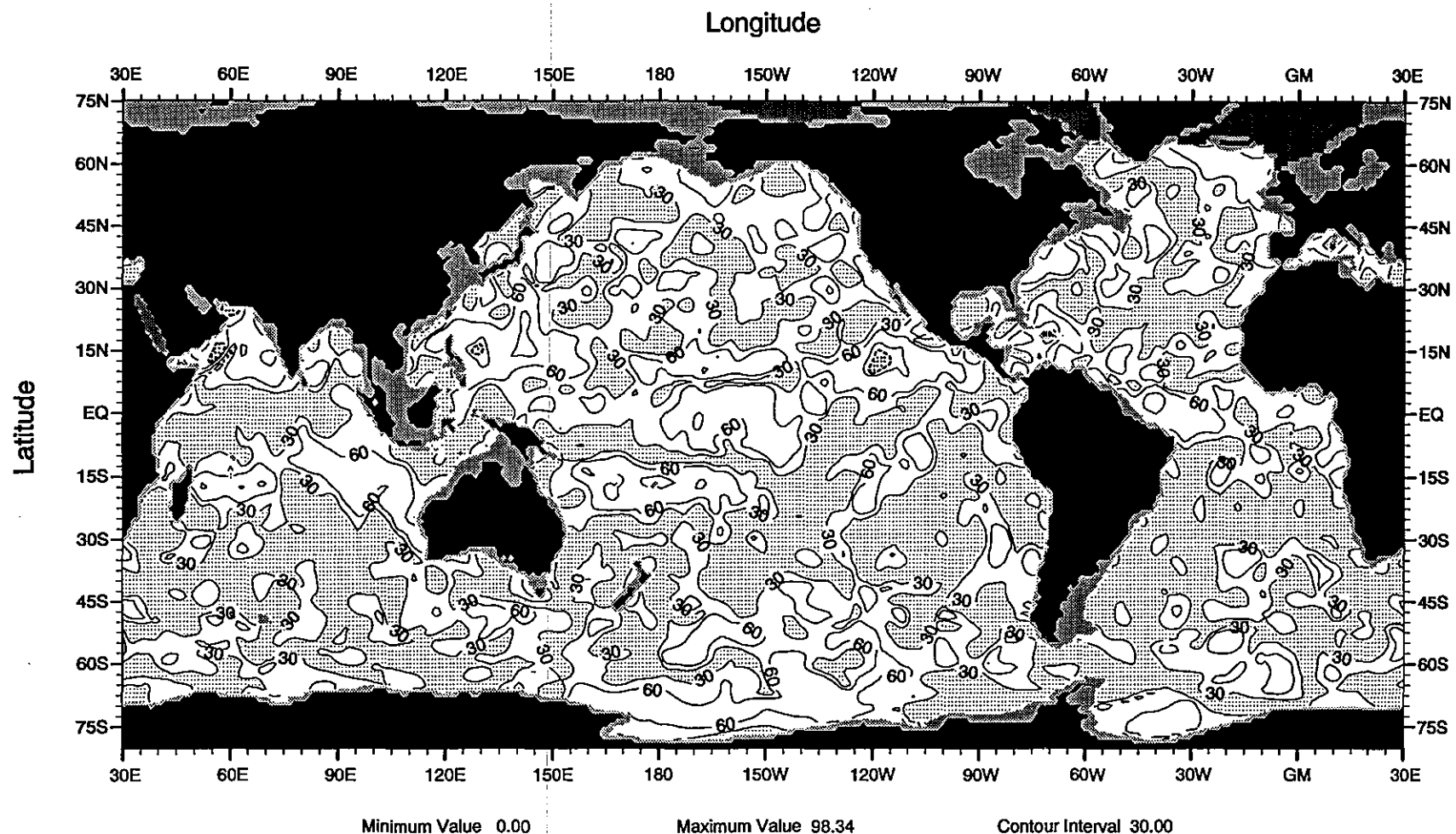


Fig. B26 Percent variance explained by 1st harmonic of the annual temperature cycle at 400 m depth

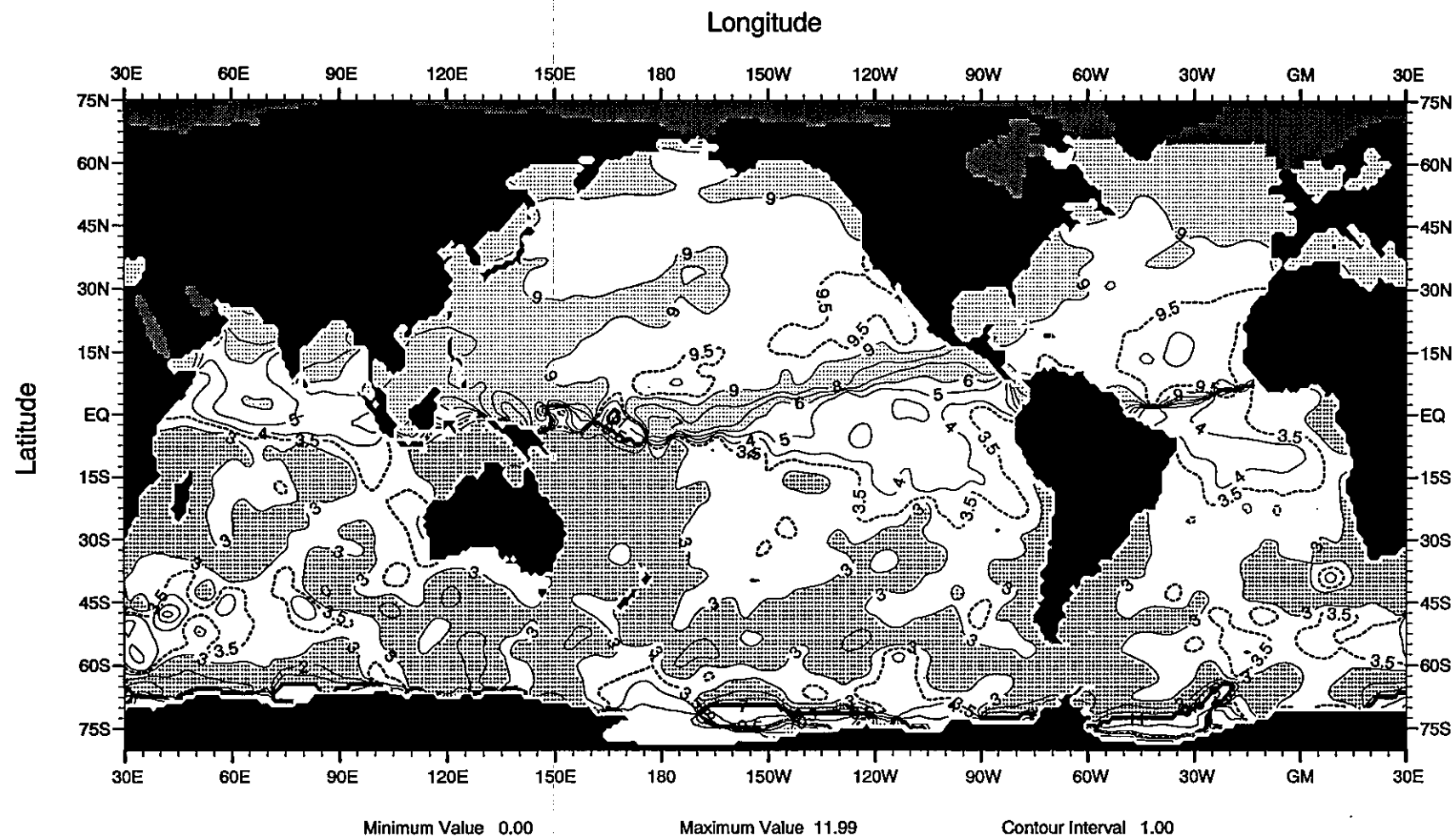


Fig. B27 Phase (months) of the 1st harmonic of the annual temperature cycle at the sea surface

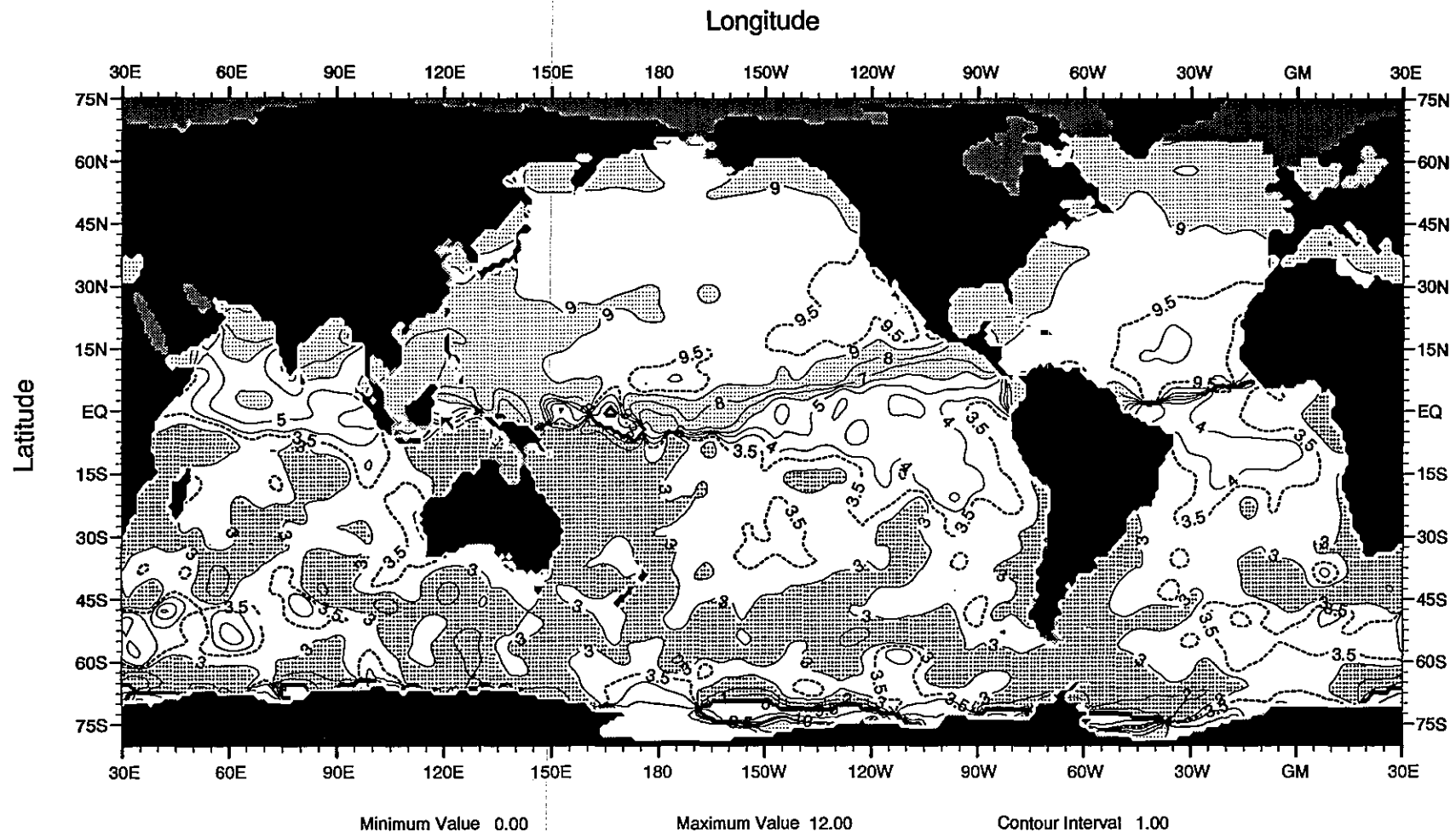


Fig. B28 Phase (months) of the 1st harmonic of the annual temperature cycle at 10 m depth

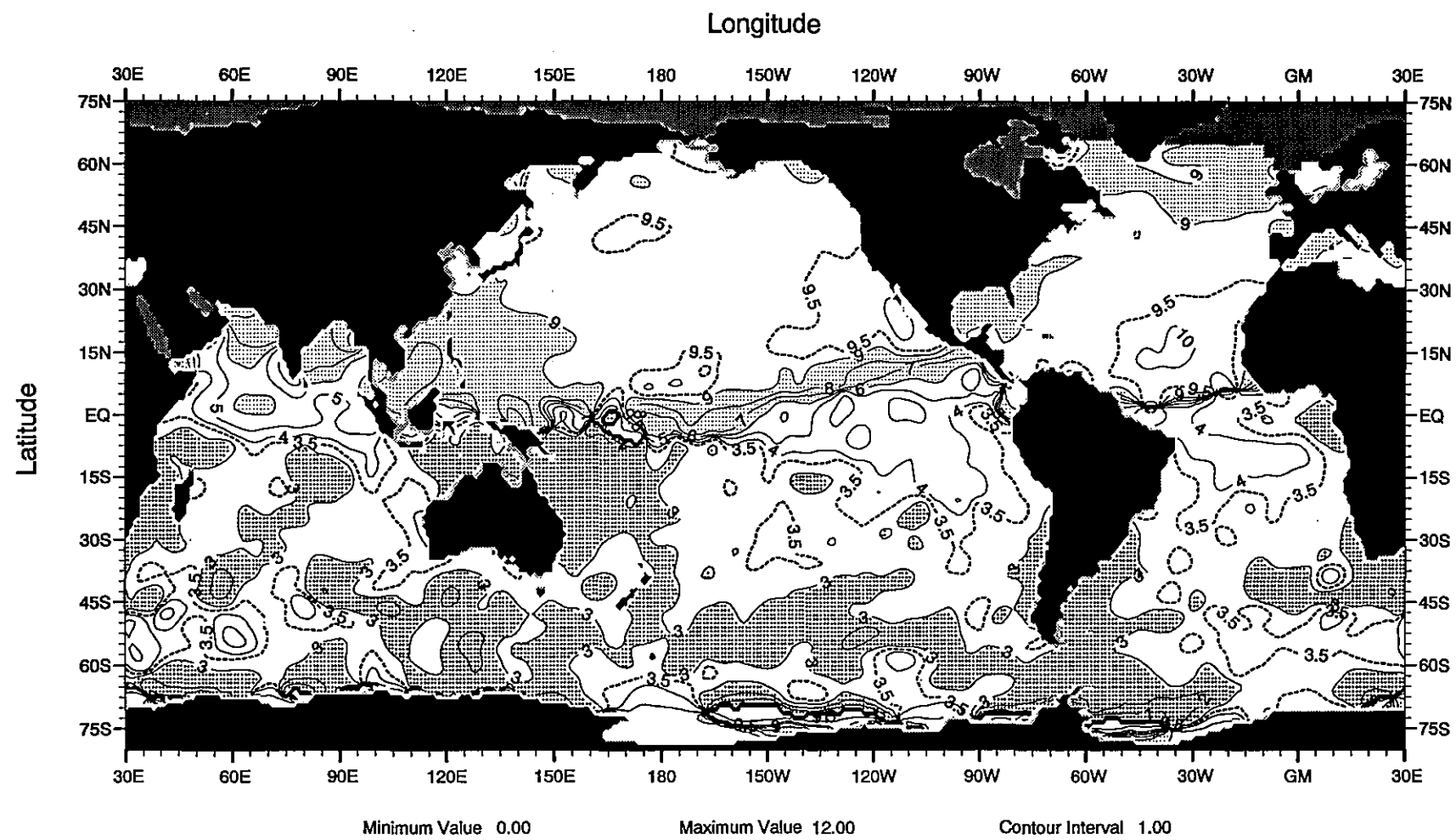


Fig. B29 Phase (months) of the 1st harmonic of the annual temperature cycle at 20 m depth

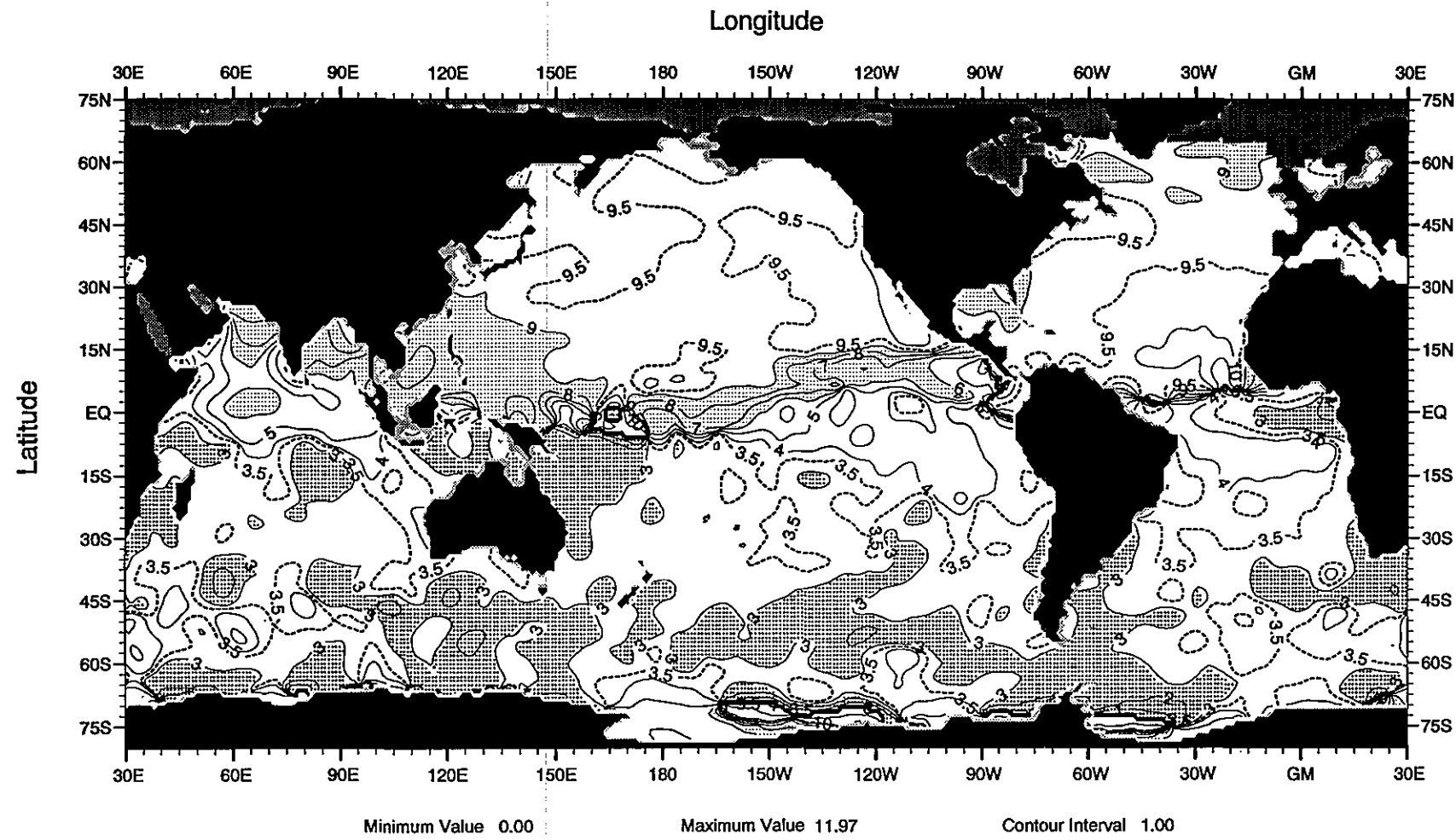


Fig. B30 Phase (months) of the 1st harmonic of the annual temperature cycle at 30 m depth

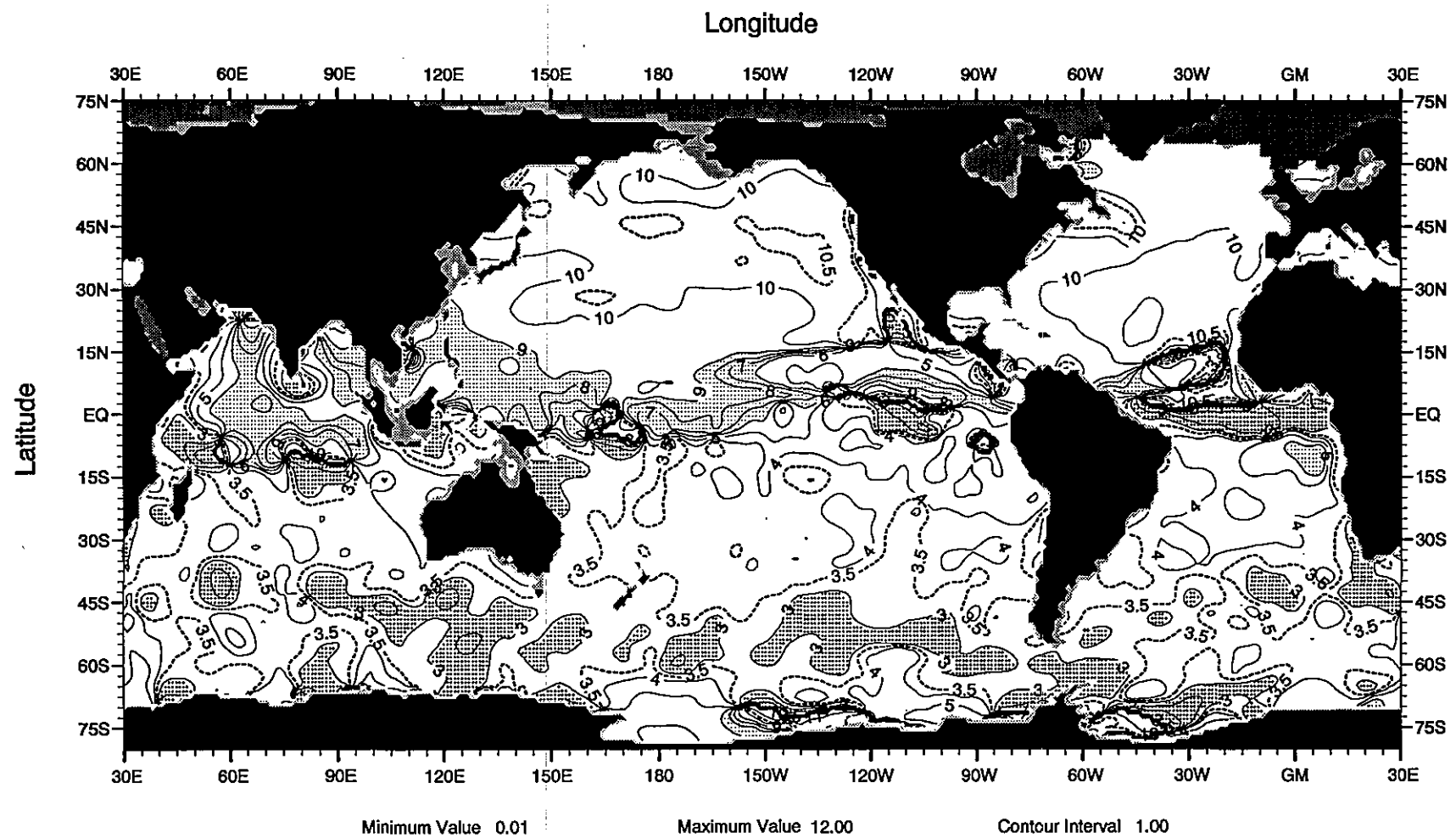


Fig. B31 Phase (months) of the 1st harmonic of the annual temperature cycle at 50 m depth

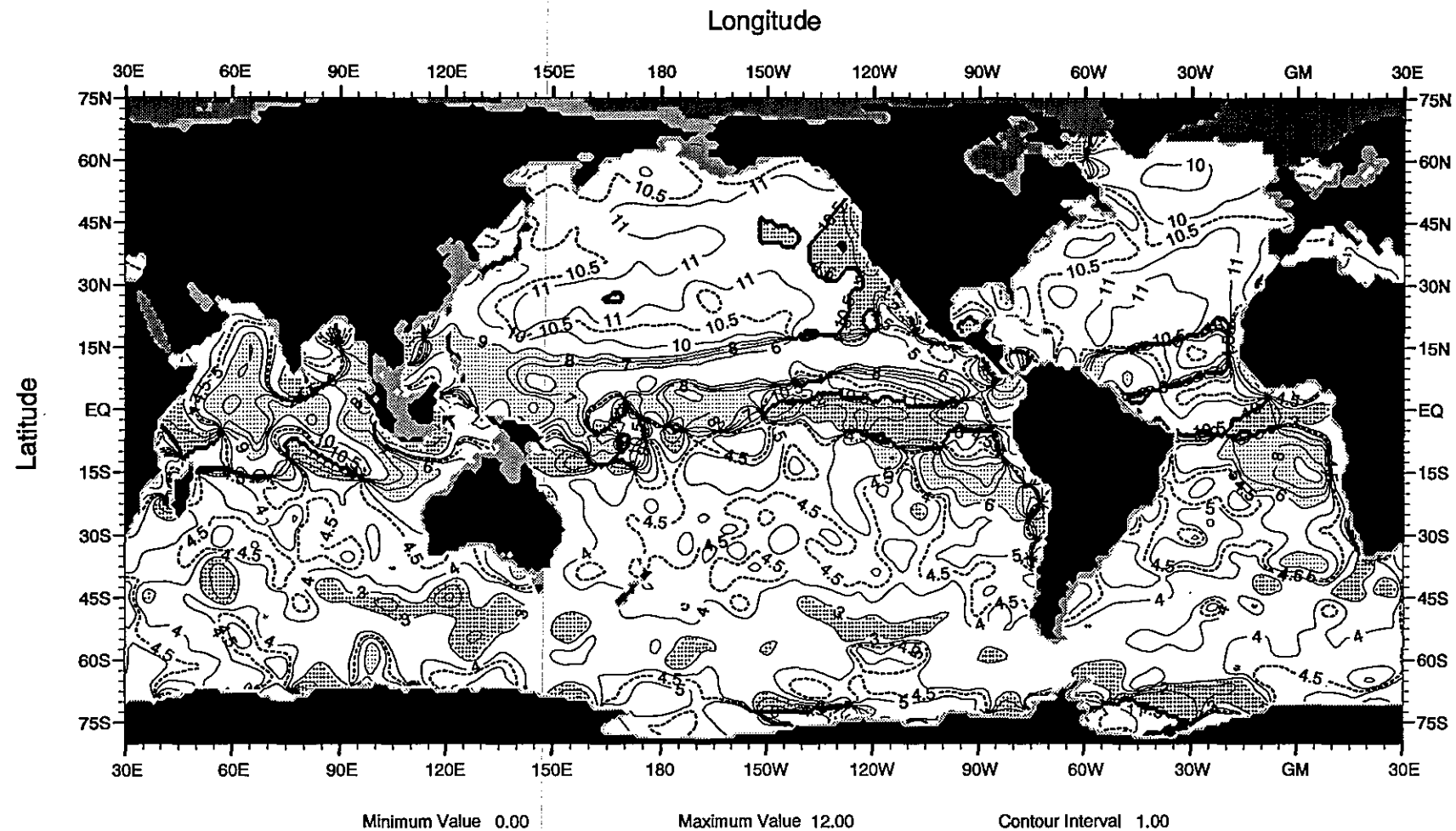


Fig. B32 Phase (months) of the 1st harmonic of the annual temperature cycle at 75 m depth

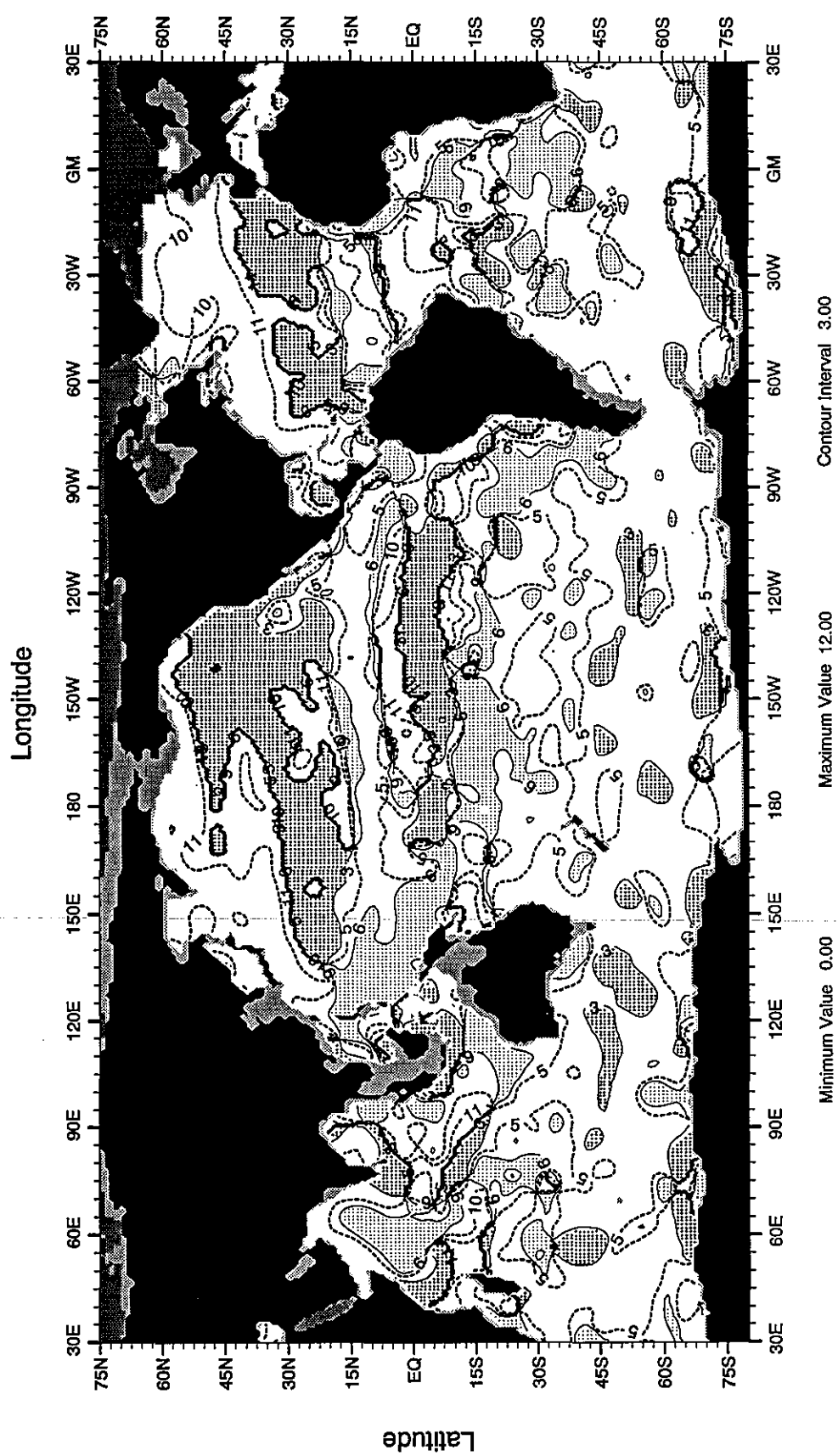


Fig. B33 Phase (months) of the 1st harmonic of the annual temperature cycle at 100 m depth

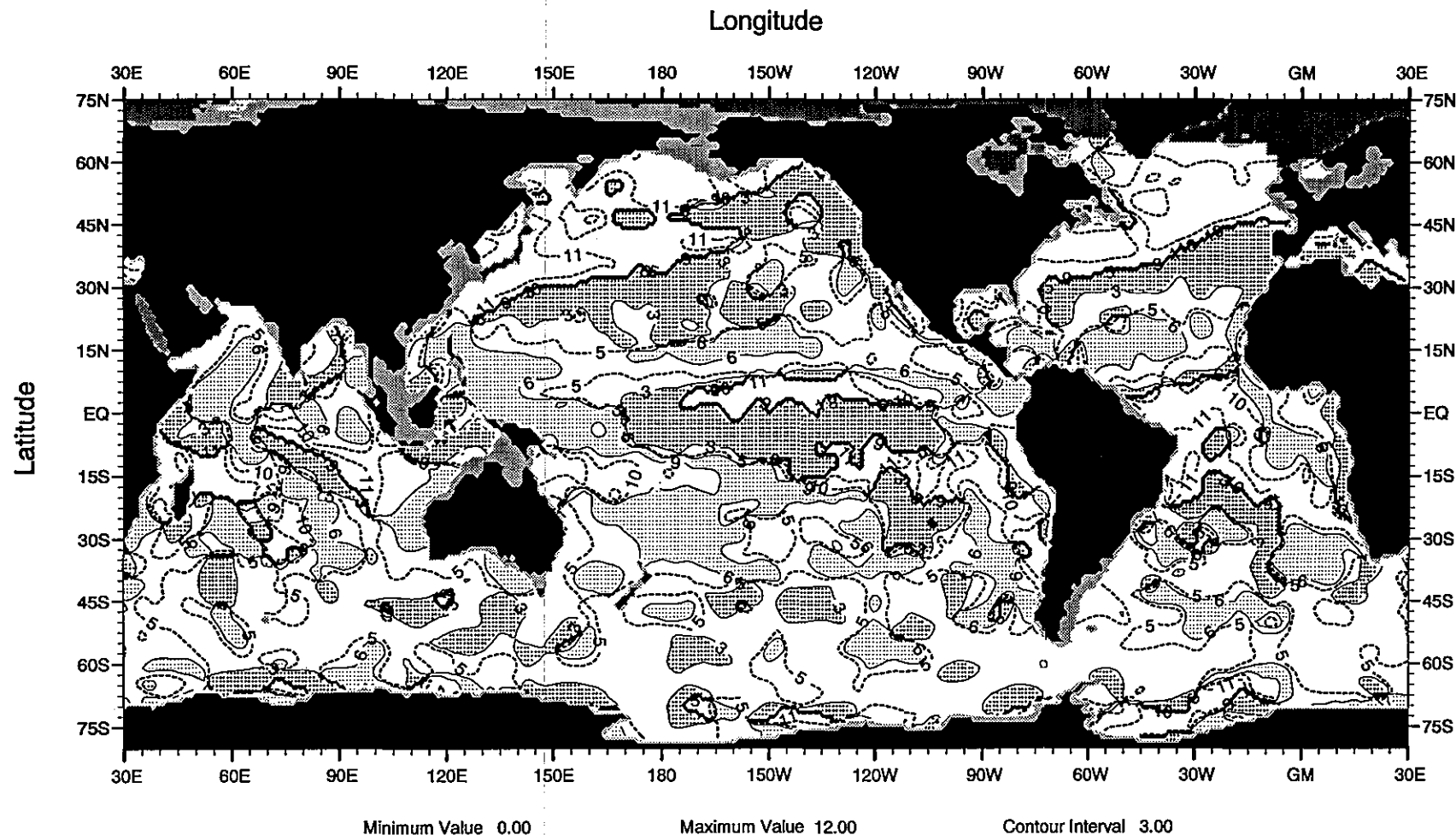


Fig. B34 Phase (months) of the 1st harmonic of the annual temperature cycle at 125 m depth

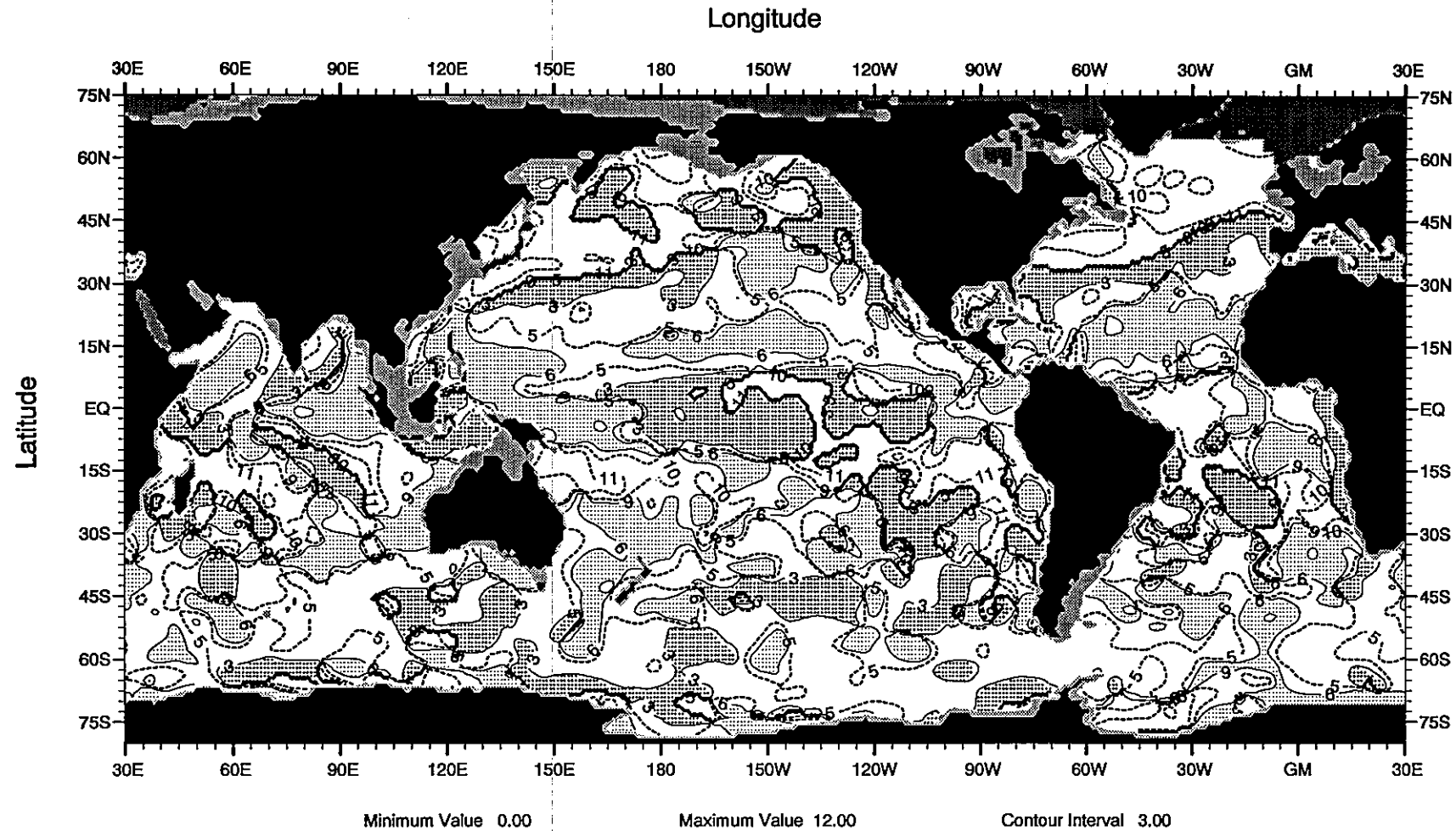


Fig. B35 Phase (months) of the 1st harmonic of the annual temperature cycle at 150 m depth

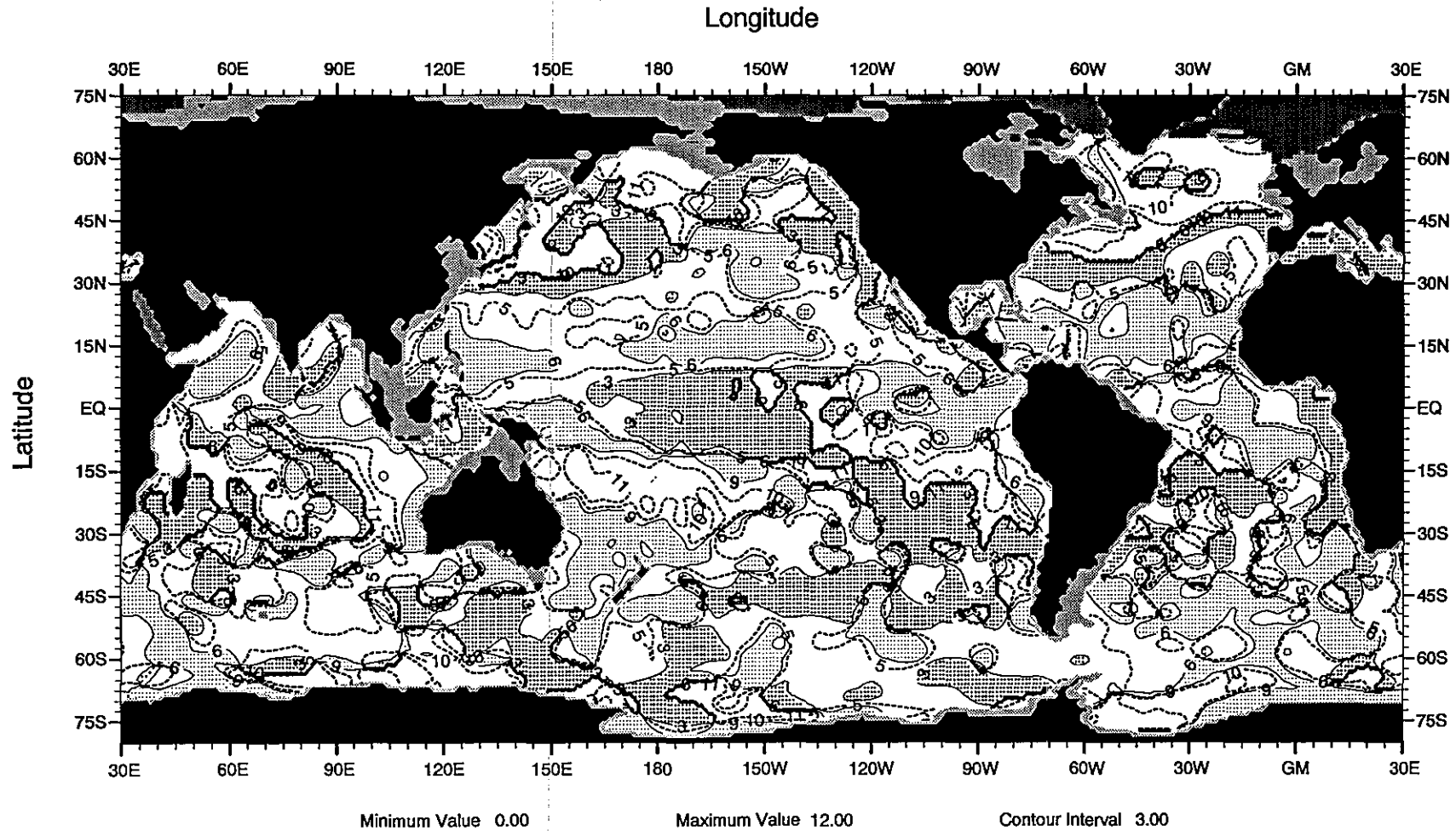


Fig. B36 Phase (months) of the 1st harmonic of the annual temperature cycle at 200 m depth

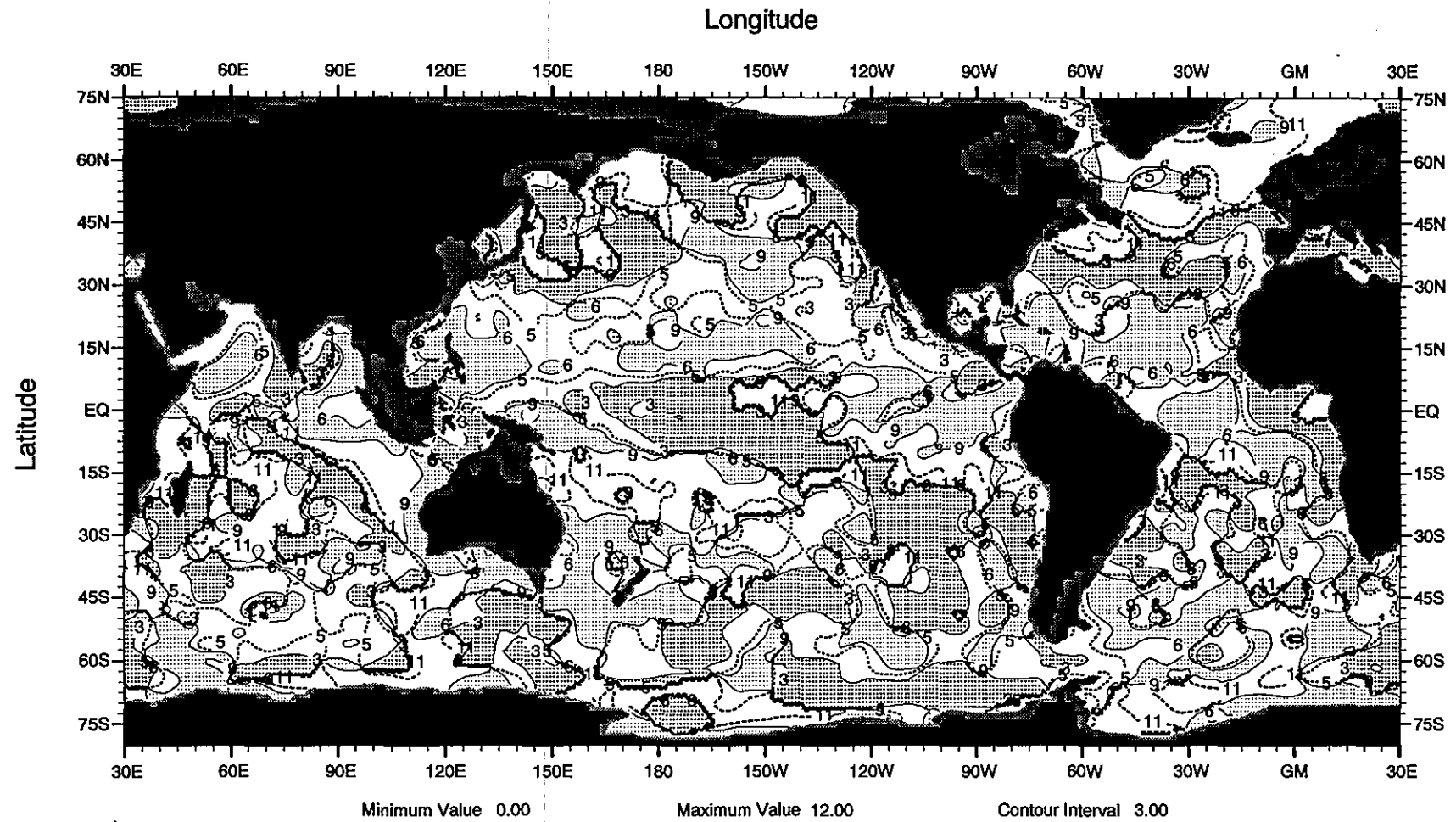


Fig.B37 Phase (months) of the 1st harmonic of the annual temperature cycle at 250 m depth

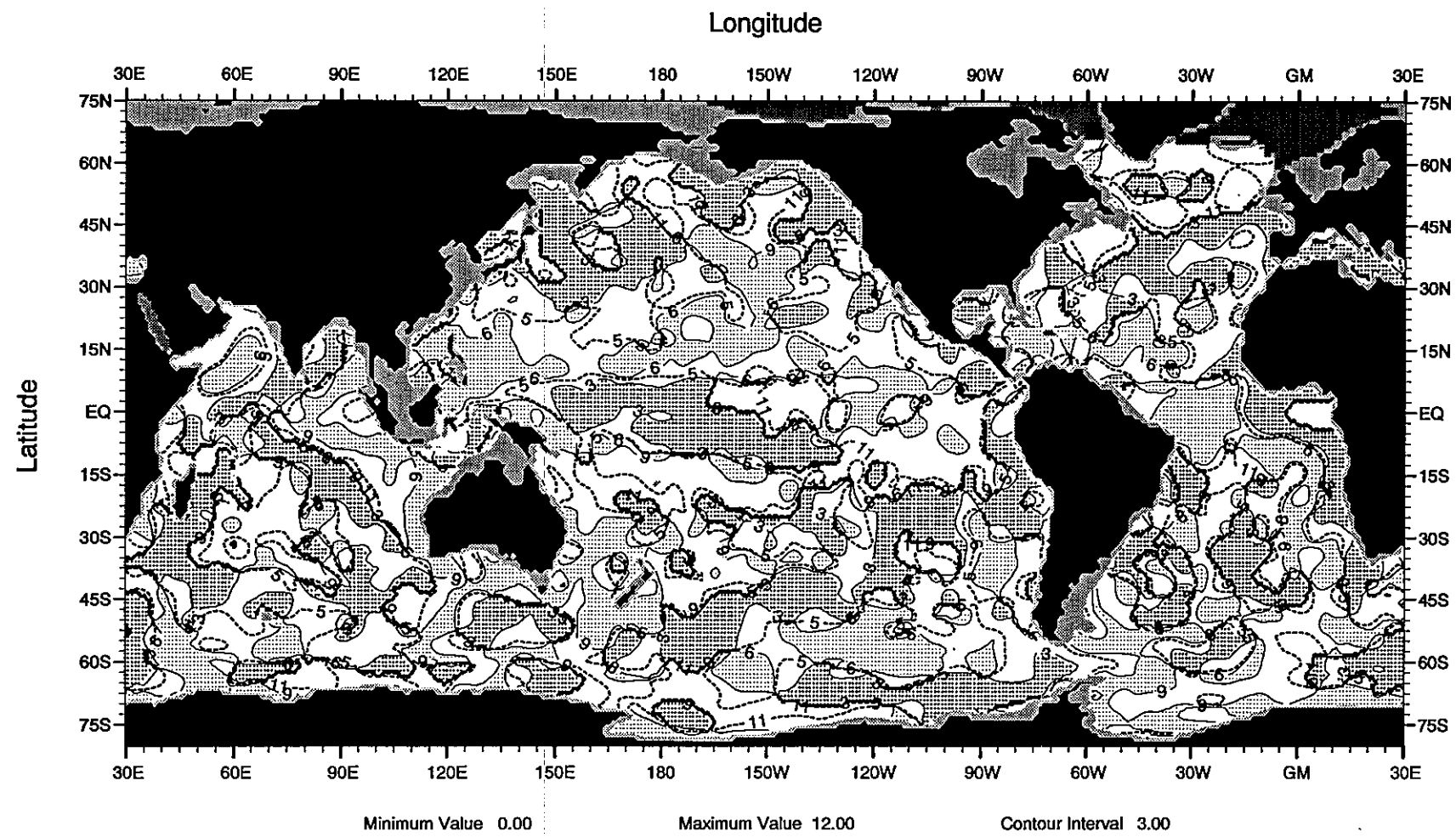


Fig. B38 Phase (months) of the 1st harmonic of the annual temperature cycle at 300 m depth

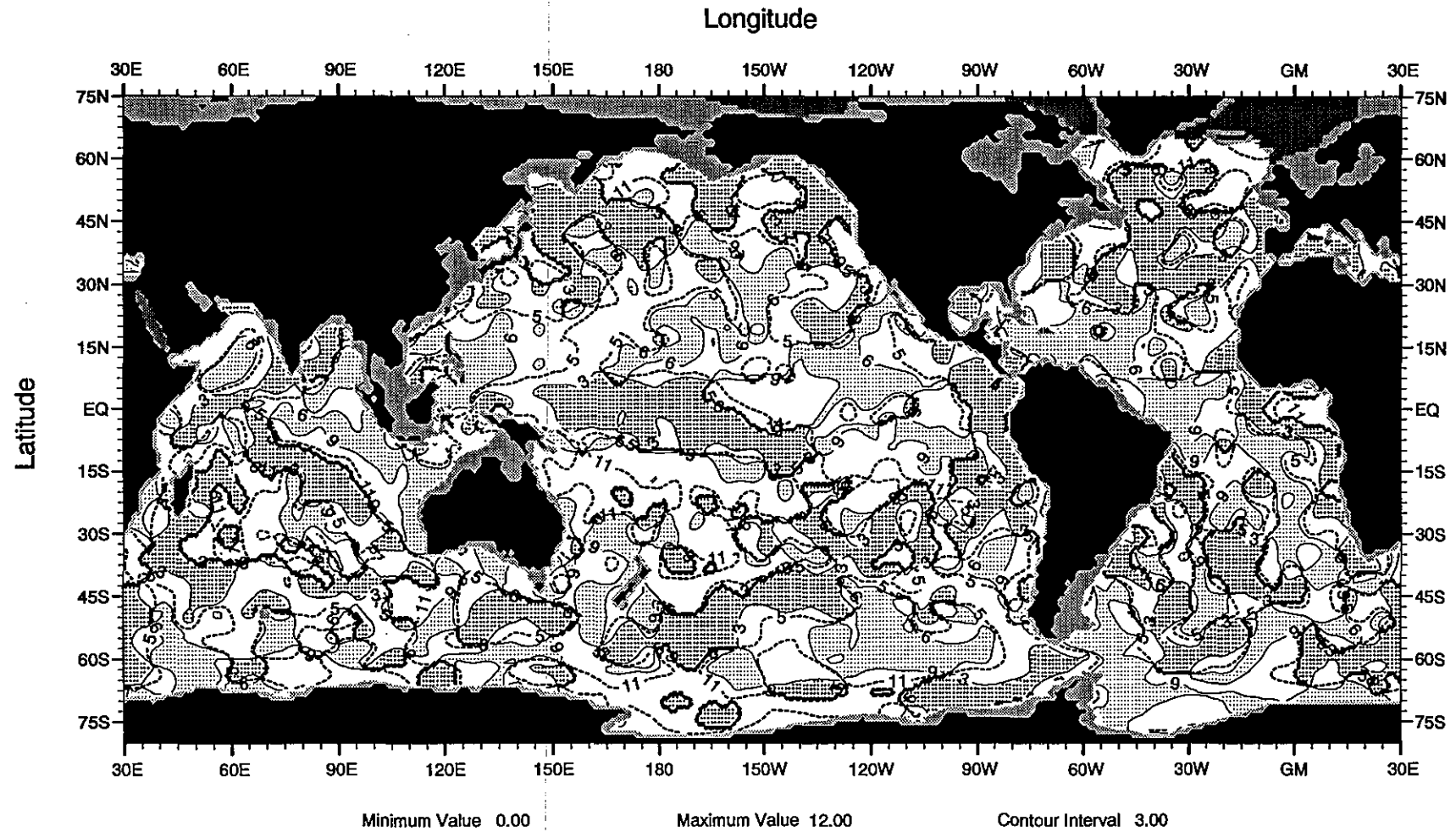


Fig. B39 Phase (months) of the 1st harmonic of the annual temperature cycle at 400 m depth

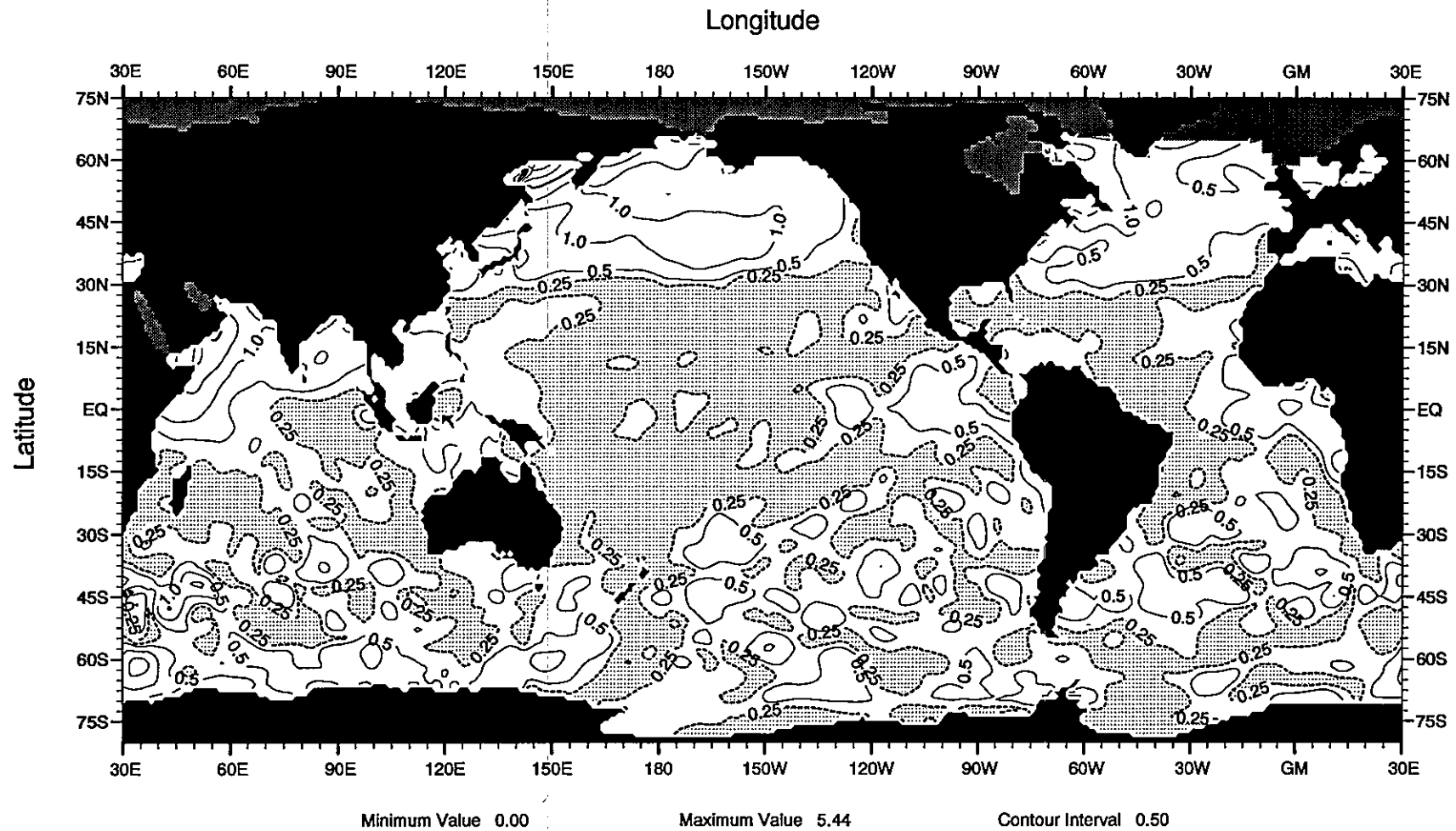


Fig. B40 Amplitude (°C) of the 2nd harmonic of the annual temperature cycle at the sea surface

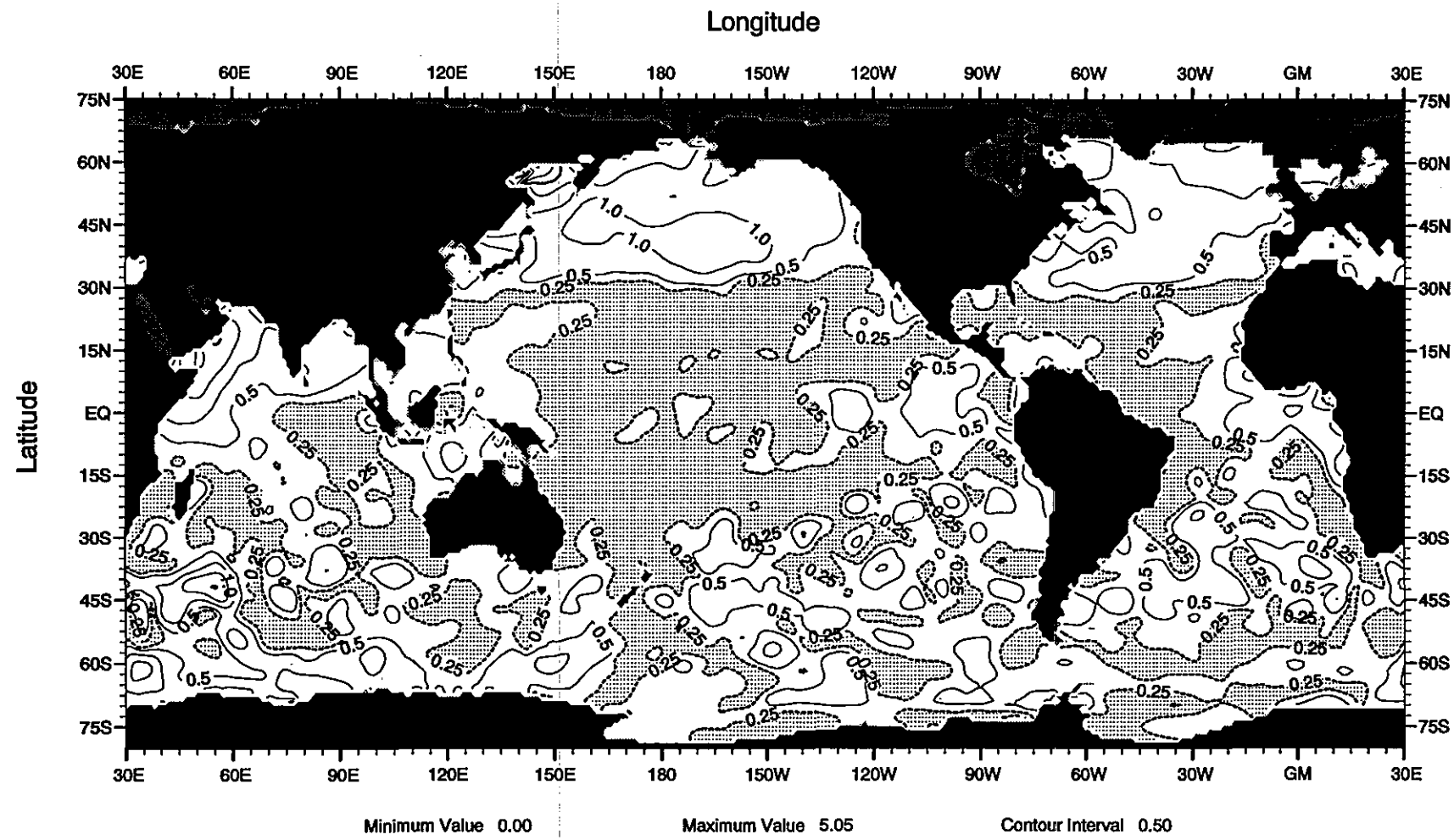


Fig. B41 Amplitude (°C) of the 2nd harmonic of the annual temperature cycle at 10 m depth

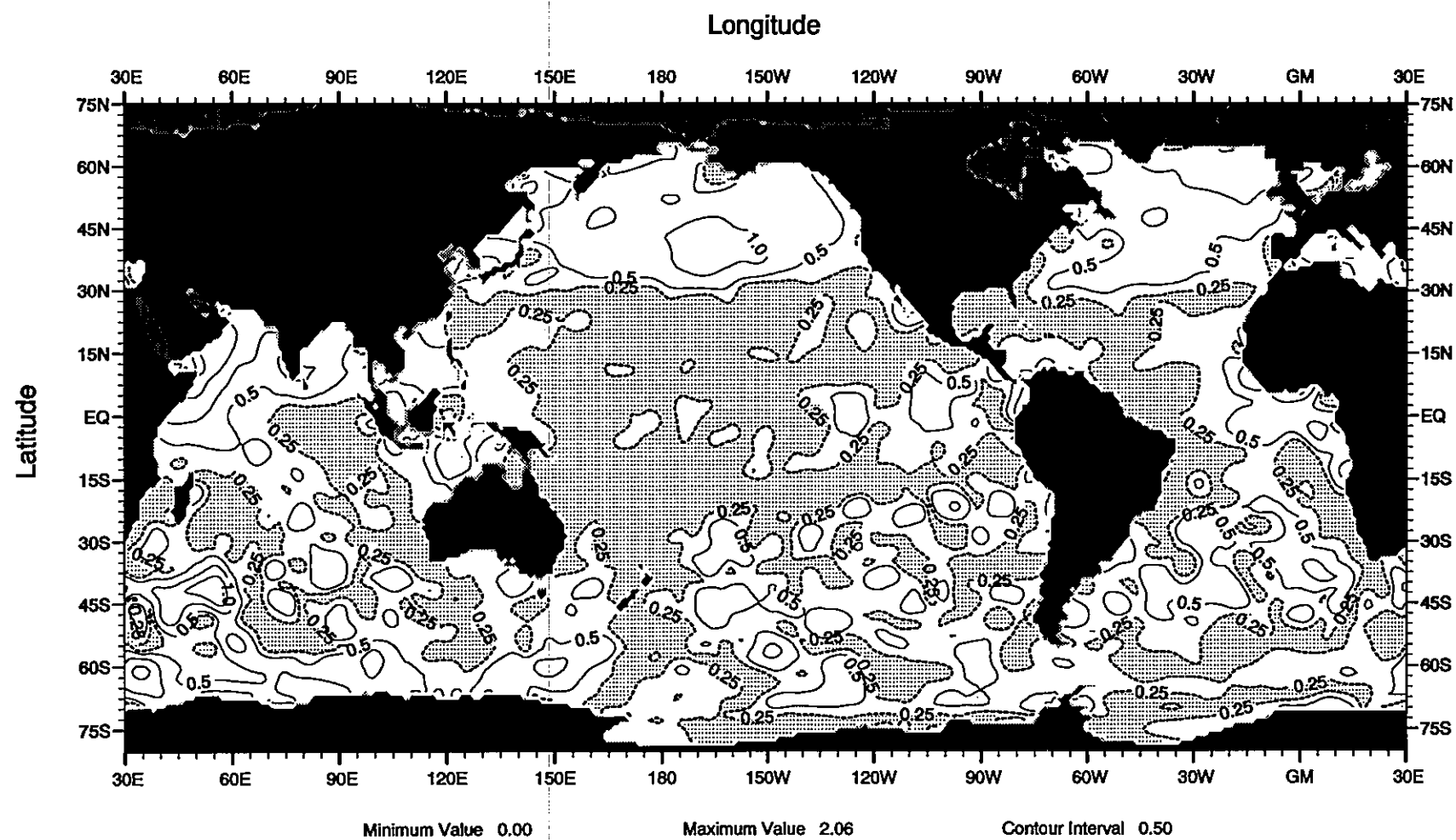


Fig. B42 Amplitude (°C) of the 2nd harmonic of the annual temperature cycle at 20 m depth

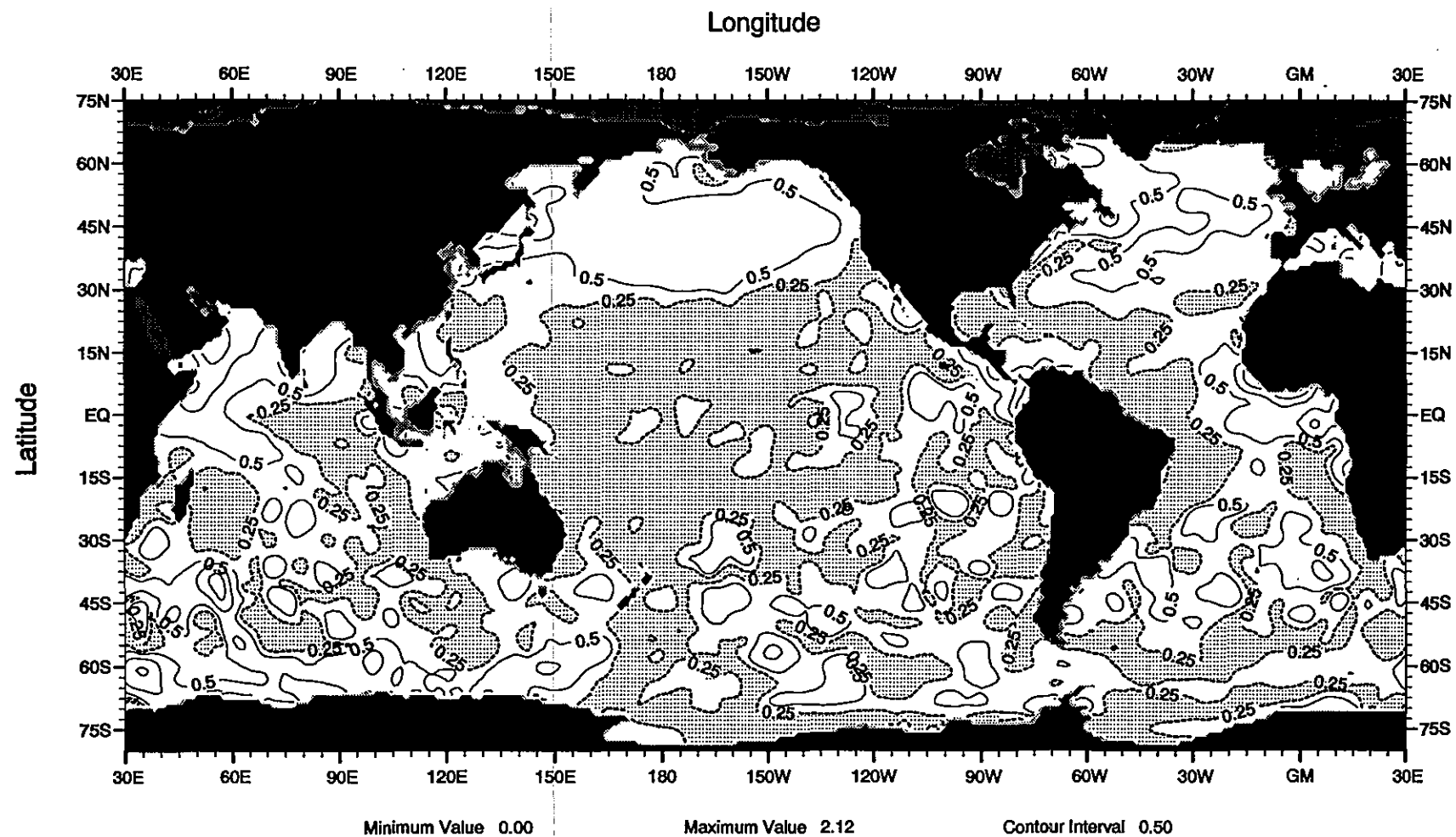


Fig. B43 Amplitude (°C) of the 2nd harmonic of the annual temperature cycle at 30 m depth

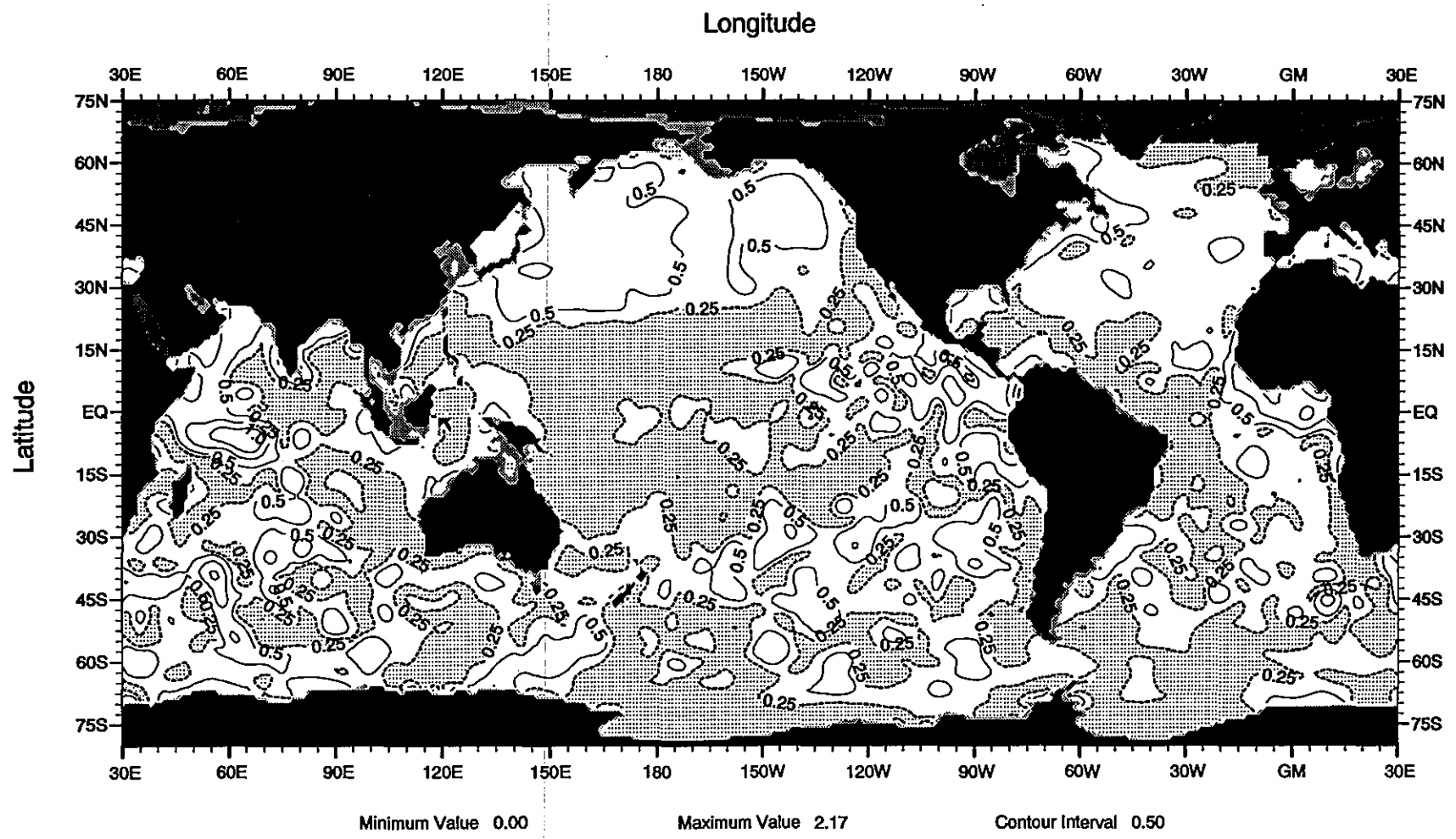


Fig. B44 Amplitude (°C) of the 2nd harmonic of the annual temperature cycle at 50 m depth

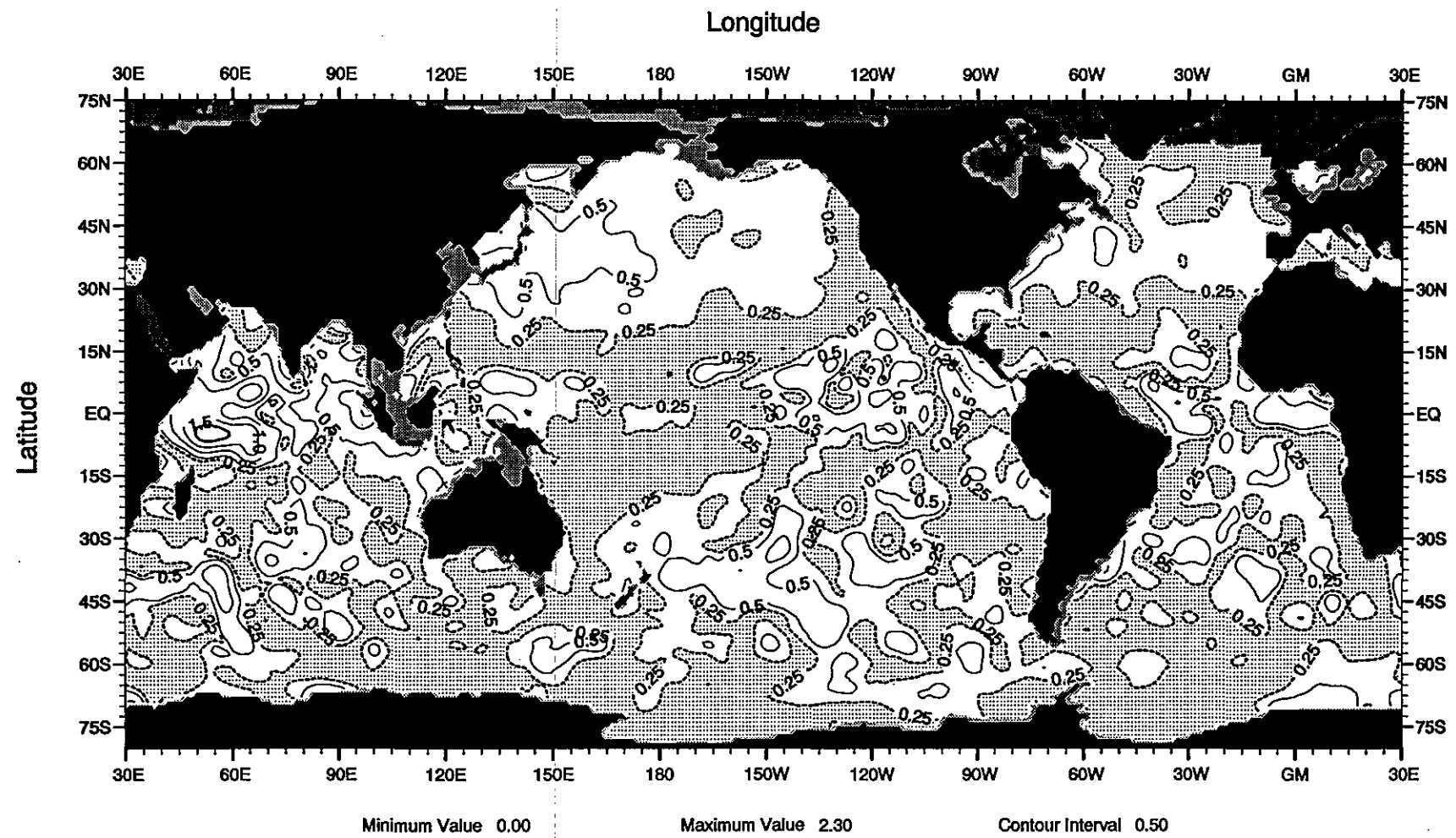


Fig. B45 Amplitude (°C) of the 2nd harmonic of the annual temperature cycle at 75 m depth

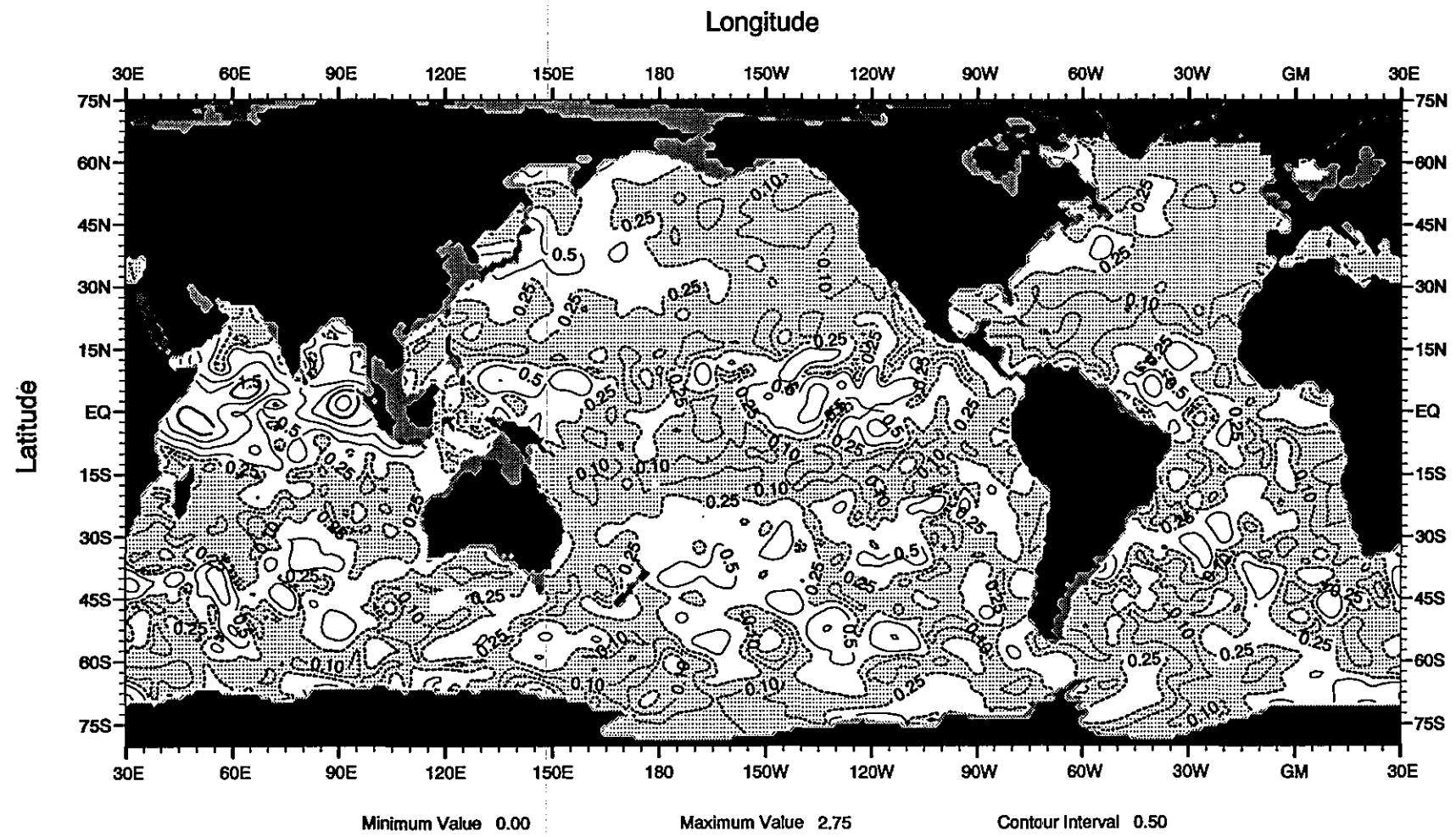


Fig. B46 Amplitude (°C) of the 2nd harmonic of the annual temperature cycle at 100 m depth

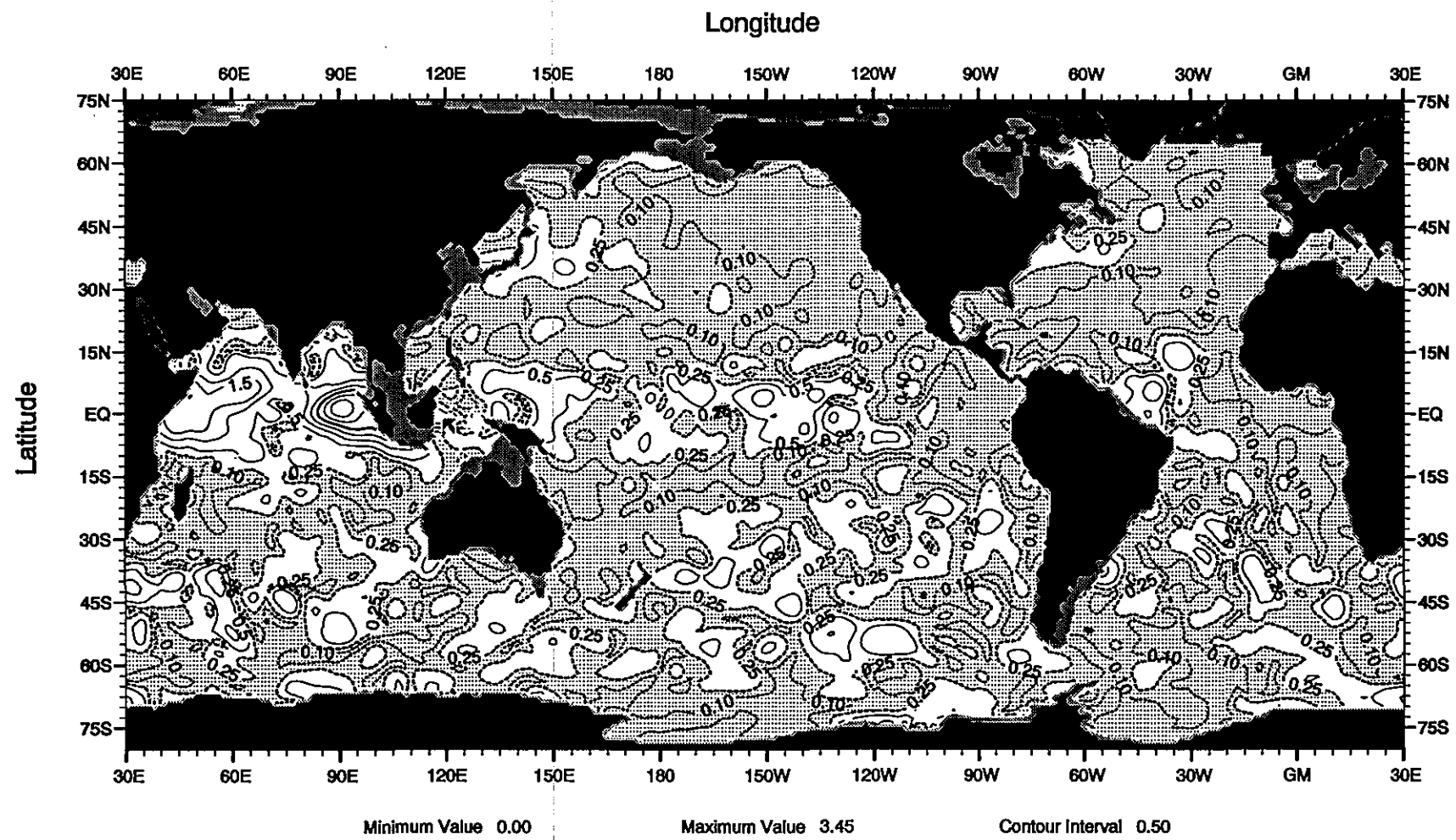


Fig. B47 Amplitude (°C) of the 2nd harmonic of the annual temperature cycle at 125 m depth

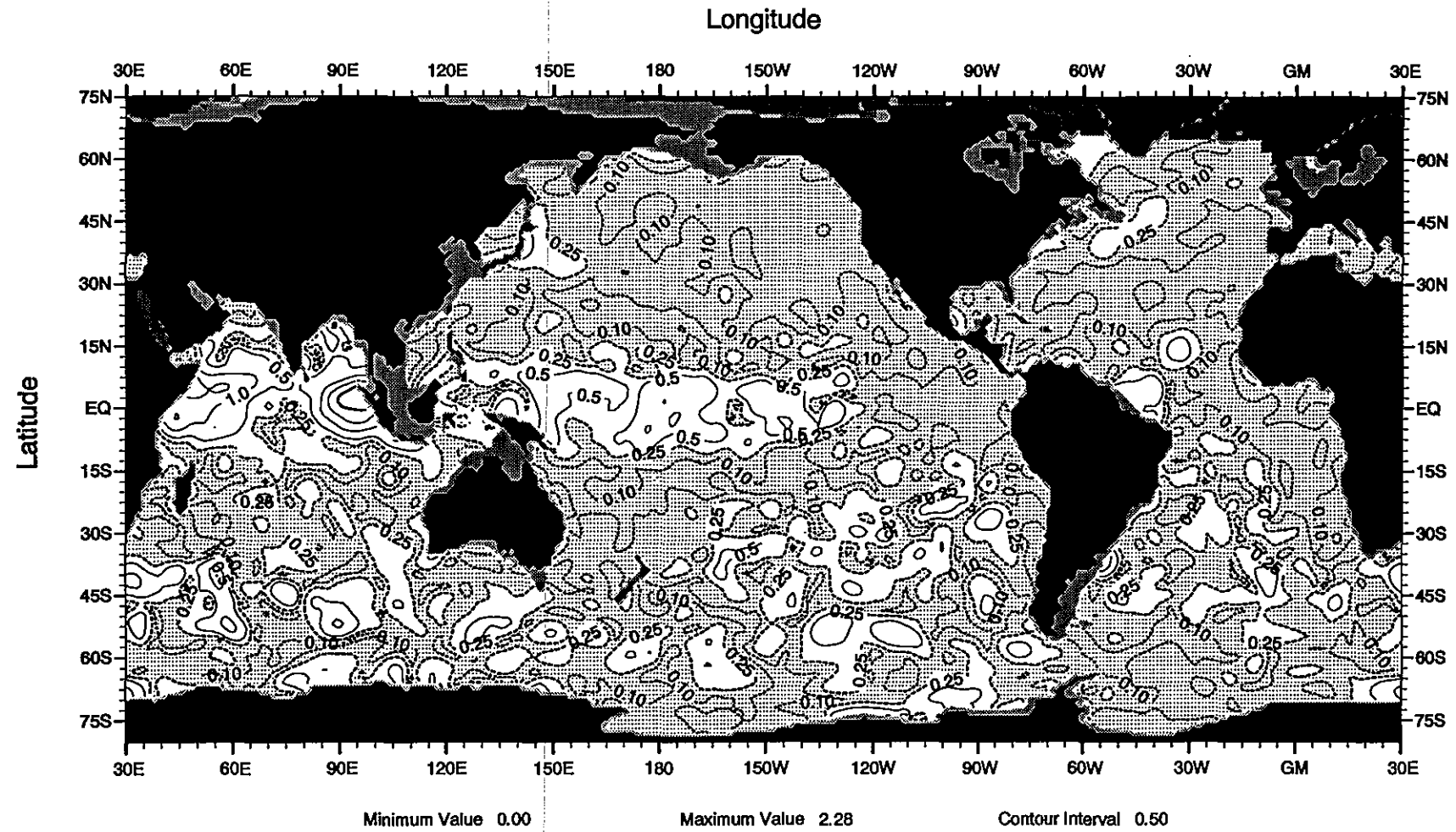


Fig. B48 Amplitude (°C) of the 2nd harmonic of the annual temperature cycle at 150 m depth

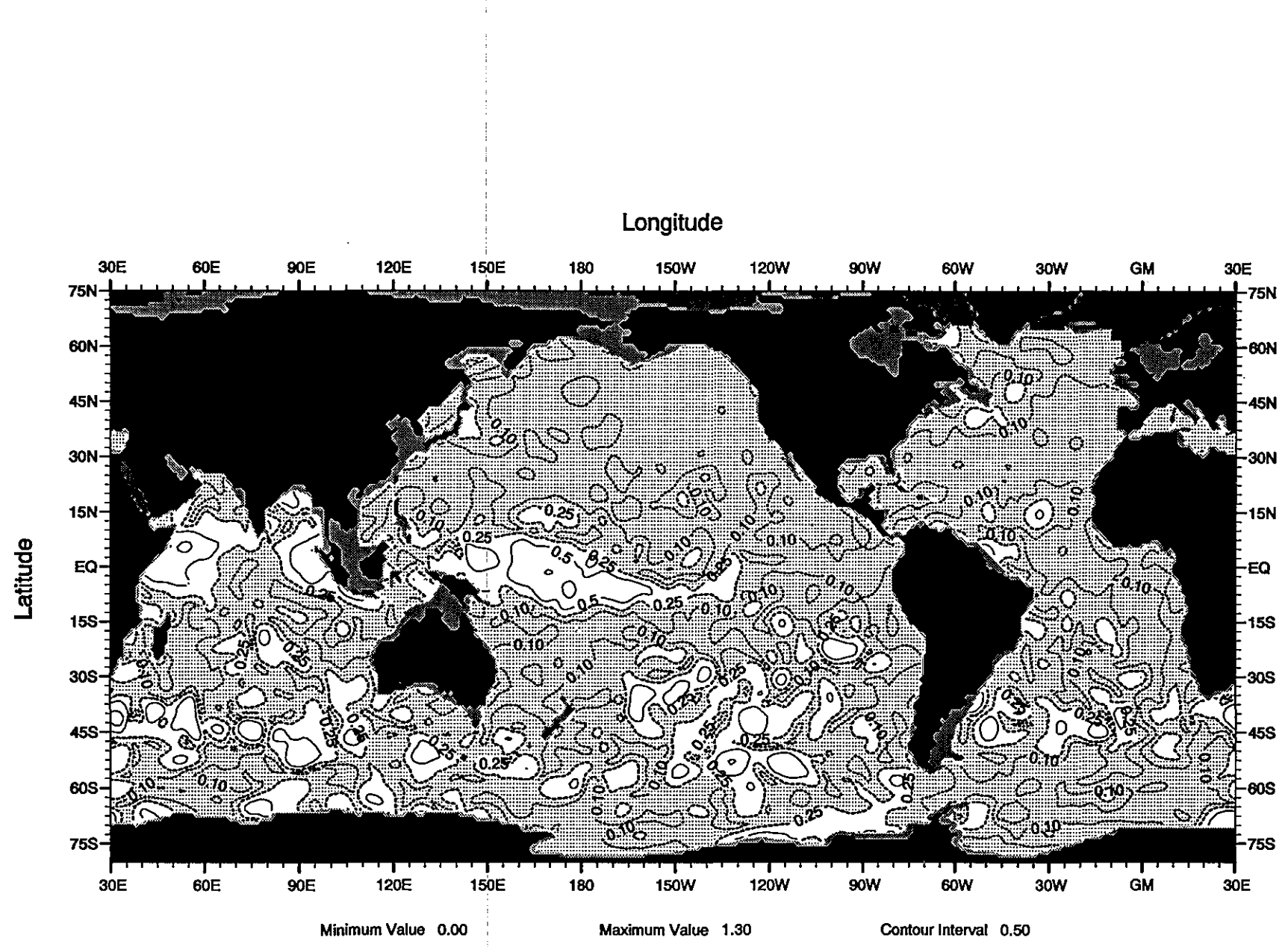


Fig. B49 Amplitude (°C) of the 2nd harmonic of the annual temperature cycle at 200 m depth

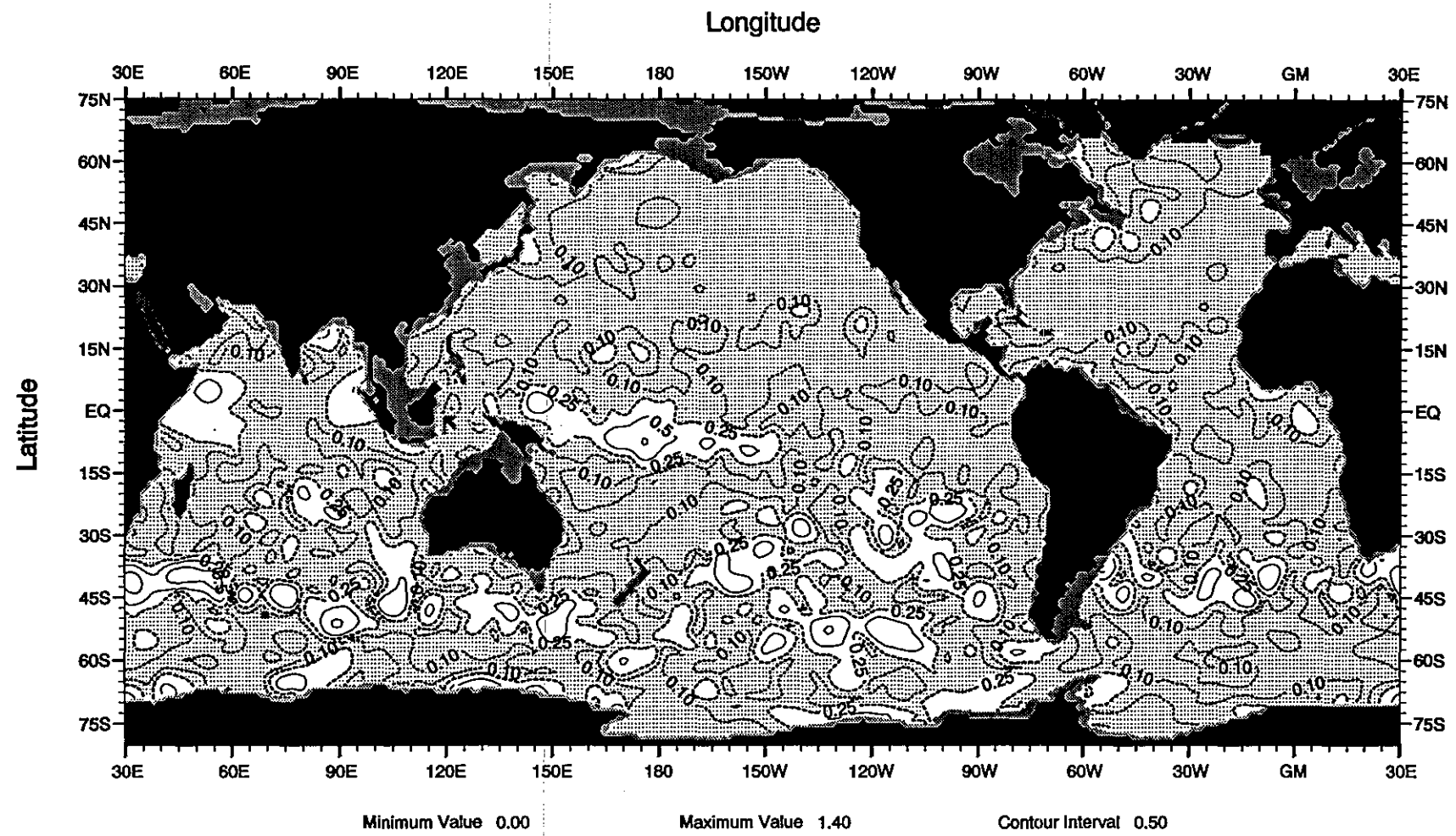


Fig. B50 Amplitude (°C) of the 2nd harmonic of the annual temperature cycle at 250 m depth

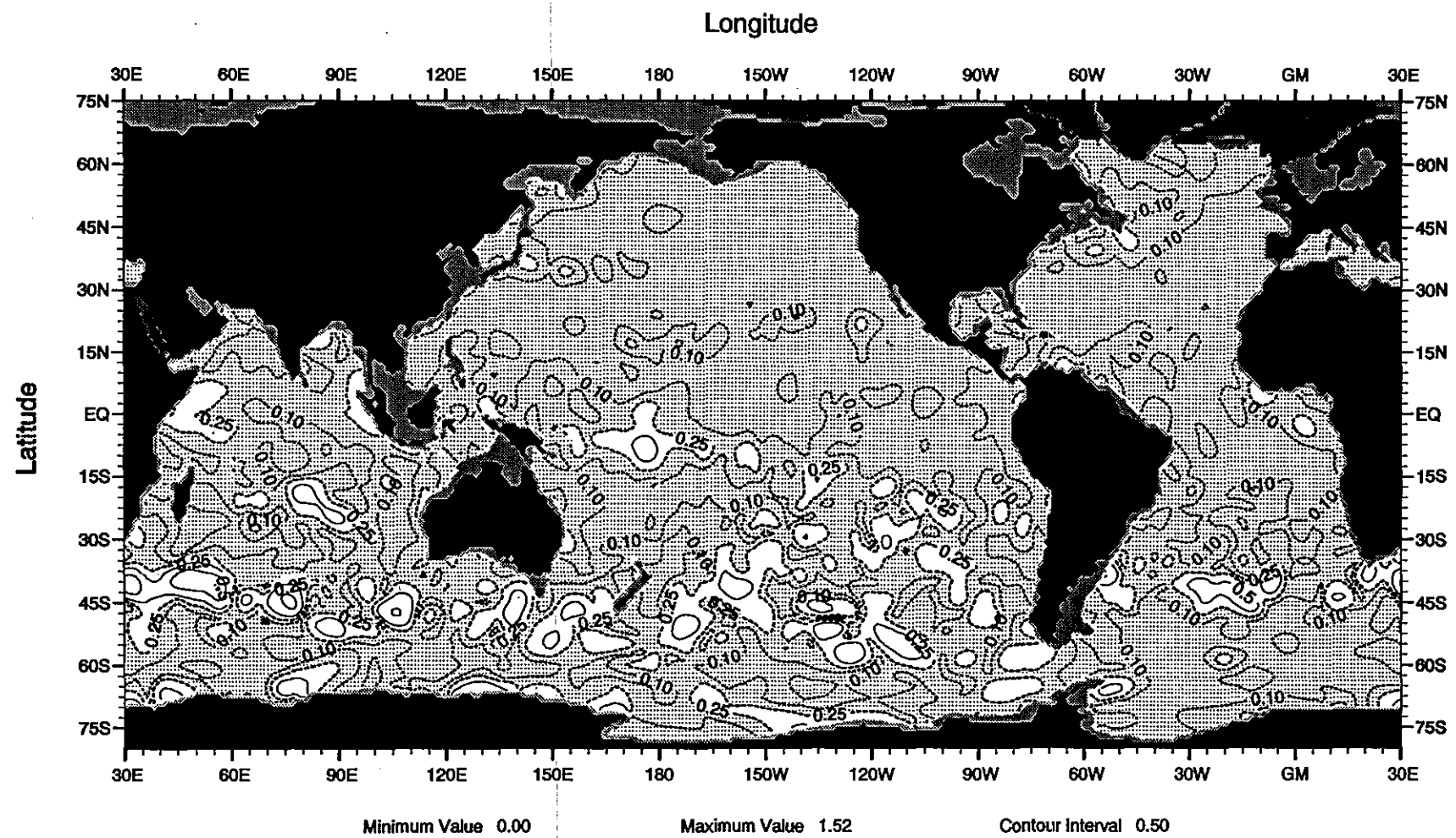


Fig. B51 Amplitude ($^{\circ}\text{C}$) of the 2nd harmonic of the annual temperature cycle at 300 m depth

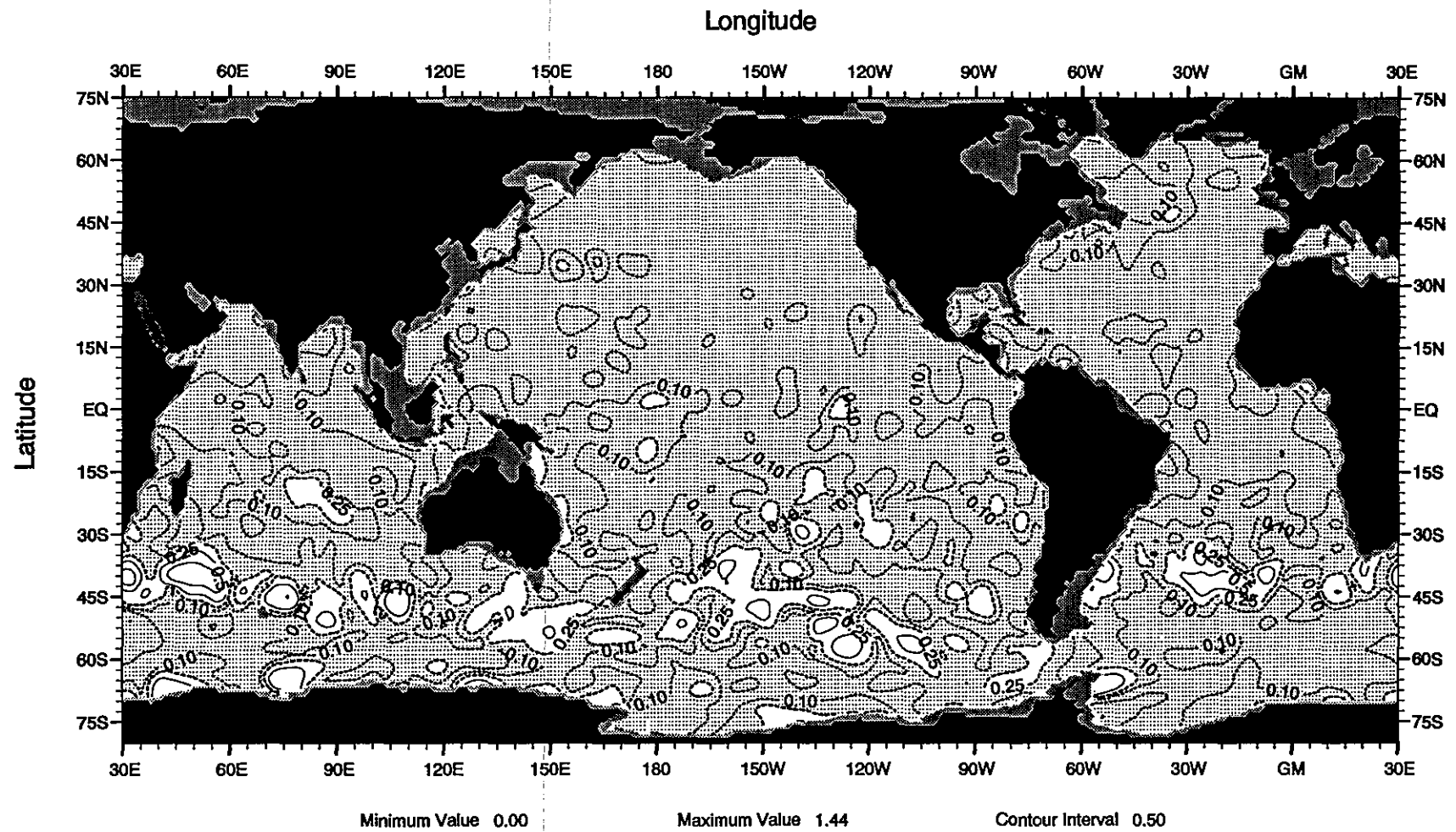


Fig. B52 Amplitude (°C) of the 2nd harmonic of the annual temperature cycle at 400 m depth

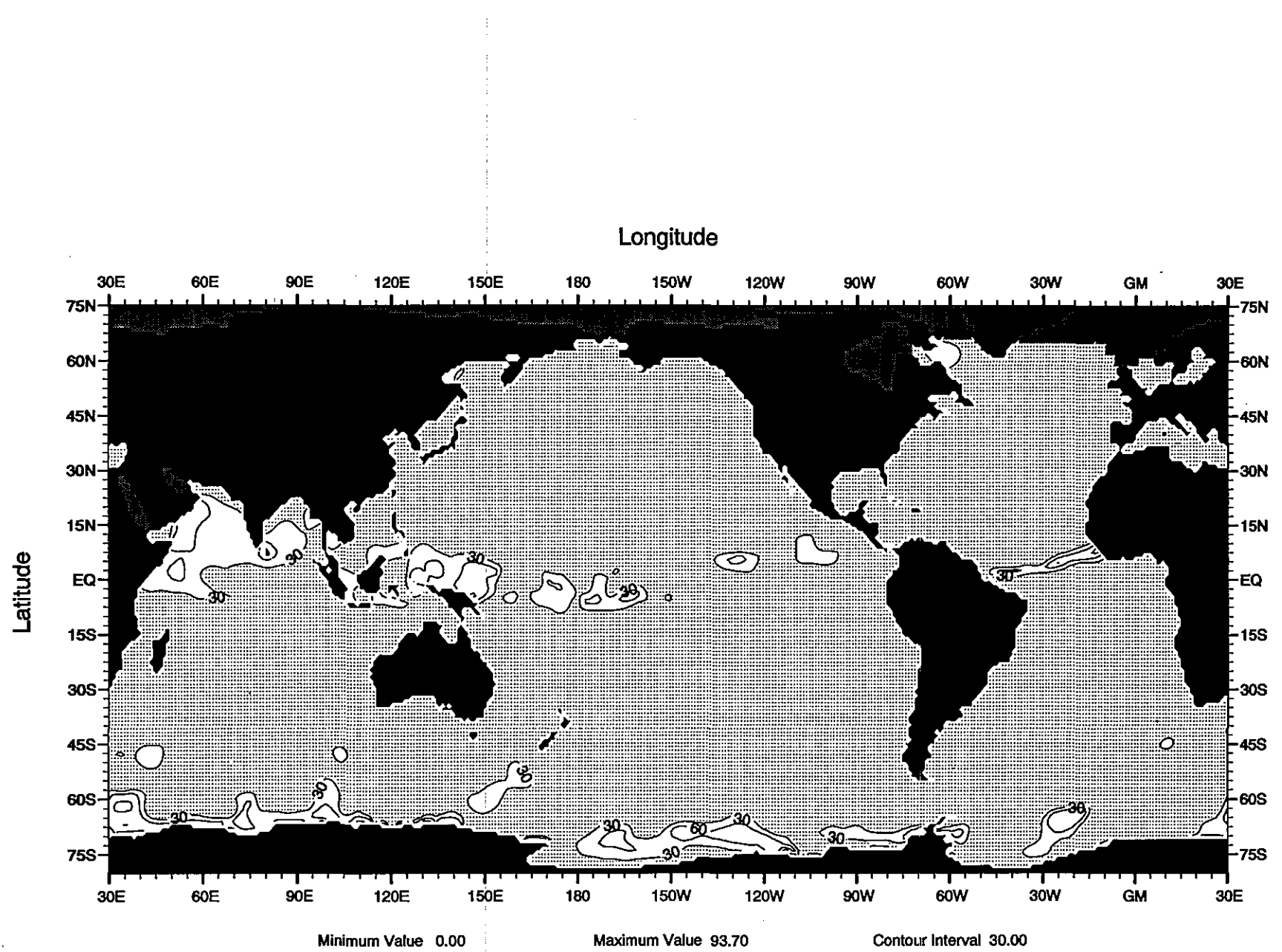


Fig. B53 Percent variance explained by 2nd harmonic of the annual temperature cycle at the surface

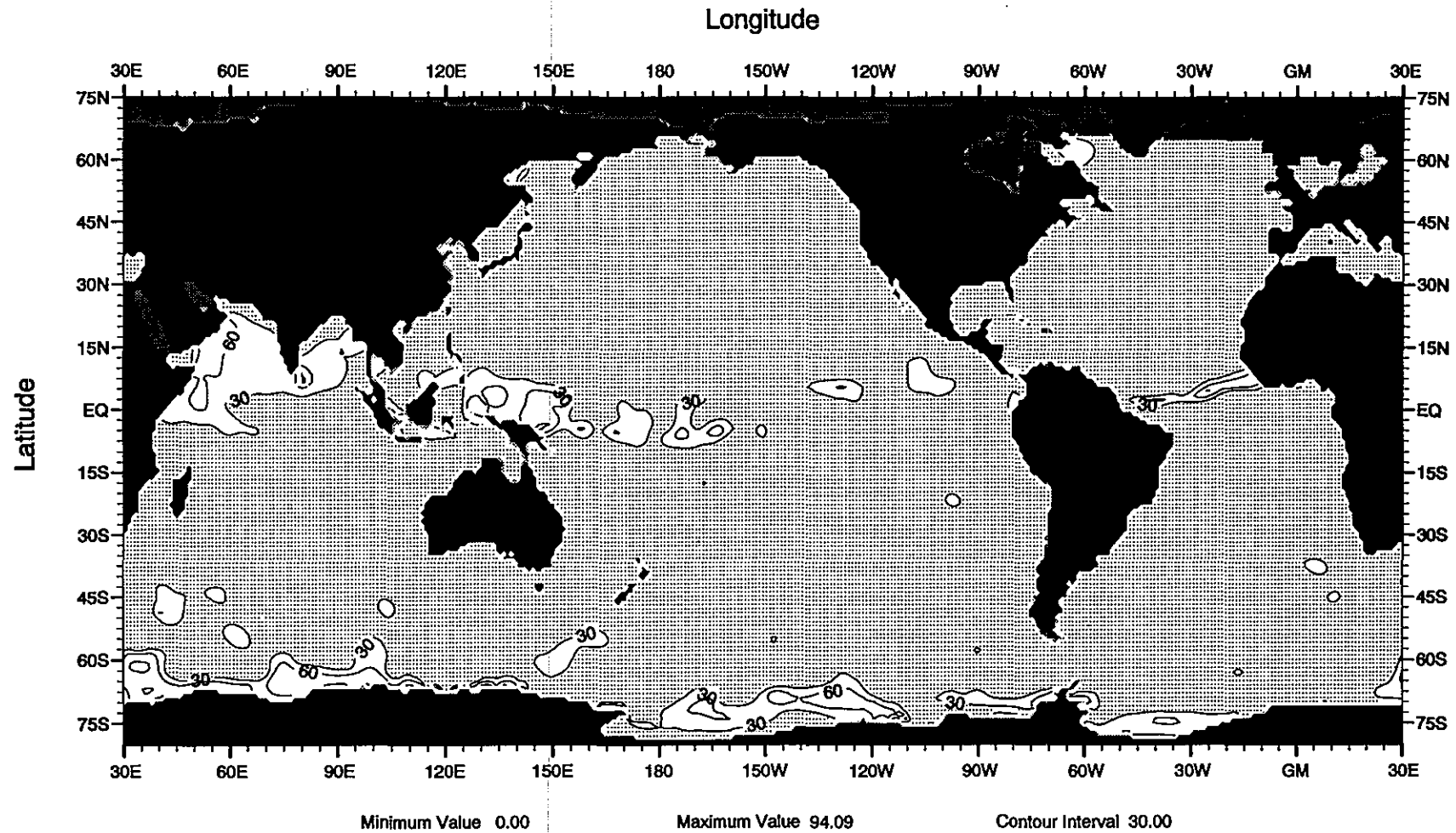


Fig. B54 Percent variance explained by 2nd harmonic of the annual temperature cycle at 10 m depth

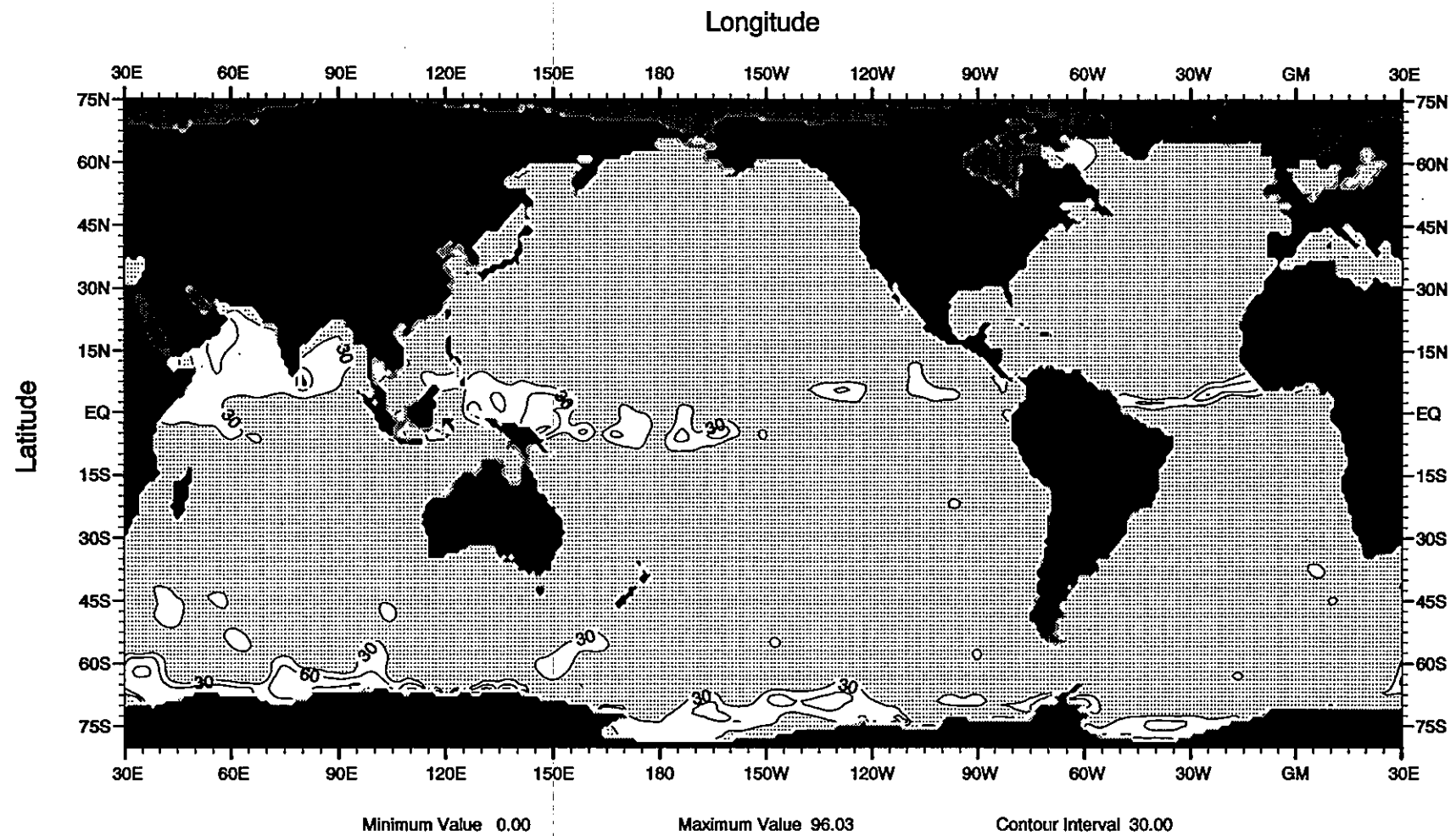


Fig. B55 Percent variance explained by 2nd harmonic of the annual temperature cycle at 20 m depth

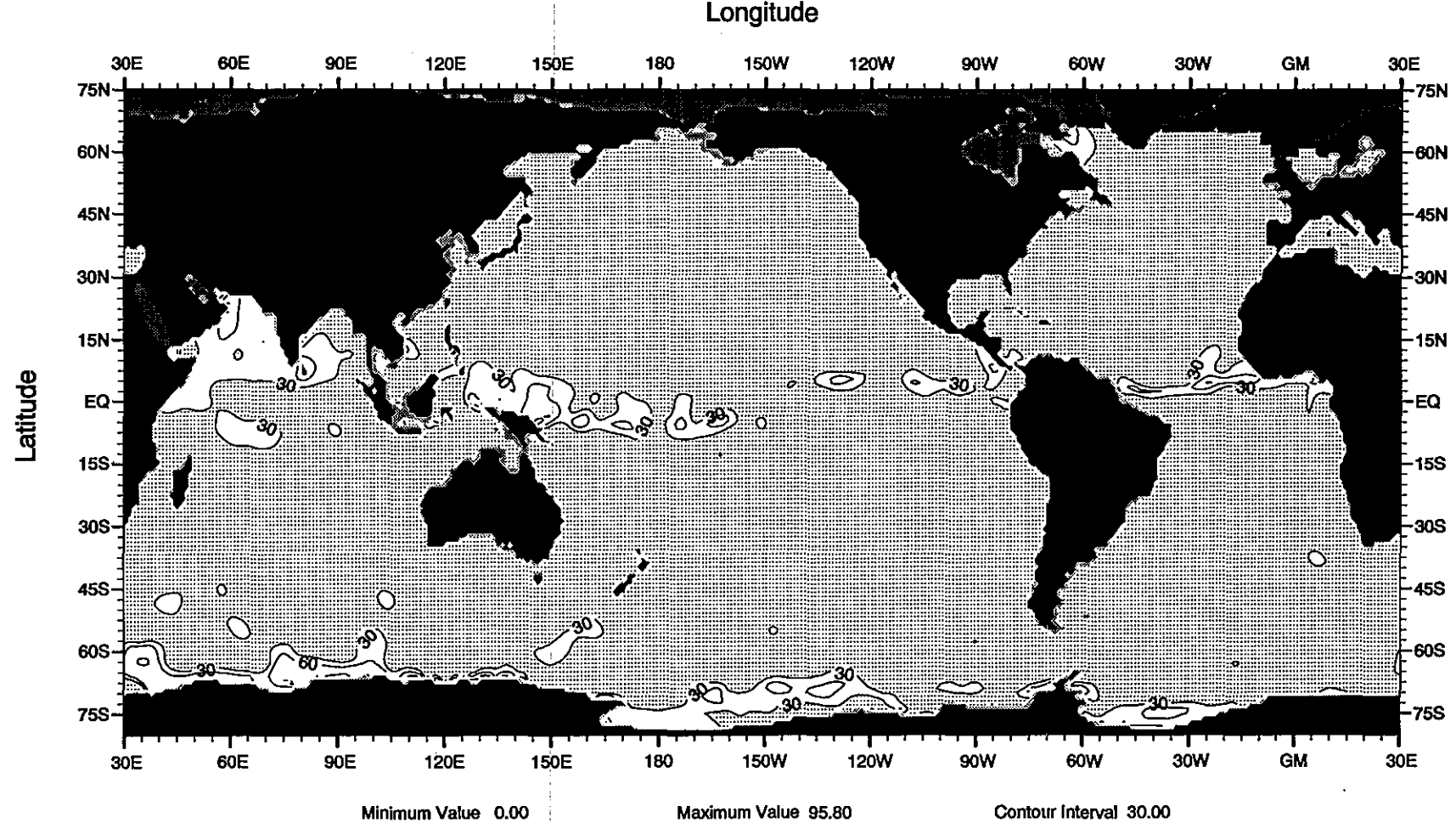


Fig. B56 Percent variance explained by 2nd harmonic of the annual temperature cycle at 30 m depth

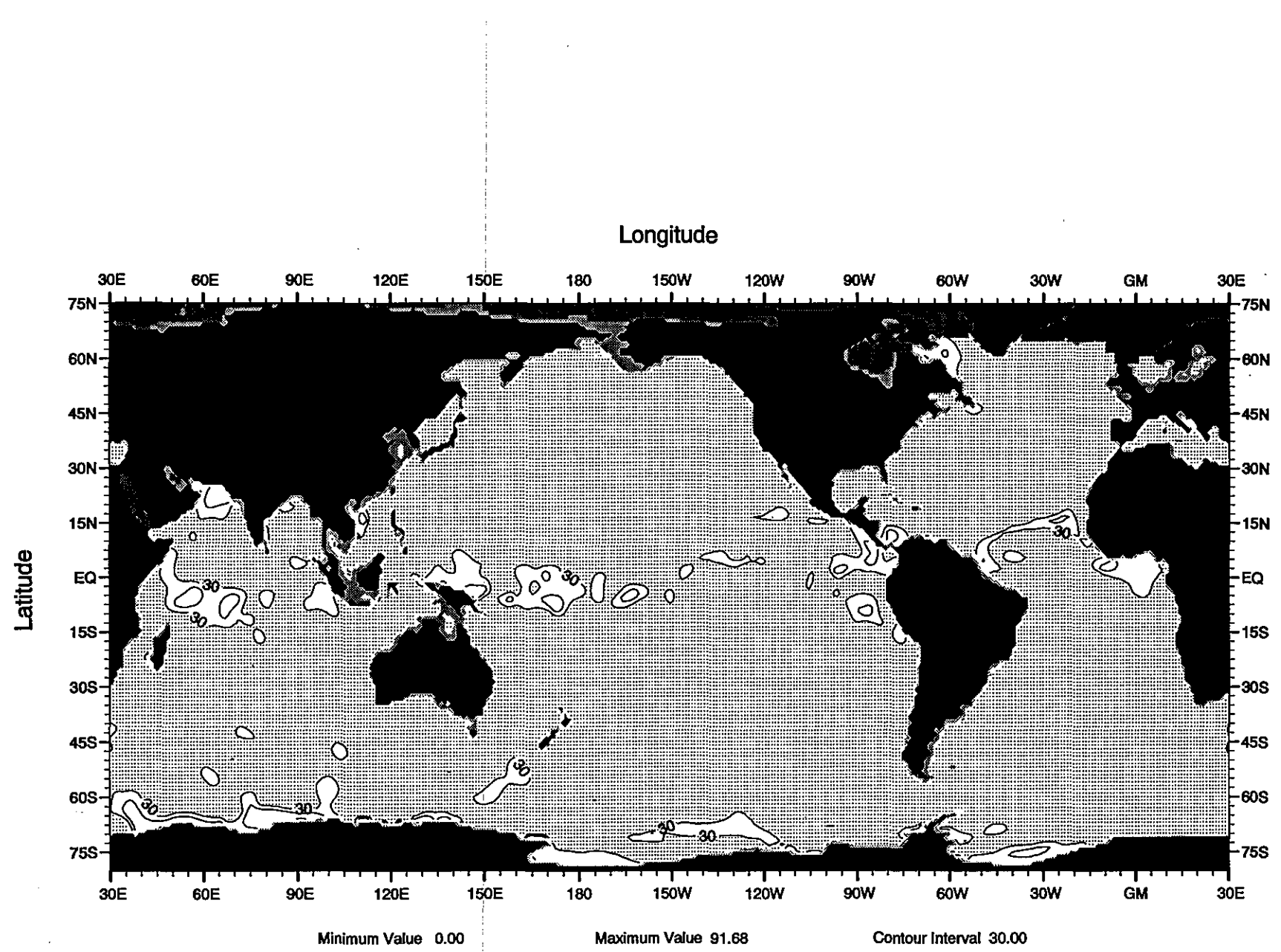


Fig. B57 Percent variance explained by 2nd harmonic of the annual temperature cycle at 50 m depth

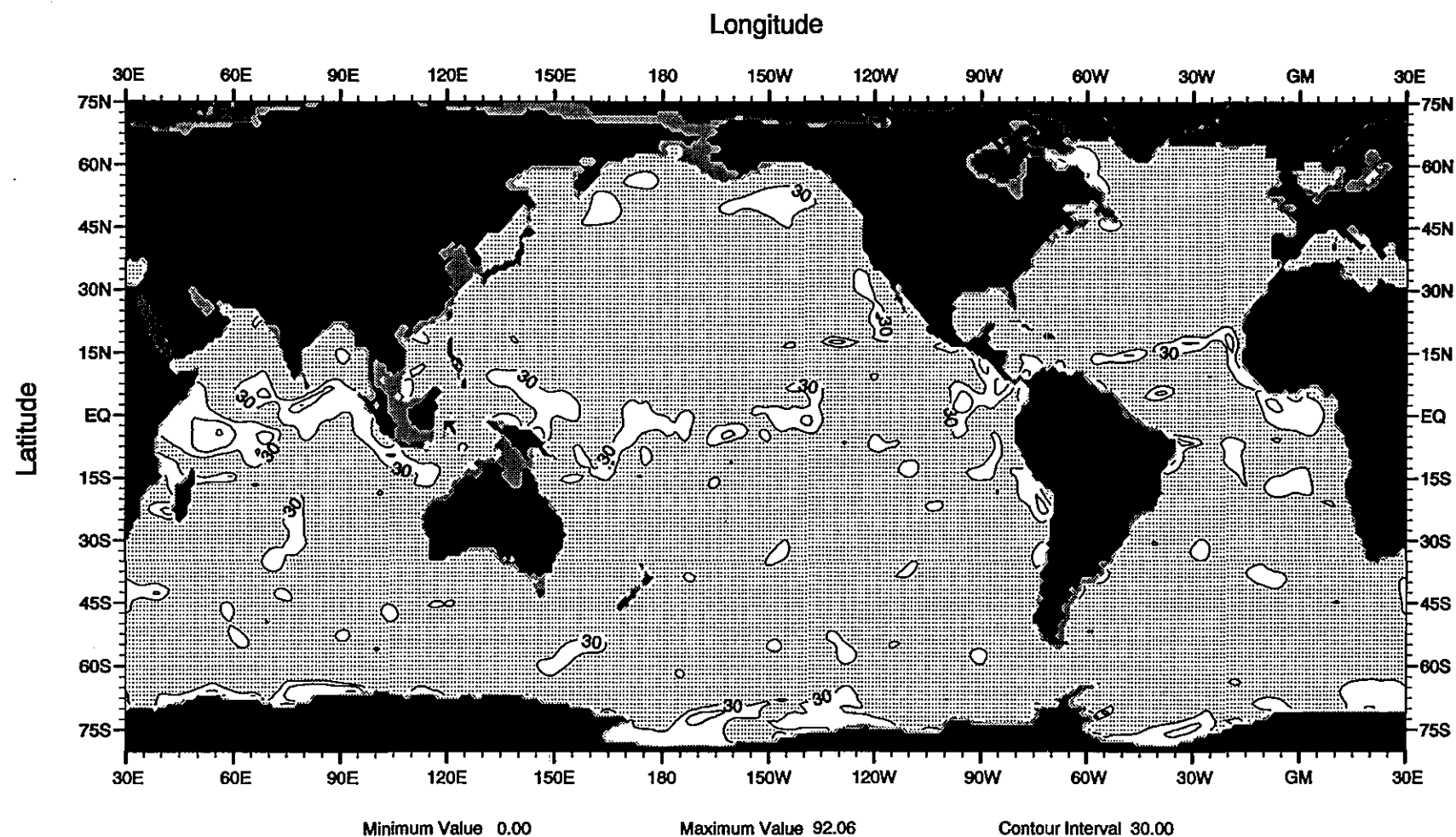


Fig. B58 Percent variance explained by 2nd harmonic of the annual temperature cycle at 75 m depth

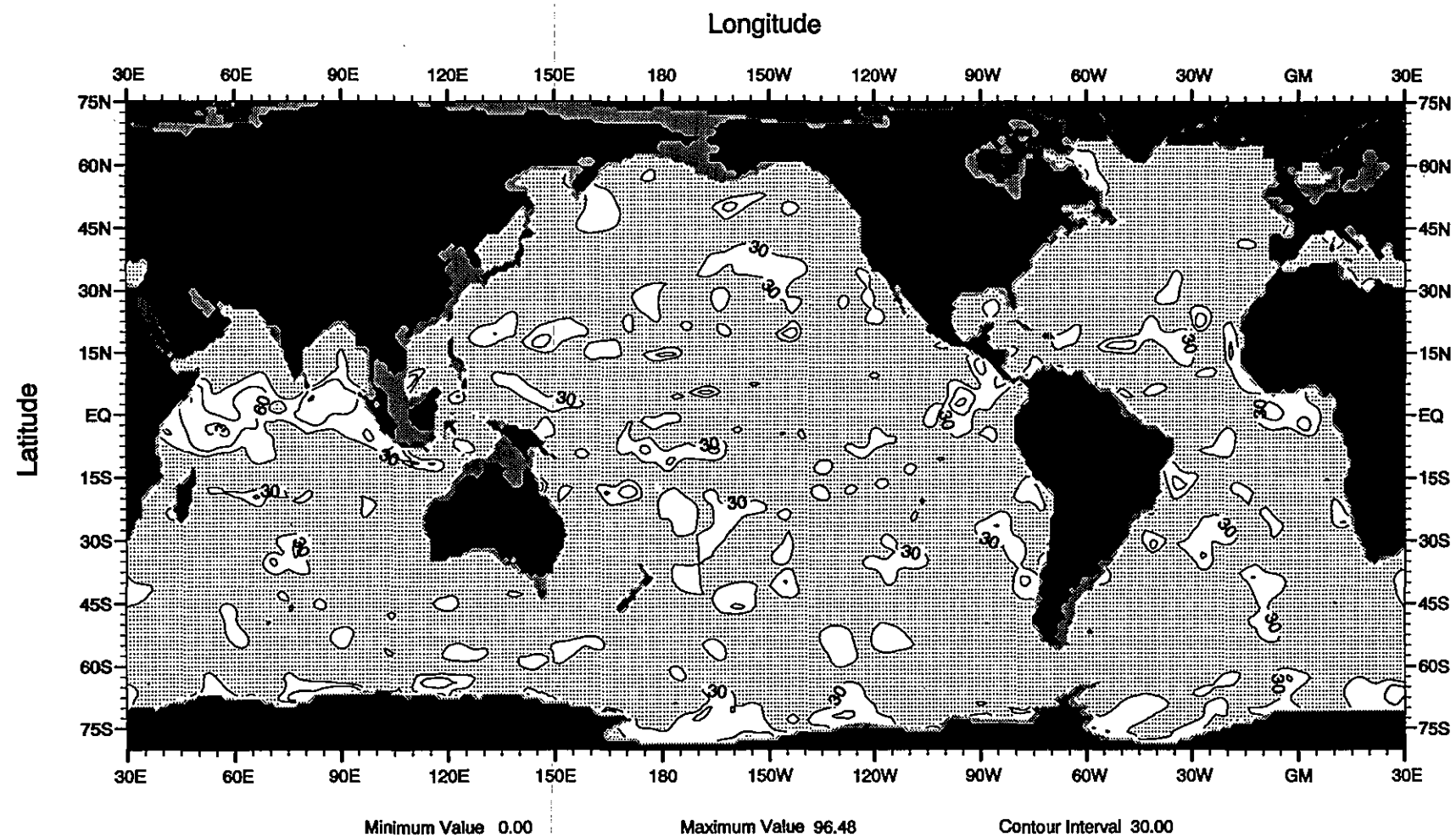


Fig. B59 Percent variance explained by 2nd harmonic of the annual temperature cycle at 100 m depth

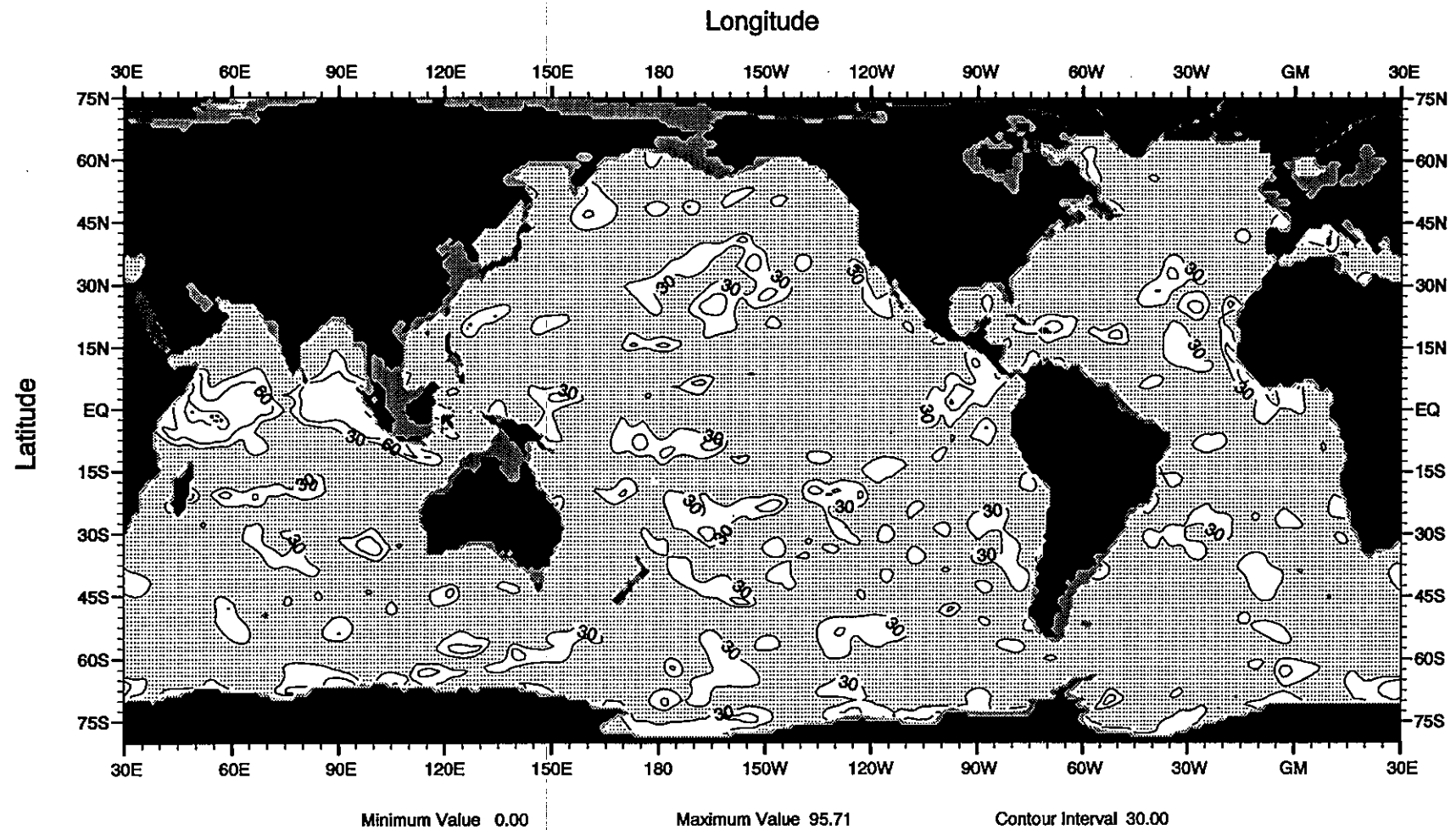


Fig. B60 Percent variance explained by 2nd harmonic of the annual temperature cycle at 125 m depth

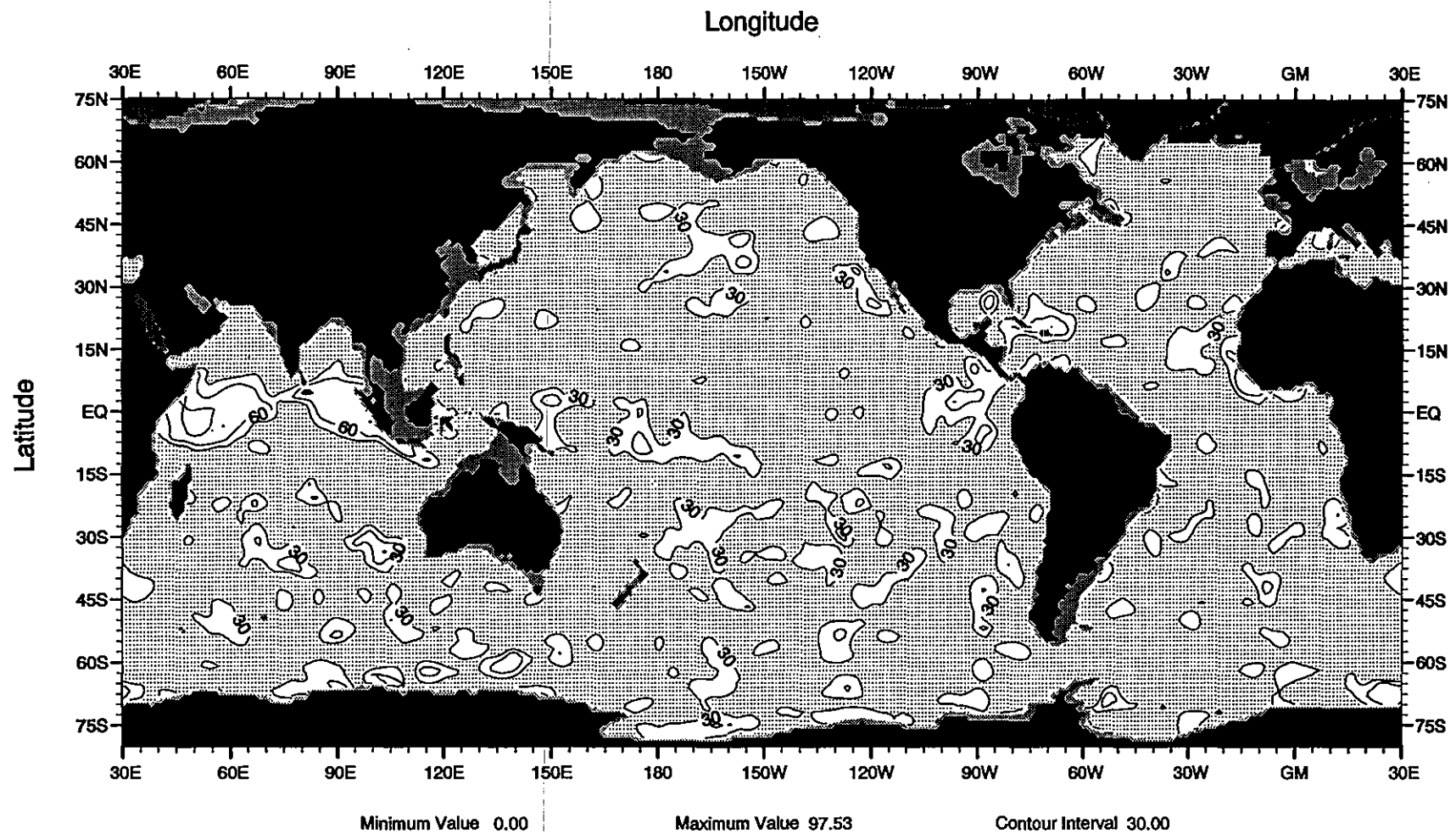


Fig. B61 Percent variance explained by 2nd harmonic of the annual temperature cycle at 150 m depth

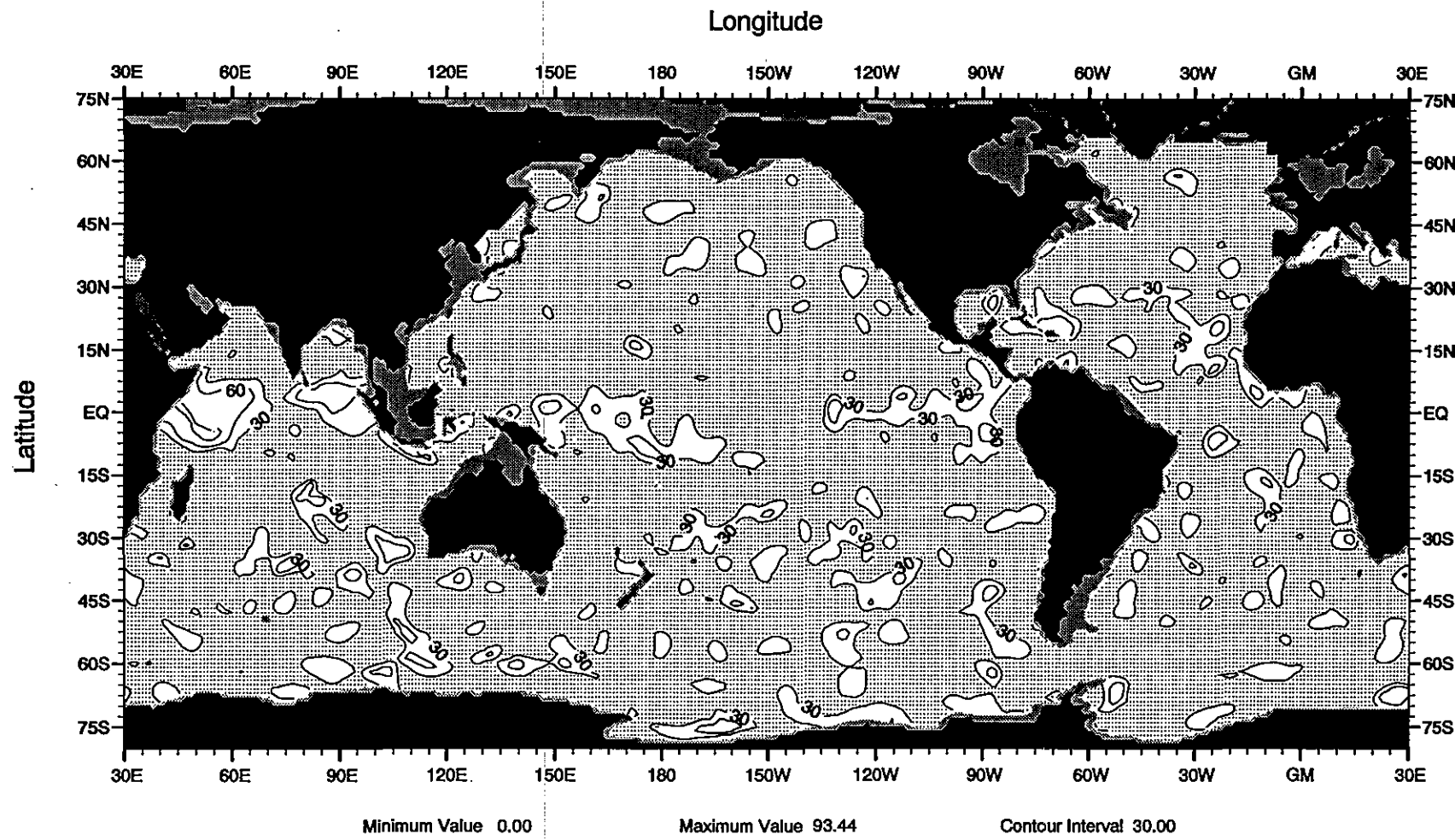


Fig. B62 Percent variance explained by 2nd harmonic of the annual temperature cycle at 200 m depth

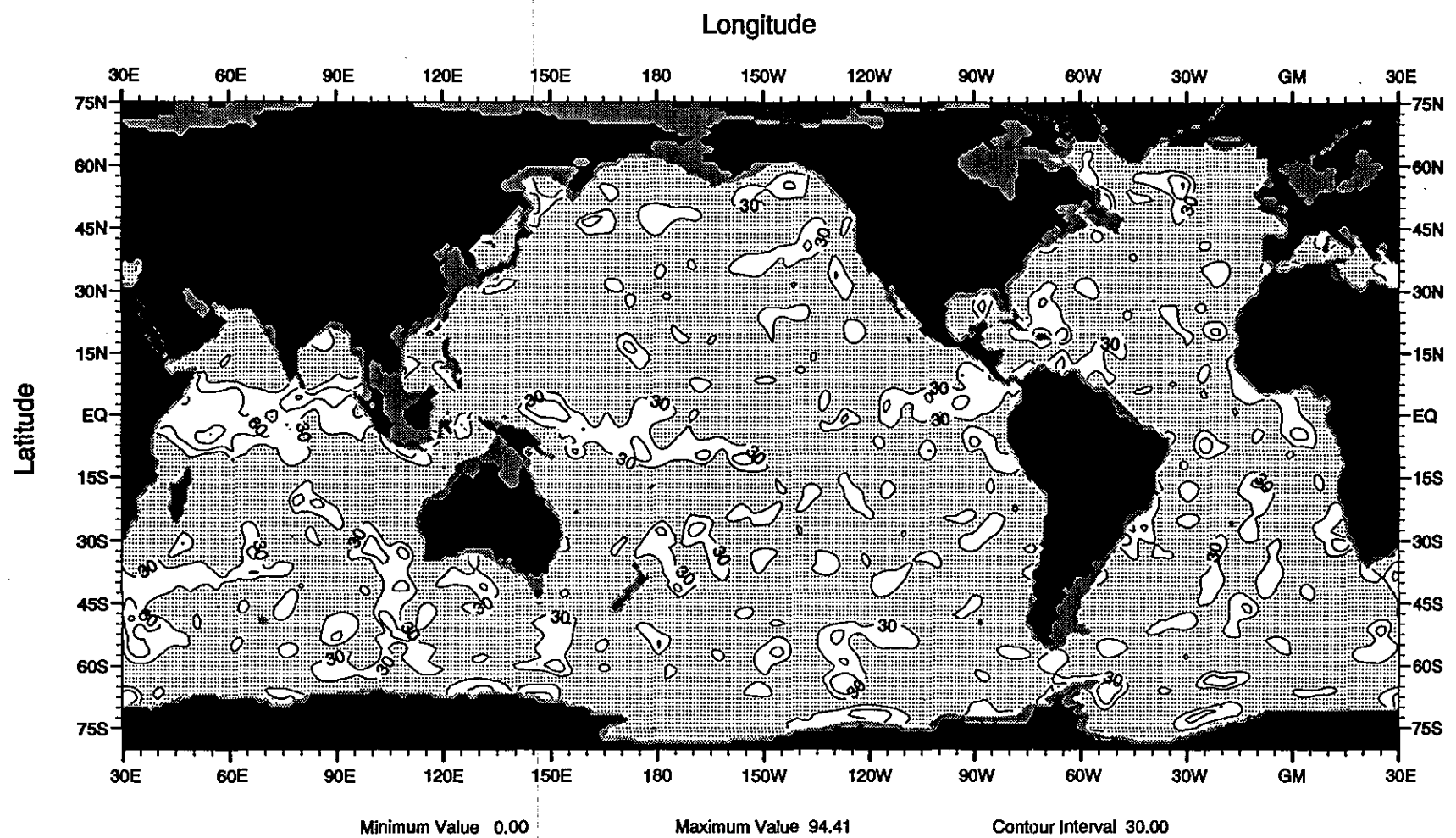


Fig. B63 Percent variance explained by 2nd harmonic of the annual temperature cycle at 250 m depth

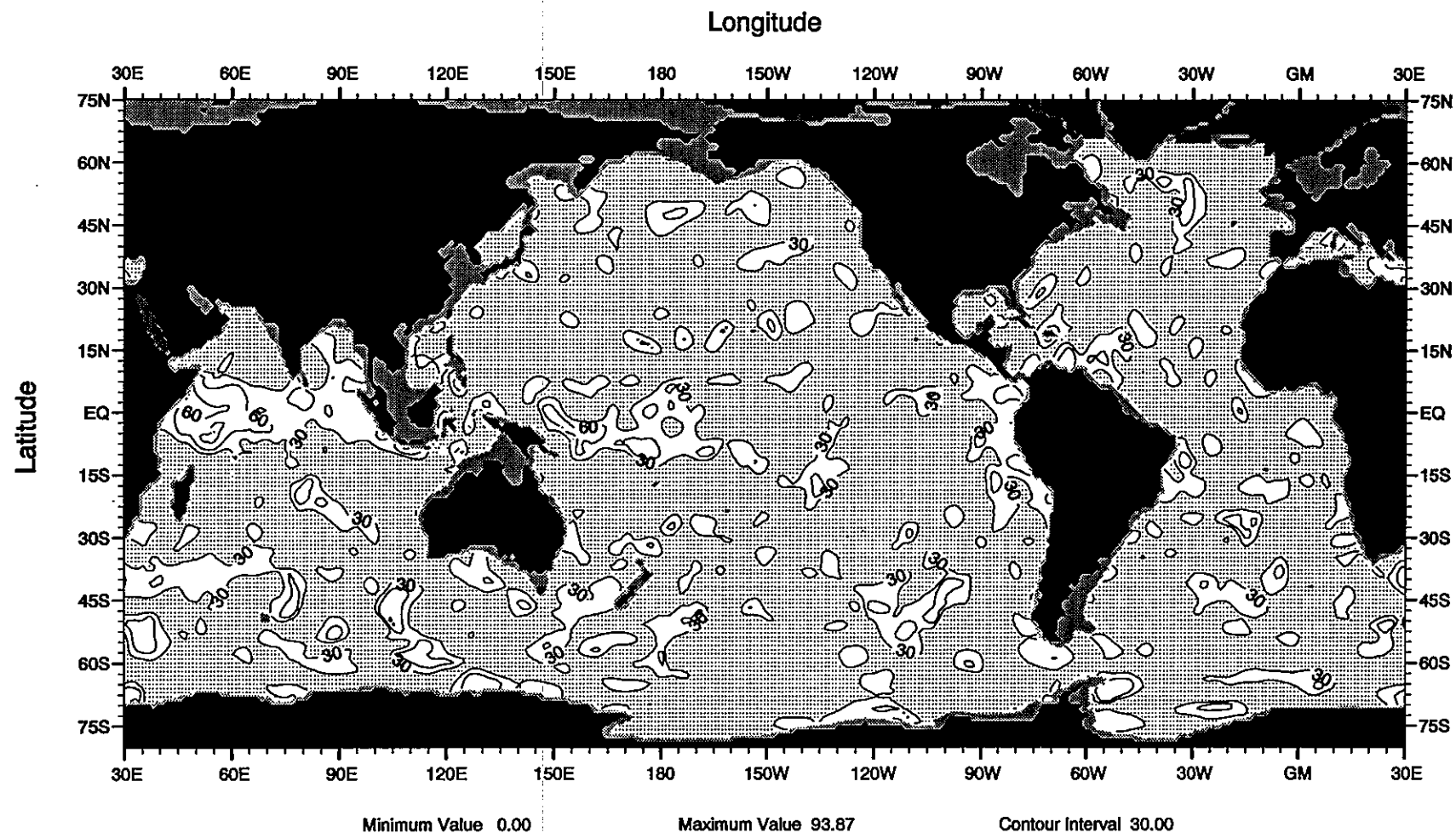


Fig. B64 Percent variance explained by 2nd harmonic of the annual temperature cycle at 300 m depth

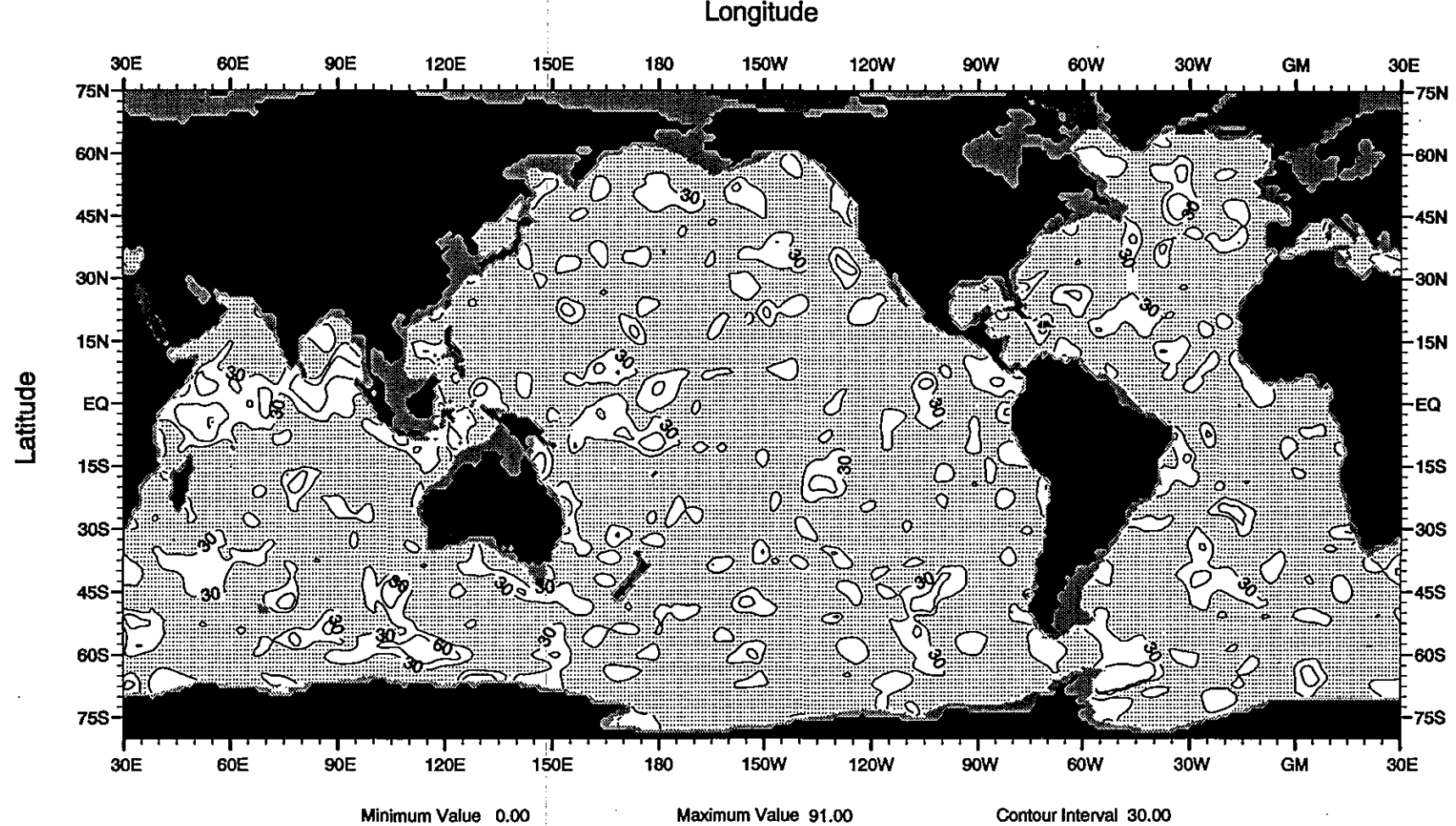


Fig. B65 Percent variance explained by 2nd harmonic of the annual temperature cycle at 400 m depth

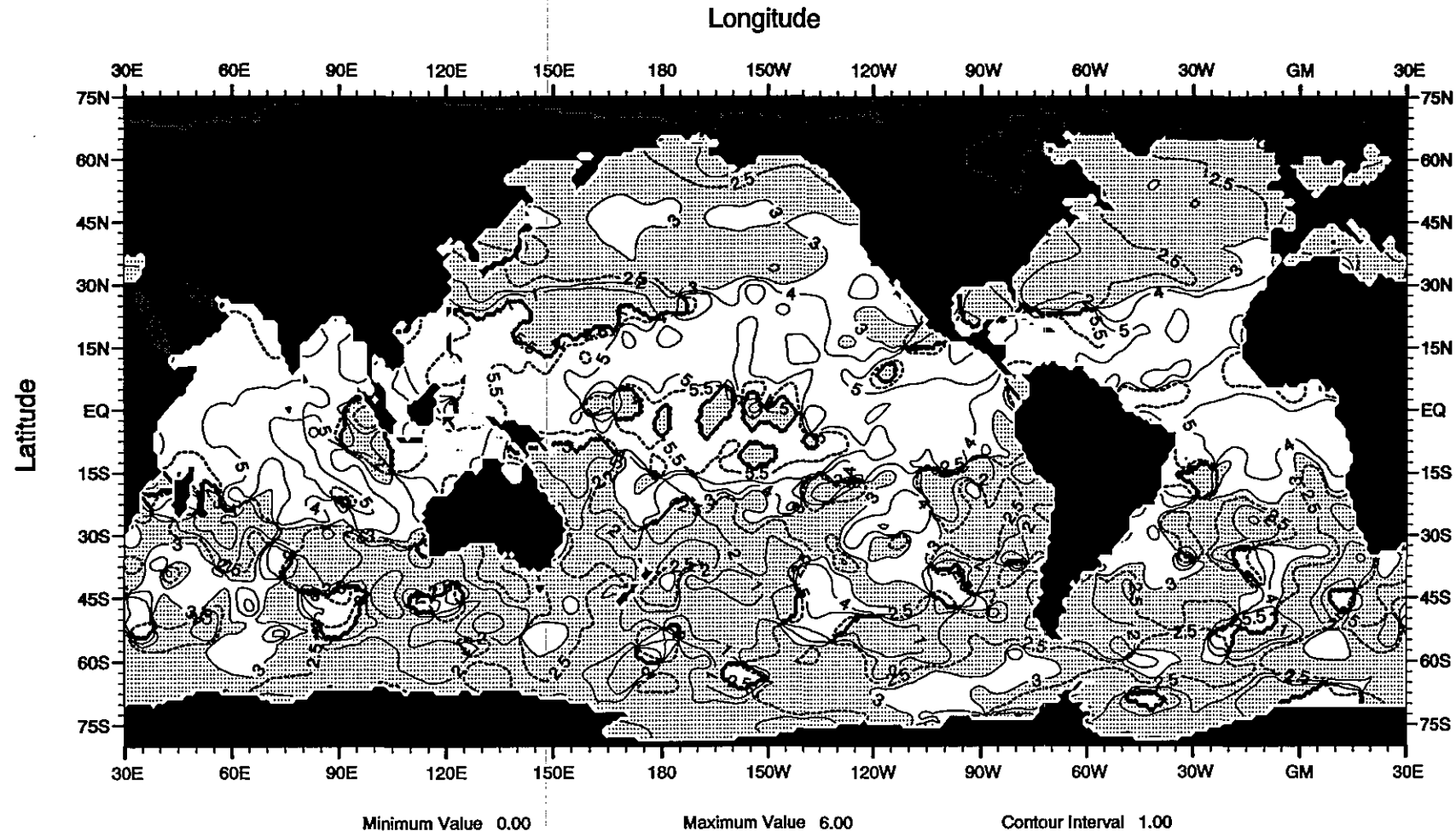


Fig. B66 Phase (months) of the 2nd harmonic of the annual temperature cycle at the sea surface

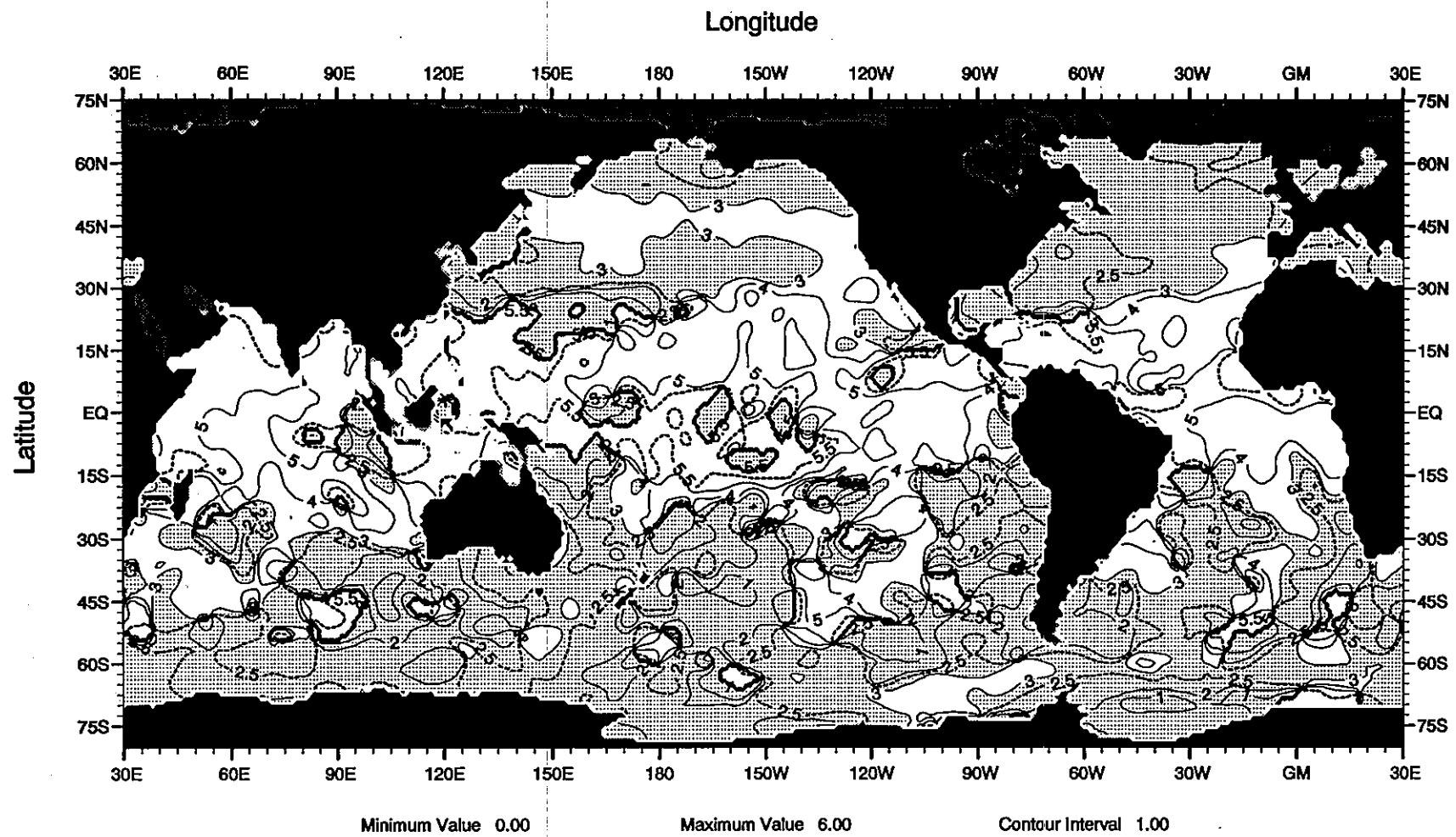


Fig. B67 Phase (months) of the 2nd harmonic of the annual temperature cycle at 10 m depth

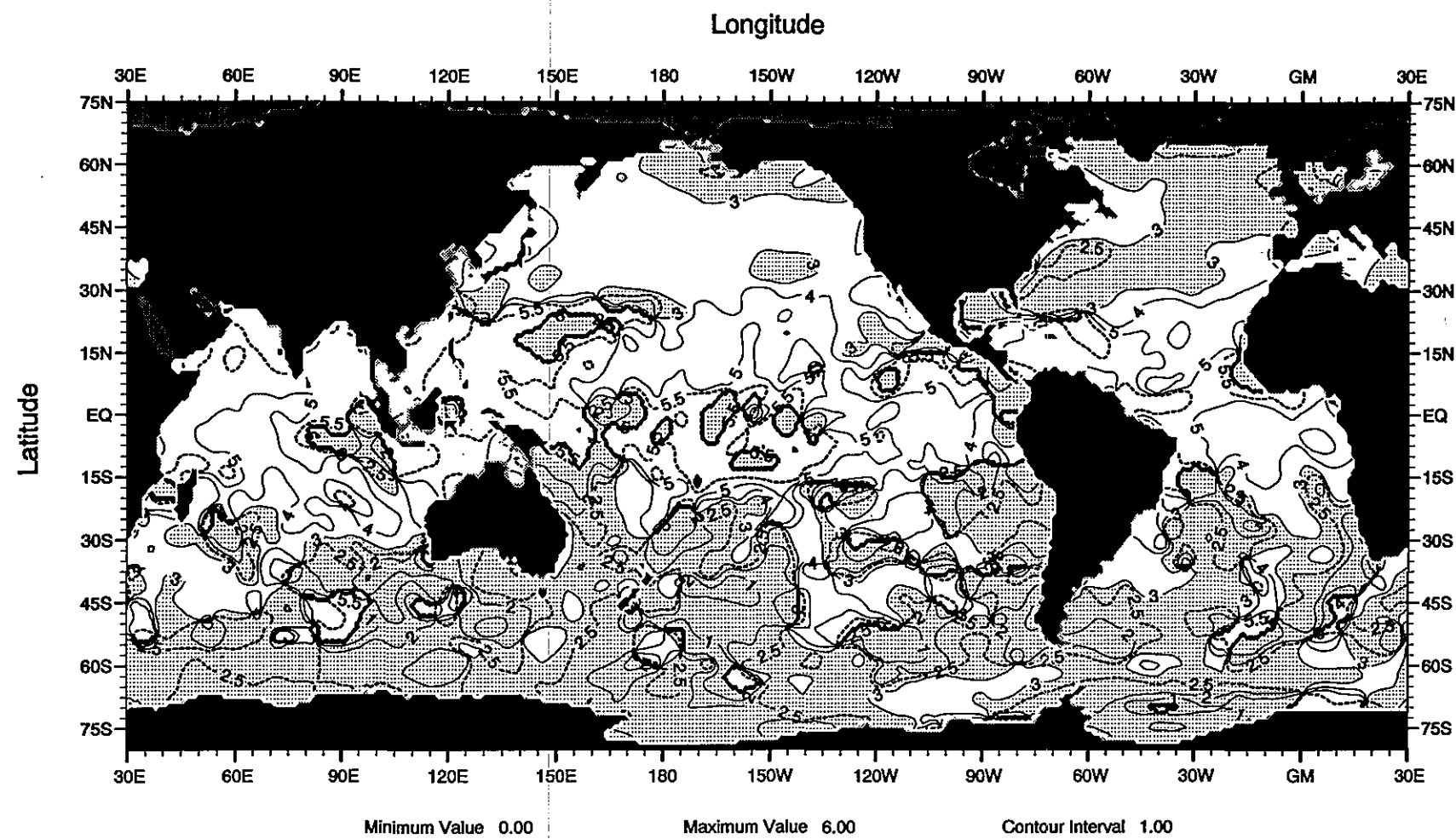


Fig. B68 Phase (months) of the 2nd harmonic of the annual temperature cycle at 20 m depth

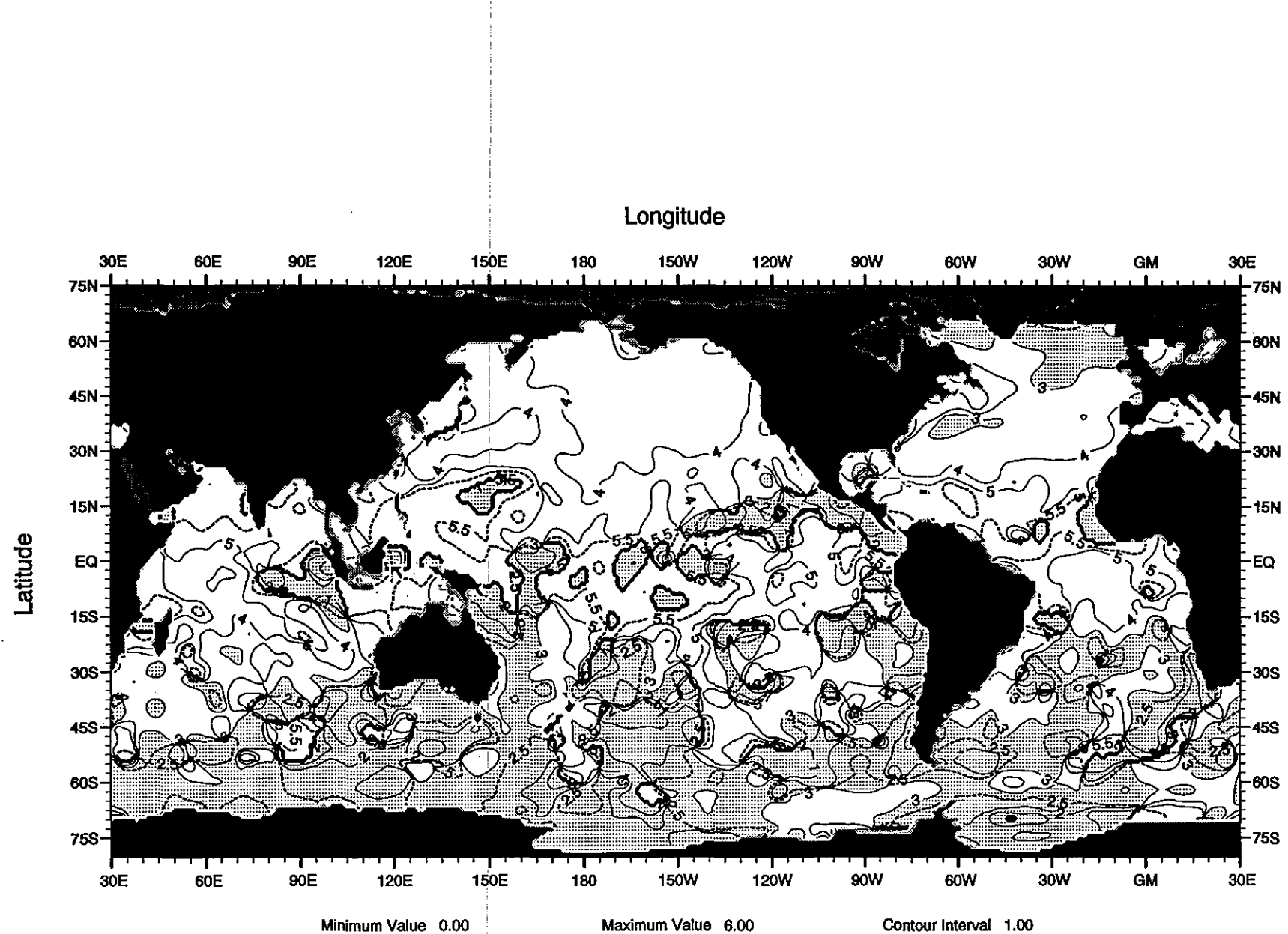


Fig. B69 Phase (months) of the 2nd harmonic of the annual temperature cycle at 30 m depth

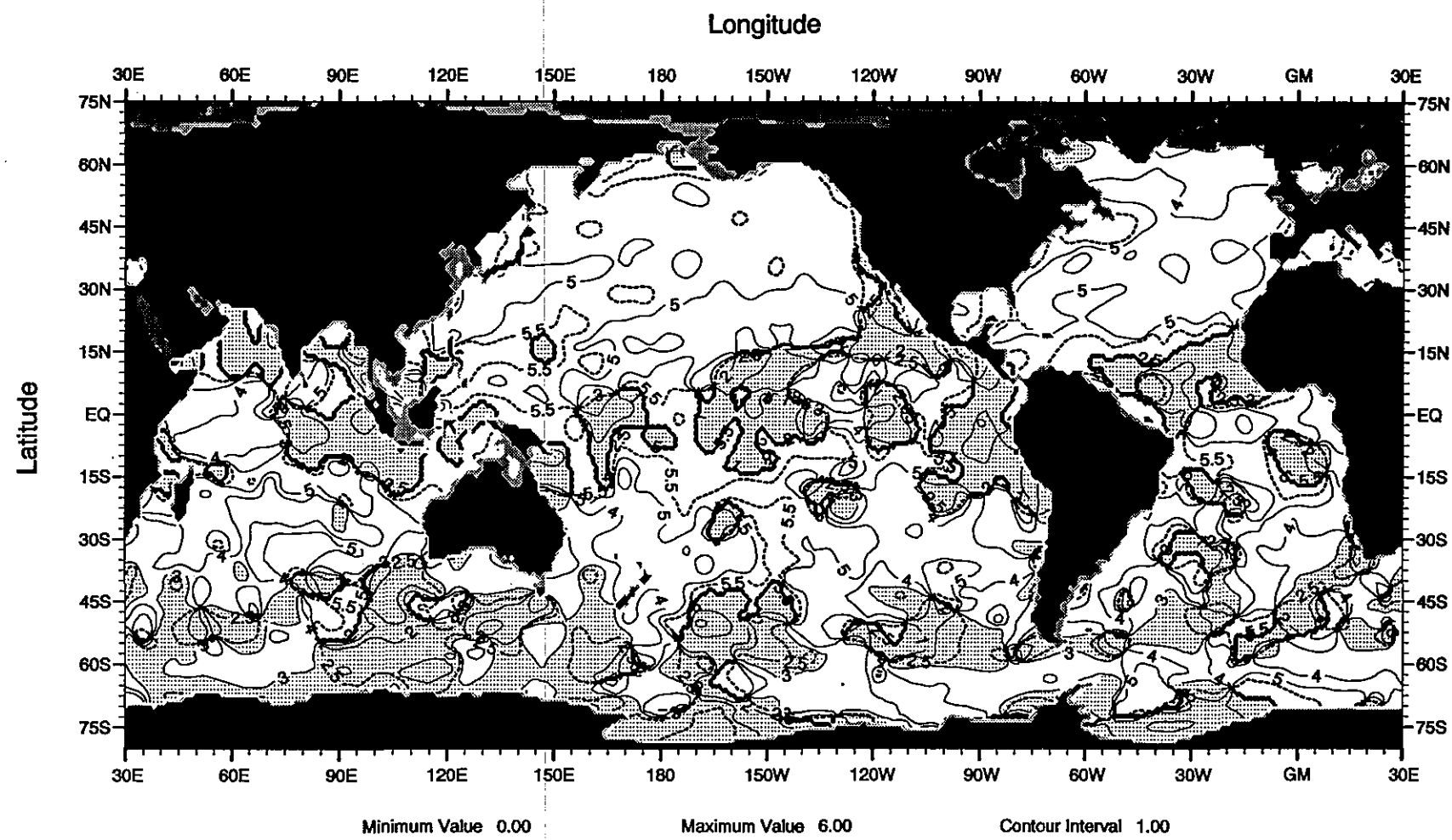


Fig. B70 Phase (months) of the 2nd harmonic of the annual temperature cycle at 50 m depth

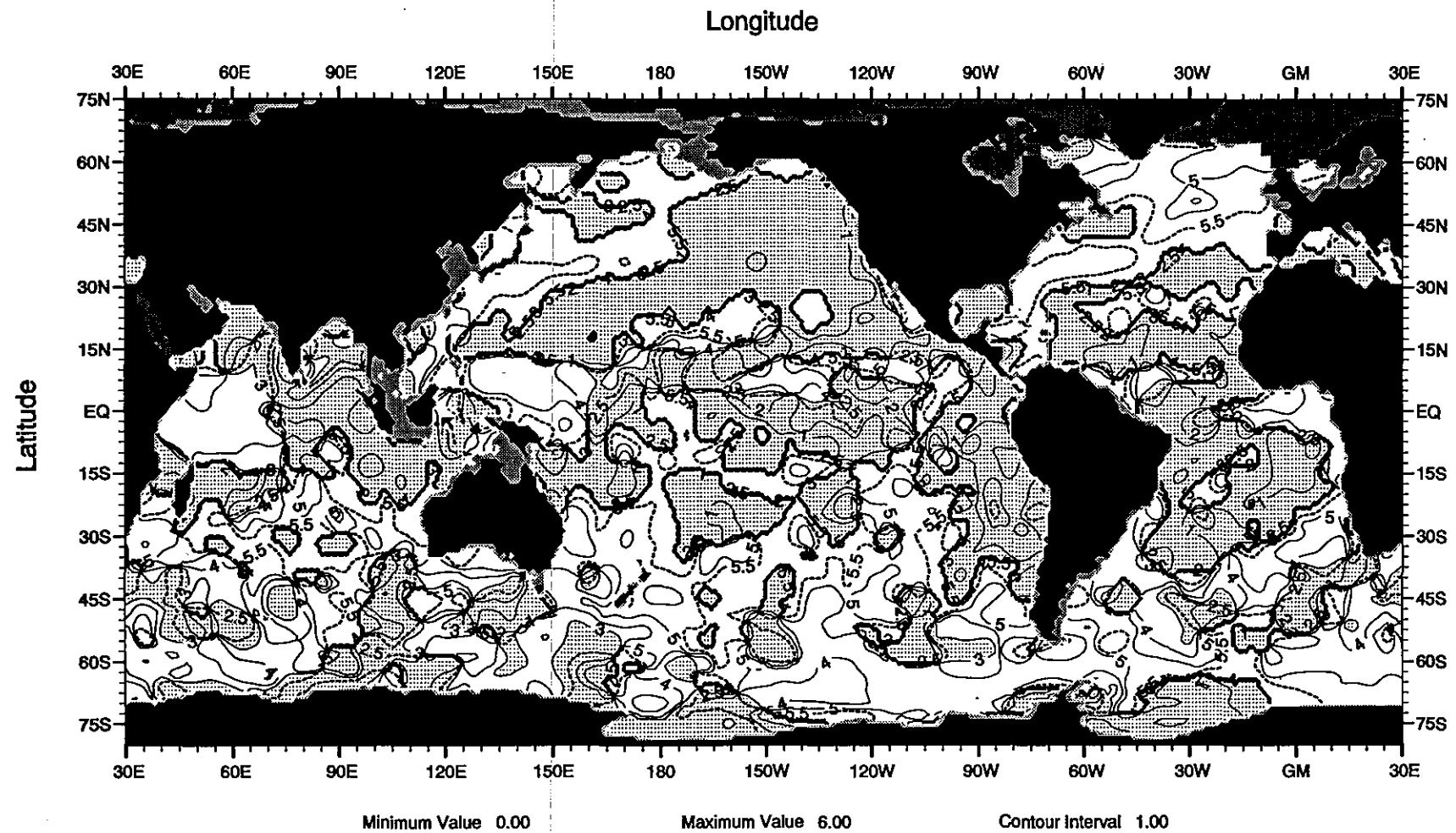


Fig. B71 Phase (months) of the 2nd harmonic of the annual temperature cycle at 75 m depth

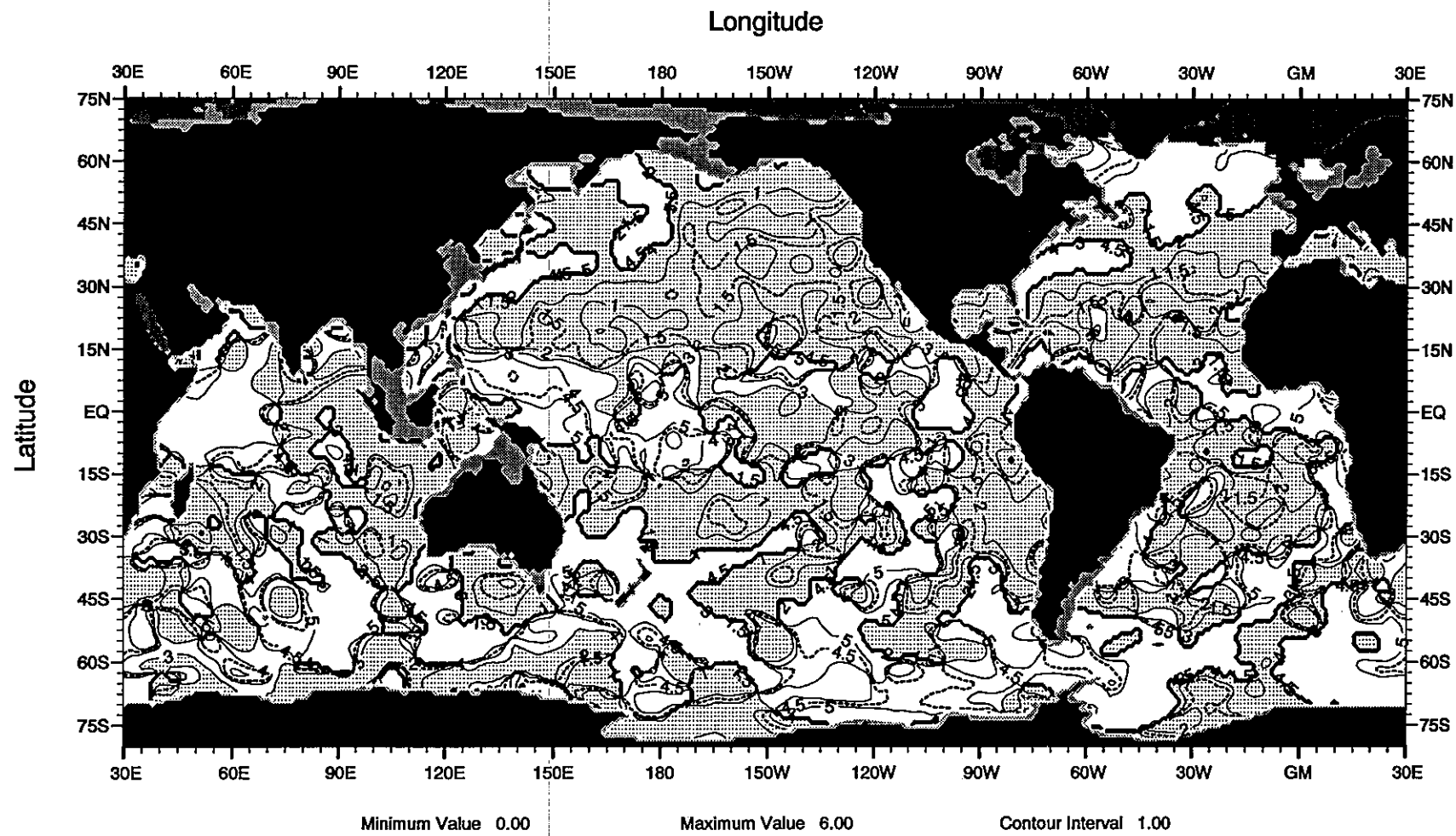


Fig. B72 Phase (months) of the 2nd harmonic of the annual temperature cycle at 100 m depth

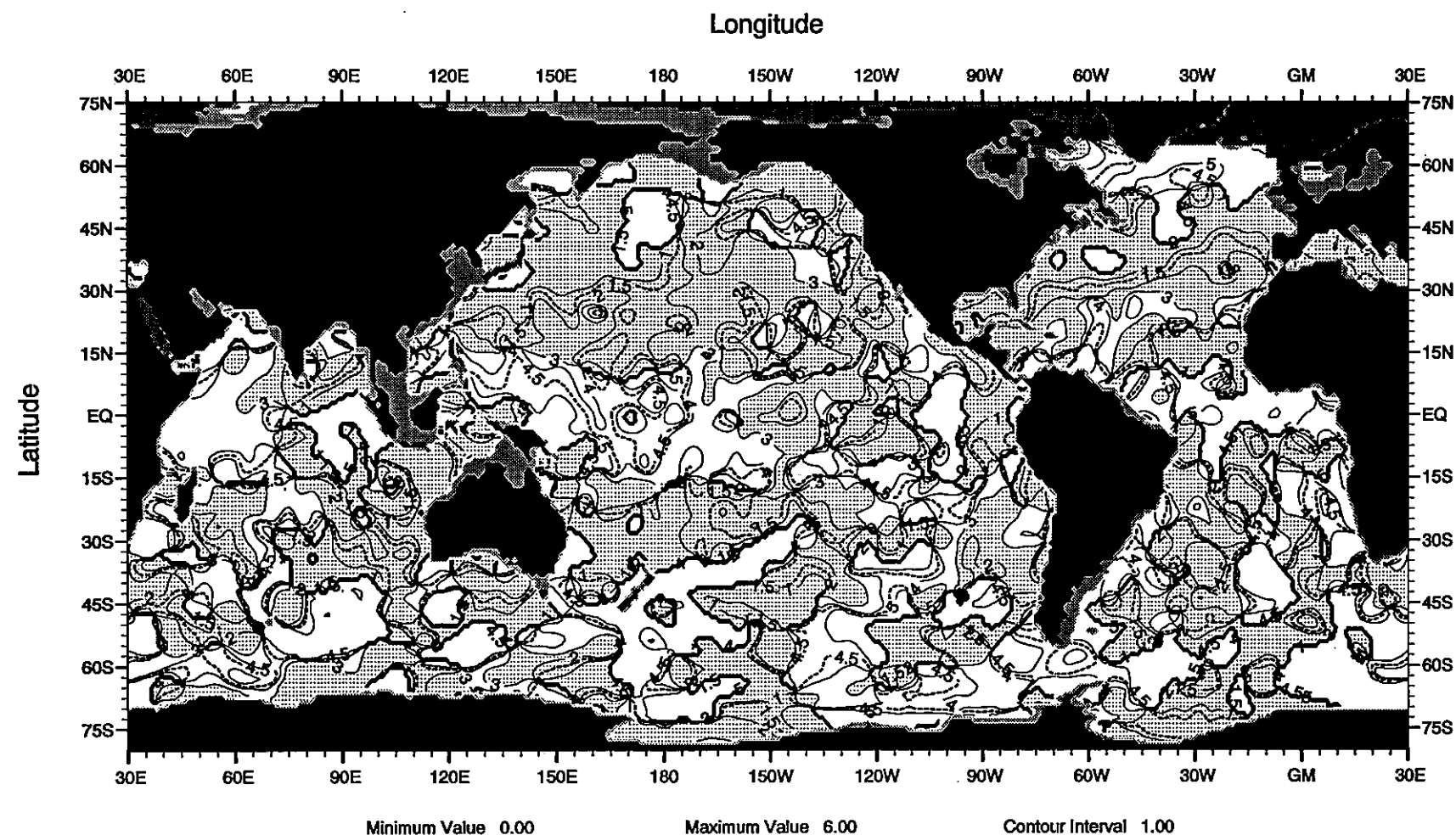


Fig. B73 Phase (months) of the 2nd harmonic of the annual temperature cycle at 125 m depth

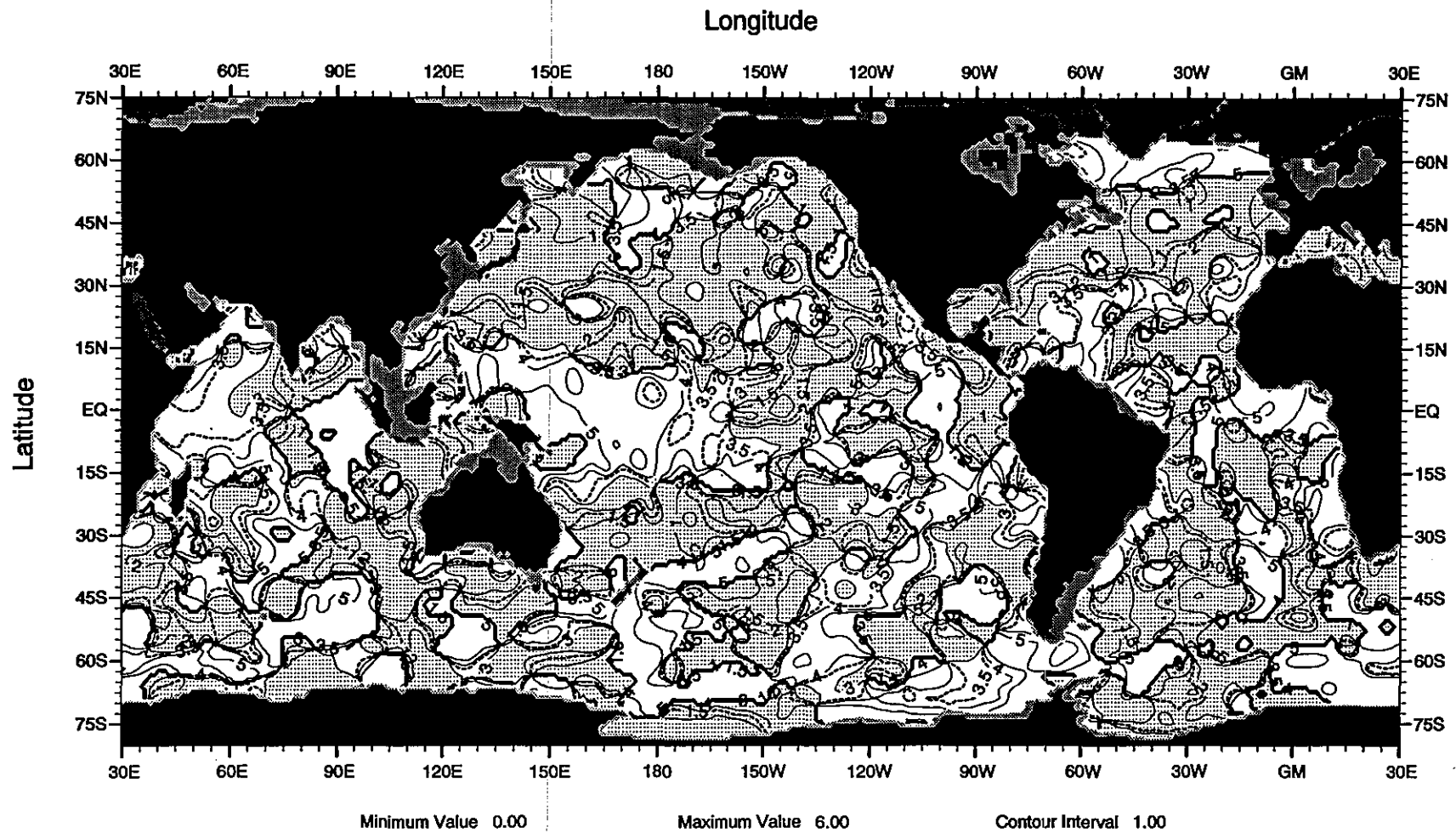


Fig. B74 Phase (months) of the 2nd harmonic of the annual temperature cycle at 150 m depth

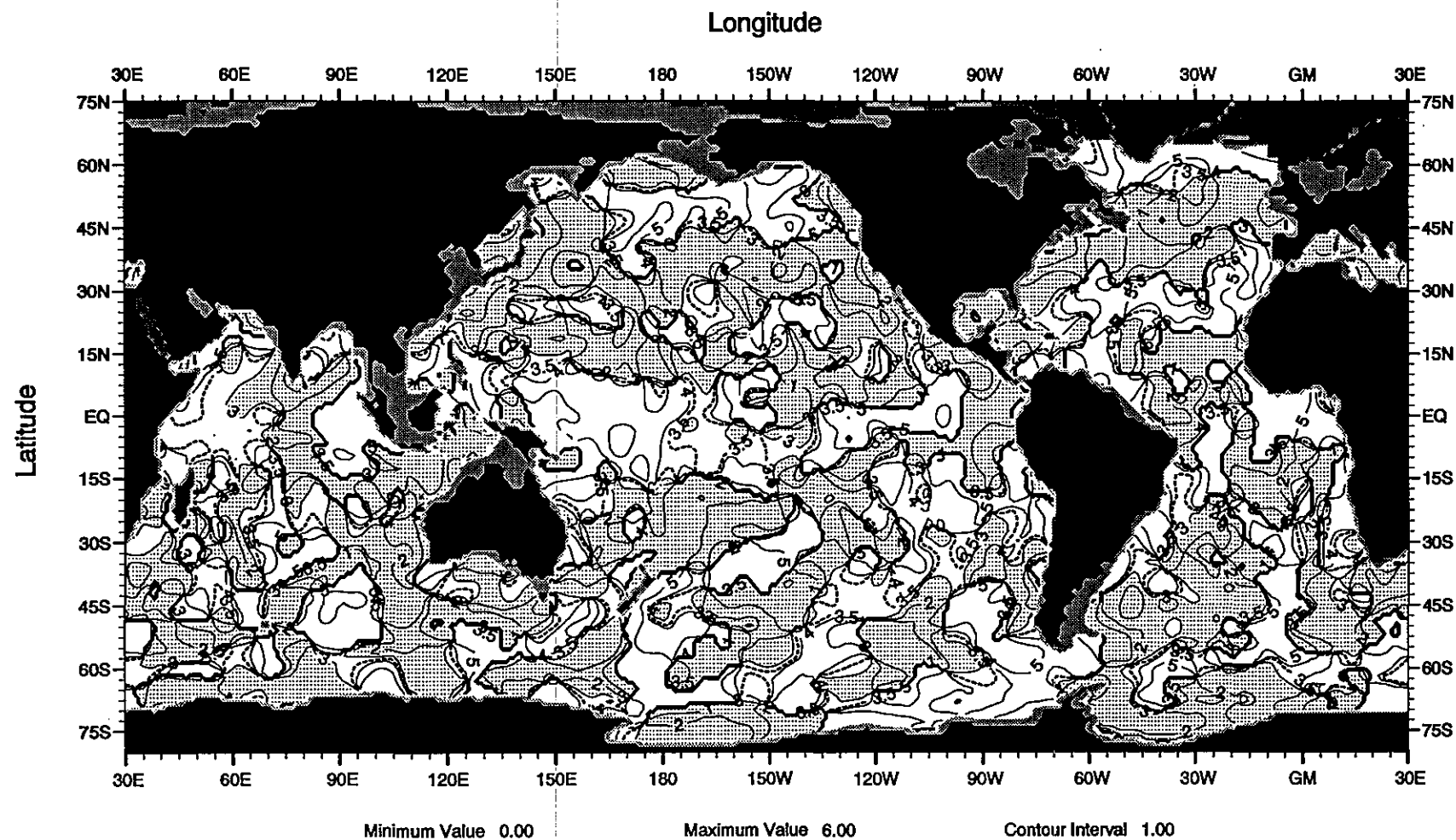


Fig. B75 Phase (months) of the 2nd harmonic of the annual temperature cycle at 200 m depth

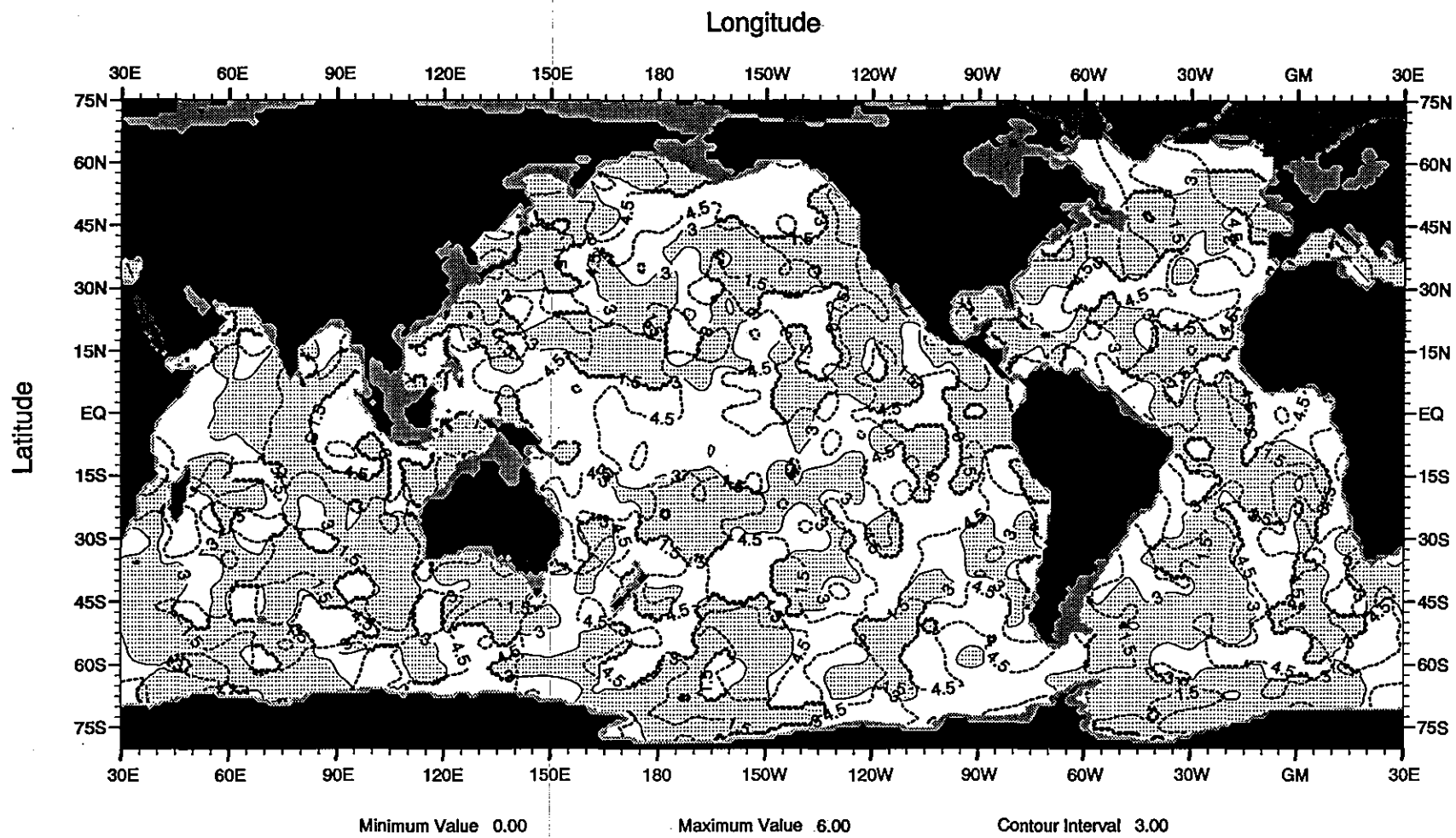


Fig. B76 Phase (months) of the 2nd harmonic of the annual temperature cycle at 250 m depth

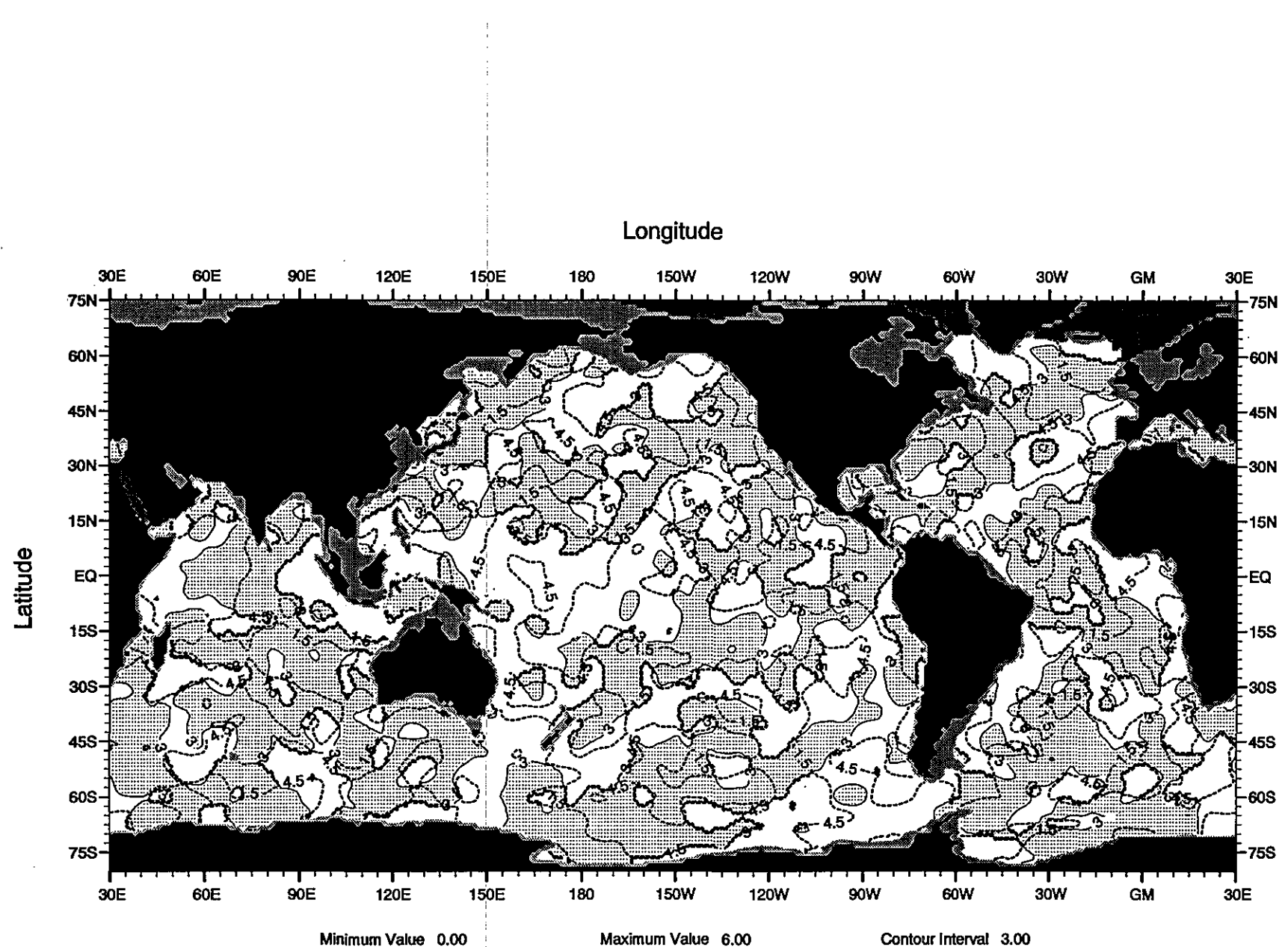


Fig. B77 Phase (months) of the 2nd harmonic of the annual temperature cycle at 300 m depth

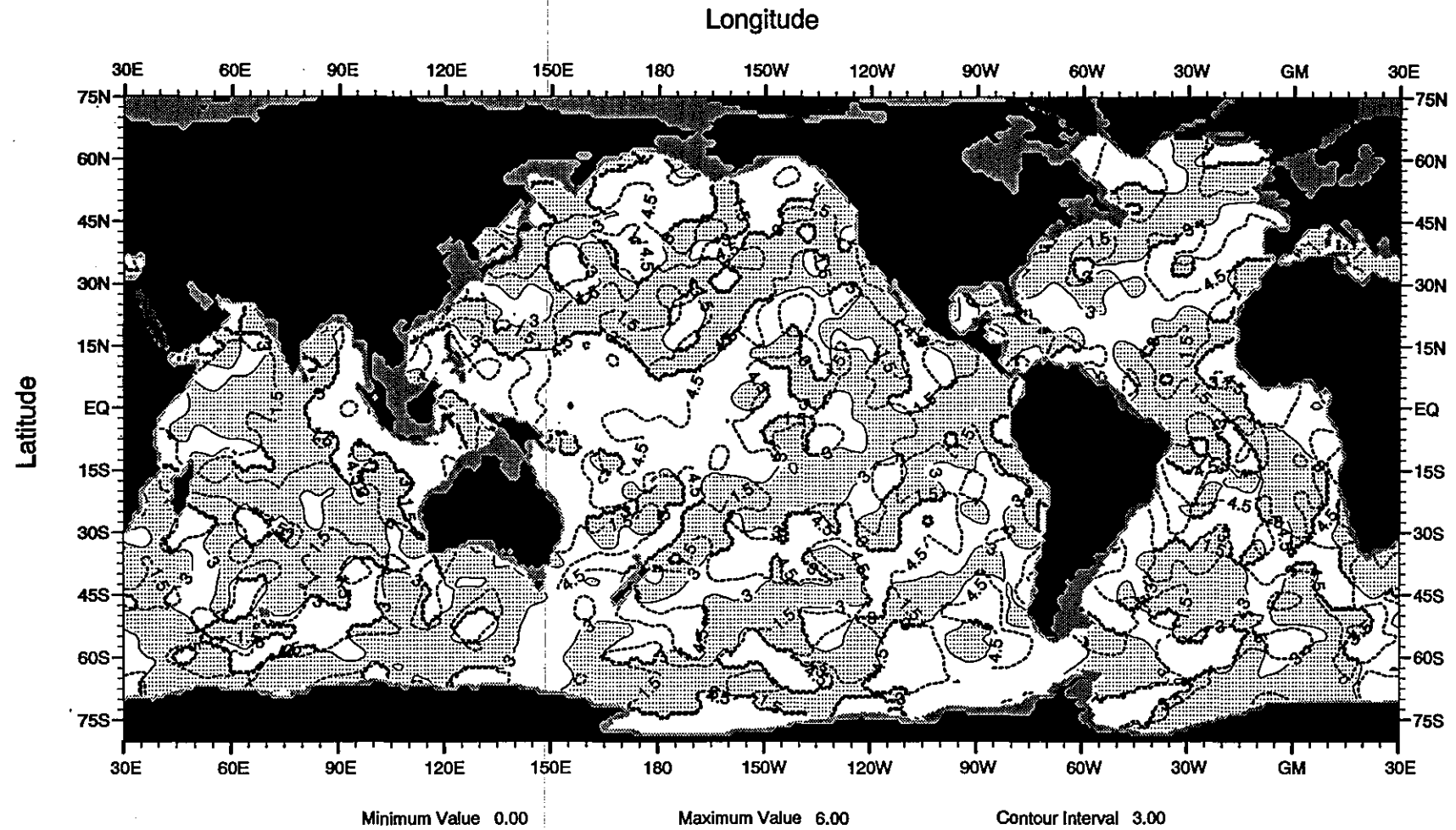


Fig. B78 Phase (months) of the 2nd harmonic of the annual temperature cycle at 400 m depth

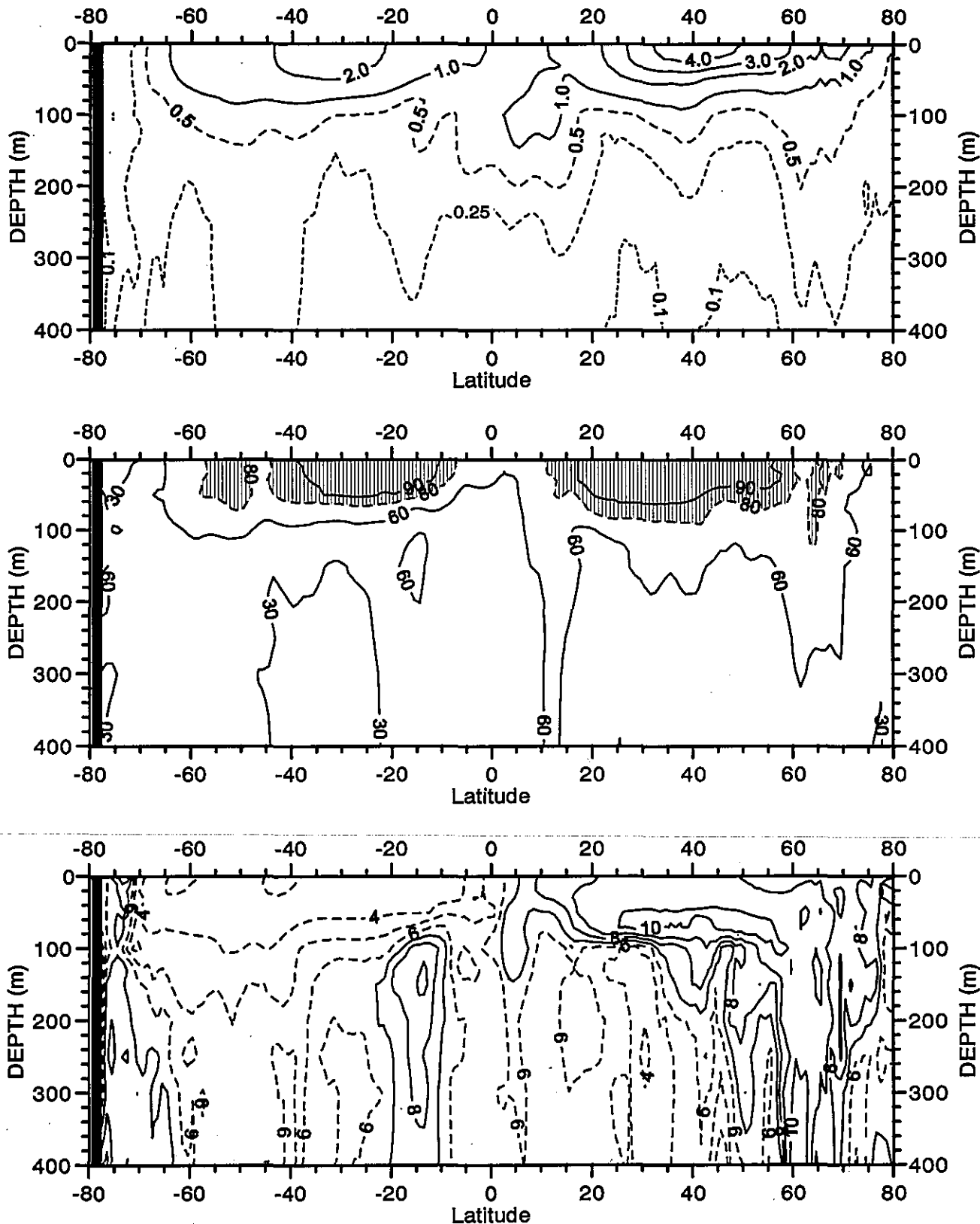


Fig. C1 Zonally averaged parameters of the 1ST harmonic of the annual temperature cycle for the World Ocean. Top panel is the amplitude ($^{\circ}\text{C}$), middle panel is the percent variance explained by this harmonic, and bottom panel is the phase (months).

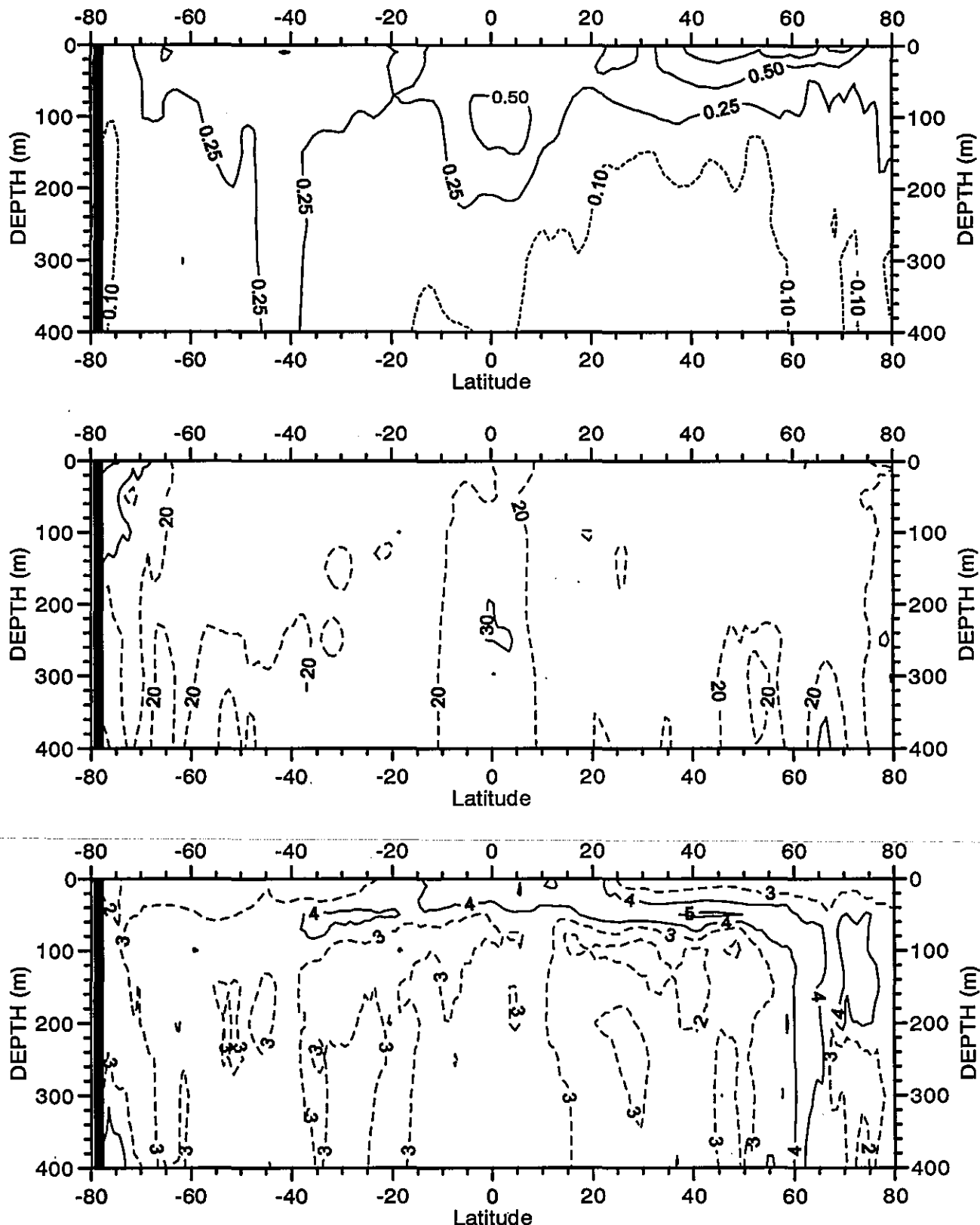


Fig. C2 Zonally averaged parameters of the 2ND harmonic of the annual temperature cycle for the World Ocean. Top panel is the amplitude ($^{\circ}\text{C}$), middle panel is the percent variance explained by this harmonic, and bottom panel is the phase (months)

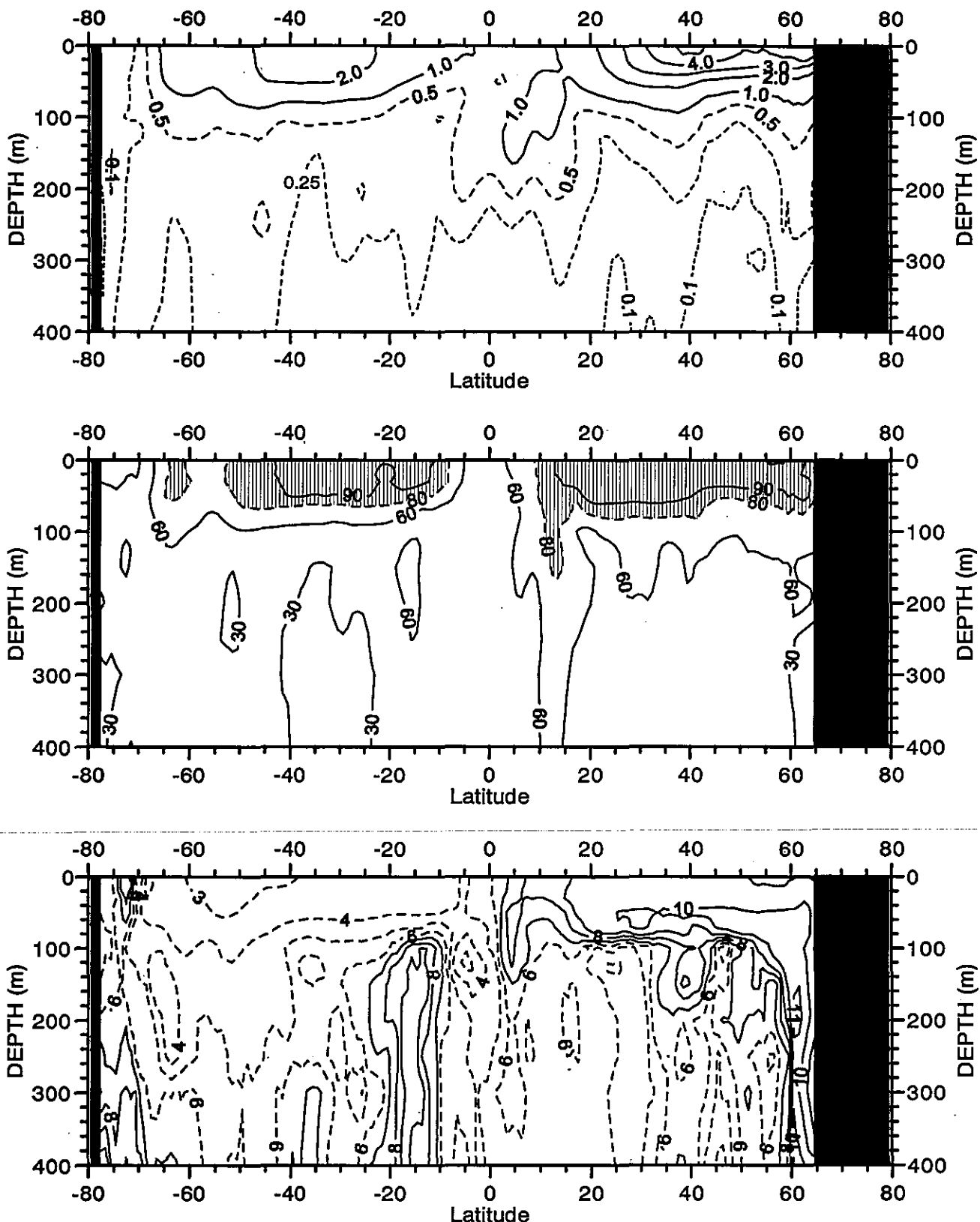


Fig. C3 Zonally averaged parameters of the 1ST harmonic of the annual temperature cycle for the Pacific Ocean. Top panel is the amplitude ($^{\circ}\text{C}$), middle panel is the percent variance explained by this harmonic, and bottom panel is the phase (months)

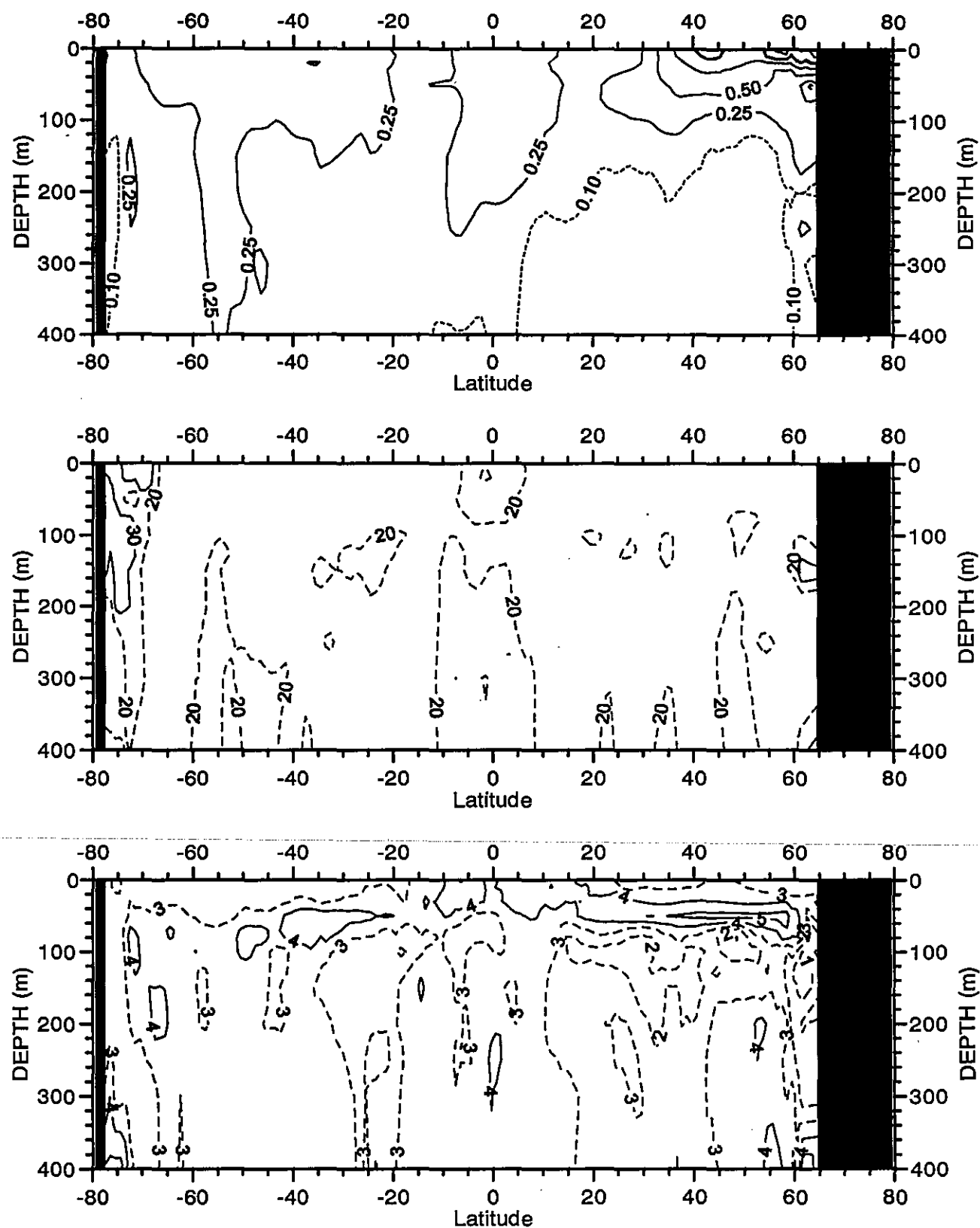


Fig. C4 Zonally averaged parameters of the 2ND harmonic of the annual temperature cycle for the Pacific Ocean. Top panel is the amplitude ($^{\circ}\text{C}$), middle panel is the percent variance explained by this harmonic, and bottom panel is the phase (months)

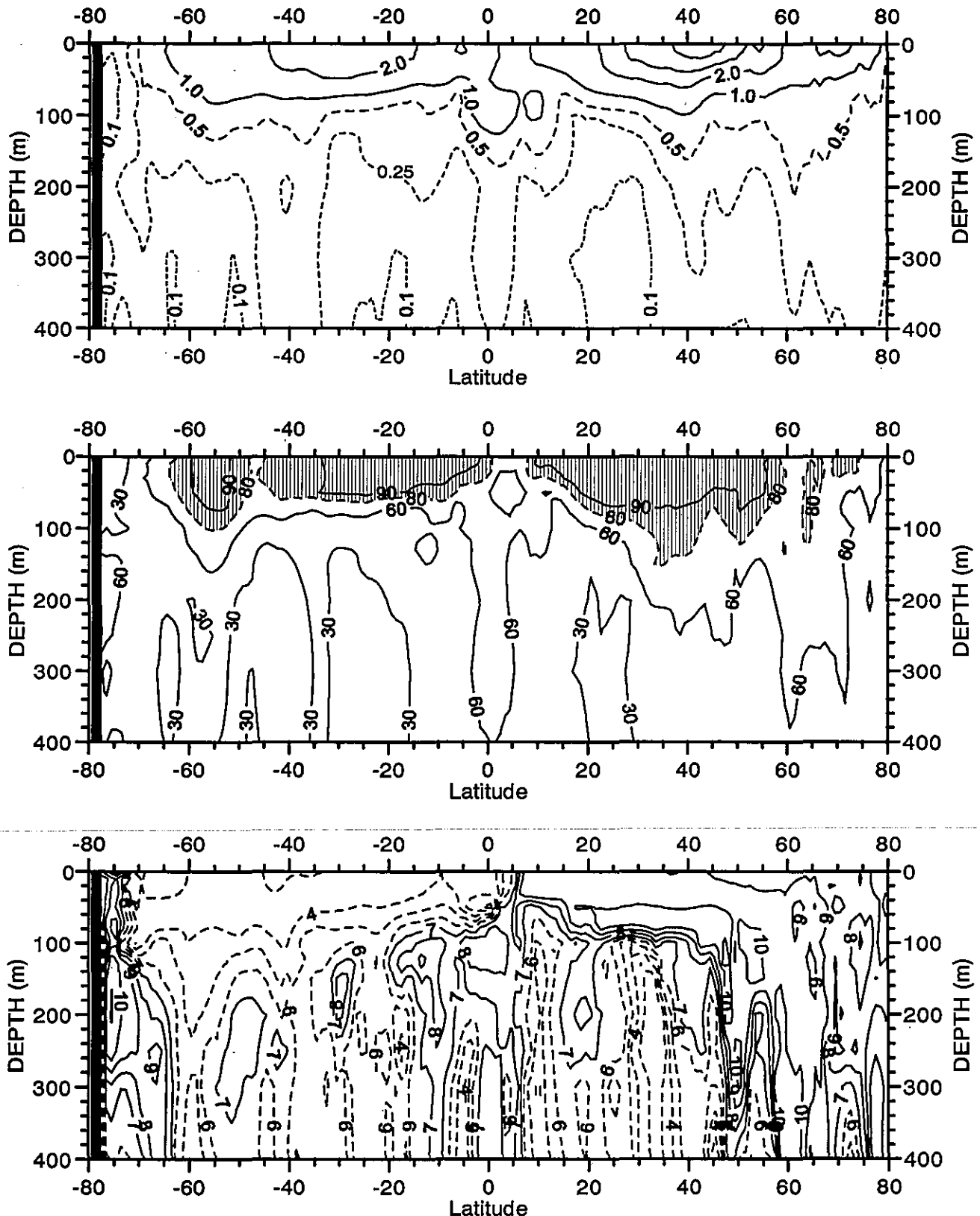


Fig. C5 Zonally averaged parameters of the 1ST harmonic of the annual temperature cycle for the Atlantic Ocean. Top panel is the amplitude ($^{\circ}\text{C}$), middle panel is the percent variance explained by this harmonic, and bottom panel is the phase (months)

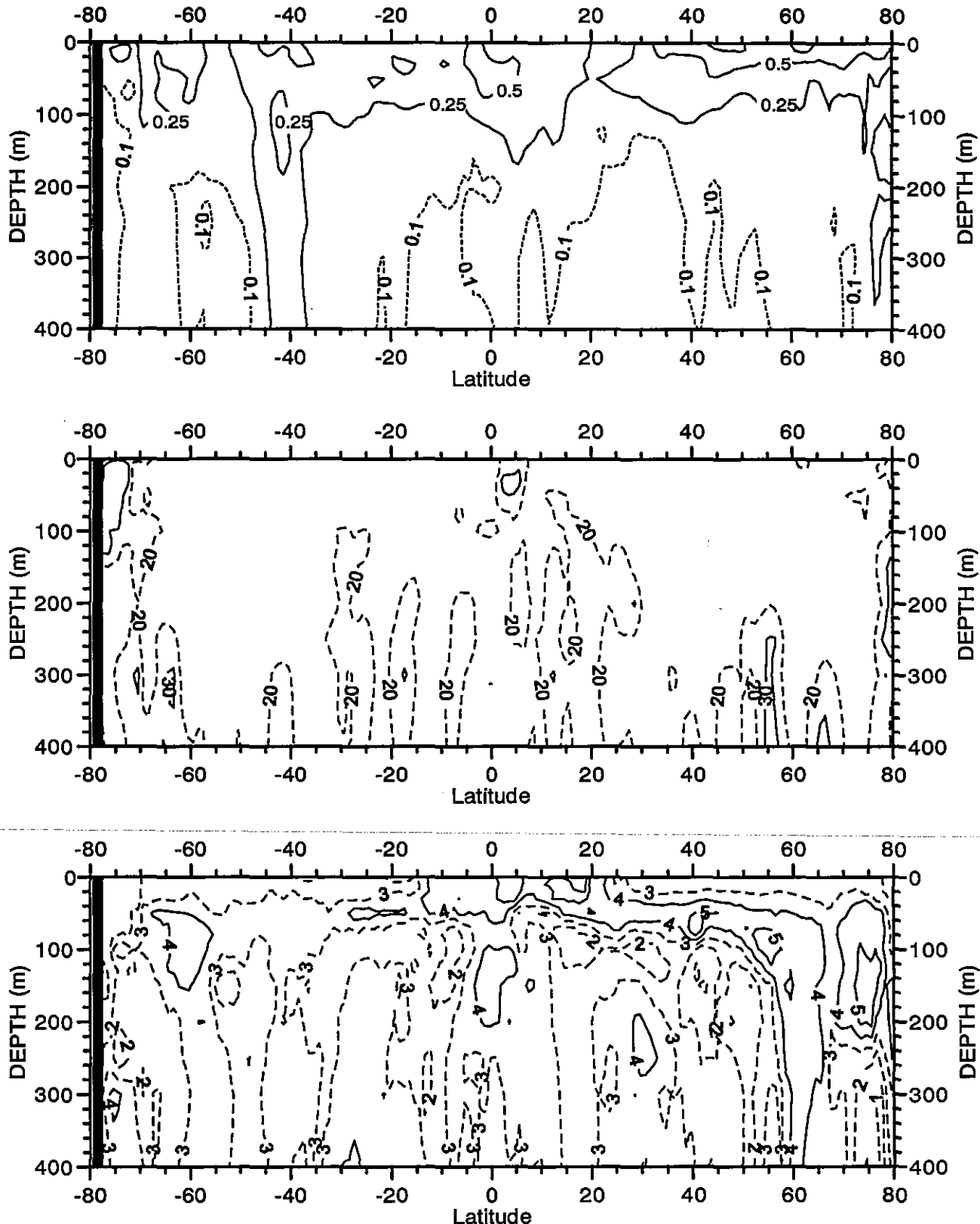


Fig. C6 Zonally averaged parameters of the 2ND harmonic of the annual temperature cycle for the Atlantic Ocean. Top panel is the amplitude ($^{\circ}\text{C}$), middle panel is the percent variance explained by this harmonic, and bottom panel is the phase (months)

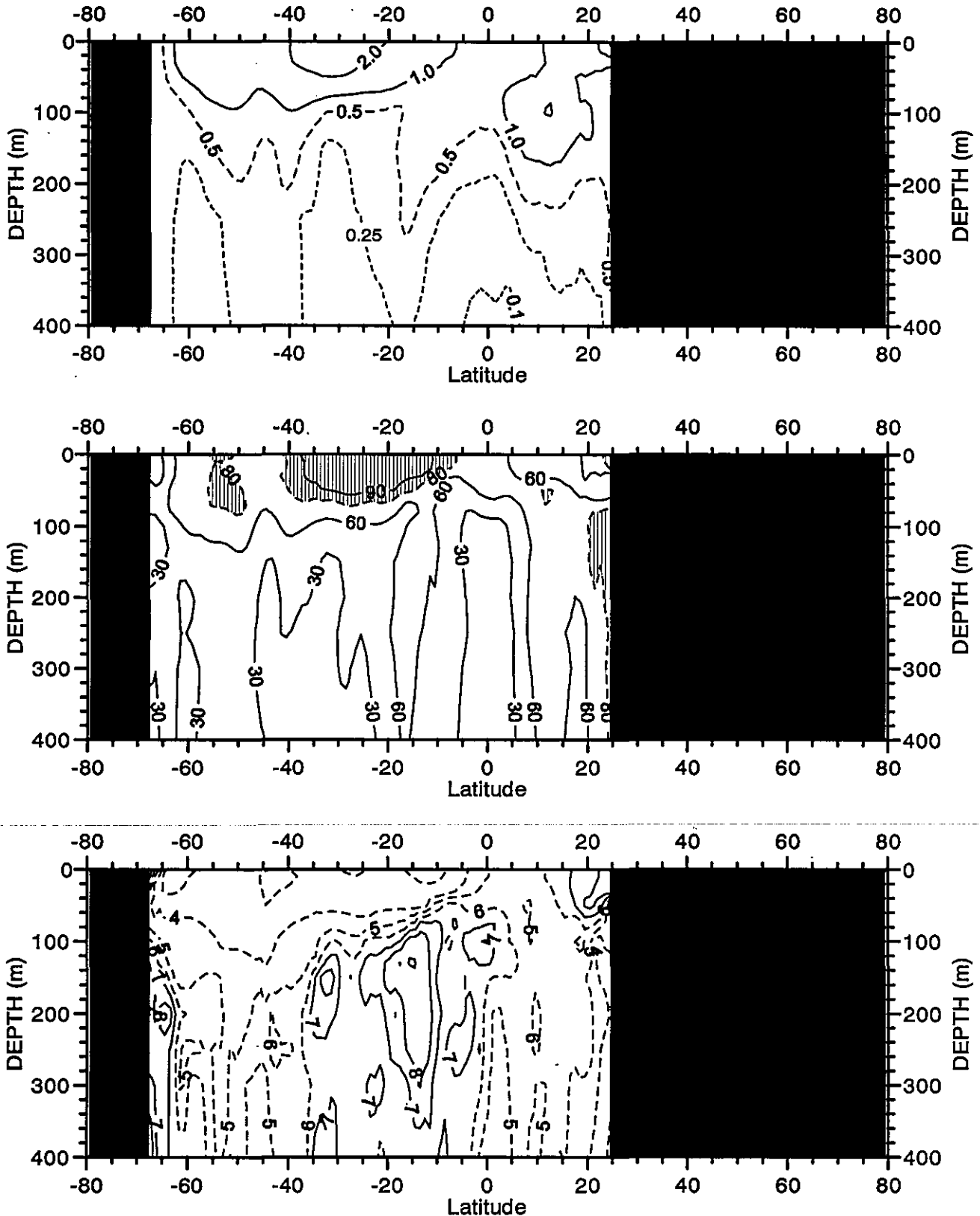


Fig. C7 Zonally averaged parameters of the 1ST harmonic of the annual temperature cycle for the Indian Ocean. Top panel is the amplitude ($^{\circ}\text{C}$), middle panel is the percent variance explained by this harmonic, and bottom panel is the phase (months)

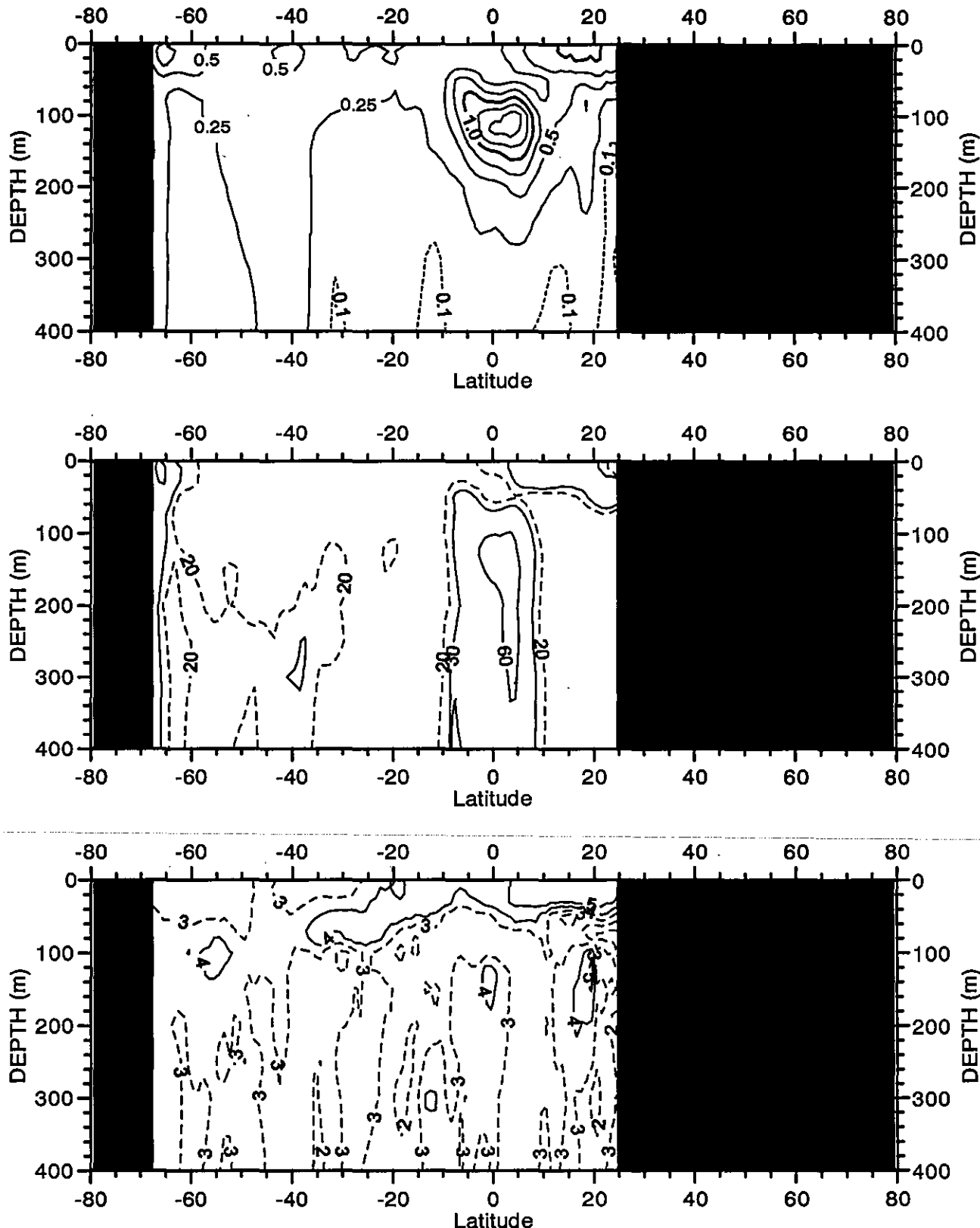


Fig. C8 Zonally averaged parameters of the 2ND harmonic of the annual temperature cycle for the Indian Ocean. Top panel is the amplitude ($^{\circ}\text{C}$), middle panel is the percent variance explained by this harmonic, and bottom panel is the phase (months)

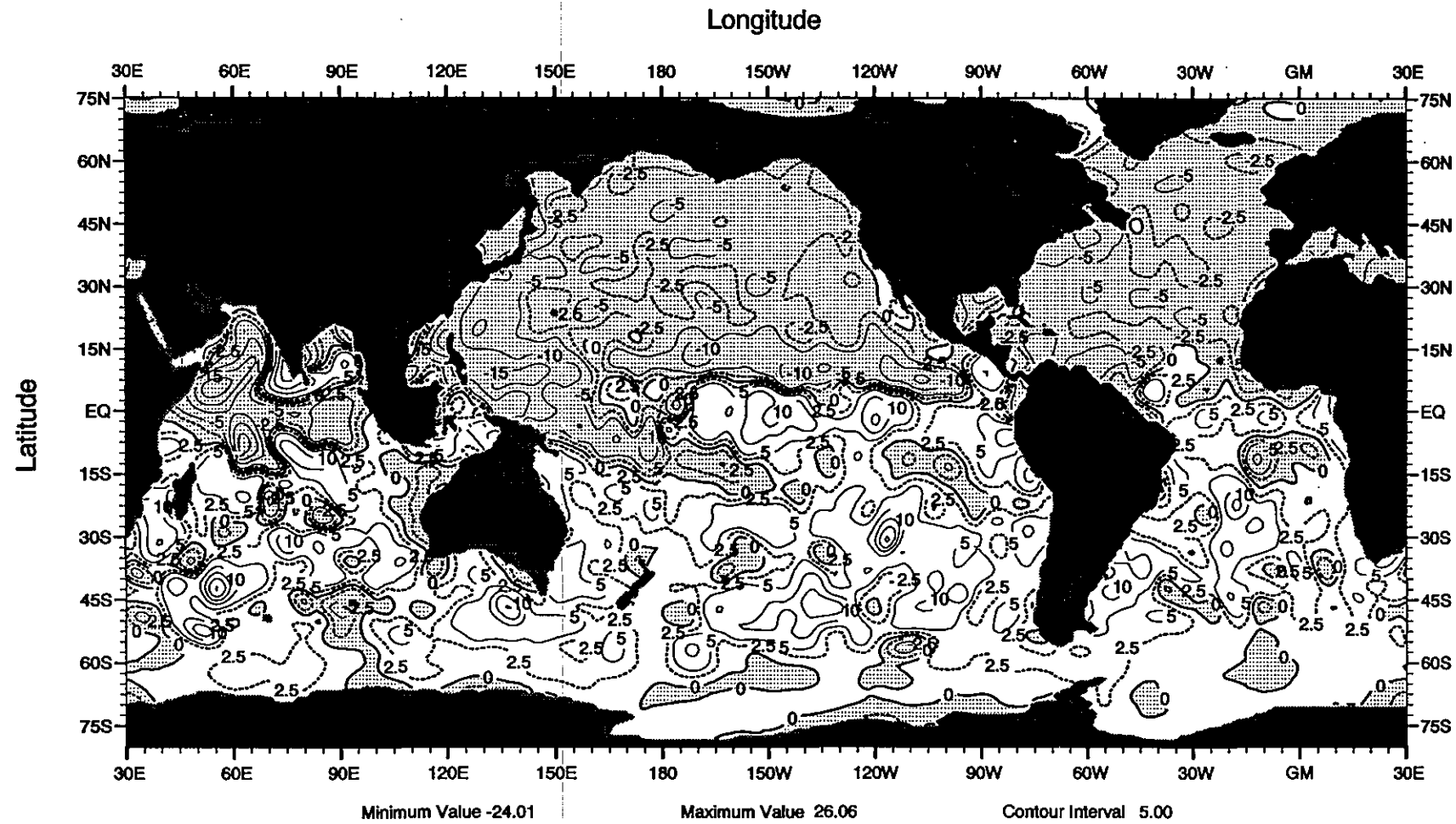


Fig.D1 January heat storage (10^{18} J) integrated through 275 m depth

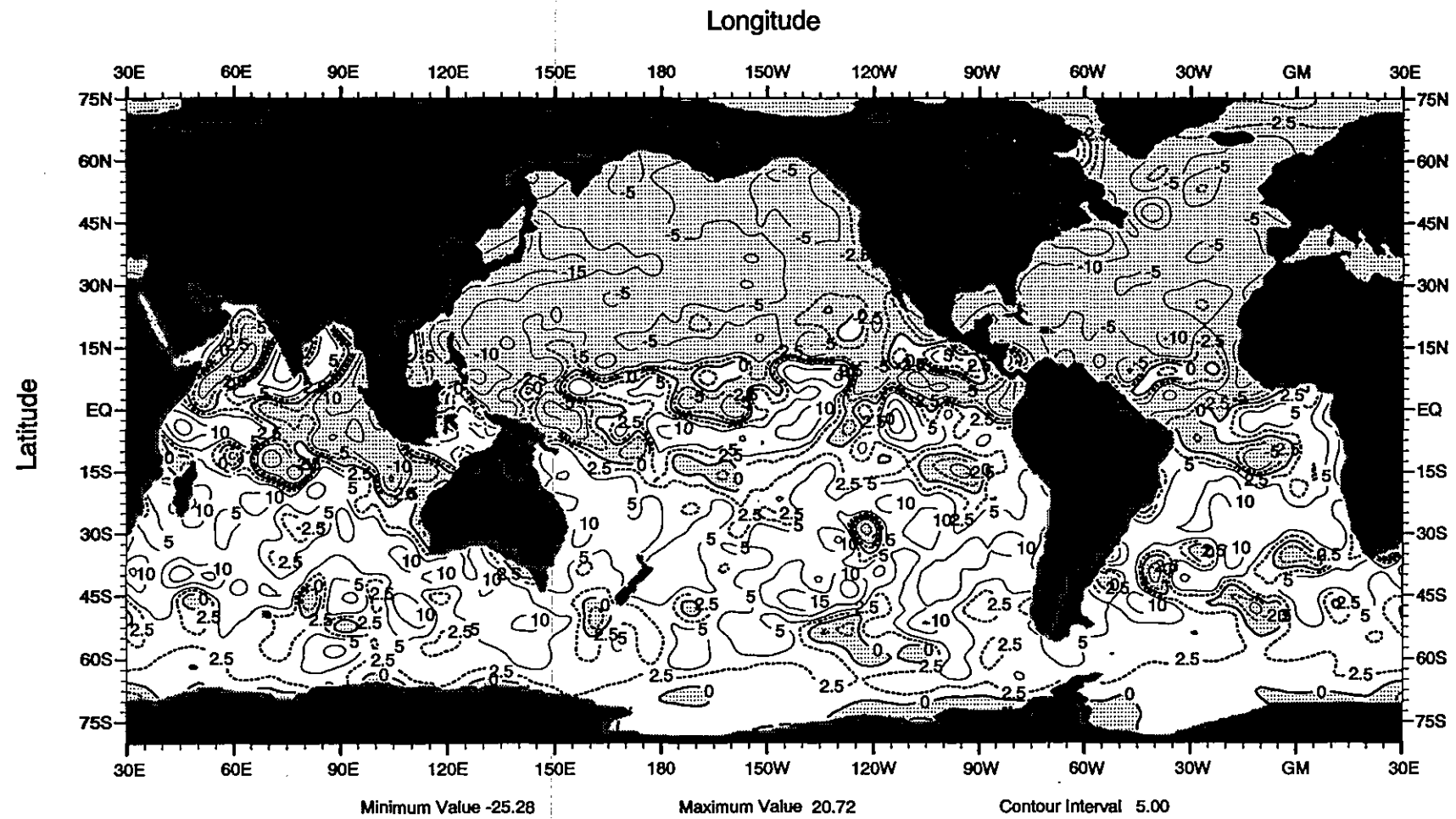


Fig.D2 February heat storage (10^{18} J) integrated through 275 m depth

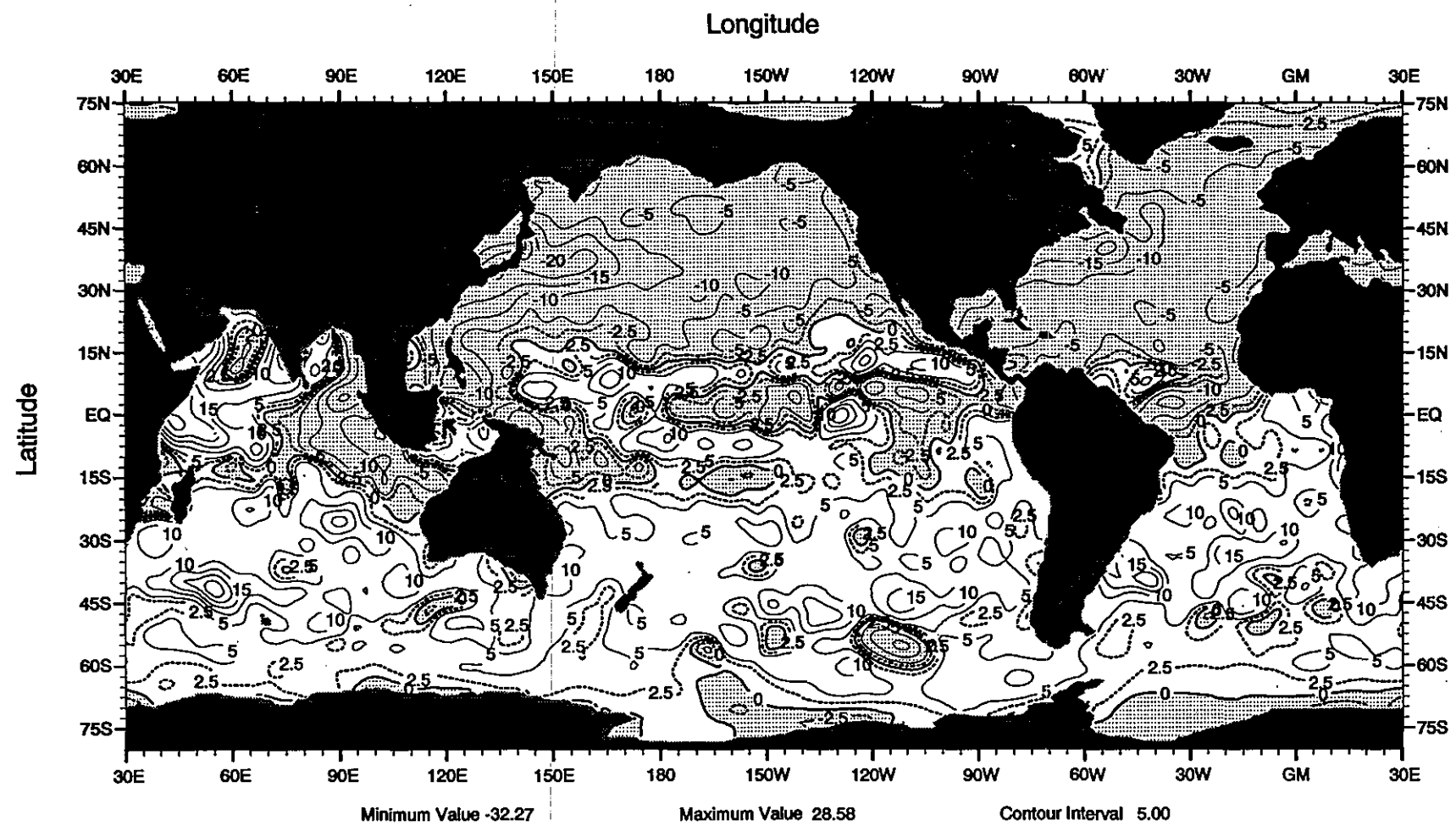


Fig.D3 March heat storage (10^{18} J) integrated through 275 m depth

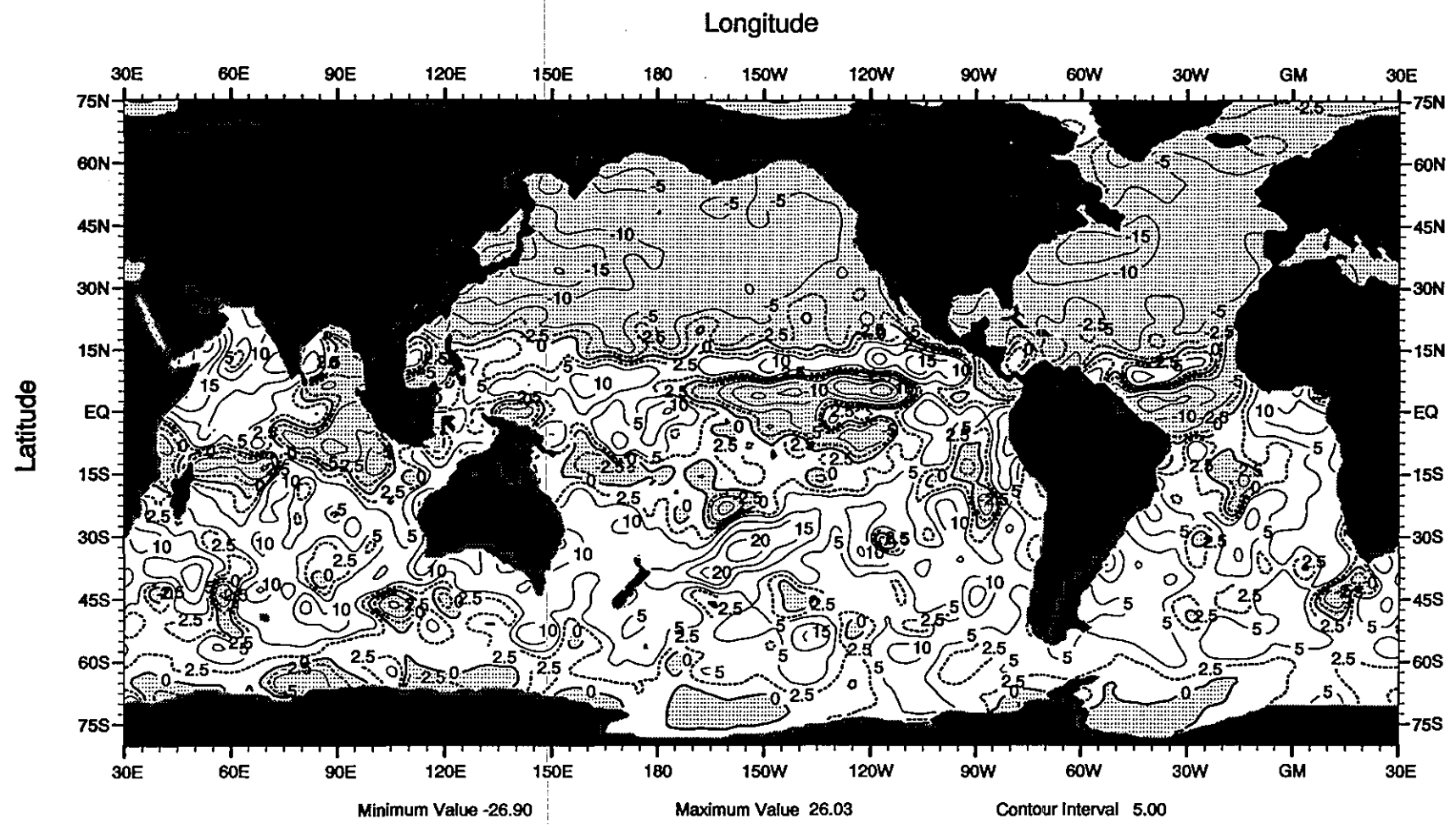


Fig.D4 April heat storage (10^{18} J) integrated through 275 m depth

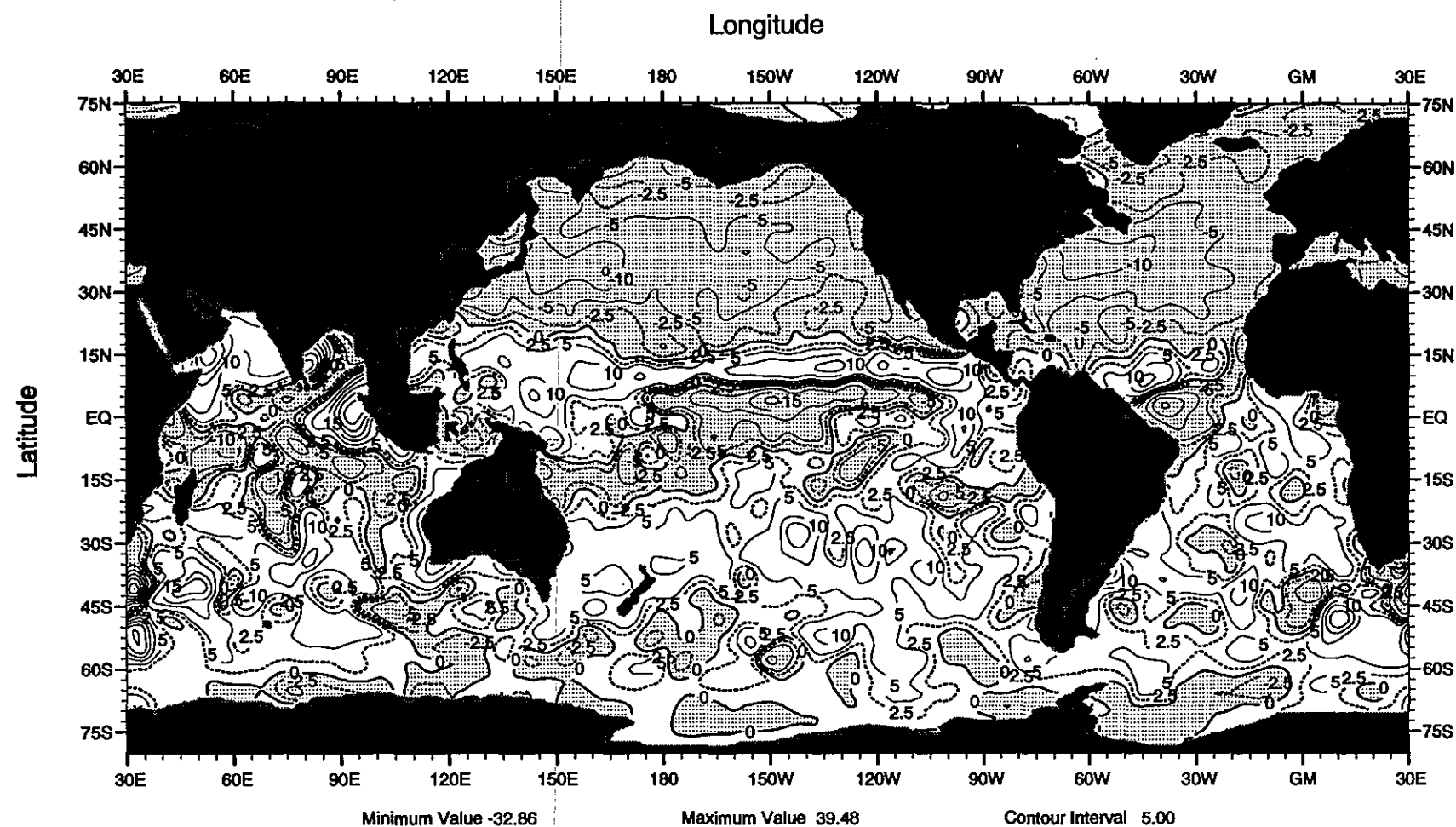


Fig.D5 May heat storage (10^{18} J) integrated through 275 m depth

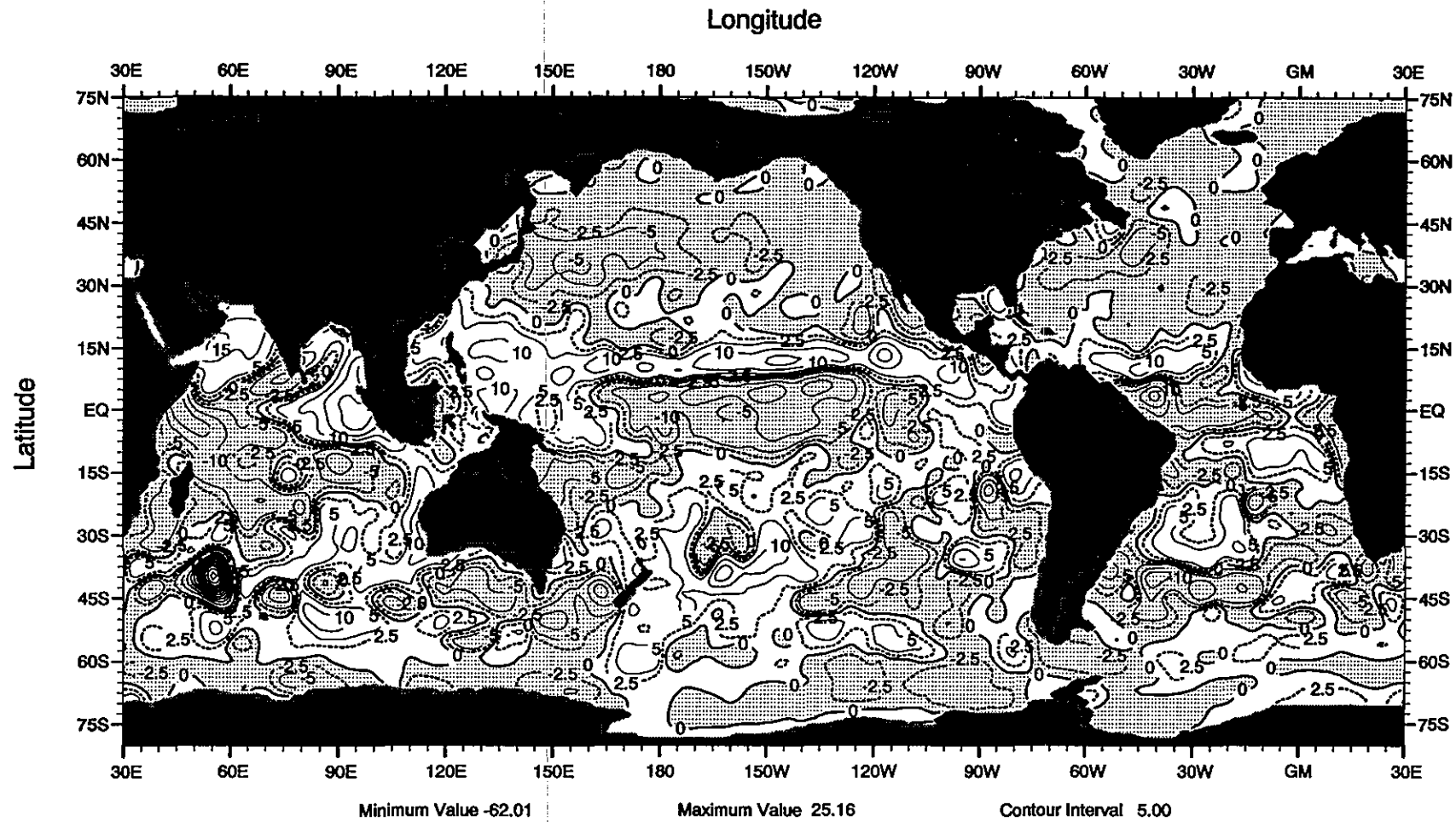


Fig.D6 June heat storage (10^{18} J) integrated through 275 m depth

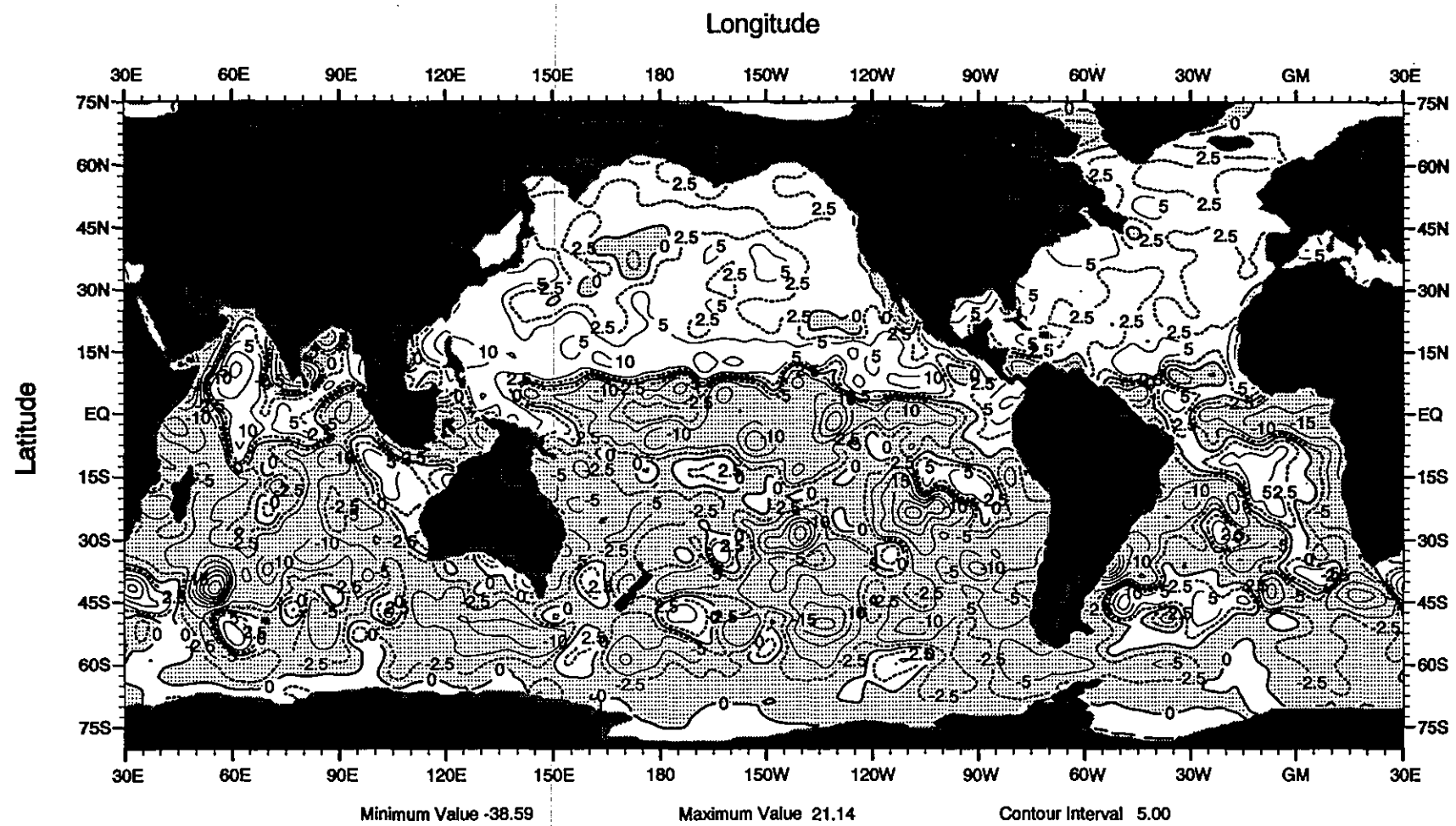


Fig.D7 July heat storage (10^{18} J) integrated through 275 m depth

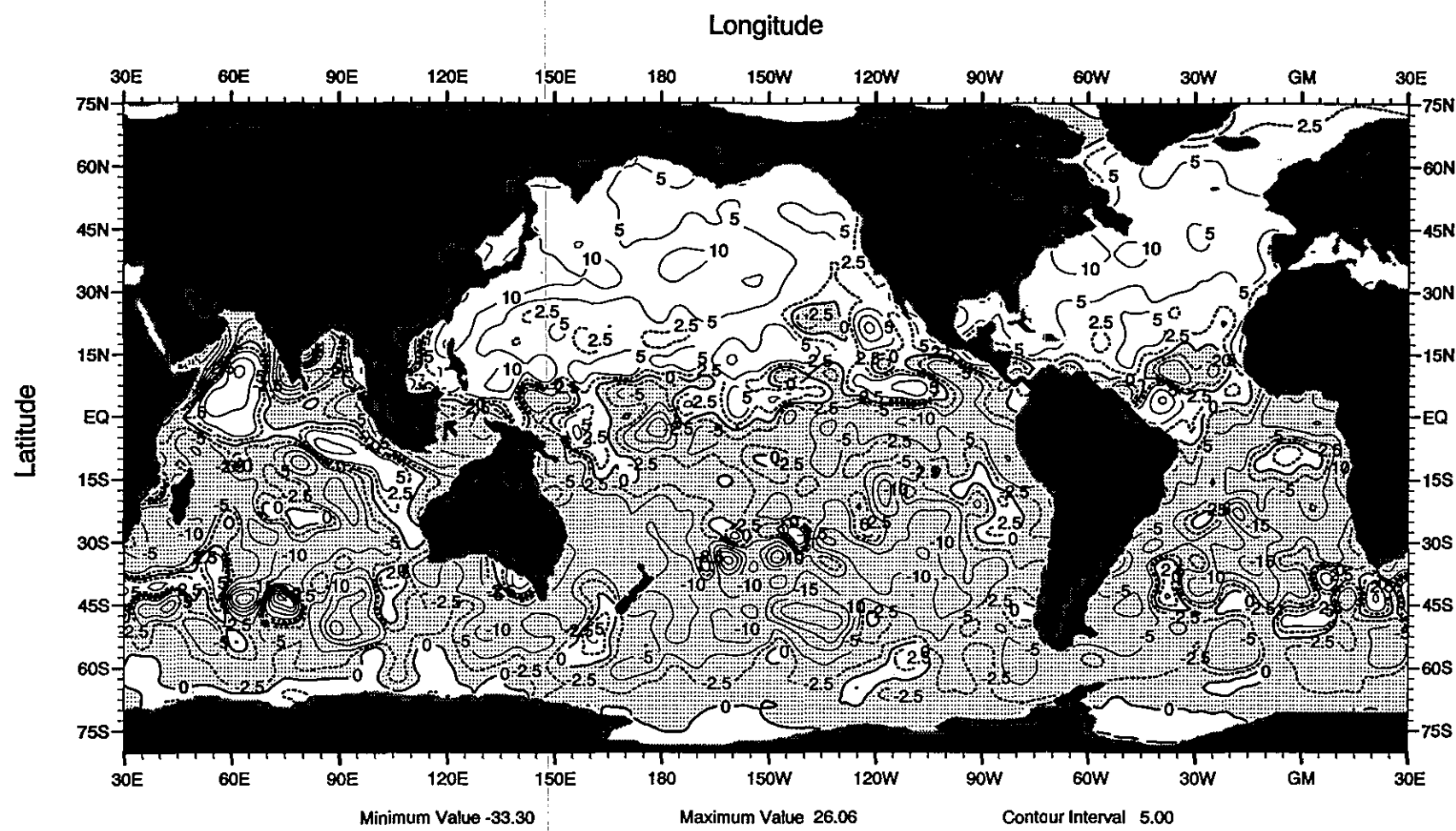


Fig.D8 August heat storage (10^{18} J) integrated through 275 m depth

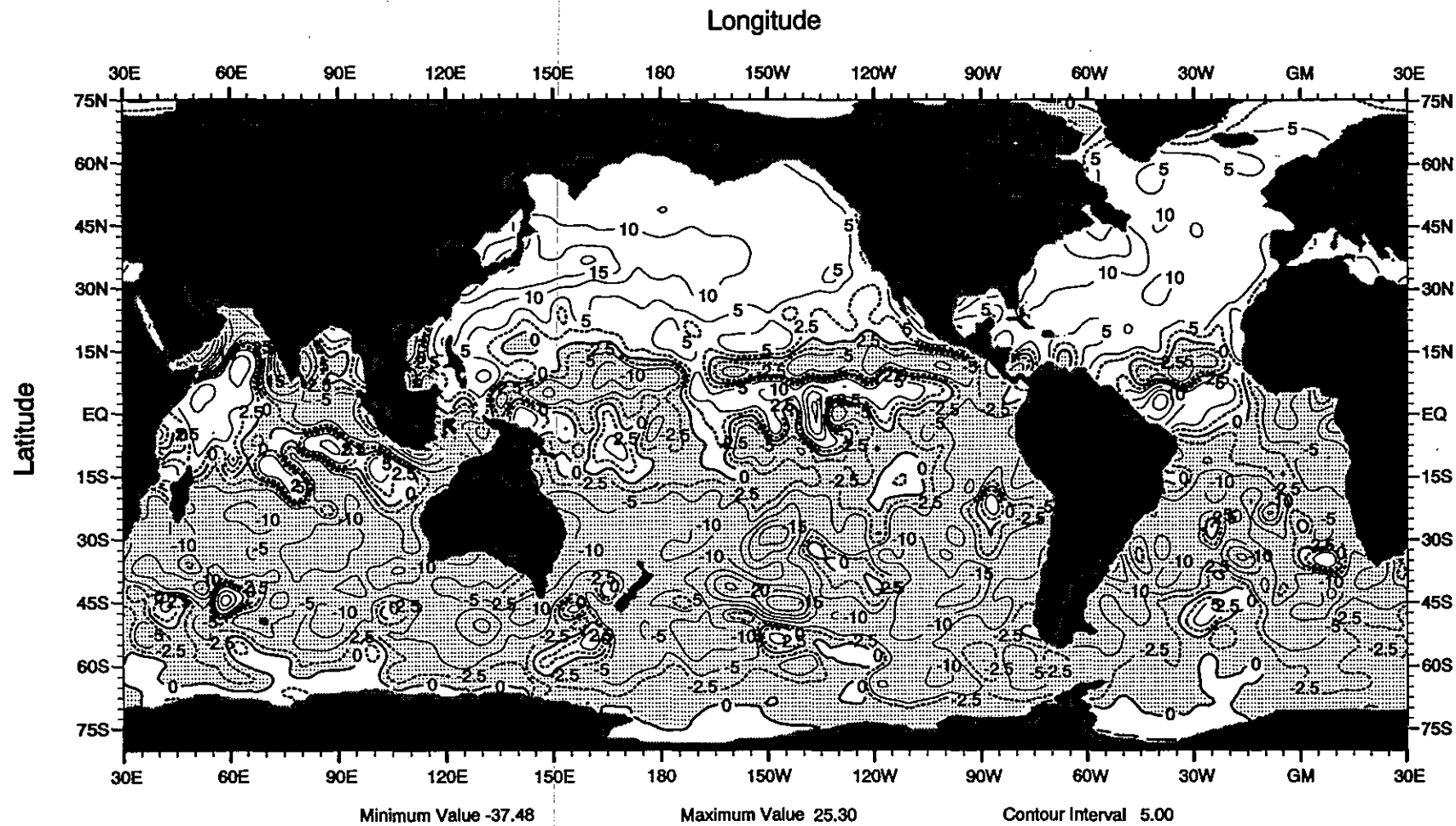


Fig.D9 September heat storage (10^{18} J) integrated through 275 m depth

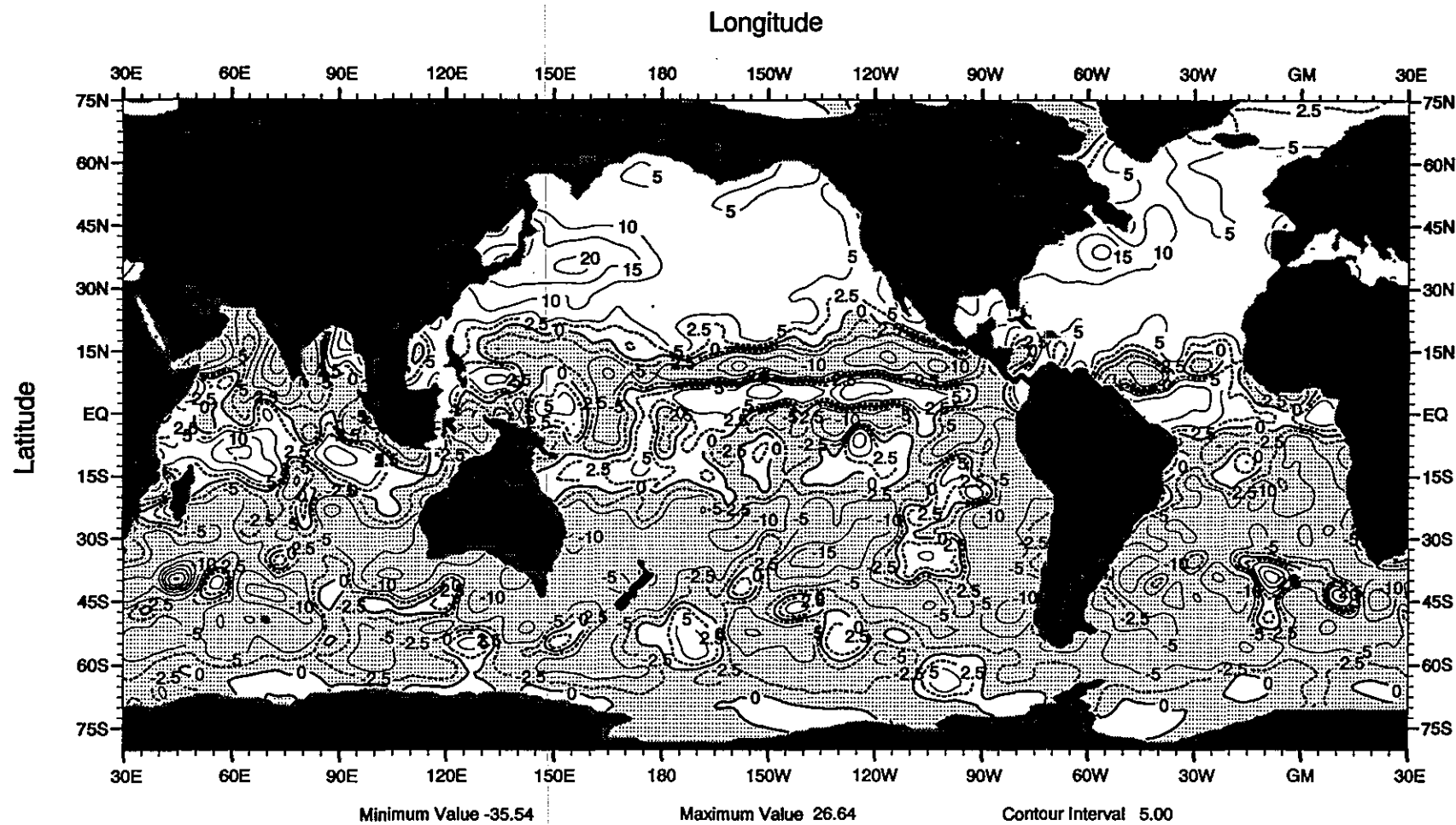


Fig.D10 October heat storage (10^{16} J) integrated through 275 m depth

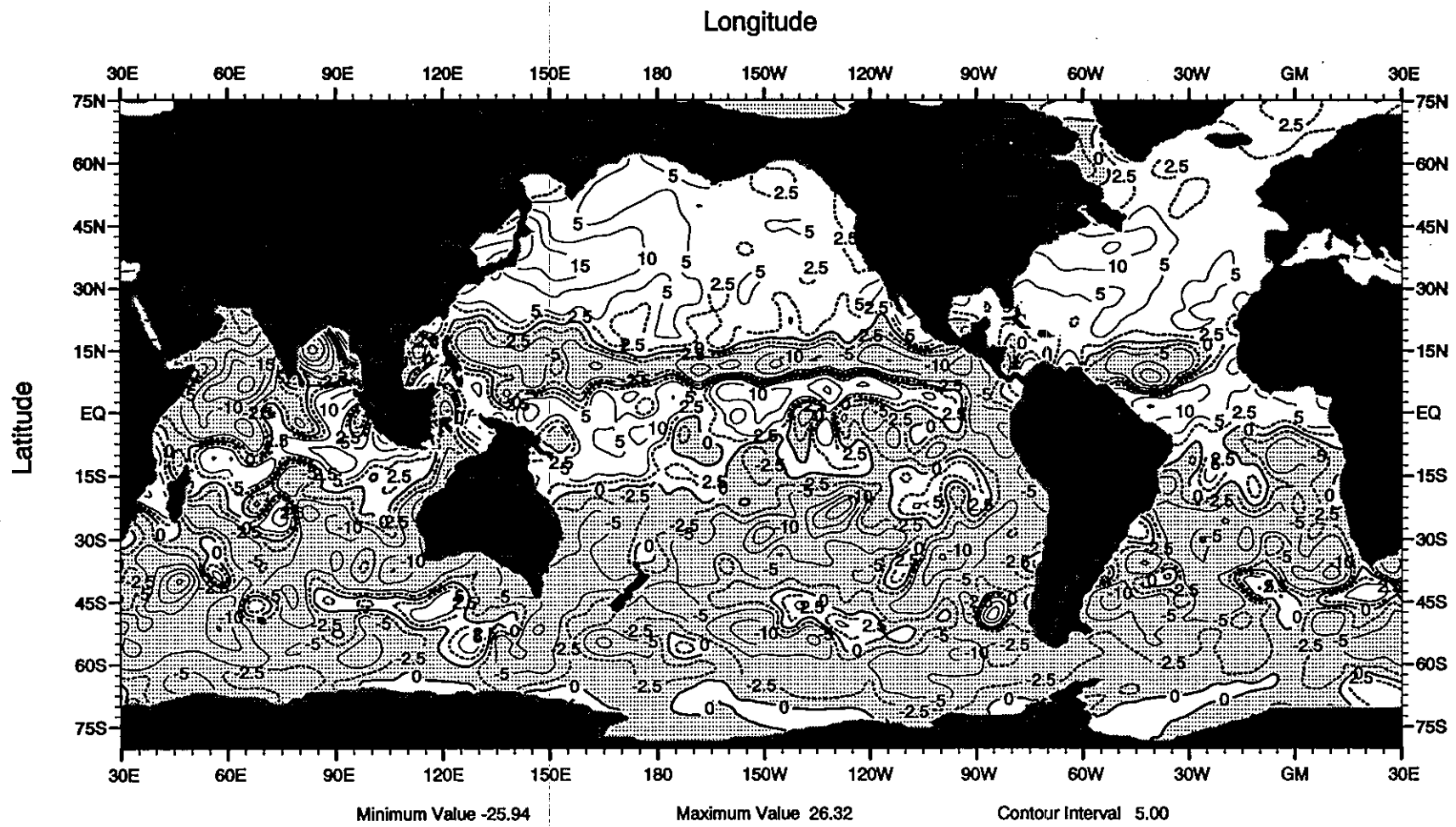


Fig.D11 November heat storage (10^{18} J) integrated through 275 m depth

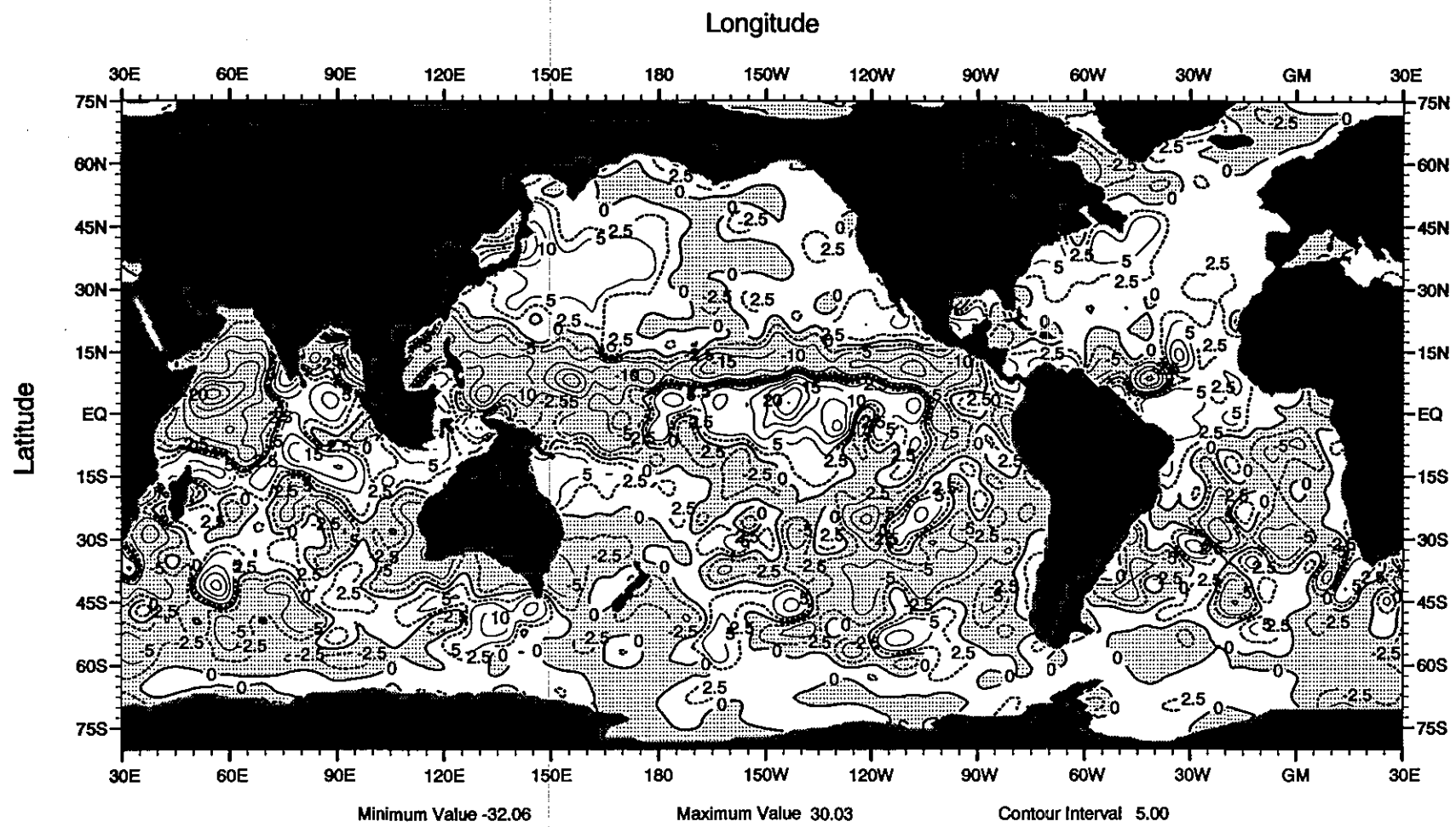


Fig.D12 December heat storage (10^{18} J) integrated through 275 m depth

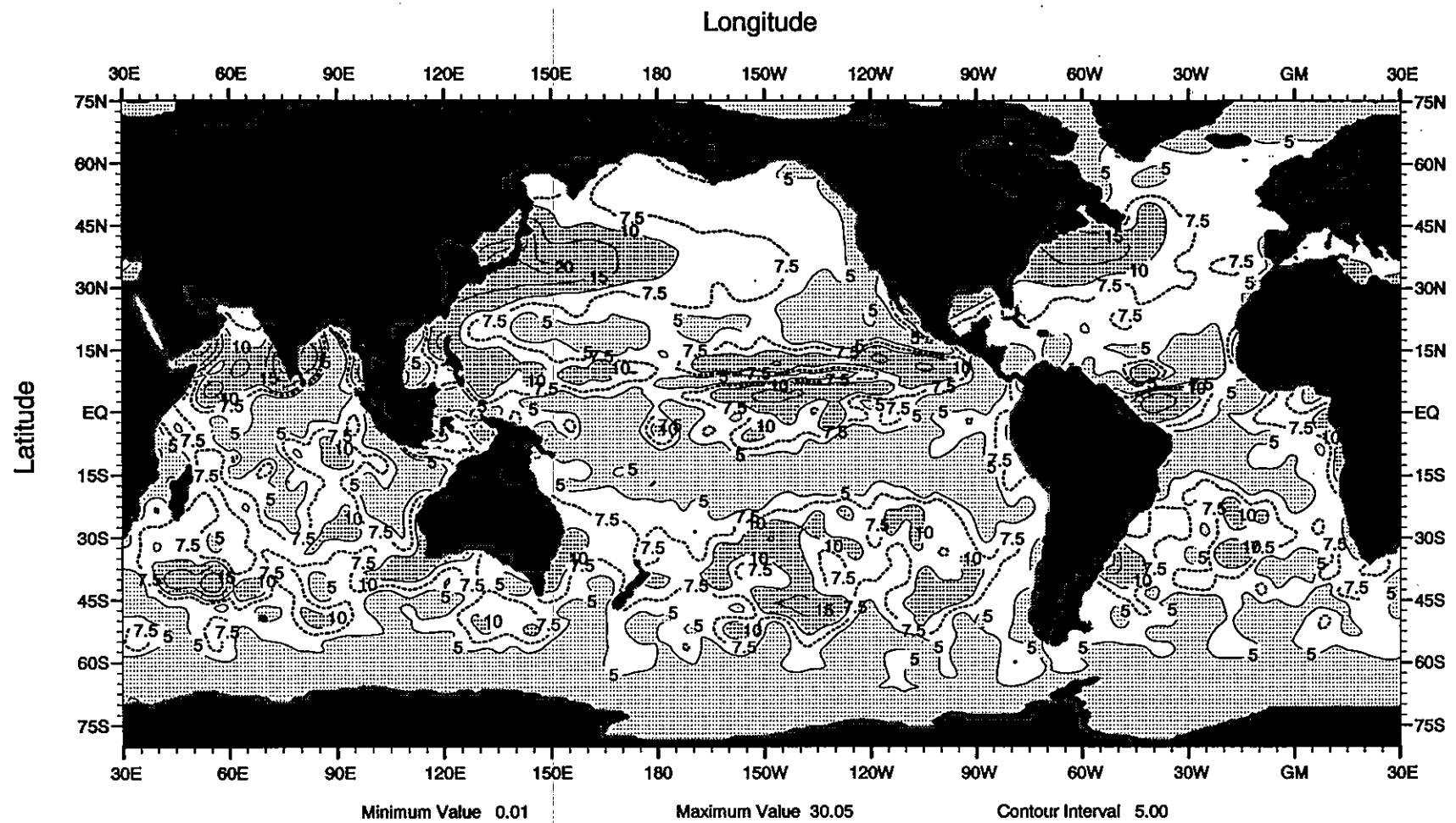


Fig.D13 Amplitude (10^{18} J) of 1st harmonic of the annual cycle of
heat storage for the 0-275 m layer

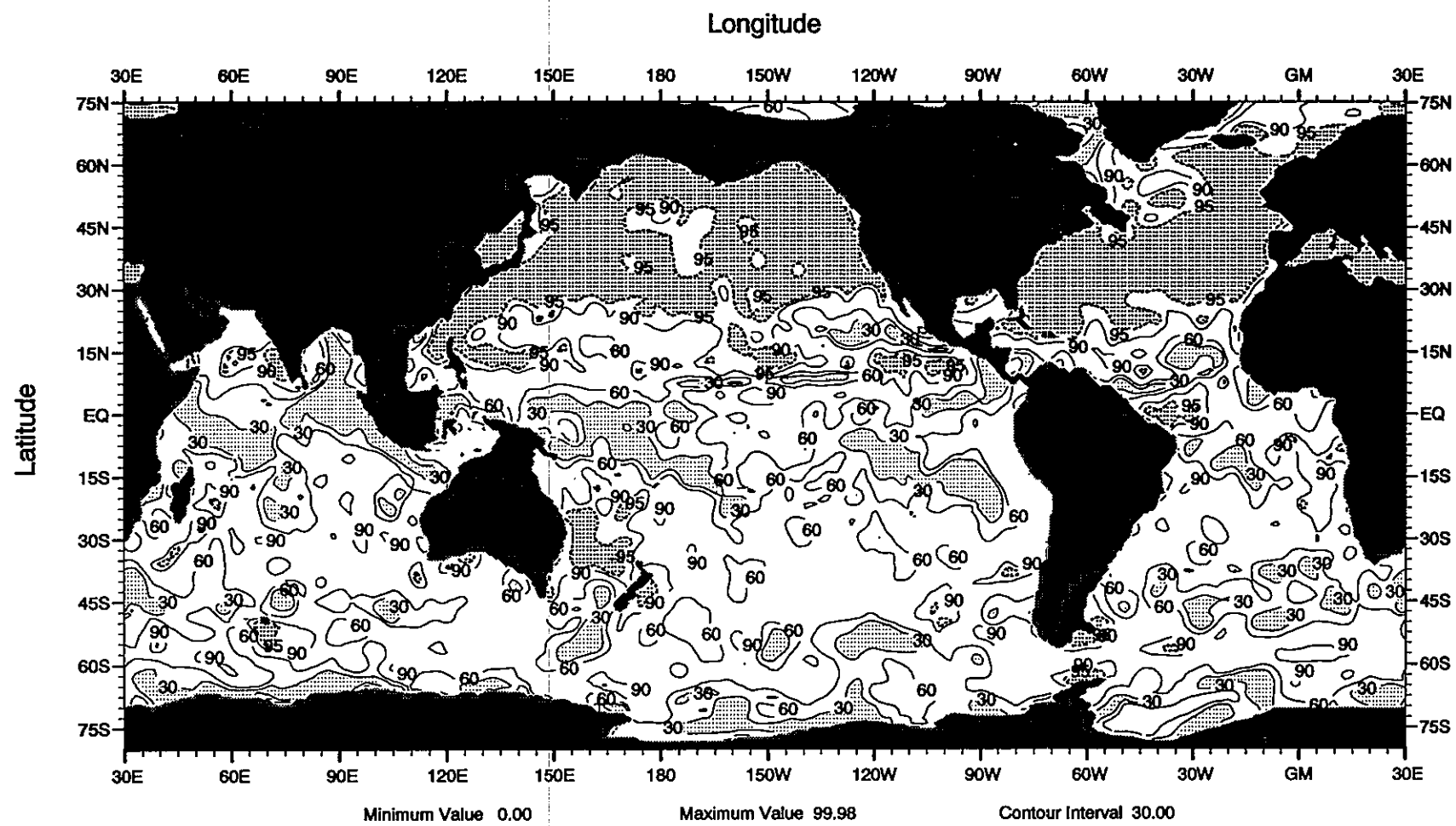


Fig.D14 Percent variance explained by 1st harmonic of the annual cycle of
heat storage for the 0-275 m layer

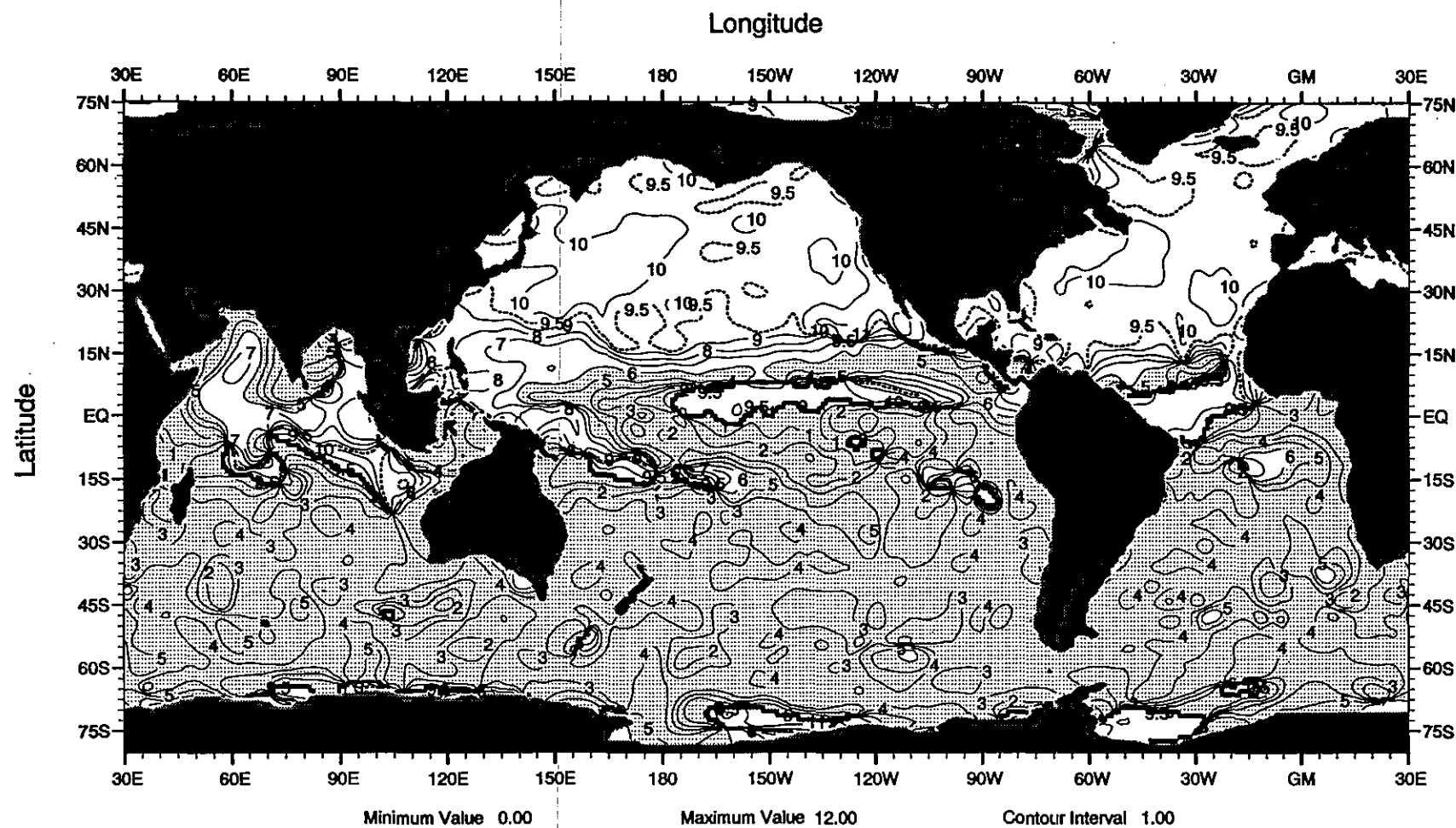


Fig.D15 Phase (months) of 1st harmonic of the annual cycle of
heat storage for the 0-275 m layer

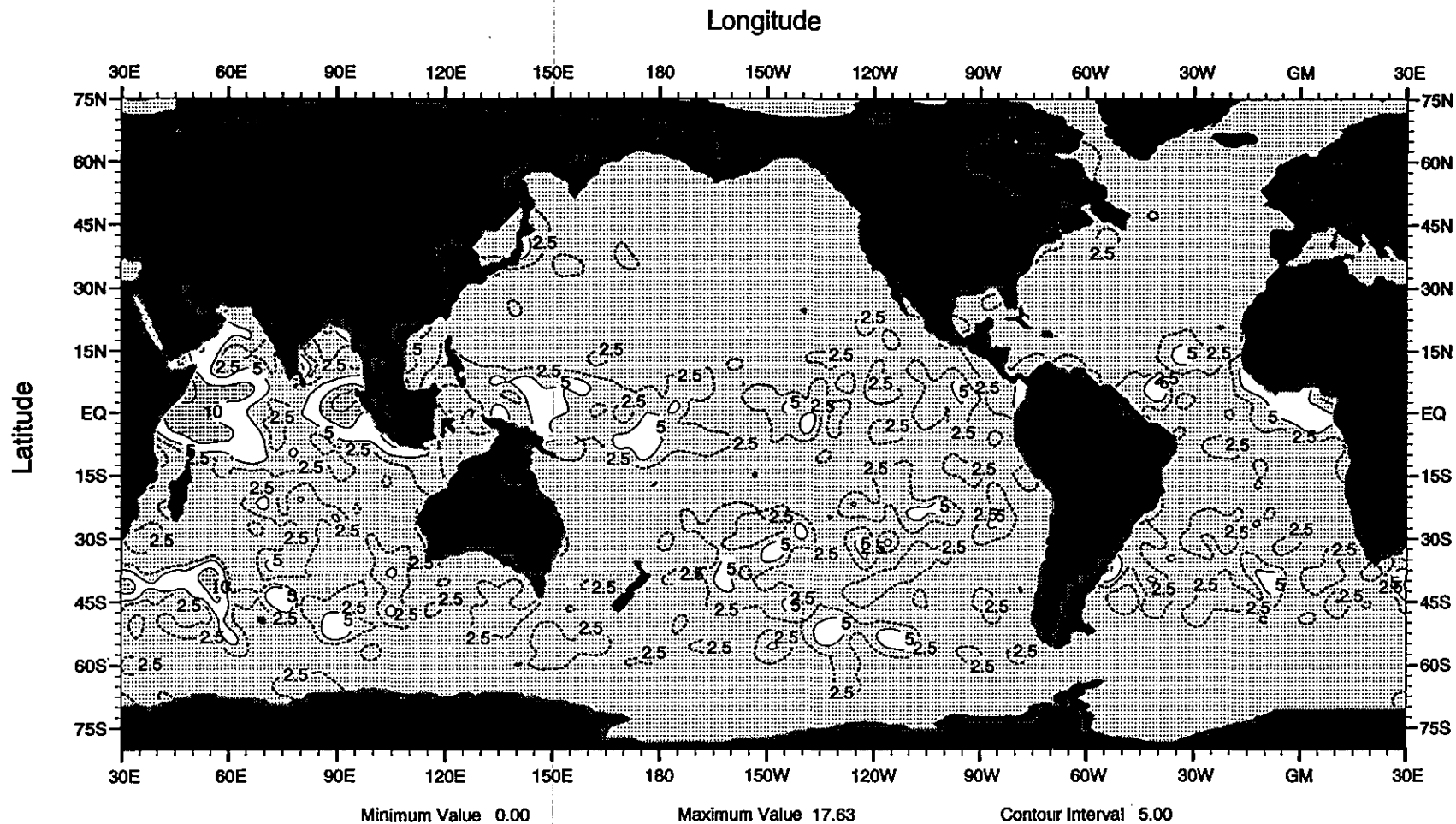


Fig.D16 Amplitude (10^{18} J) of 2nd harmonic of the annual cycle of
heat storage for the 0-275 m layer

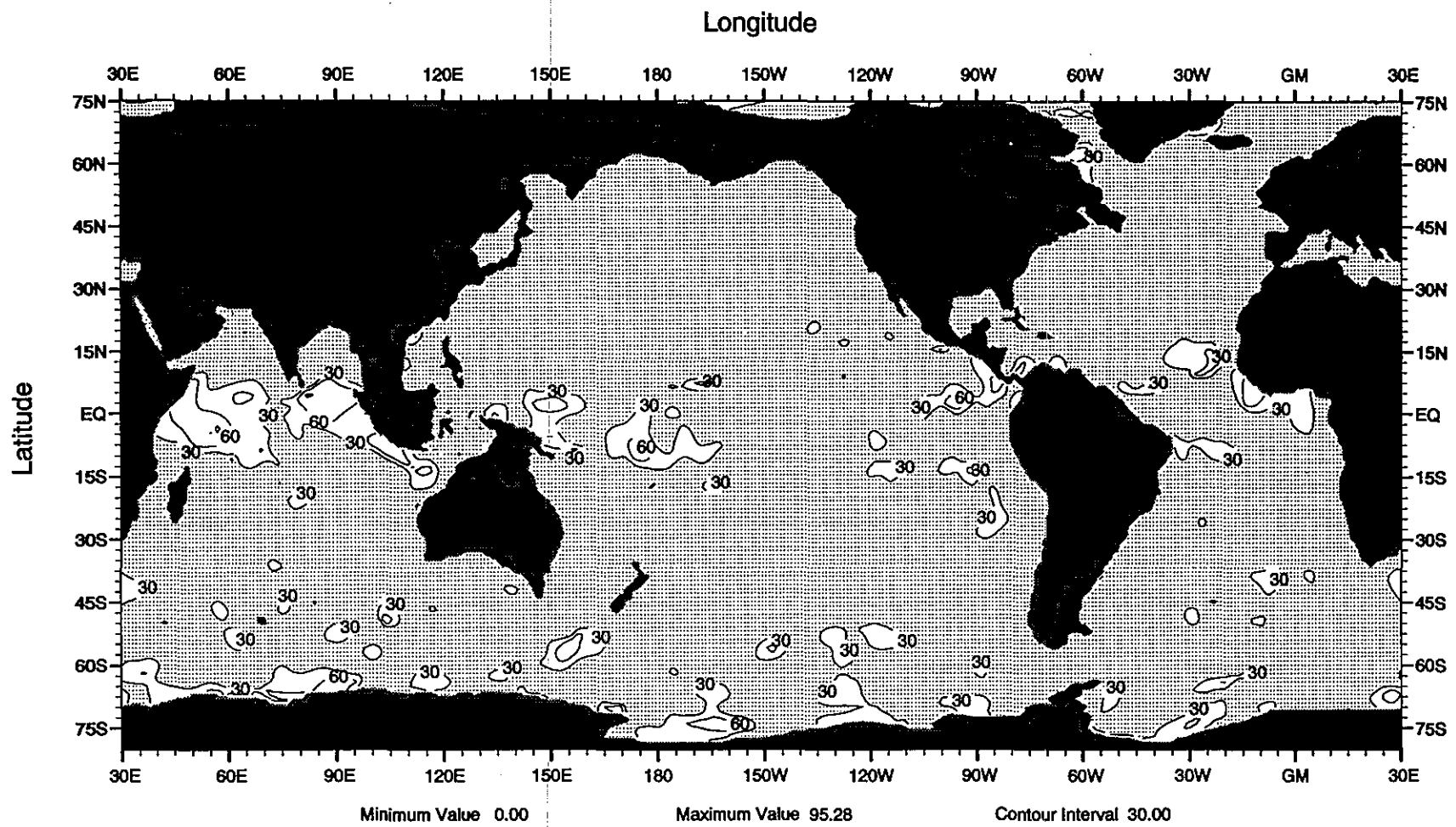


Fig.D17 Percent variance explained by 2nd harmonic of the annual cycle of
heat storage for the 0-275 m layer

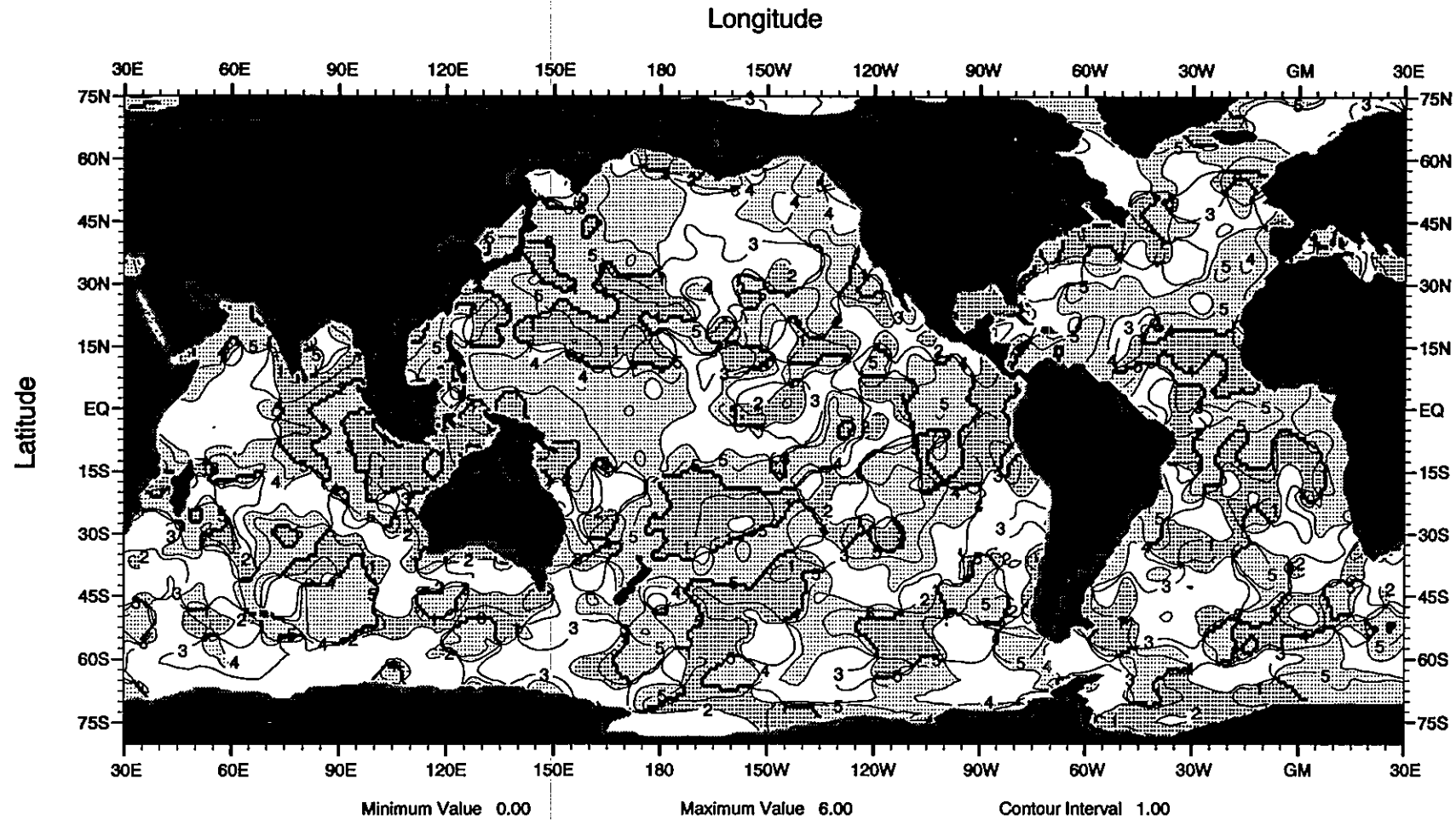


Fig.D18 Phase (months) of 2nd harmonic of the annual cycle of
heat storage for the 0-275 m layer

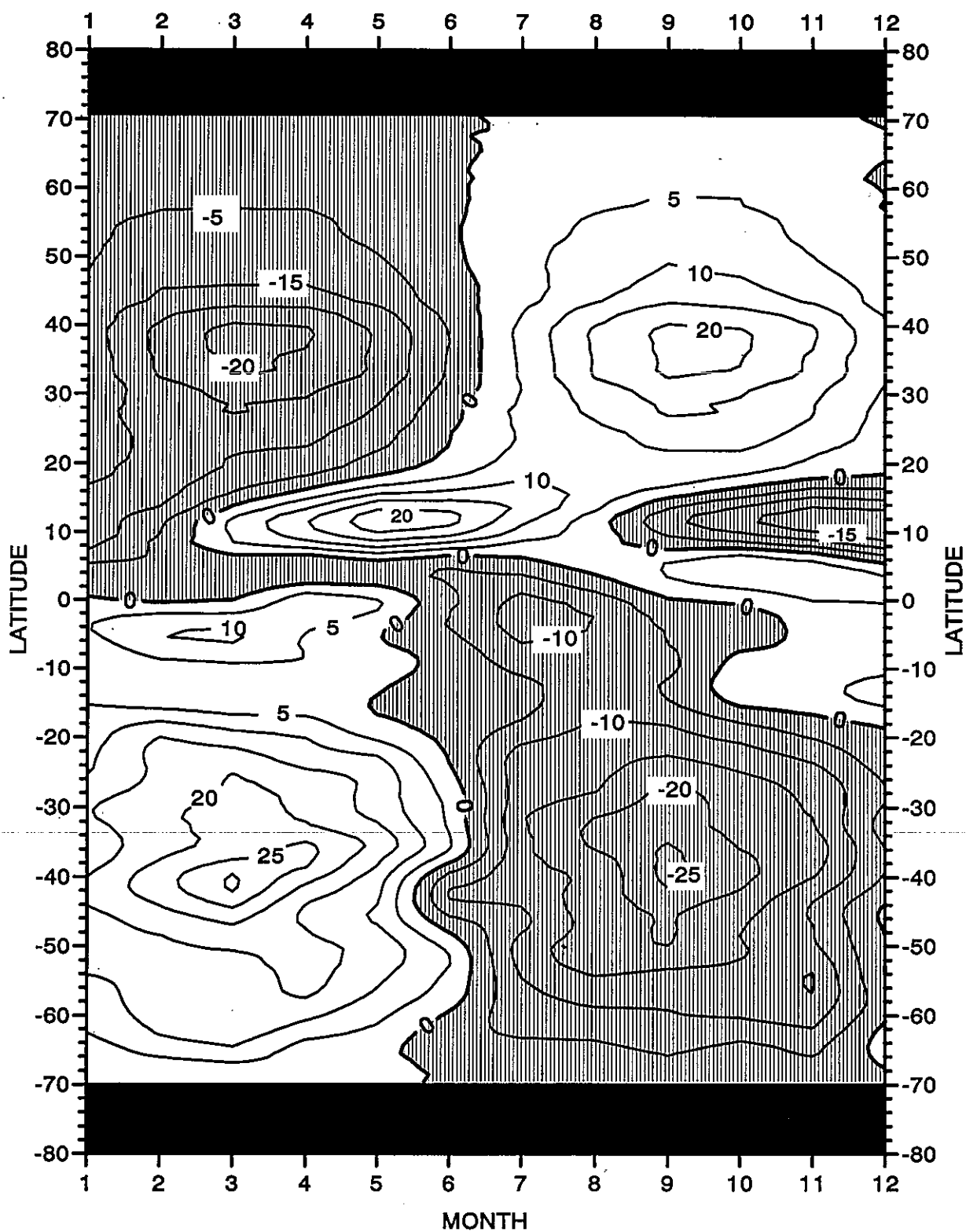


Fig. D19 Zonally integrated heat storage (10^{20} J) vertically integrated through 275 m depth for the World Ocean

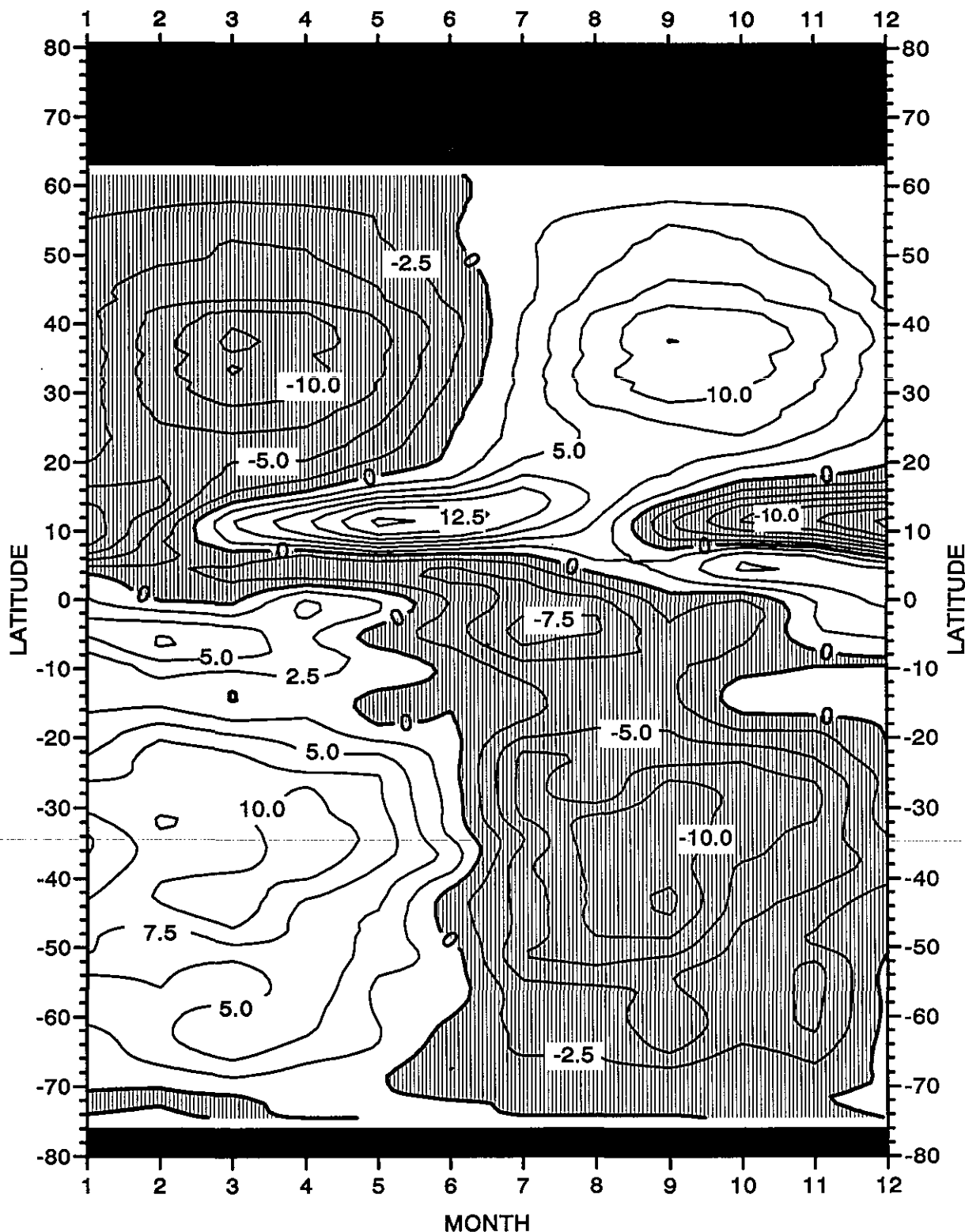


Fig. D20 Zonally integrated heat storage (10^{20} J) vertically integrated through 275 m depth for the Pacific Ocean

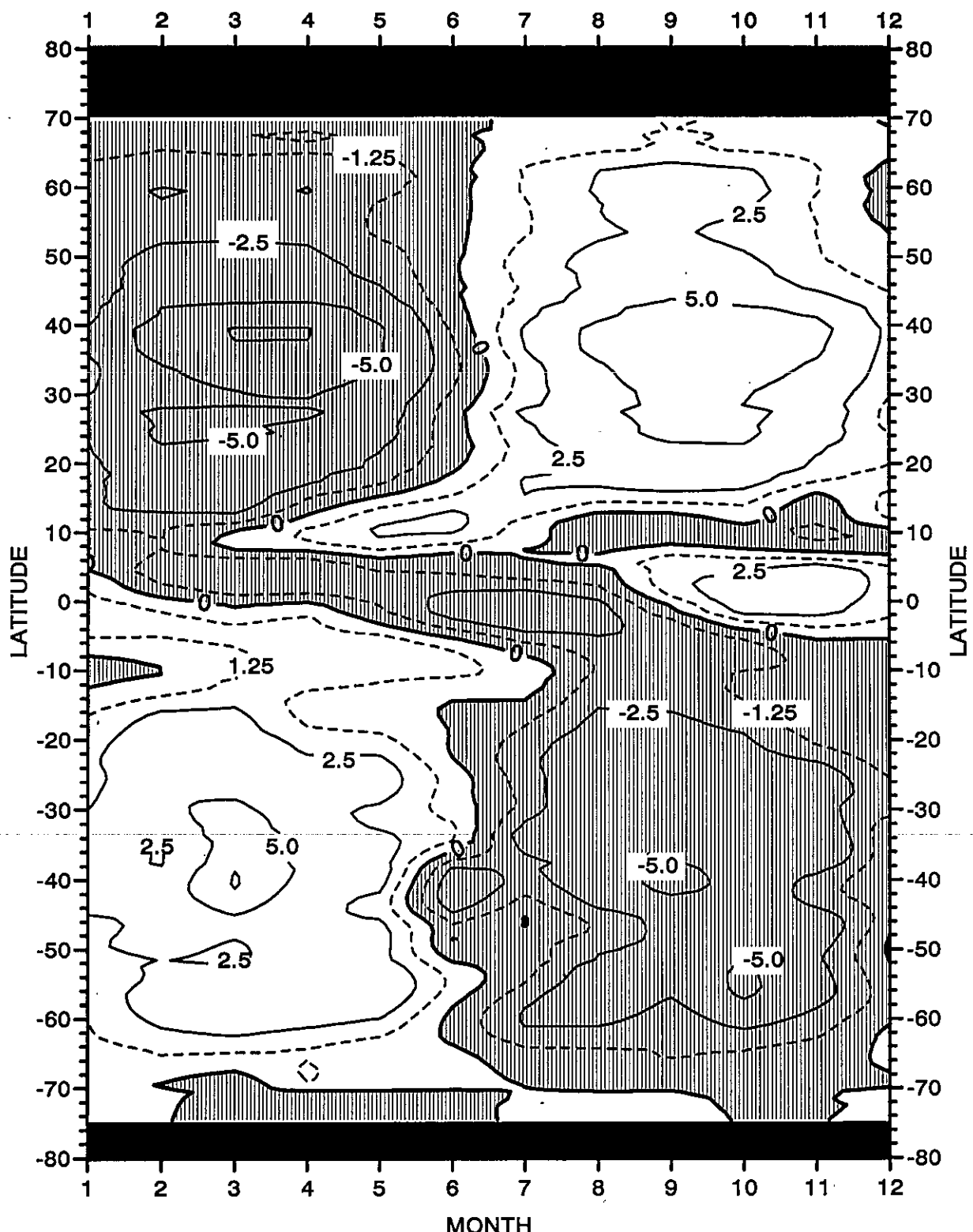


Fig. D21 Zonally integrated heat storage (10^{20} J) vertically integrated through 275 m depth for the Atlantic Ocean

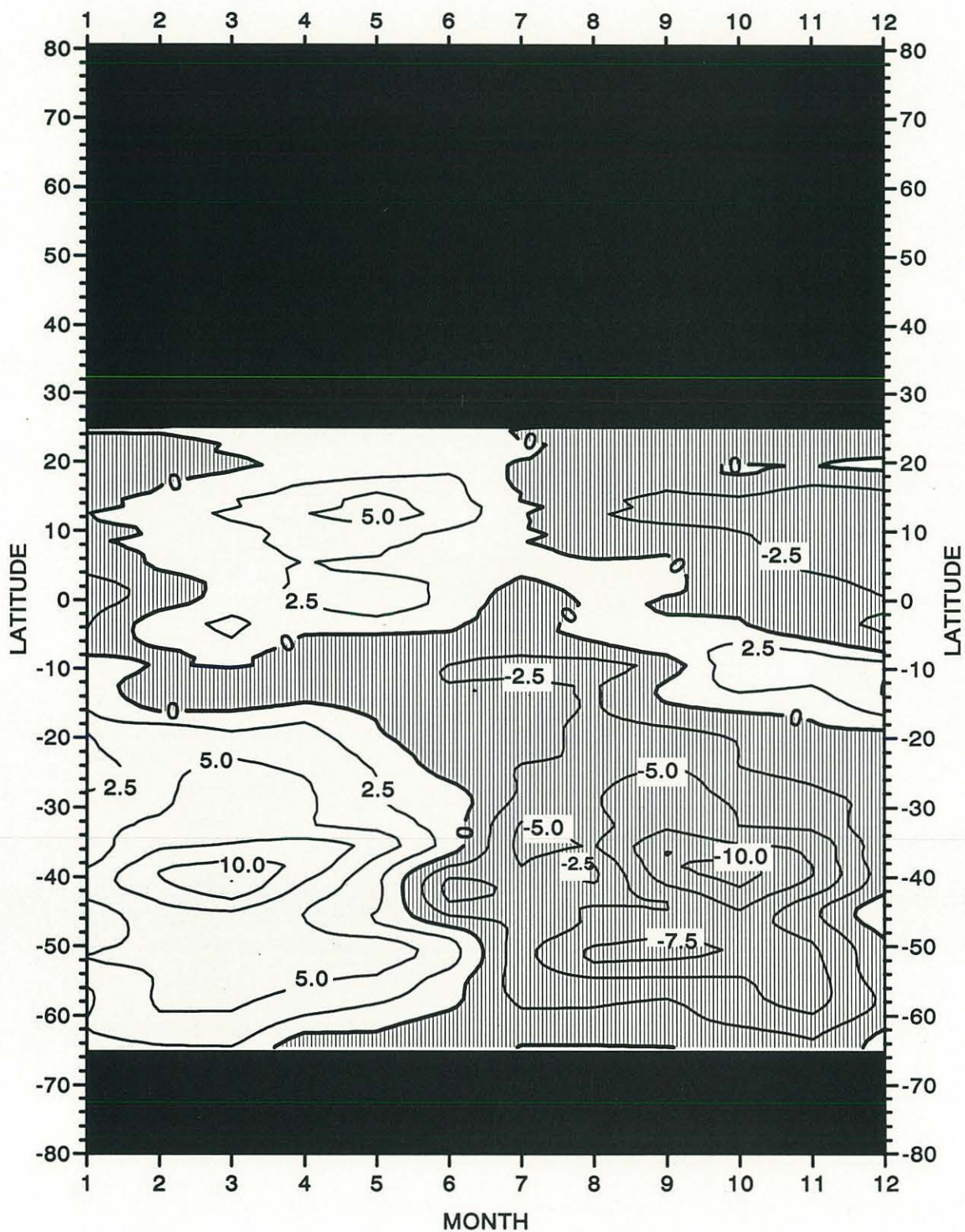


Fig. D22 Zonally integrated heat storage (10^{20} J) vertically integrated through 275 m depth for the Indian Ocean

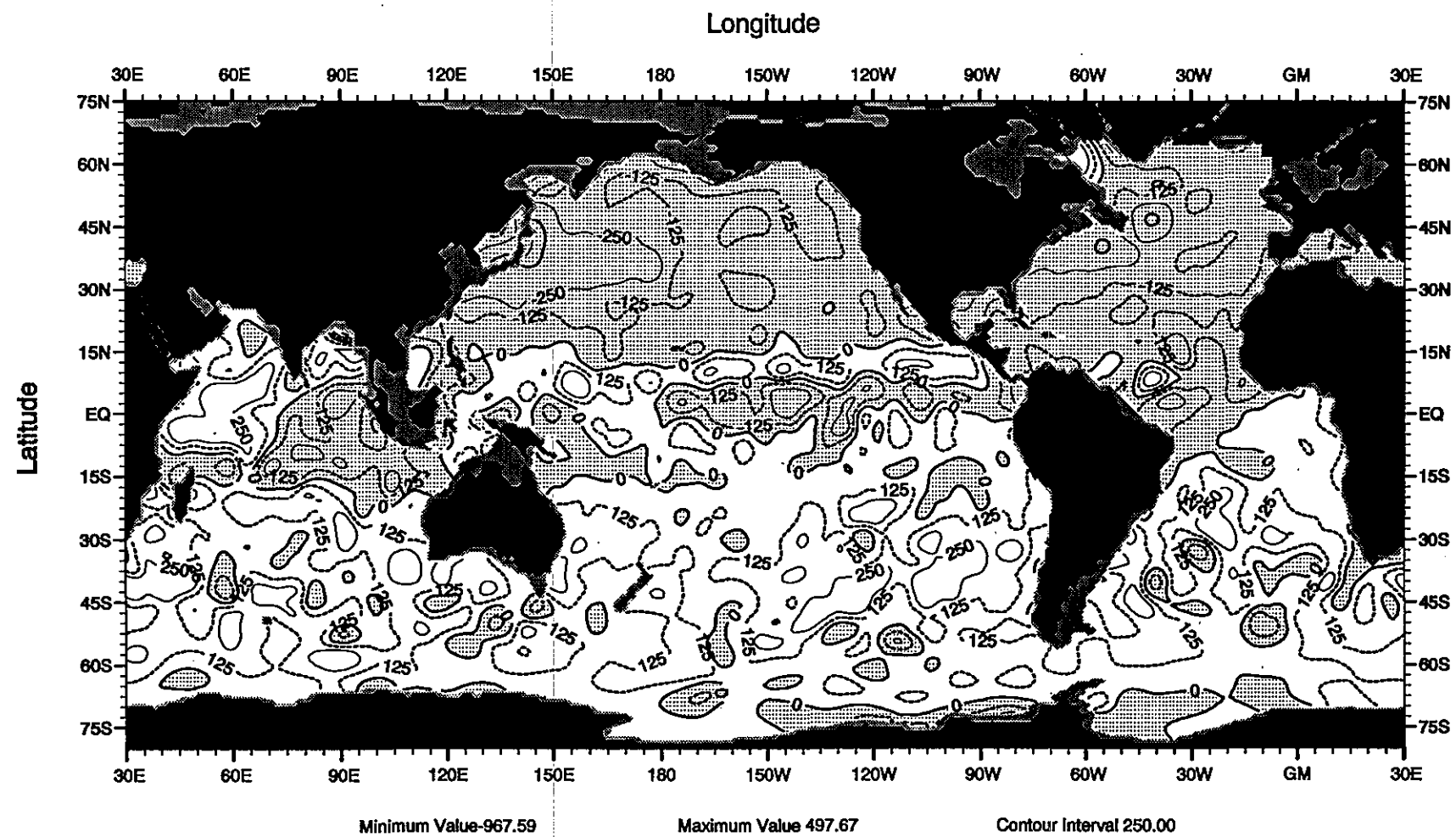


Fig. E1 Rate of heat storage (W/M^2) integrated through 275 m depth for January

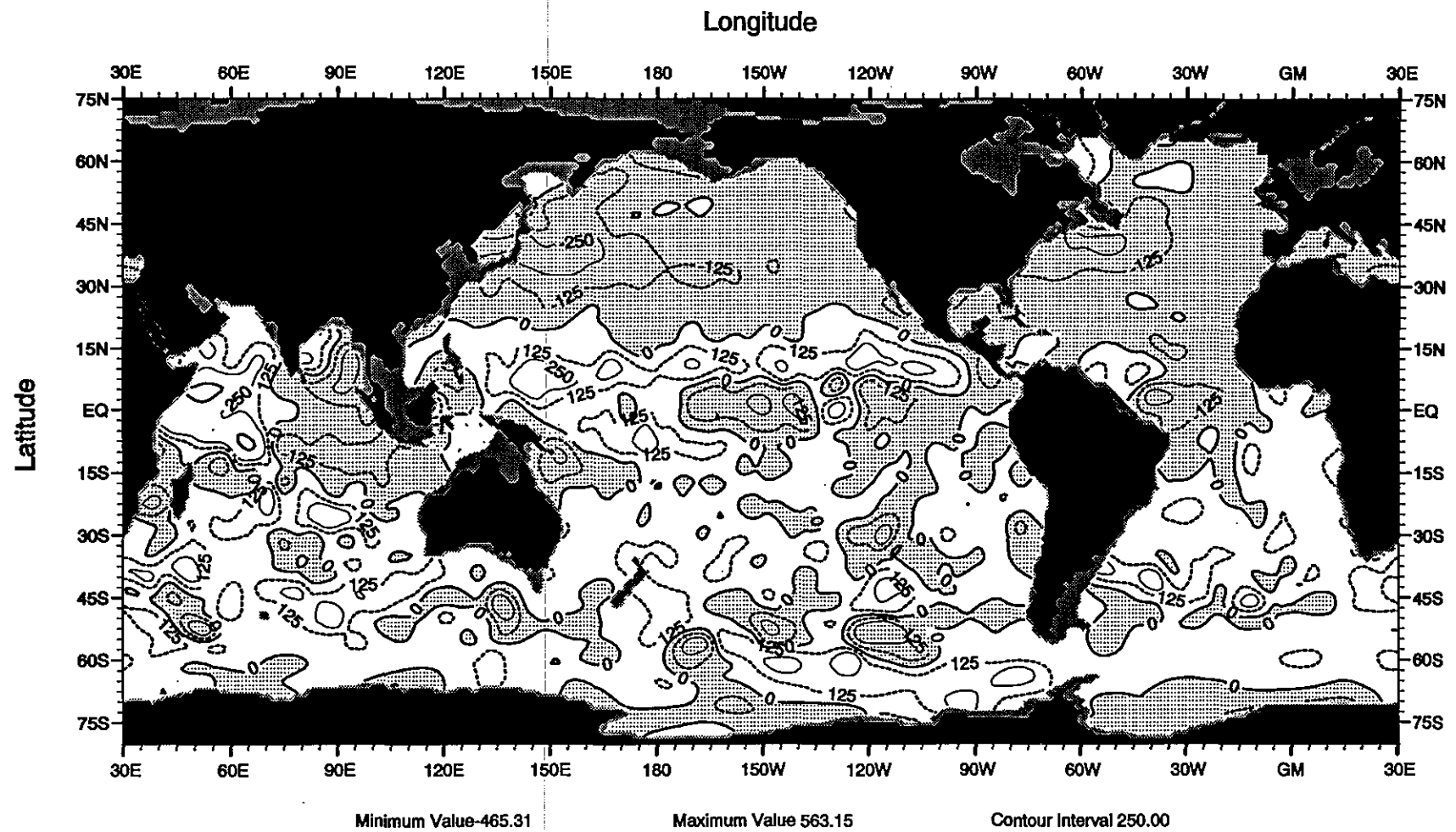


Fig. E2 Rate of heat storage (W/m^2) integrated through 275 m depth for February

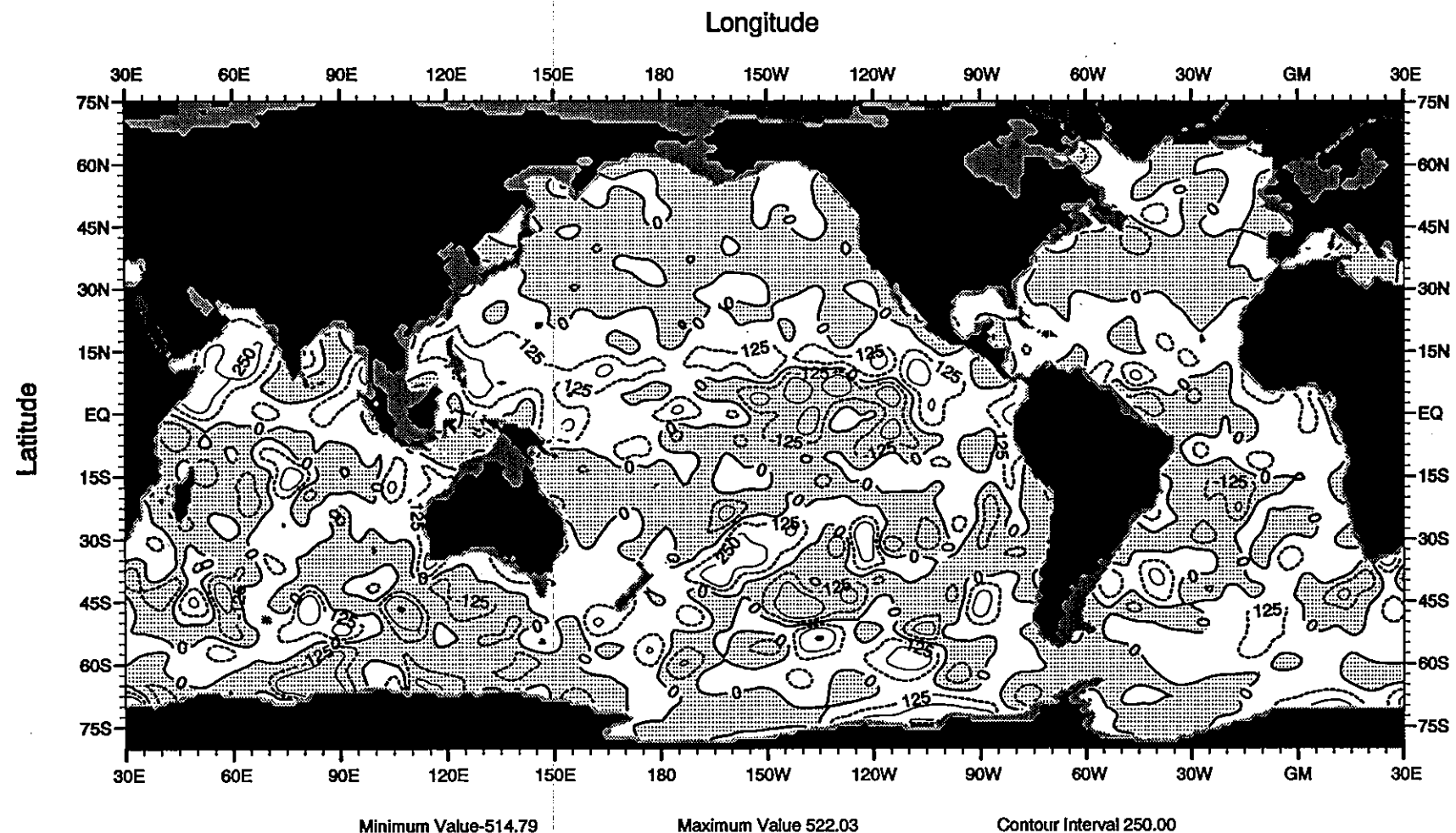


Fig. E3 Rate of heat storage (W/M^2) integrated through 275 m depth for March

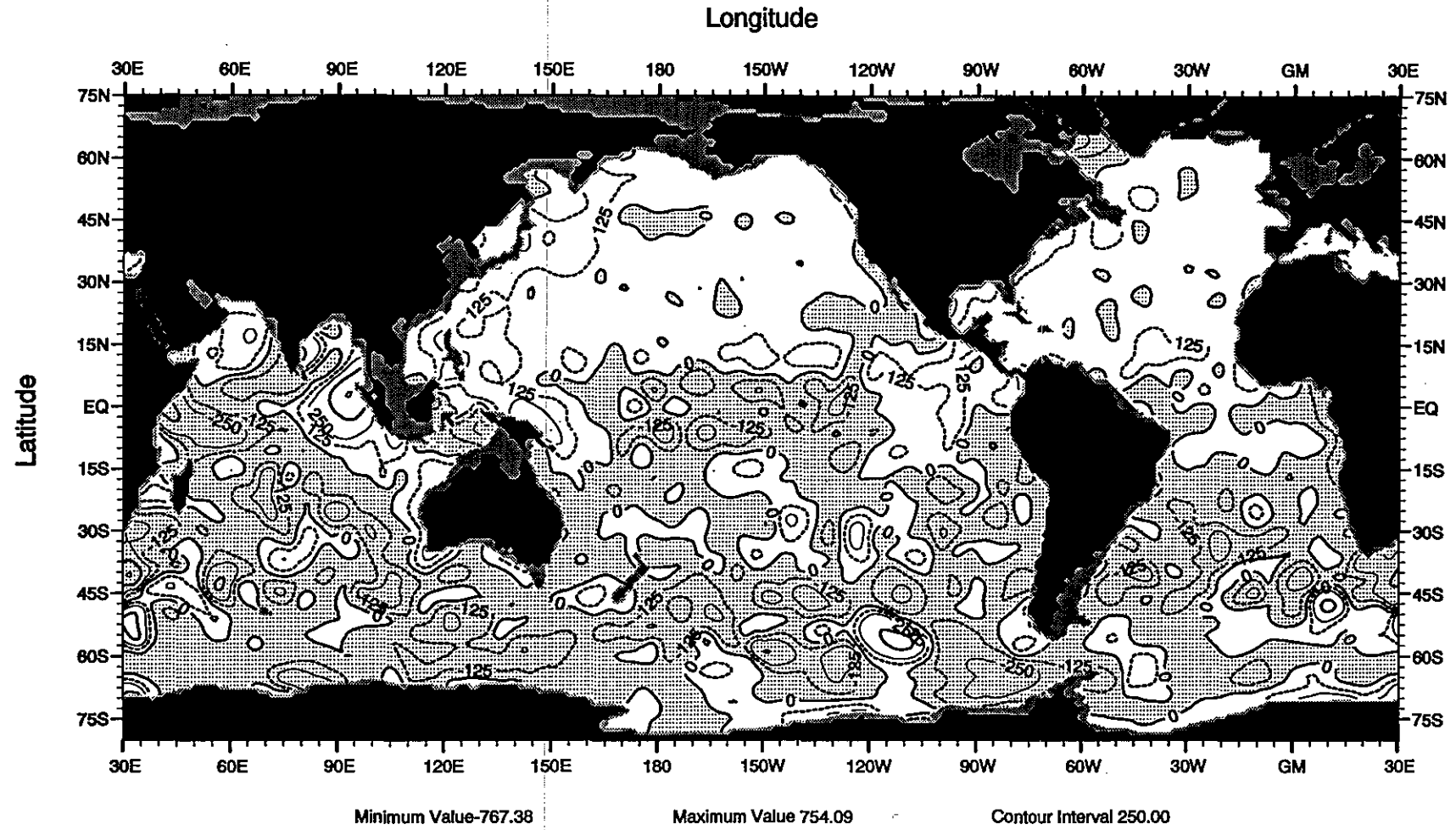


Fig. E4 Rate of heat storage (W/M²) integrated through 275 m depth for April

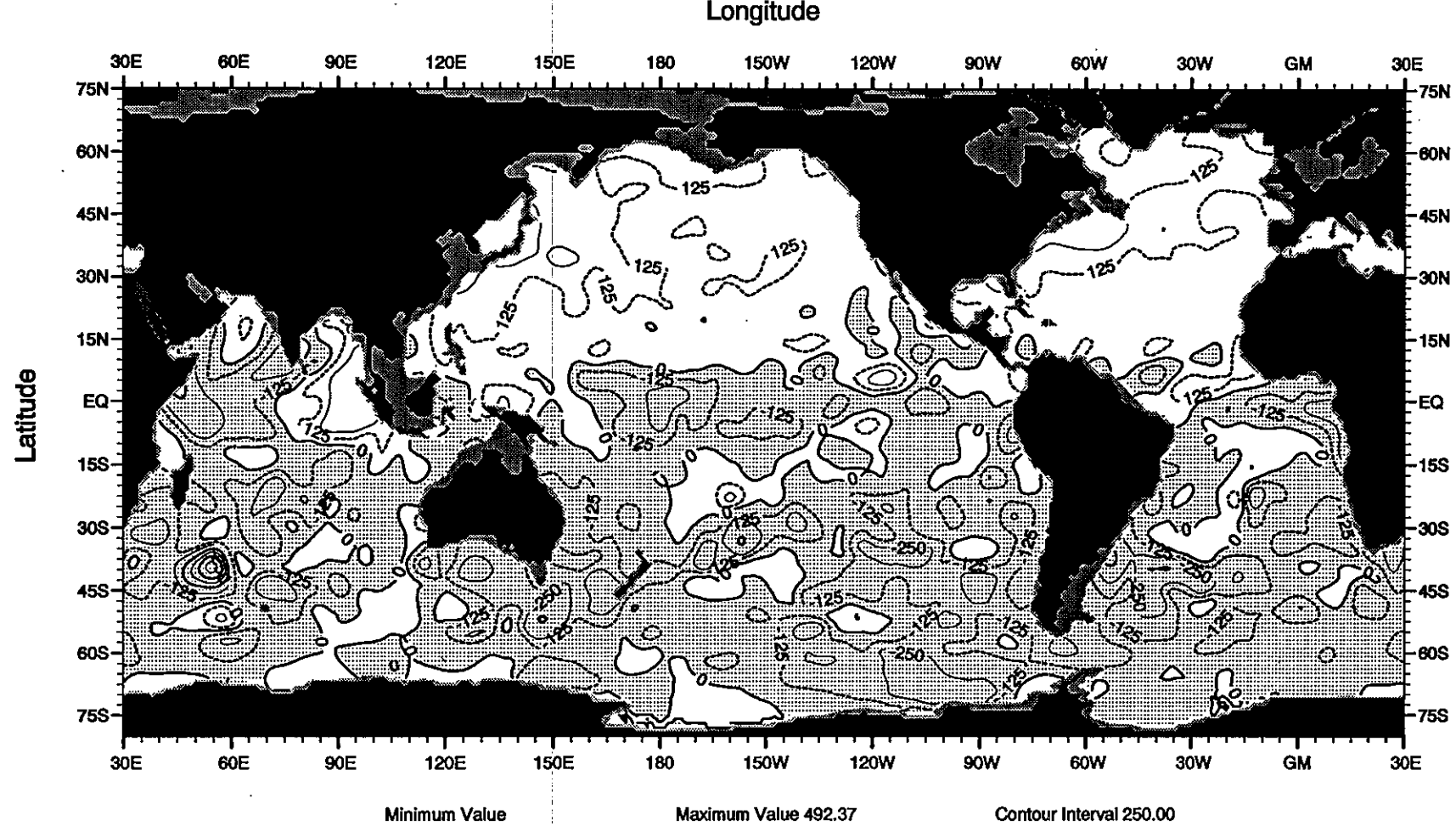


Fig. E5 Rate of heat storage (W/M^2) integrated through 275 m depth for May

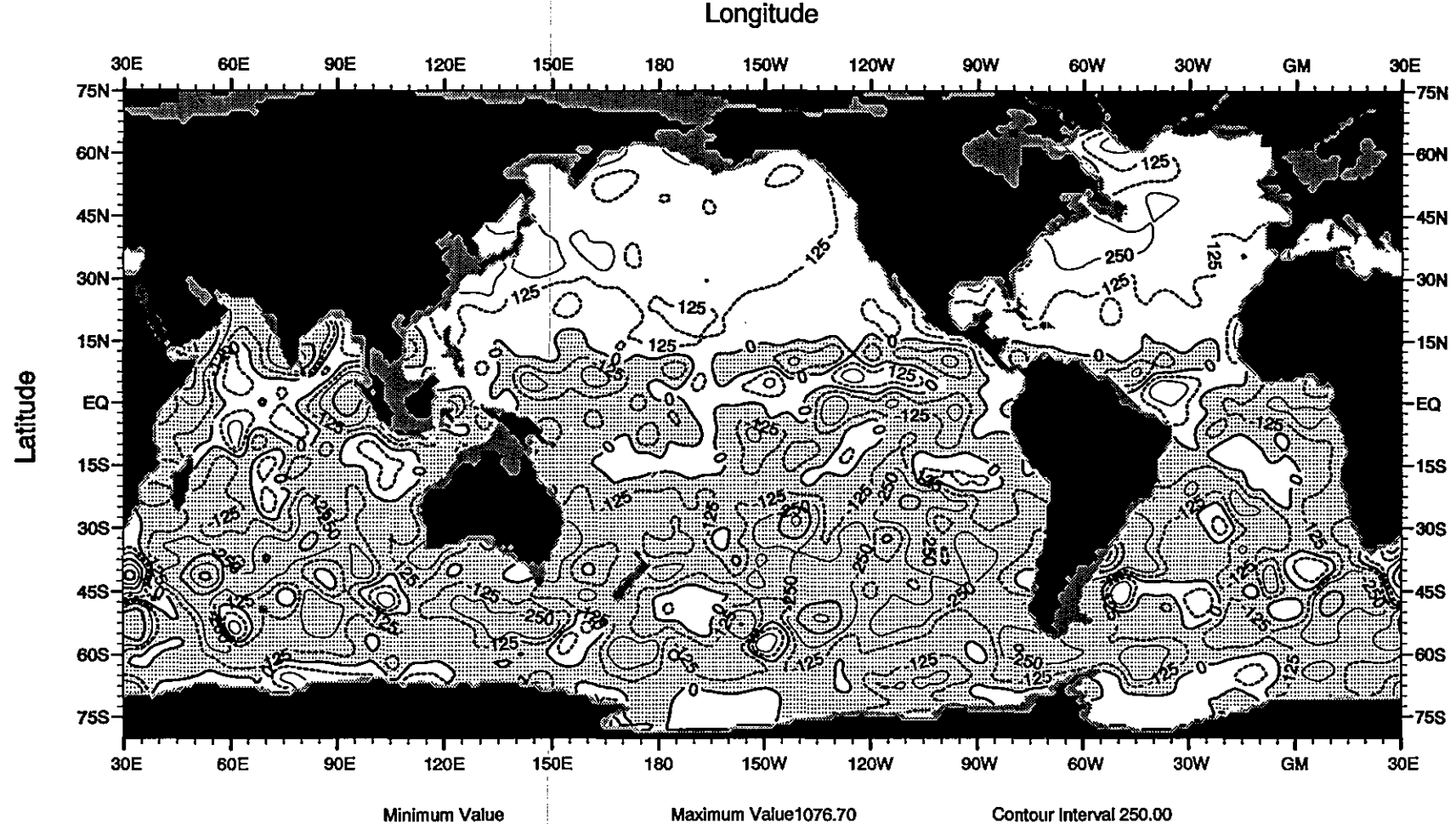


Fig. E6 Rate of heat storage (W/M^2) integrated through 275 m depth for June

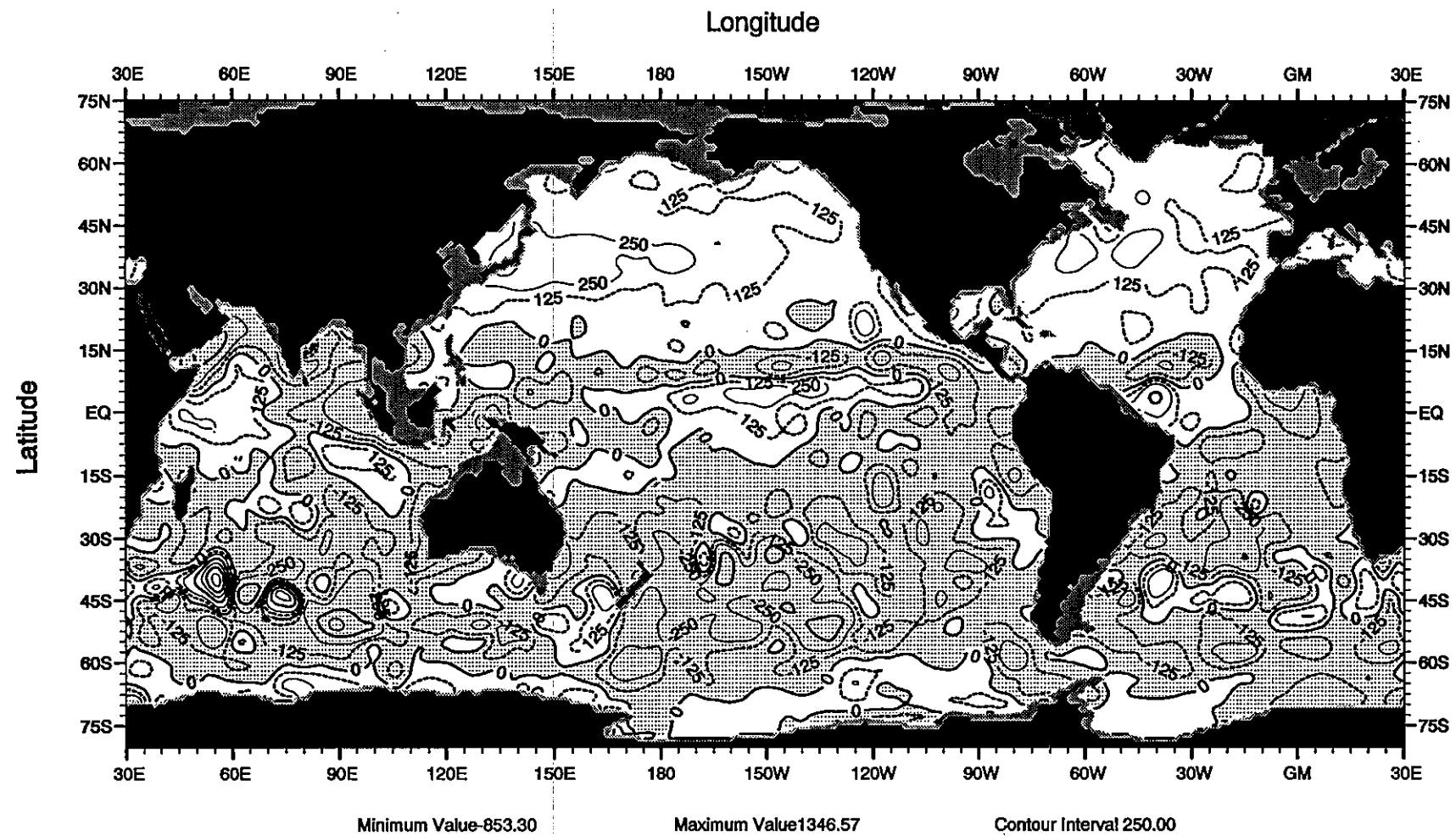


Fig. E7 Rate of heat storage (W/M^2) integrated through 275 m depth for July

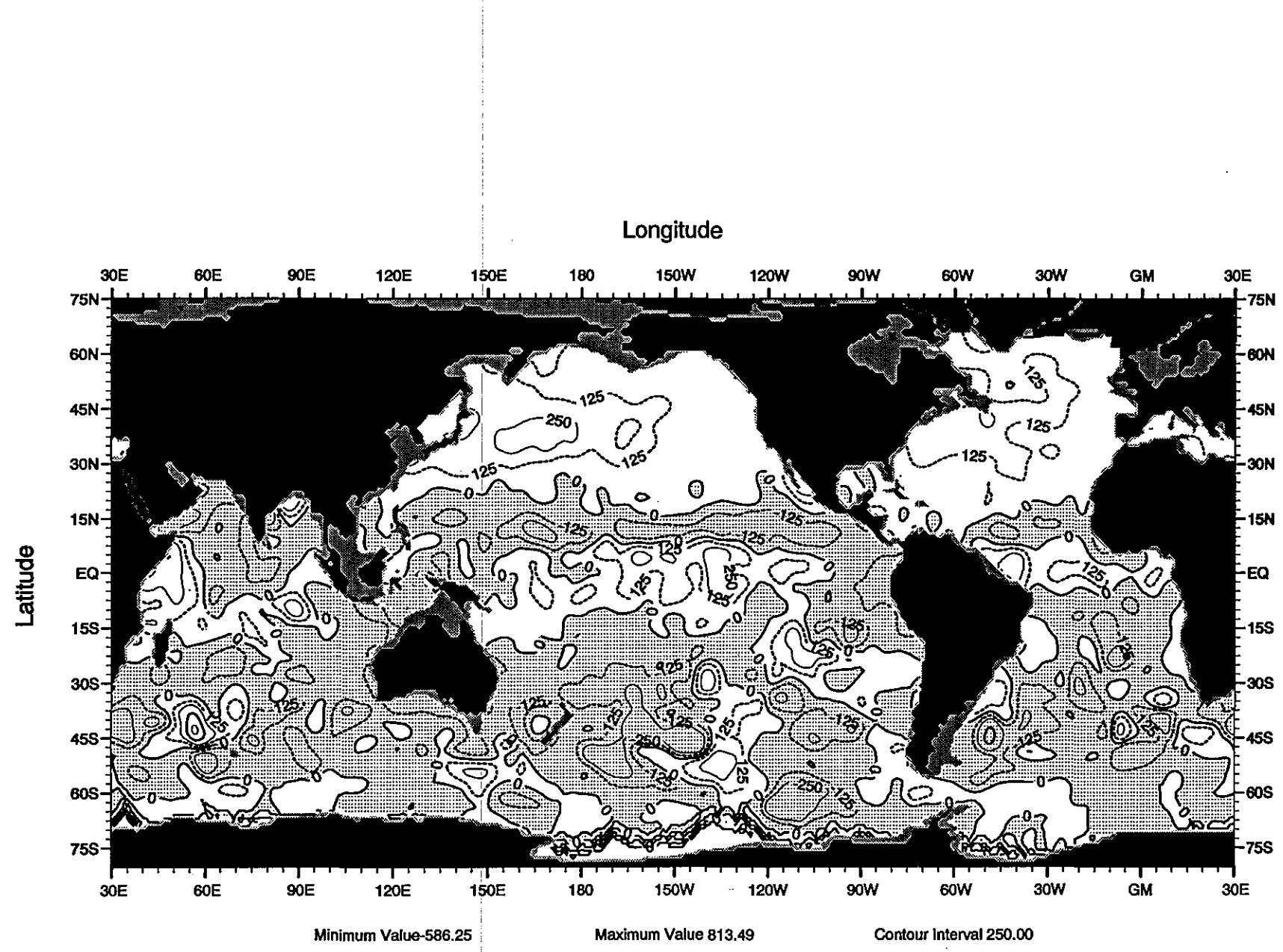


Fig. E8 Rate of heat storage (W/M^2) integrated through 275 m depth for August

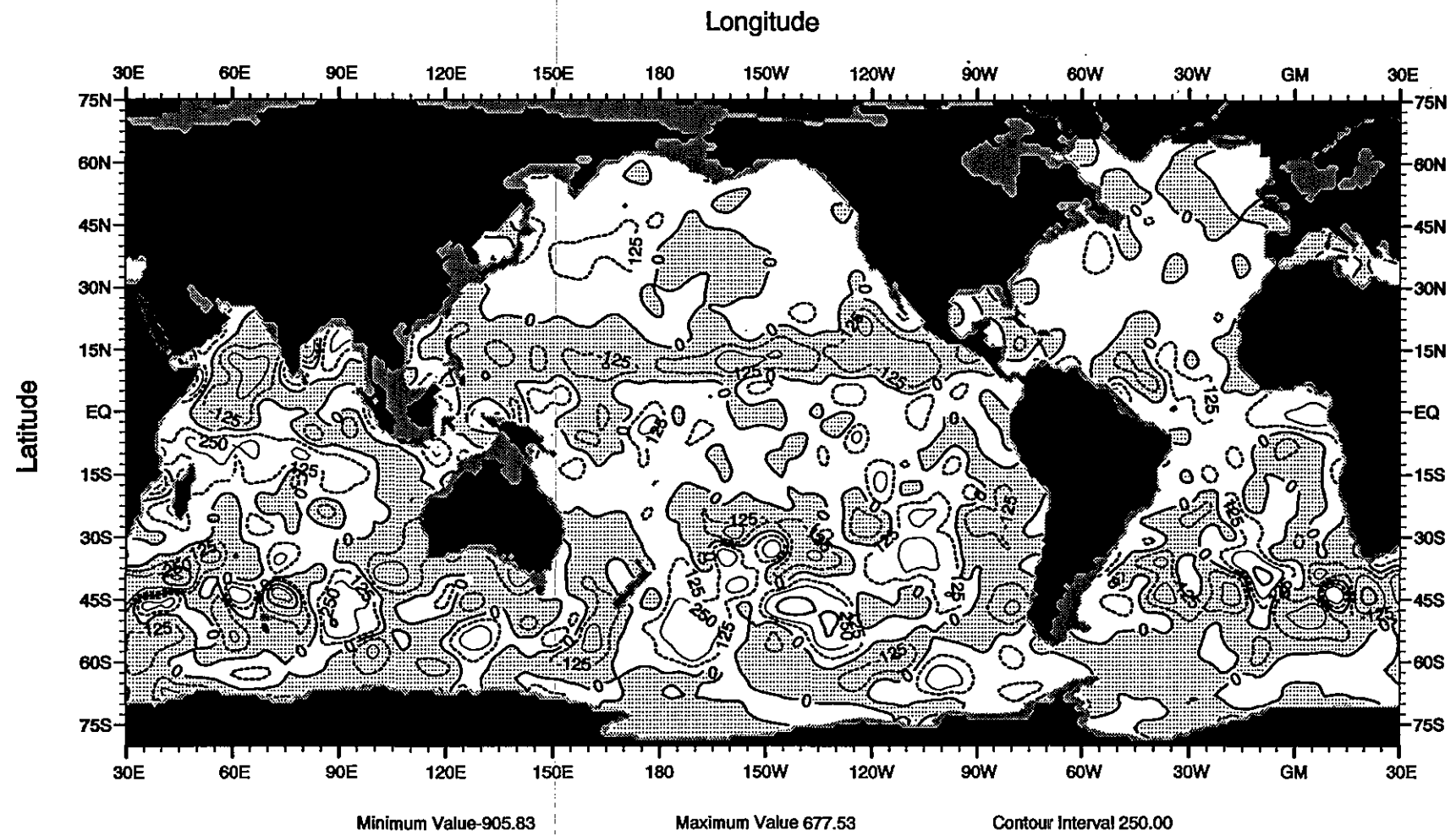


Fig. E9 Rate of heat storage (W/m^2) integrated through 275 m depth for September

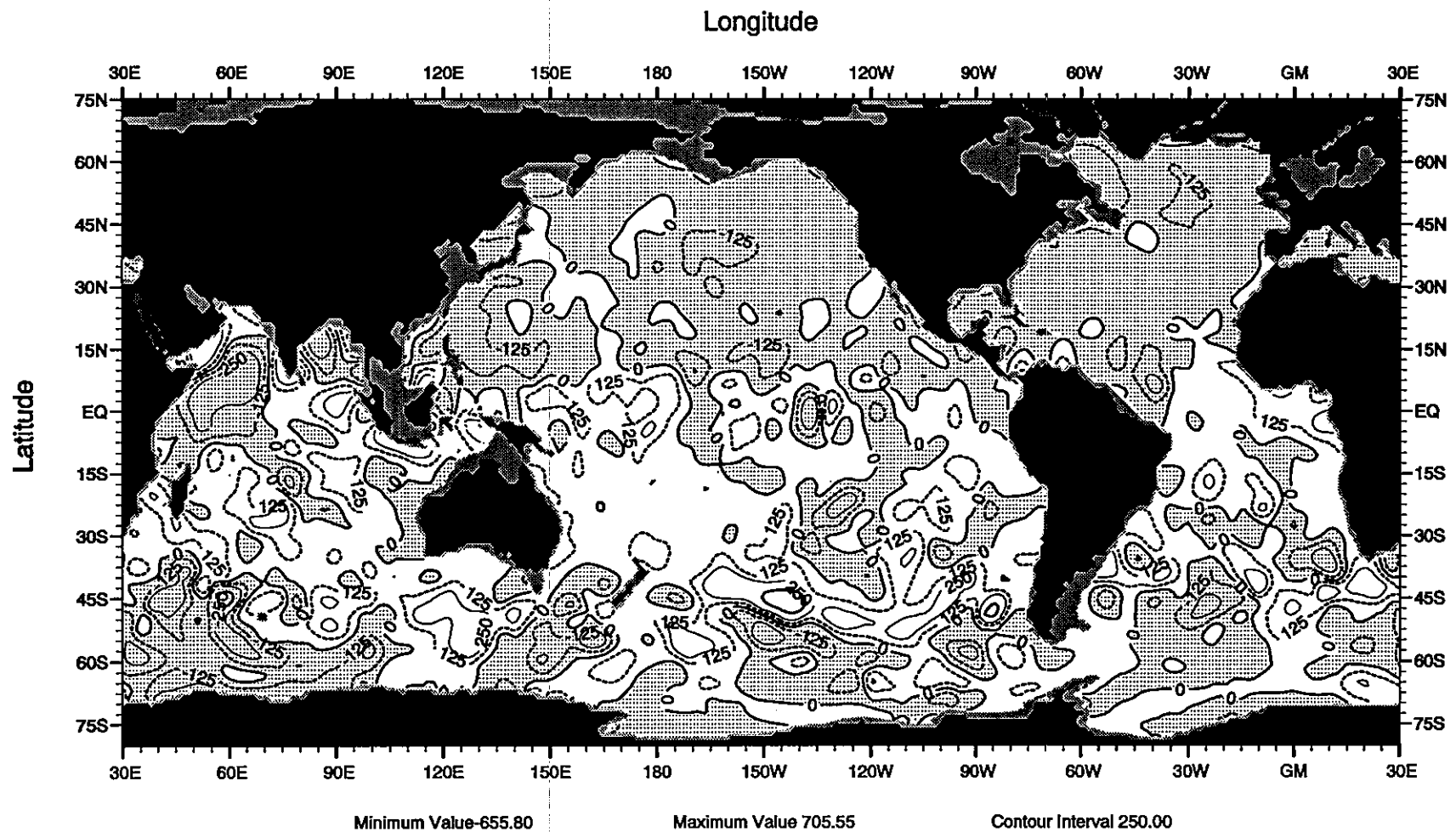


Fig. E10 Rate of heat storage (W/m^2) integrated through 275 m depth for October

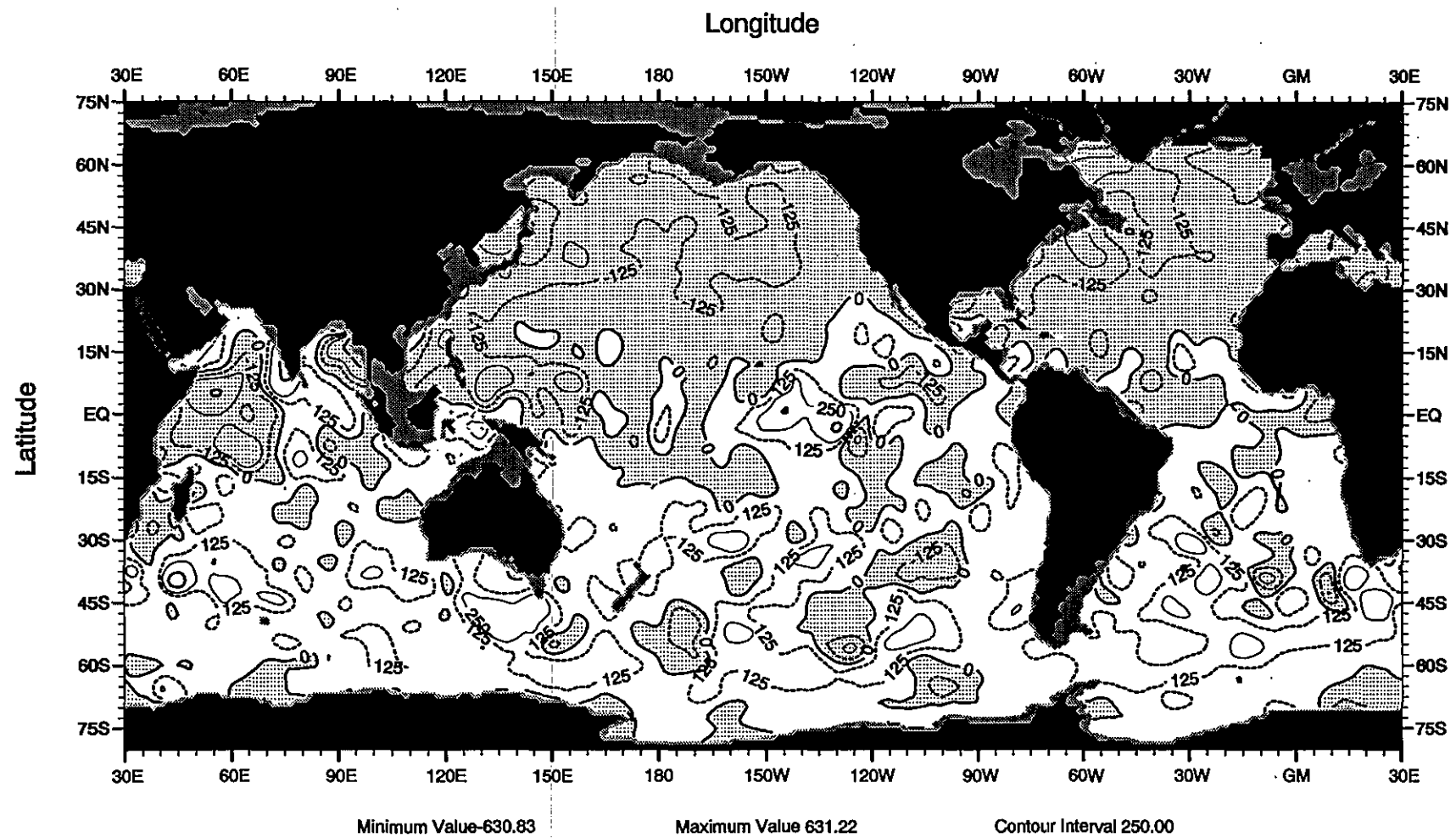


Fig. E11 Rate of heat storage (W/M^2) integrated through 275 m depth for November

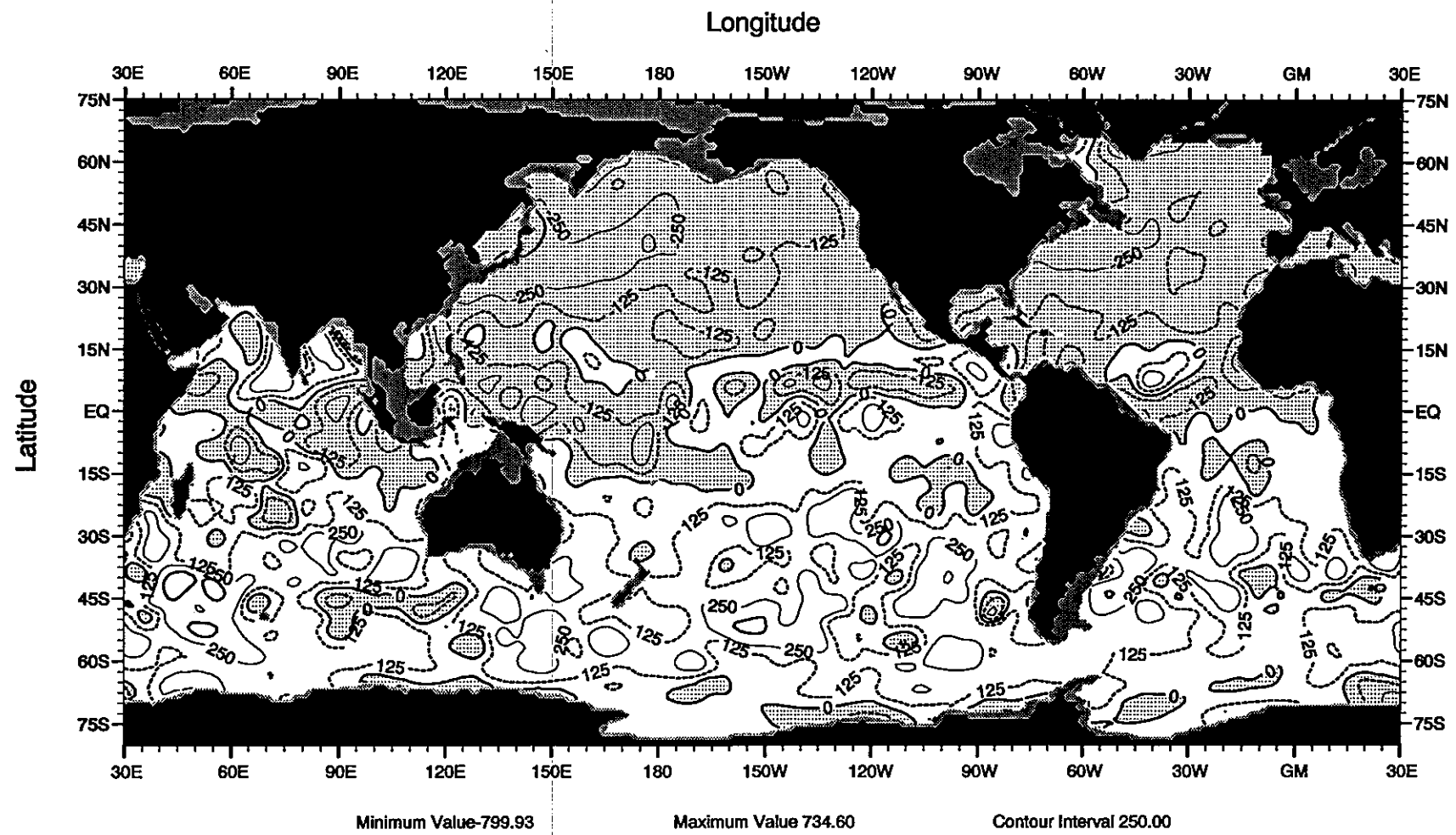


Fig. E12 Rate of heat storage (W/m^2) integrated through 275 m depth for December

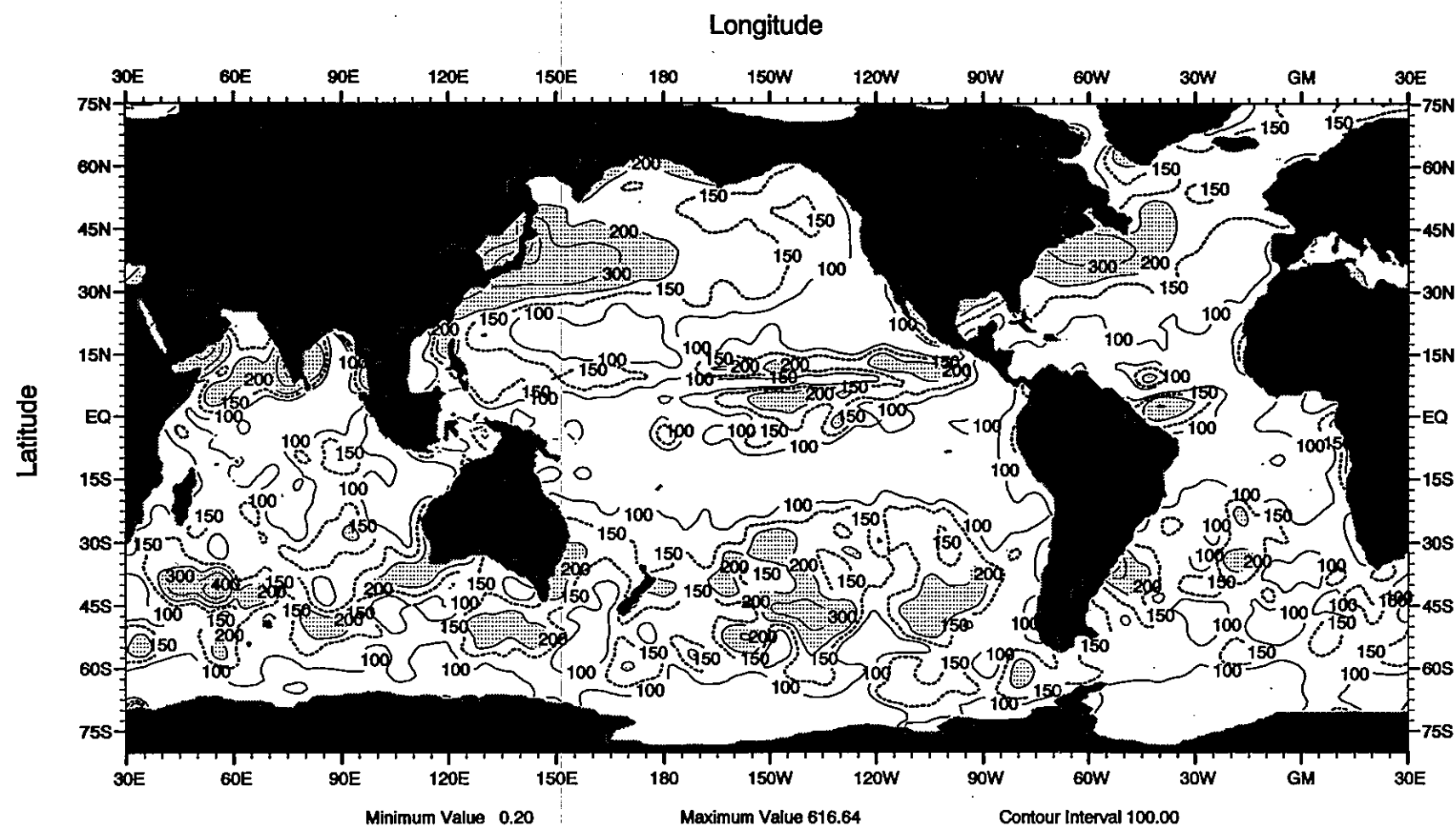


Fig.E13 Amplitude (W/M^3) of 1st harmonic of the annual cycle of
the rate of heat storage for the 0-275 m layer

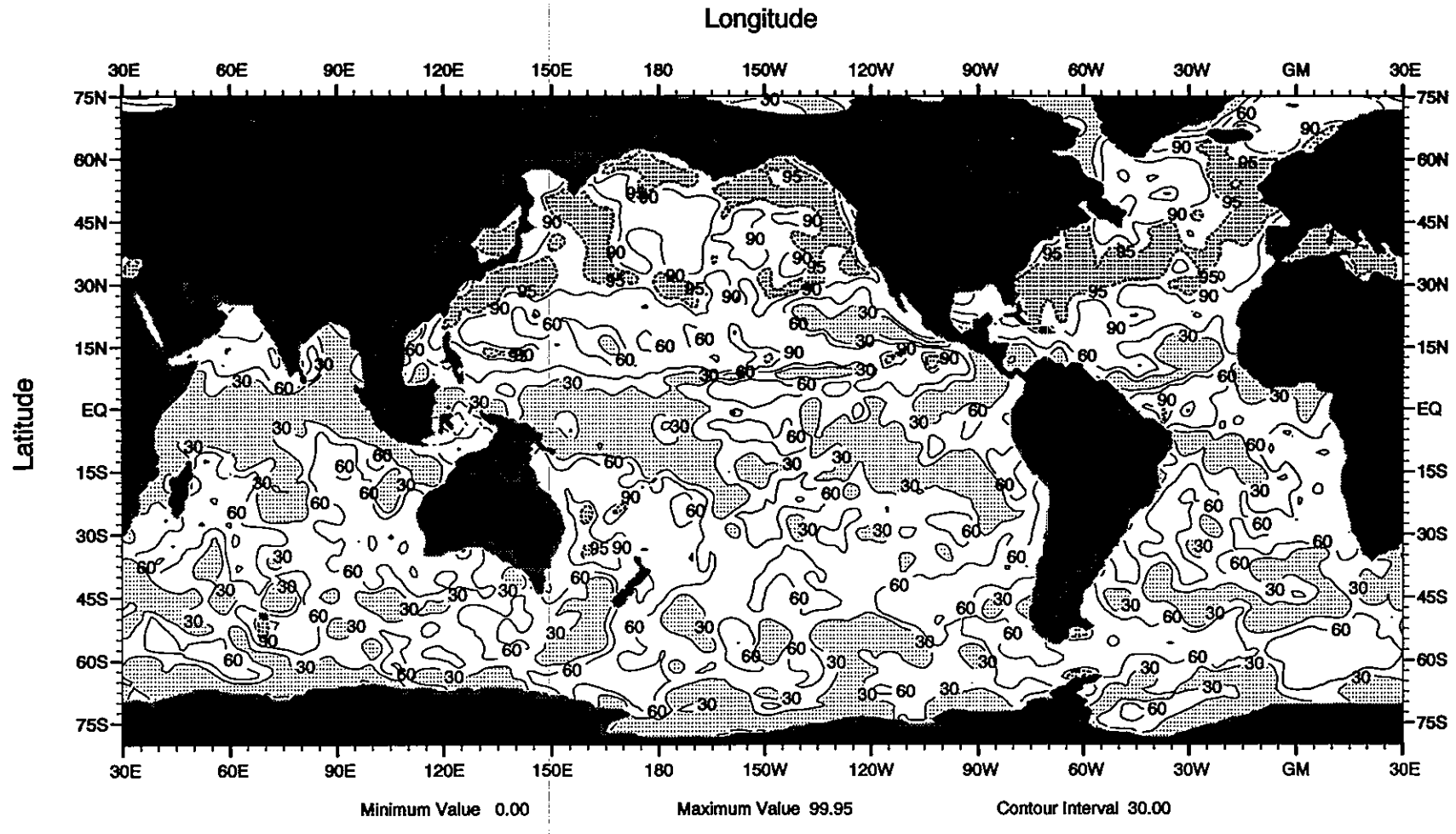


Fig.E14 Percent variance explained by 1st harmonic of the annual cycle of the rate of heat storage for the 0-275 m layer

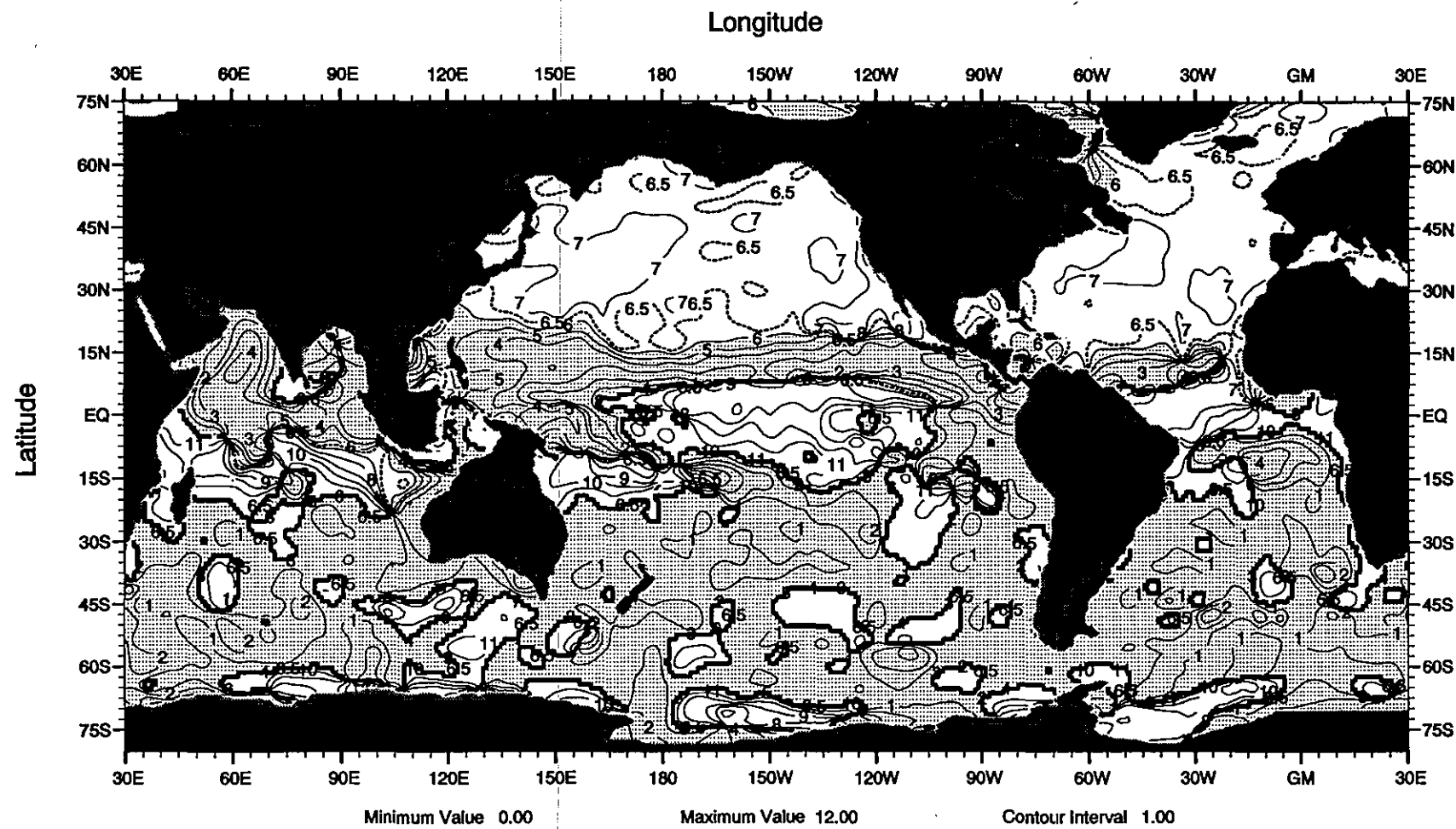


Fig.E15 Phase (months) of 1st harmonic of the annual cycle of
the rate of heat storage for the 0-275 m layer

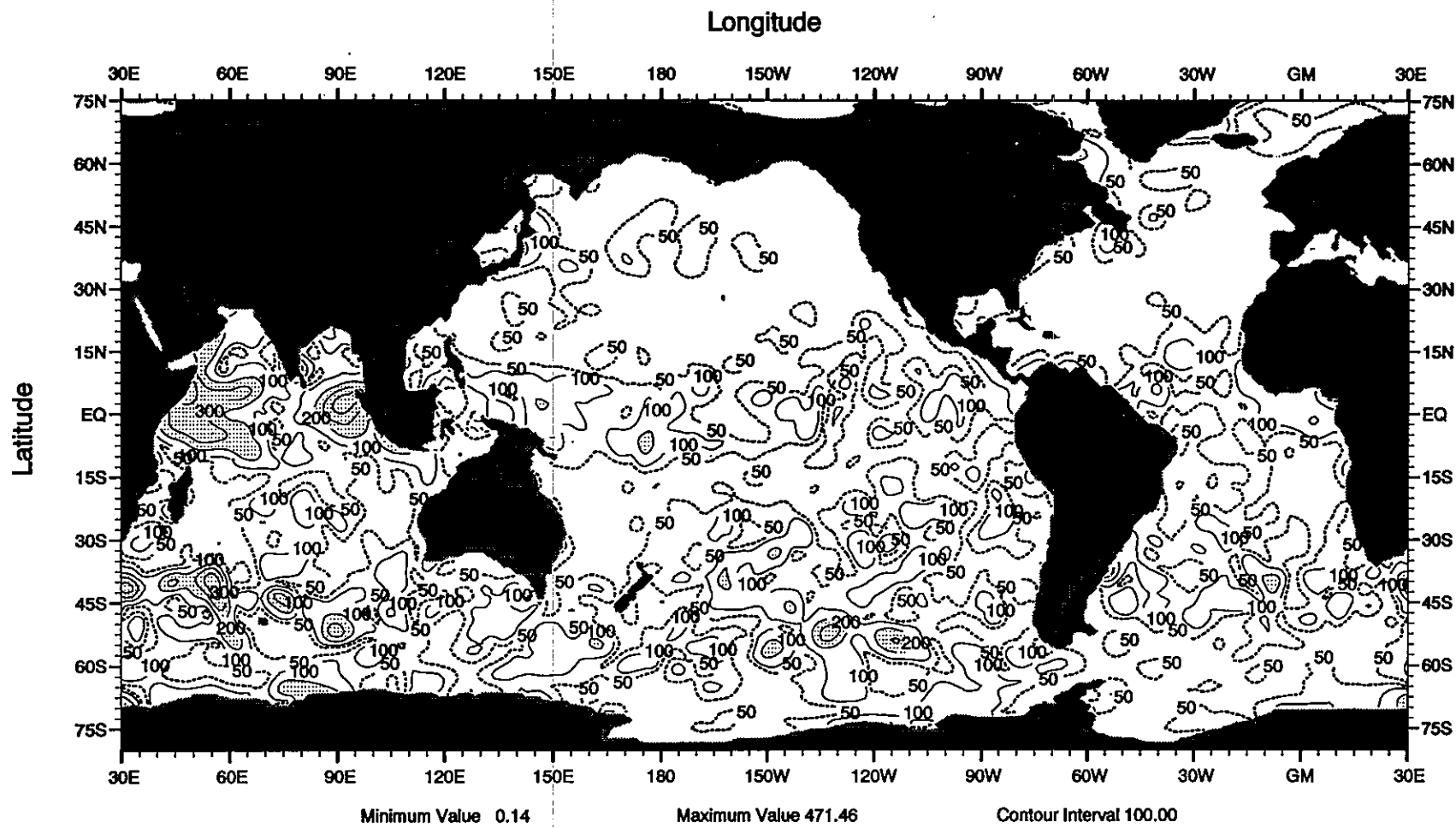


Fig.E16 Amplitude (W/M^2) of 2nd harmonic of the annual cycle of the rate of heat storage for the 0-275 m layer

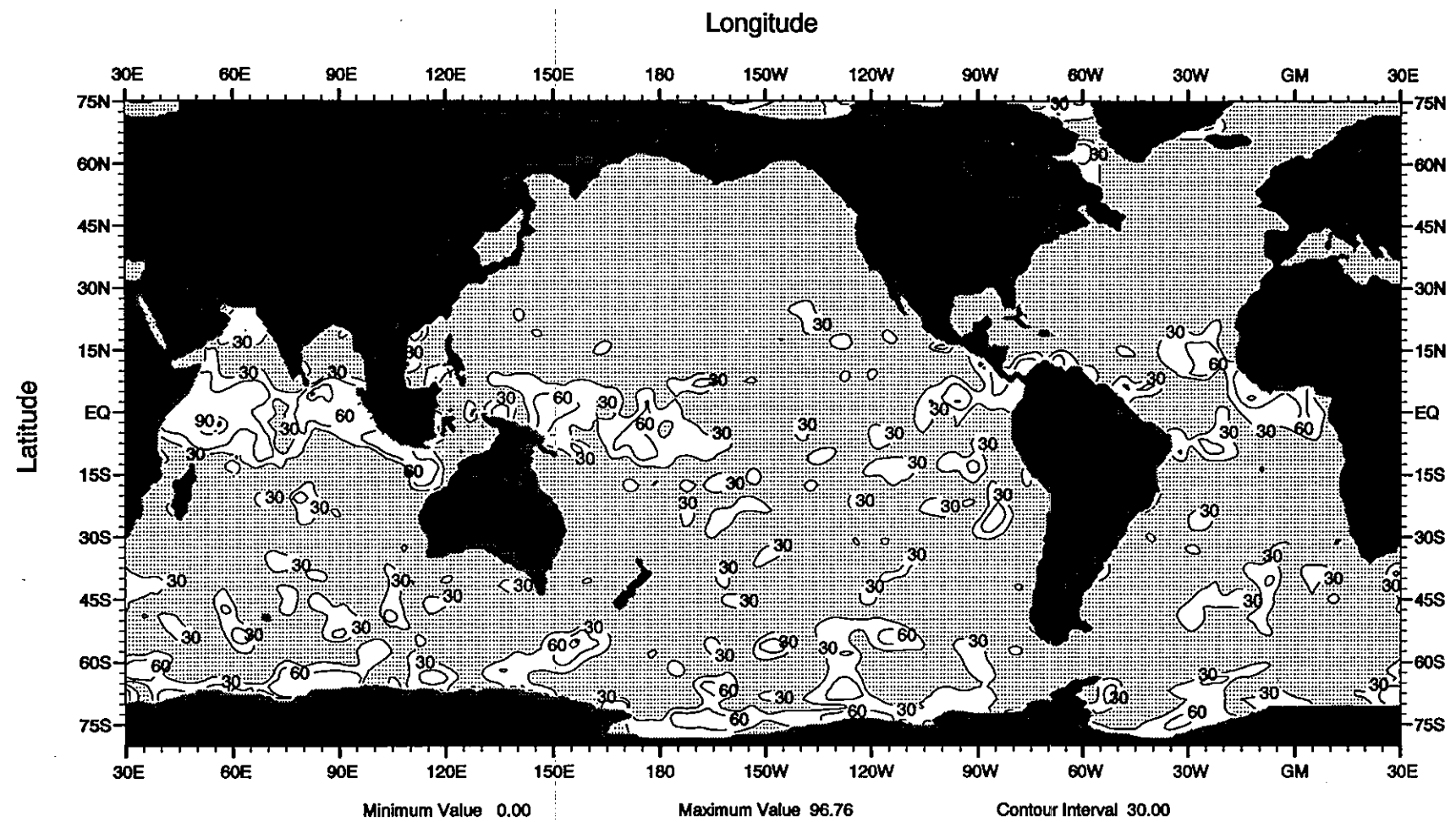


Fig.E17 Percent variance explained by 2nd harmonic of the annual cycle of
the rate of heat storage for the 0-275 m layer

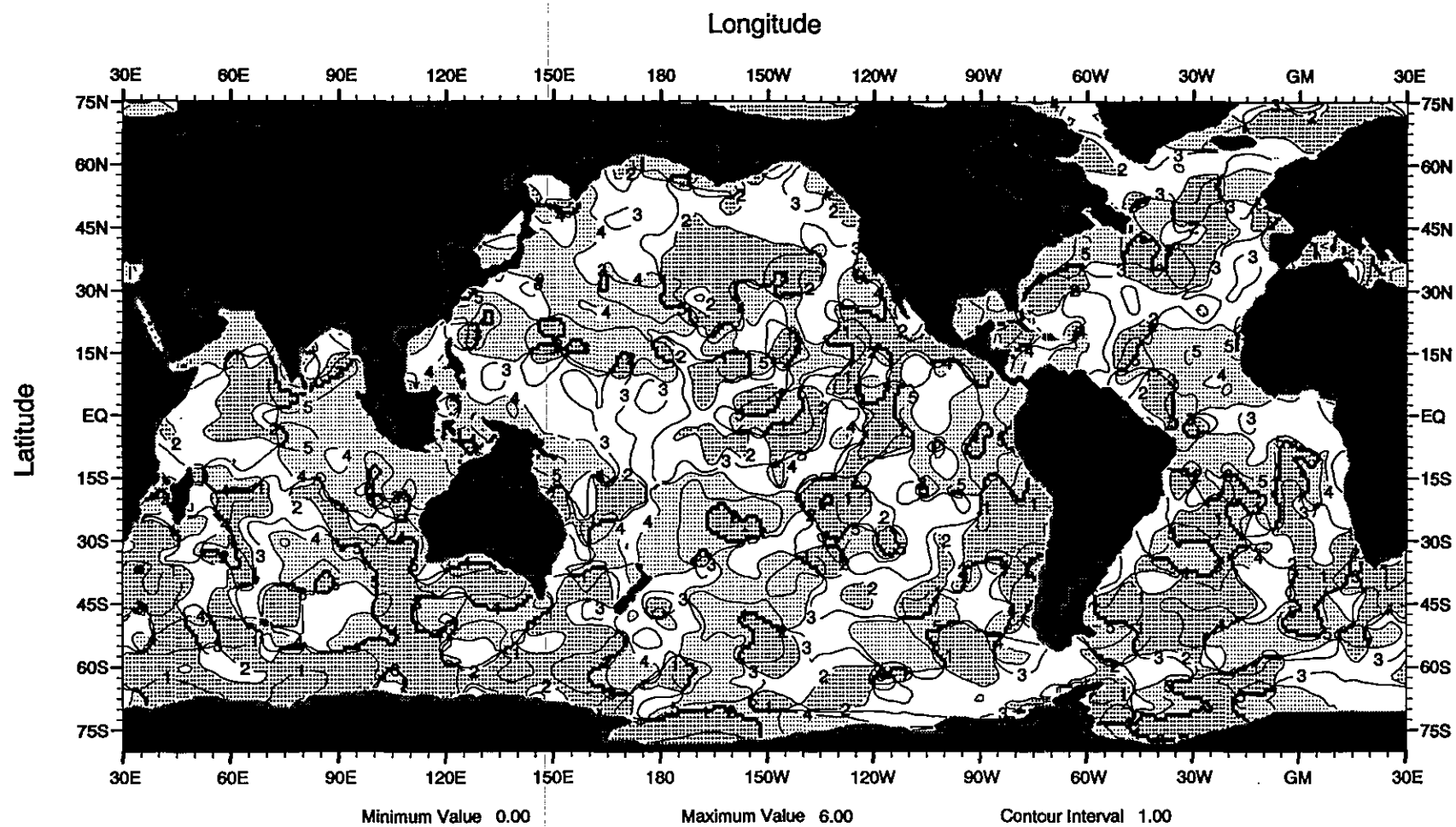


Fig.E18 Phase (months) of 2nd harmonic of the annual cycle of the rate of heat storage for the 0-275 m layer

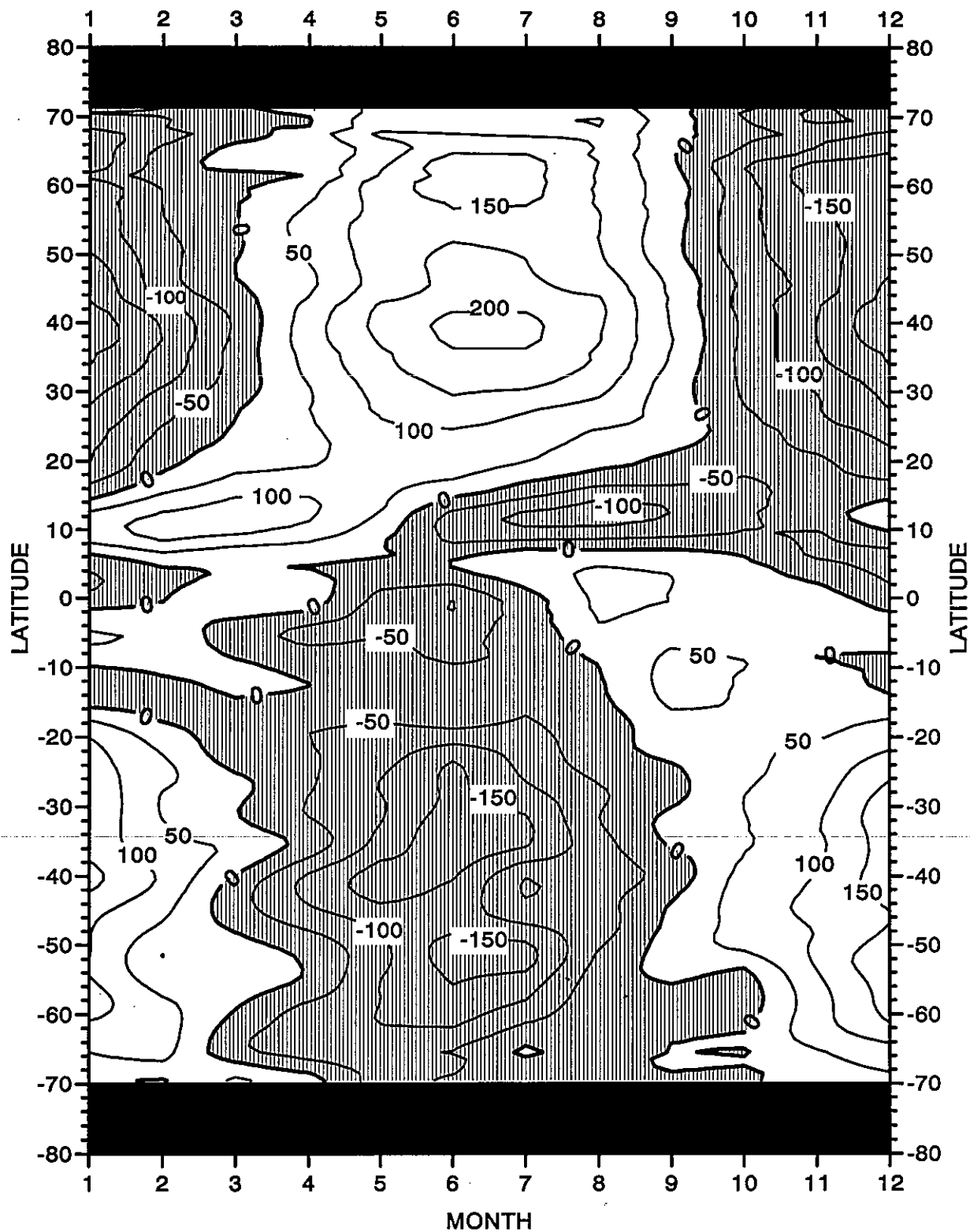


Fig. E19 Zonally averaged rate of heat storage ($\text{W} \cdot \text{m}^{-2}$) vertically integrated through 275 m depth for the World Ocean

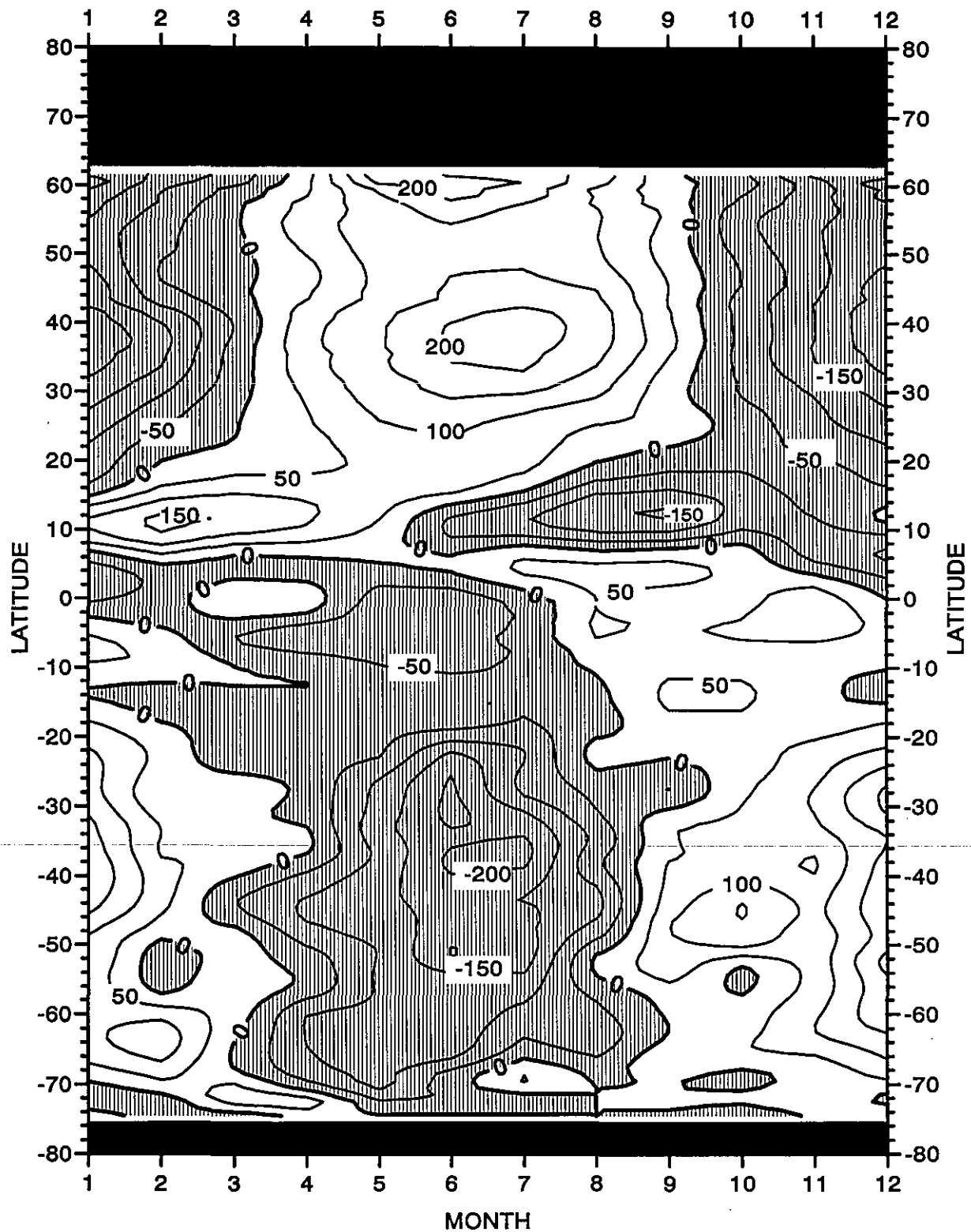


Fig. E20 Zonally averaged rate of heat storage (W^*M^{-2}) vertically integrated through 275 m depth for the Pacific Ocean

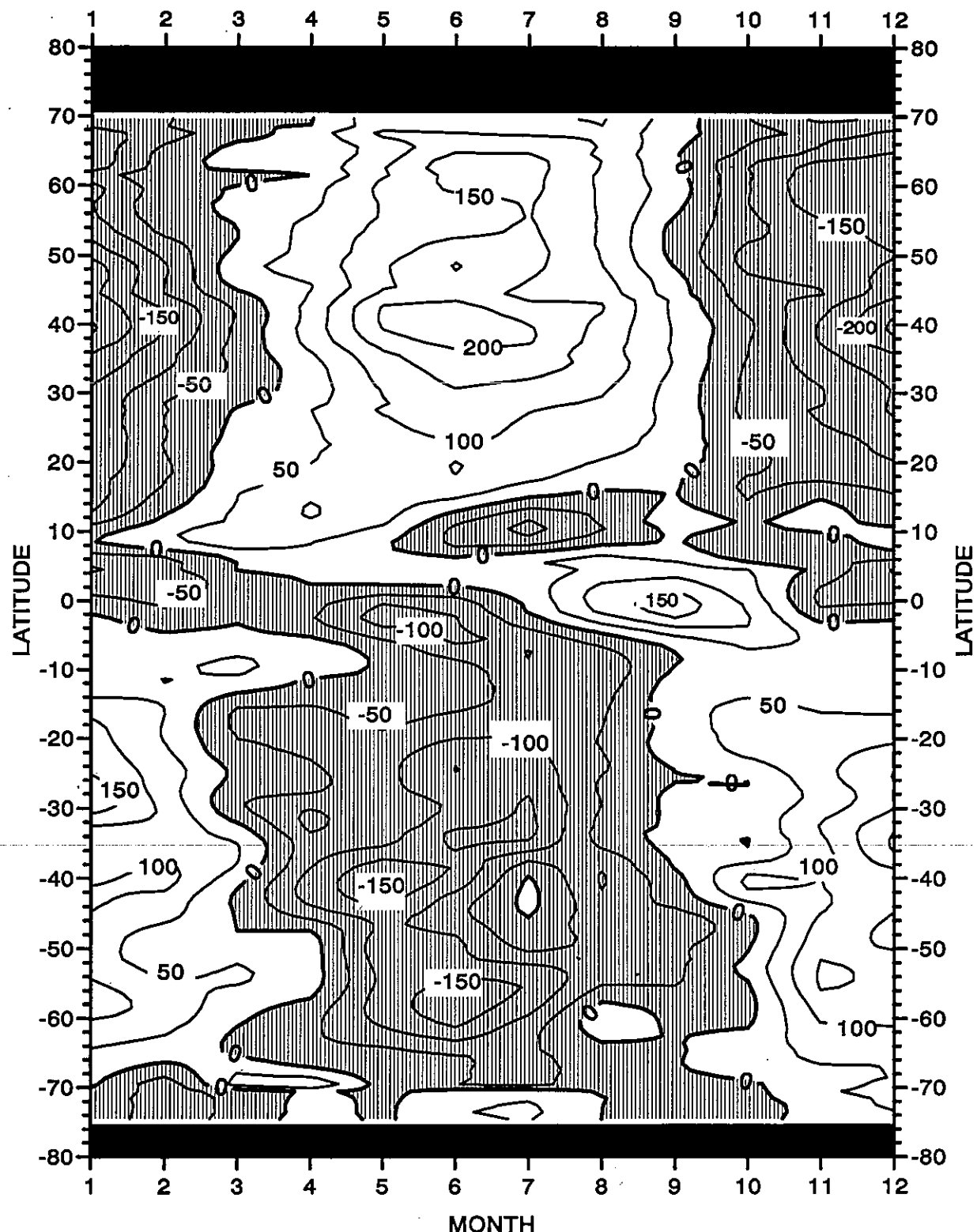


Fig. E21 Zonally averaged rate of heat storage ($\text{W}\cdot\text{m}^{-2}$) vertically integrated through 275 m depth for the Atlantic Ocean

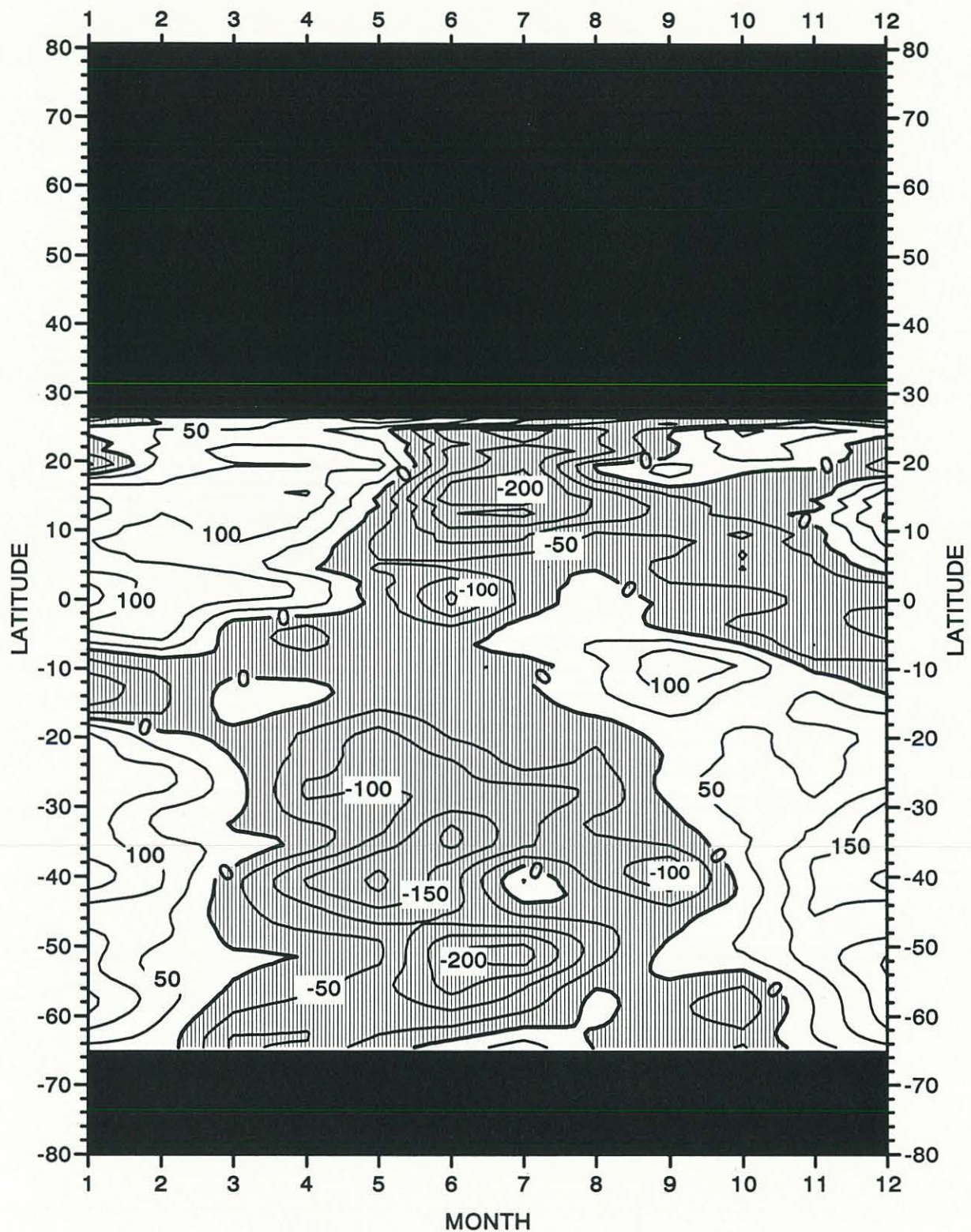


Fig. E22 Zonally averaged rate of heat storage (W^*m^{-2}) vertically integrated through 275 m depth for the Indian Ocean

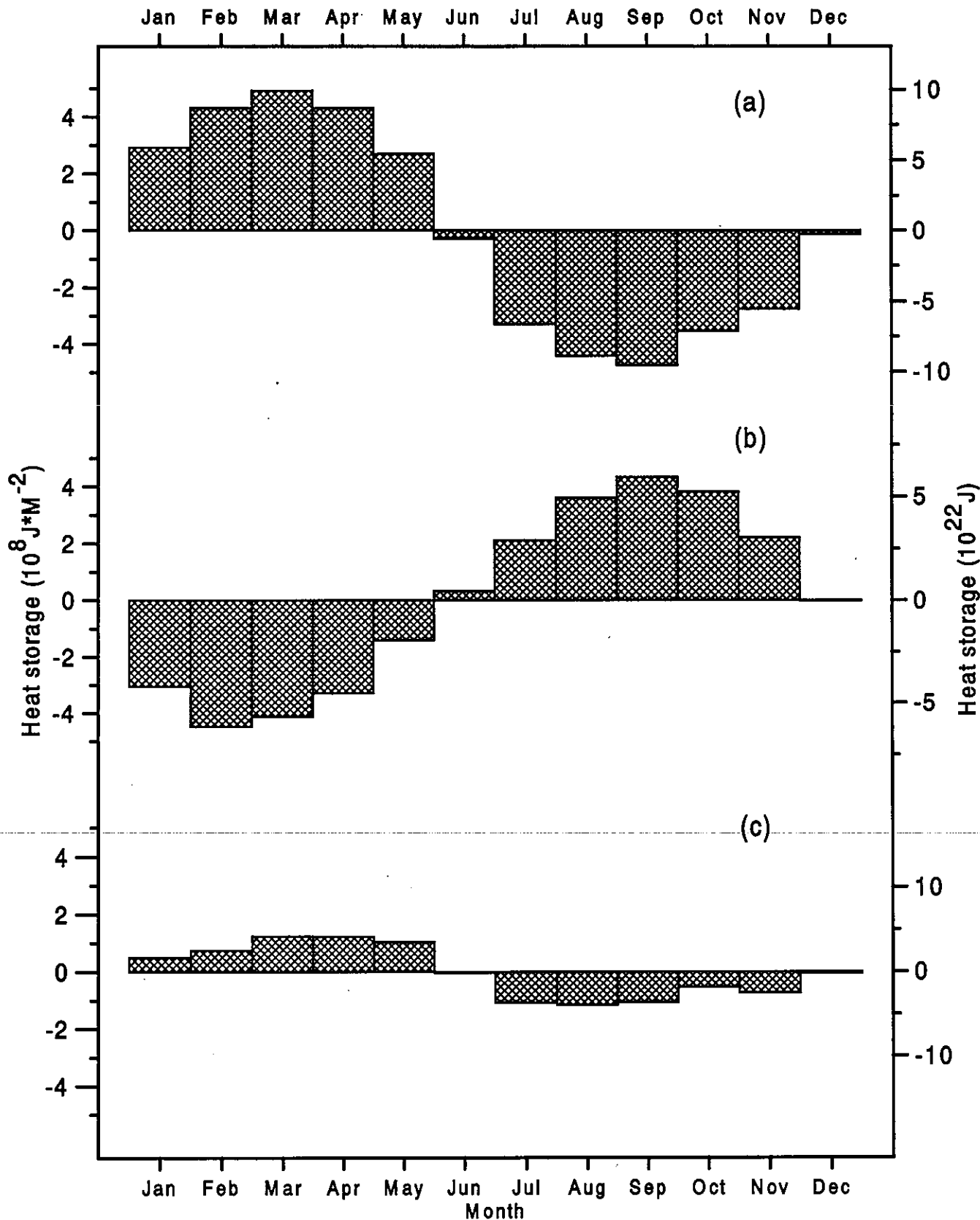


Fig. F1 Heat storage ($10^8 \text{ J} \cdot \text{m}^{-2}$ and 10^{22} J) integrated through 275 m depth
for (a) the Southern, and (b) the Northern Hemispheres, and (c) the World Ocean

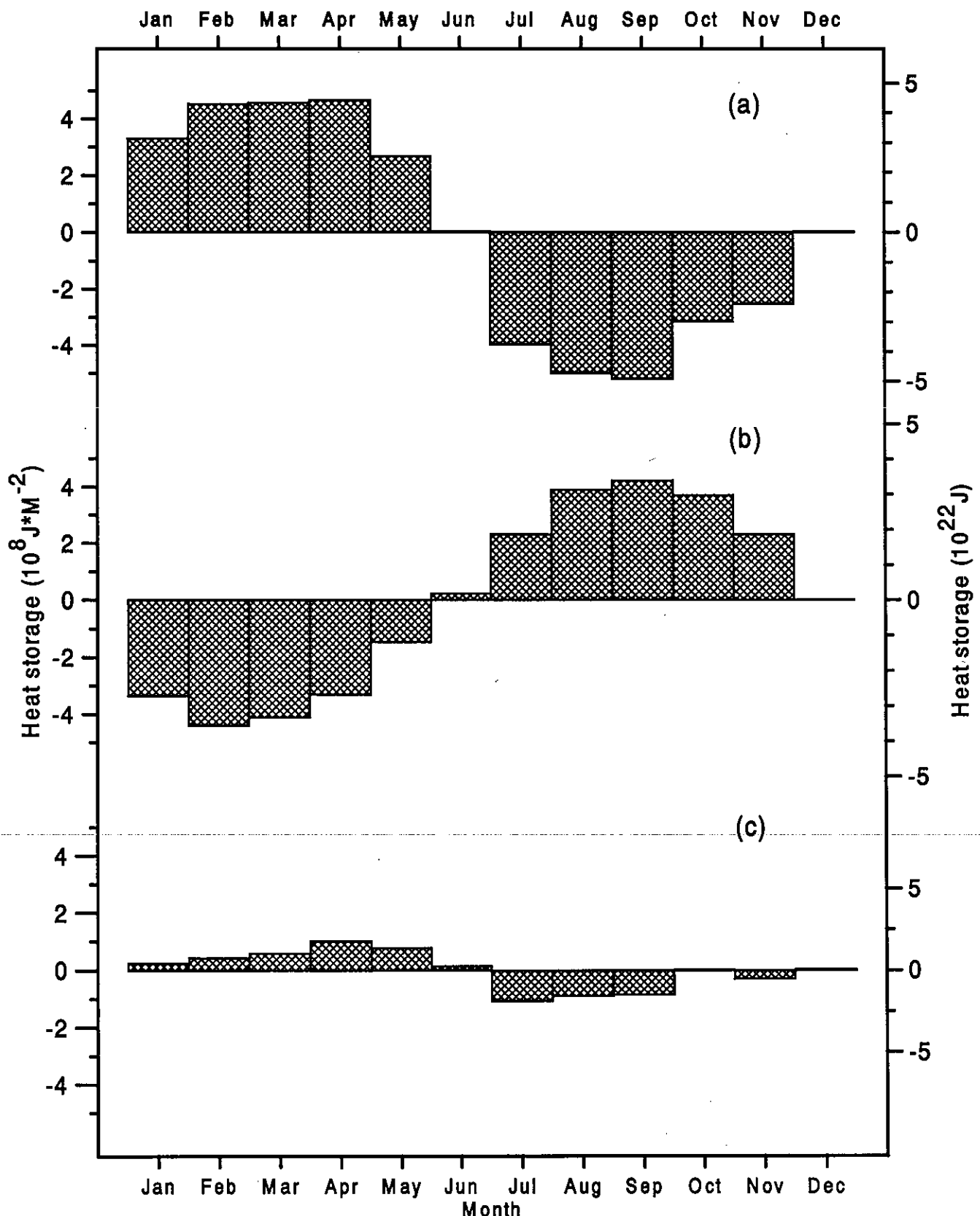


Fig. F2 Heat storage ($10^8 \text{ J} \cdot \text{m}^{-2}$ and 10^{22} J) integrated through 275 m depth for (a) the South Pacific, (b) the North Pacific, and (c) the Pacific Ocean

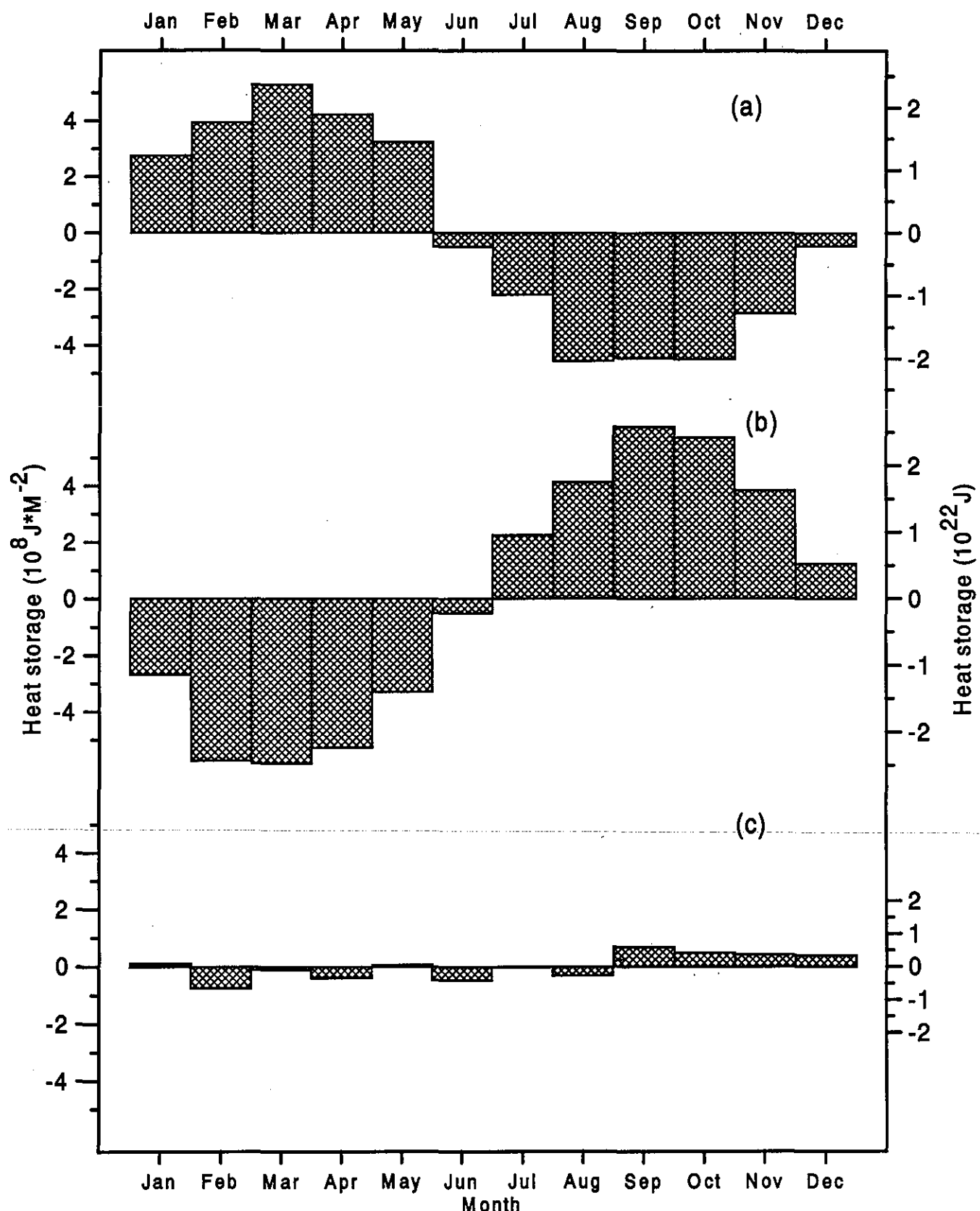


Fig. F3 Heat storage ($10^8 \text{ J} \cdot \text{m}^{-2}$ and 10^{22} J) integrated through 275 m depth for (a) the South Atlantic, (b) the North Atlantic, and (c) the Atlantic Ocean

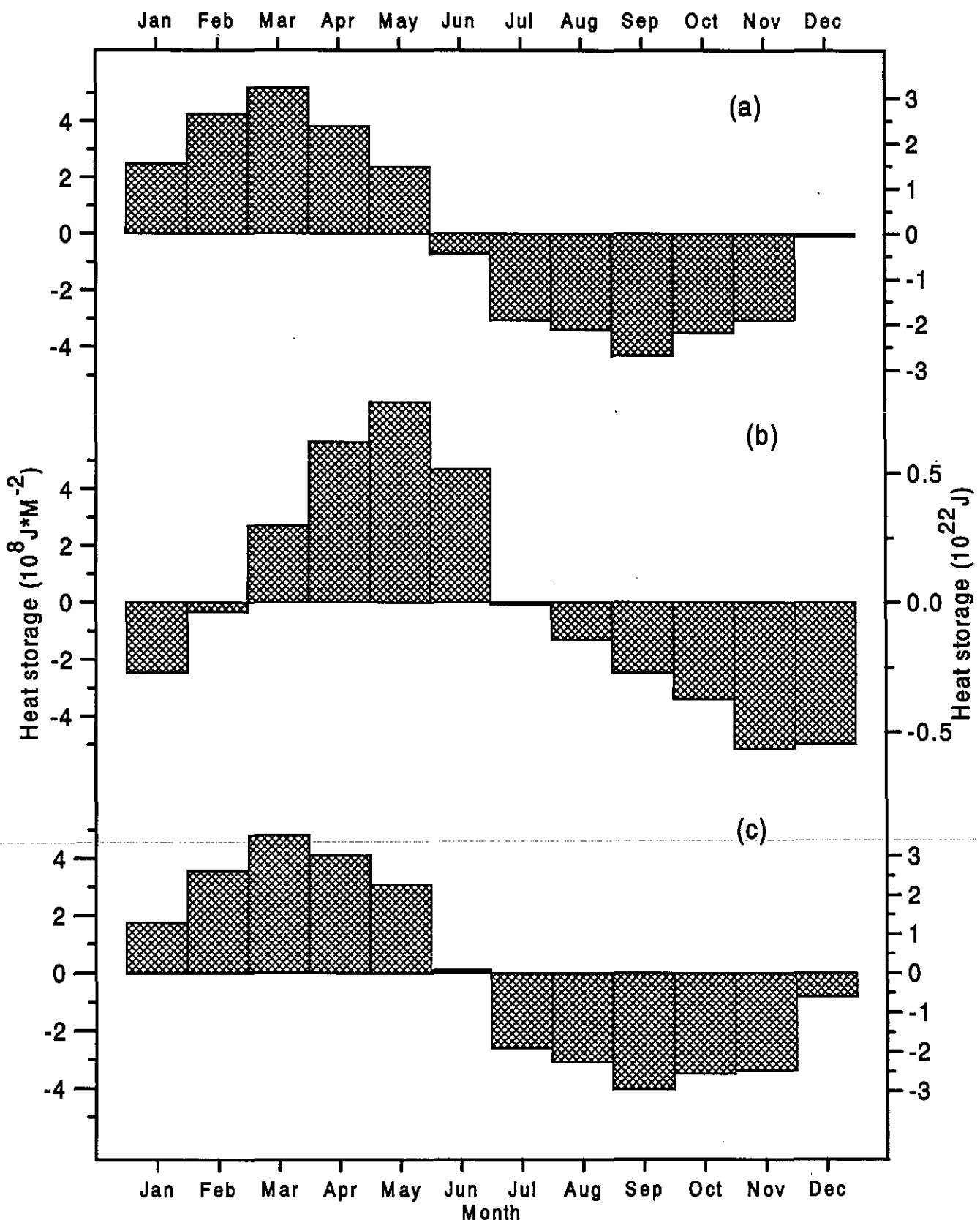


Fig. F4 Heat storage ($10^8 \text{ J} * \text{M}^{-2}$ and 10^{22} J) integrated through 275 m depth for (a) the South Indian, (b) the North Indian, and (c) the Indian Ocean

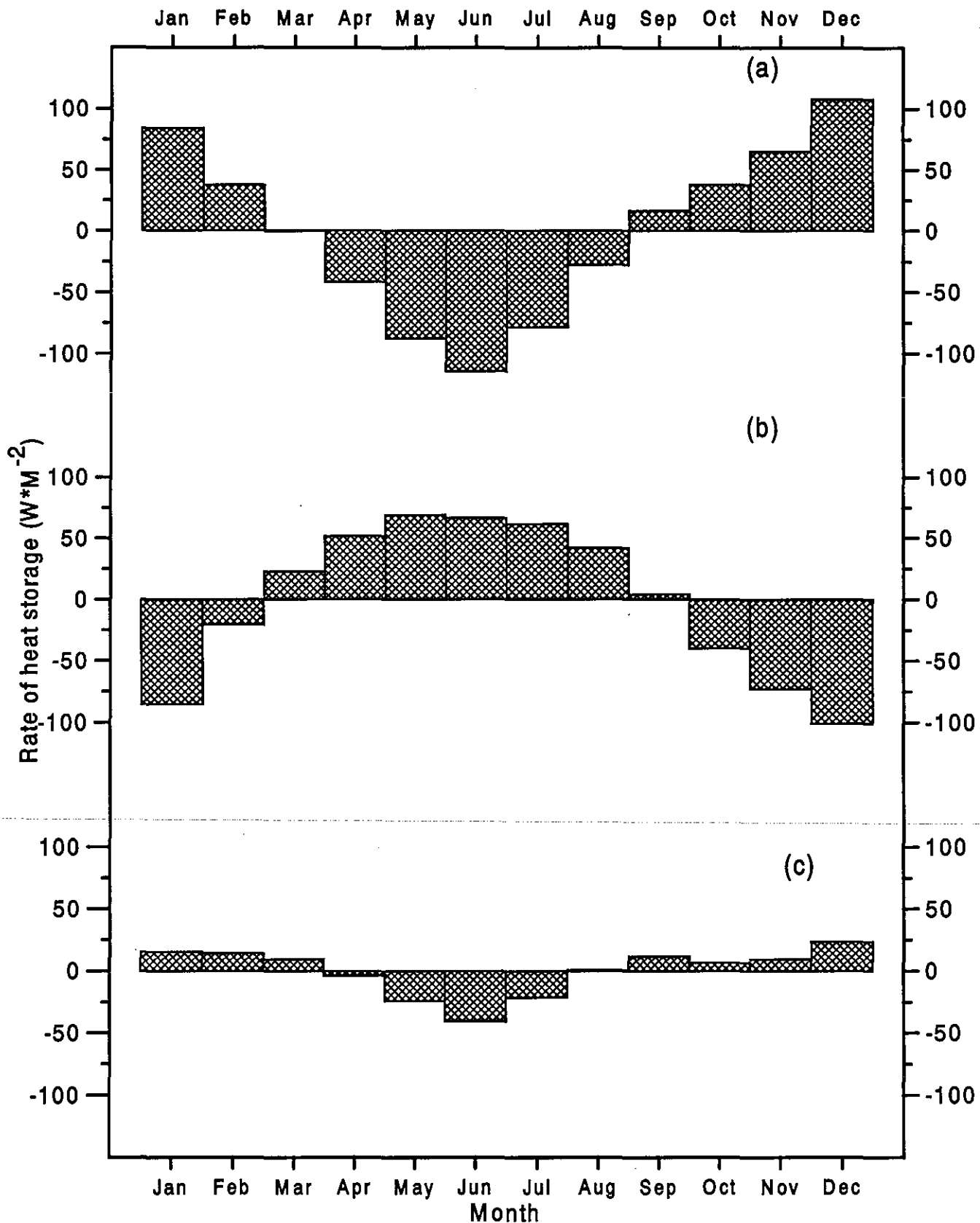


Fig. F5 Rate of heat storage ($\text{W} \cdot \text{M}^{-2}$) integrated through 275 m depth for
 (a) the Southern, and (b) the Northern Hemispheres, and (c) the World Ocean

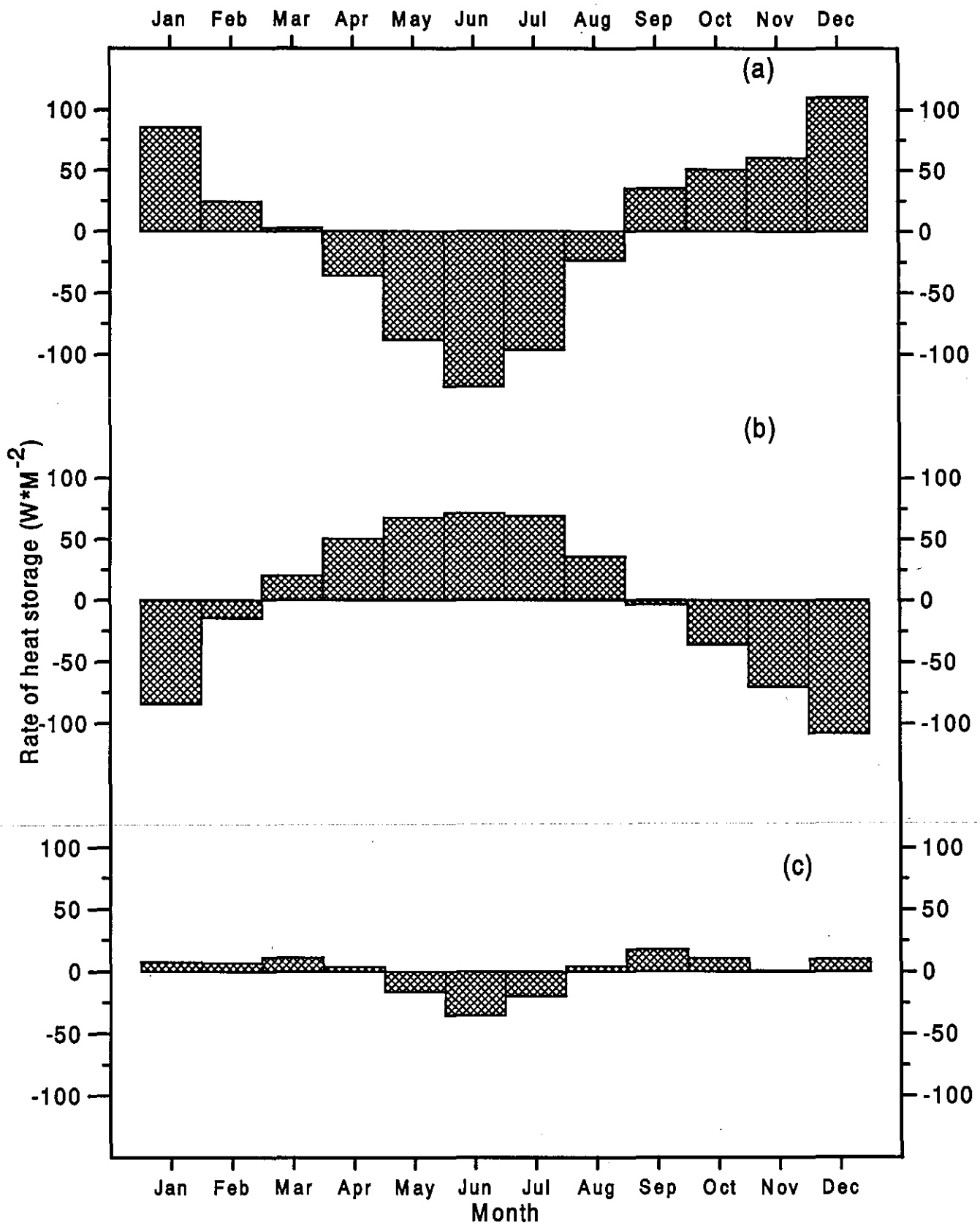


Fig. F6 Rate of heat storage ($\text{W} \cdot \text{m}^{-2}$) integrated through 275 m depth for (a) the South Pacific, (b) the North Pacific, and (c) the Pacific Ocean

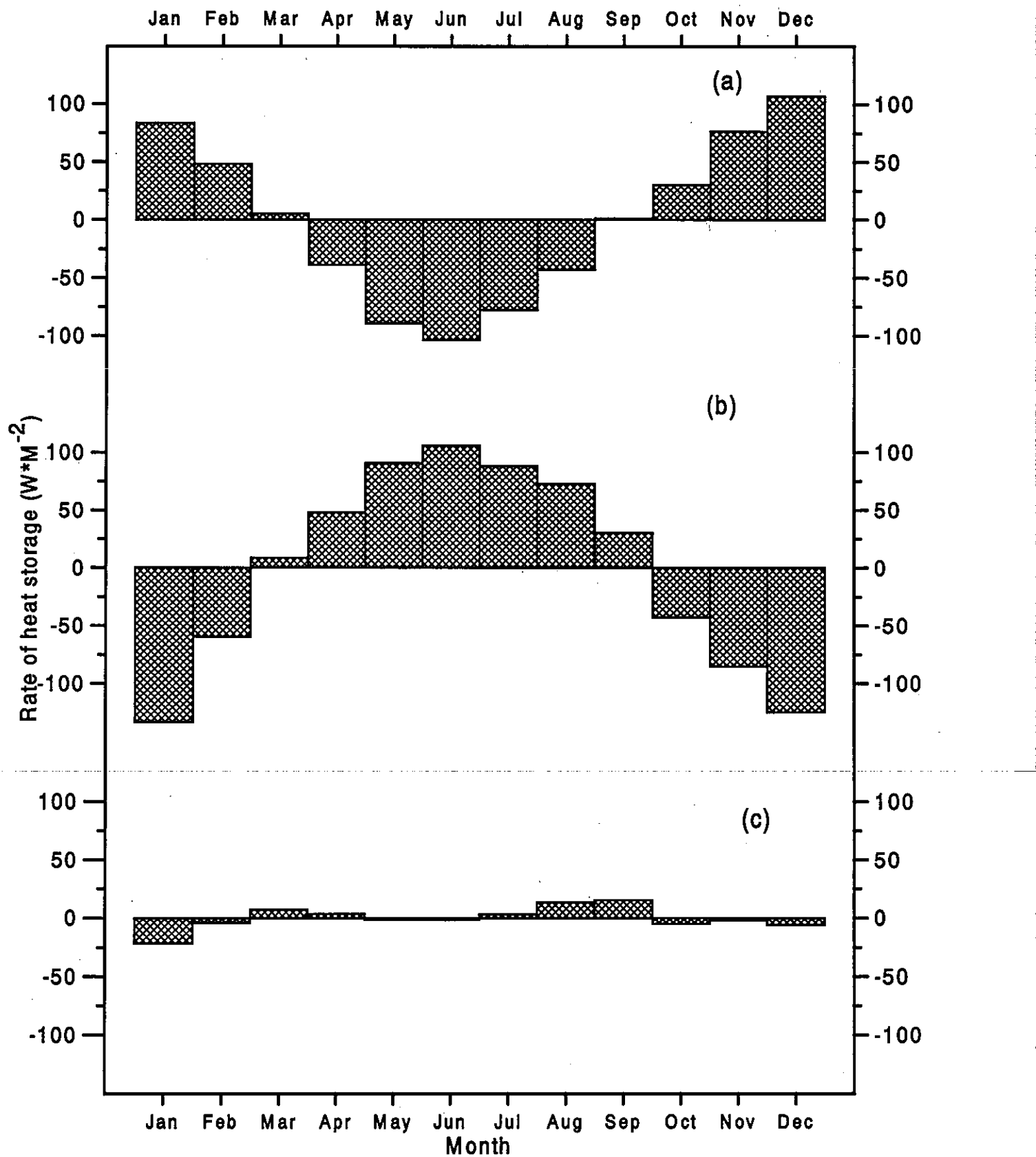


Fig. F7 Rate of heat storage ($\text{W} \cdot \text{m}^{-2}$) integrated through 275 m depth for (a) the South Atlantic, (b) the North Atlantic, and (c) the Atlantic Ocean

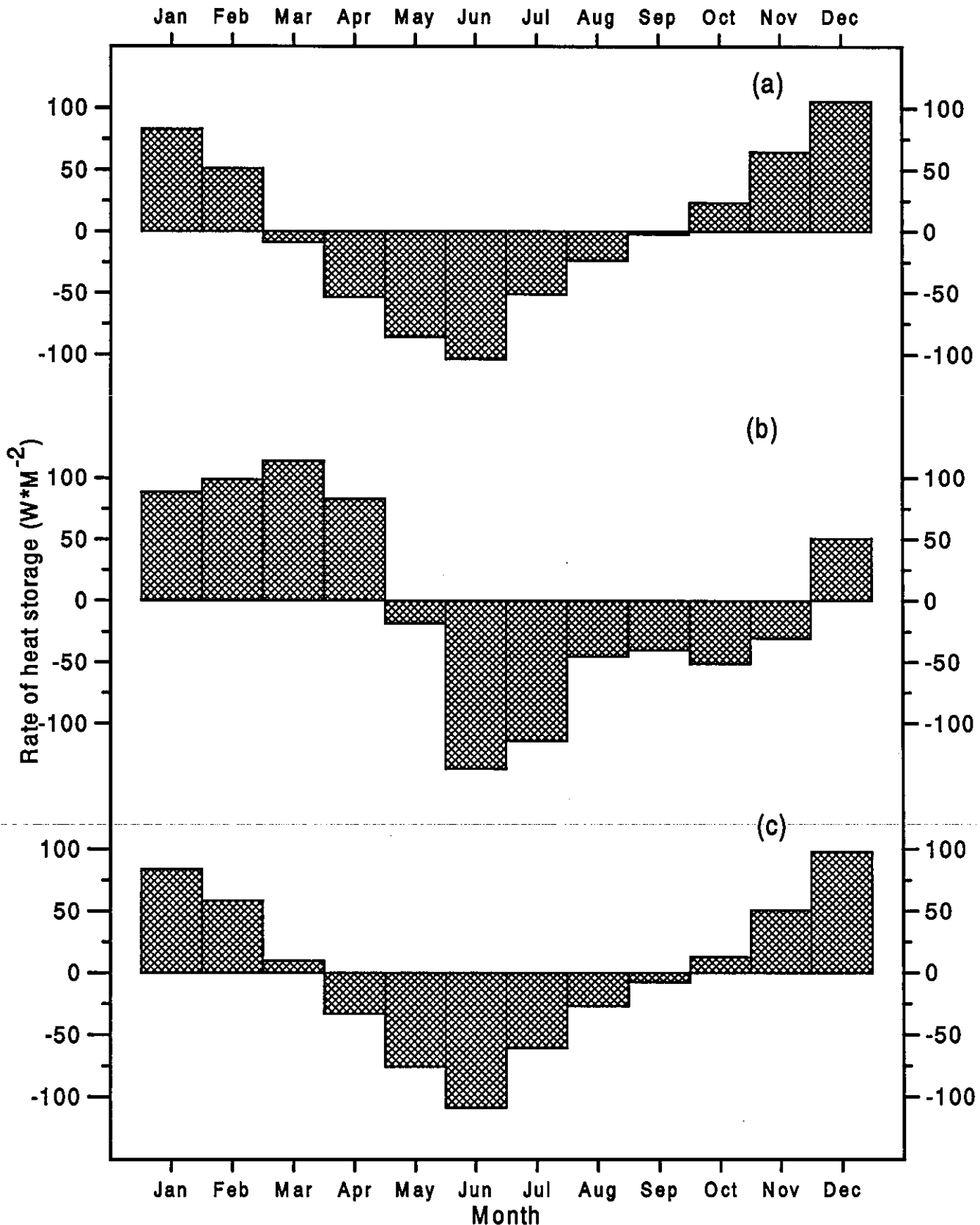


Fig. F8 Rate of heat storage ($\text{W} \cdot \text{M}^{-2}$) integrated through 275 m depth
for (a) the South Indian, (b) the North Indian, and (c) the Indian Ocean

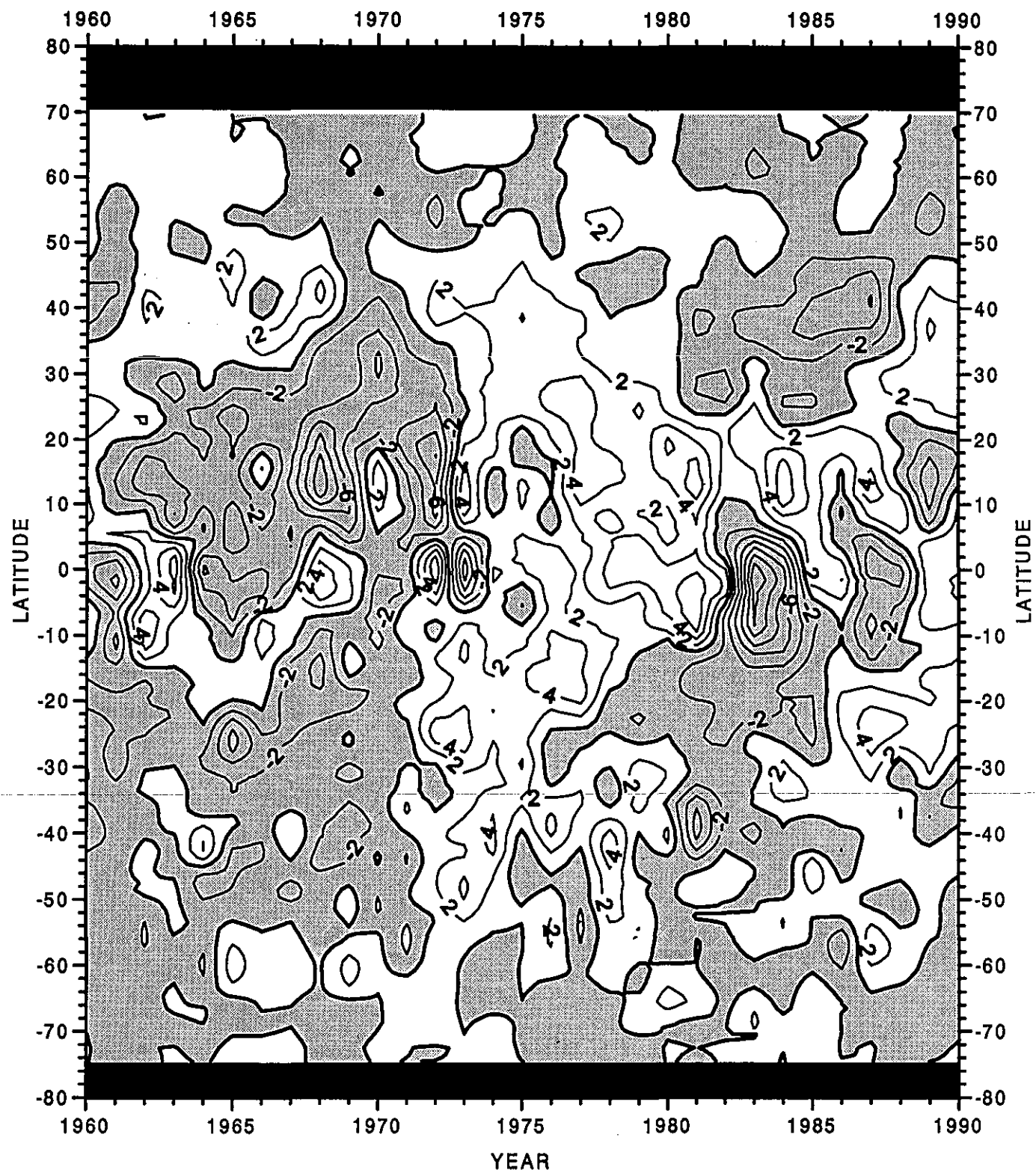


Fig. G1 Zonally integrated heat storage (10^{20} J) integrated through 275 meters depth for the World Ocean

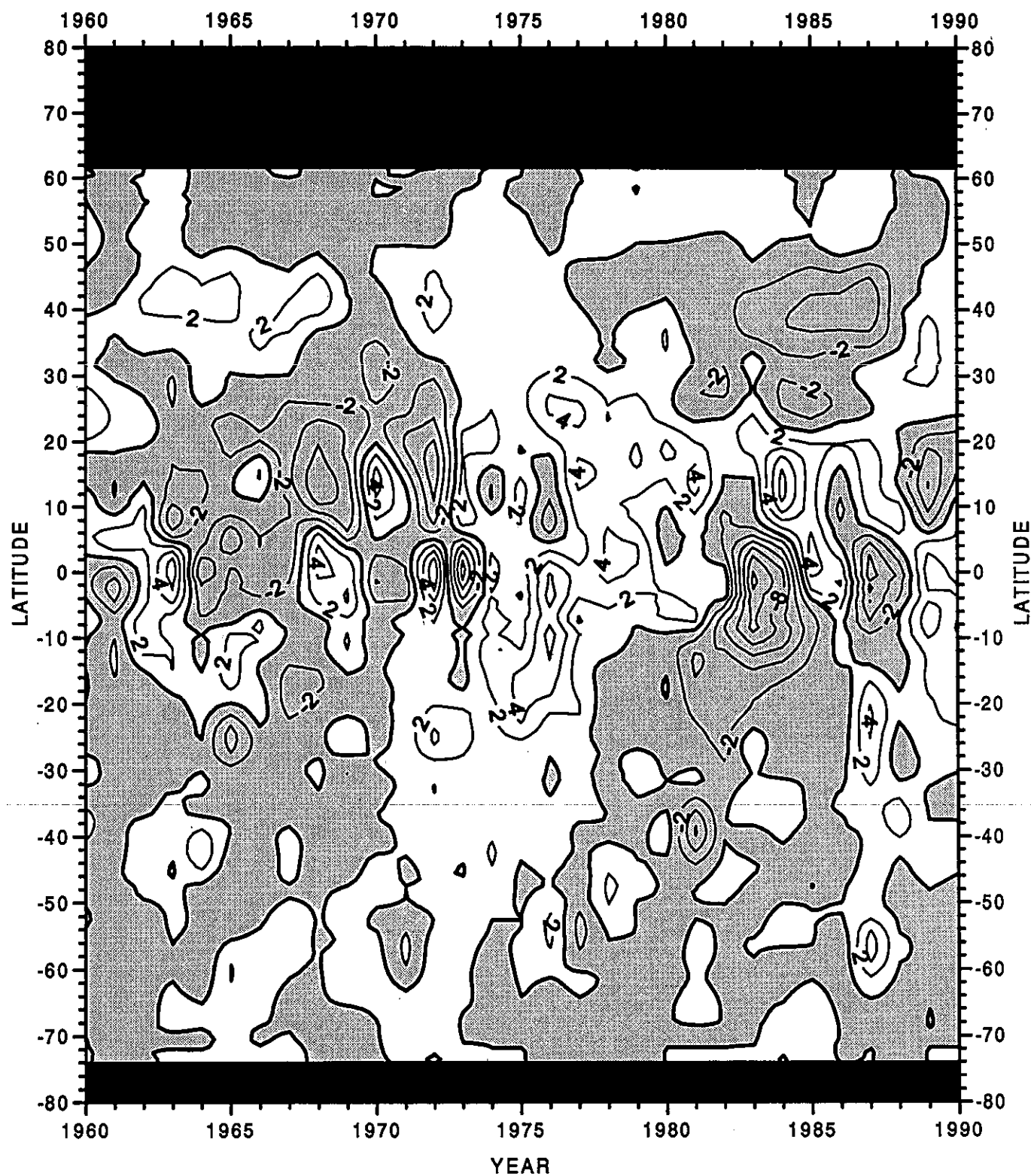


Fig. G2 Zonally integrated heat storage (10^{20} J) integrated through 275 meters depth for the Pacific Ocean

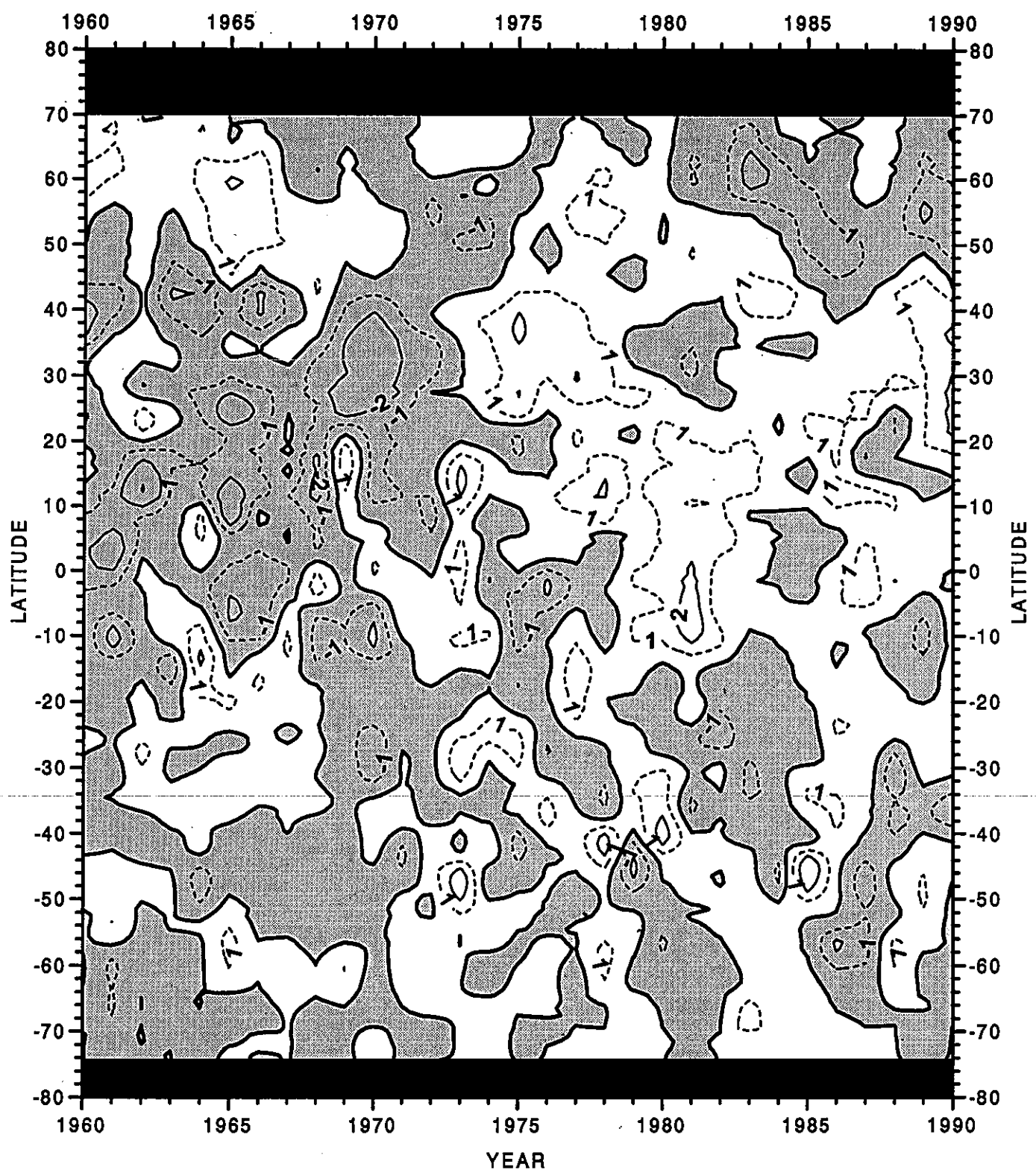


Fig. G3 Zonally integrated heat storage (10^{20} J) integrated through 275 meters depth for the Atlantic Ocean

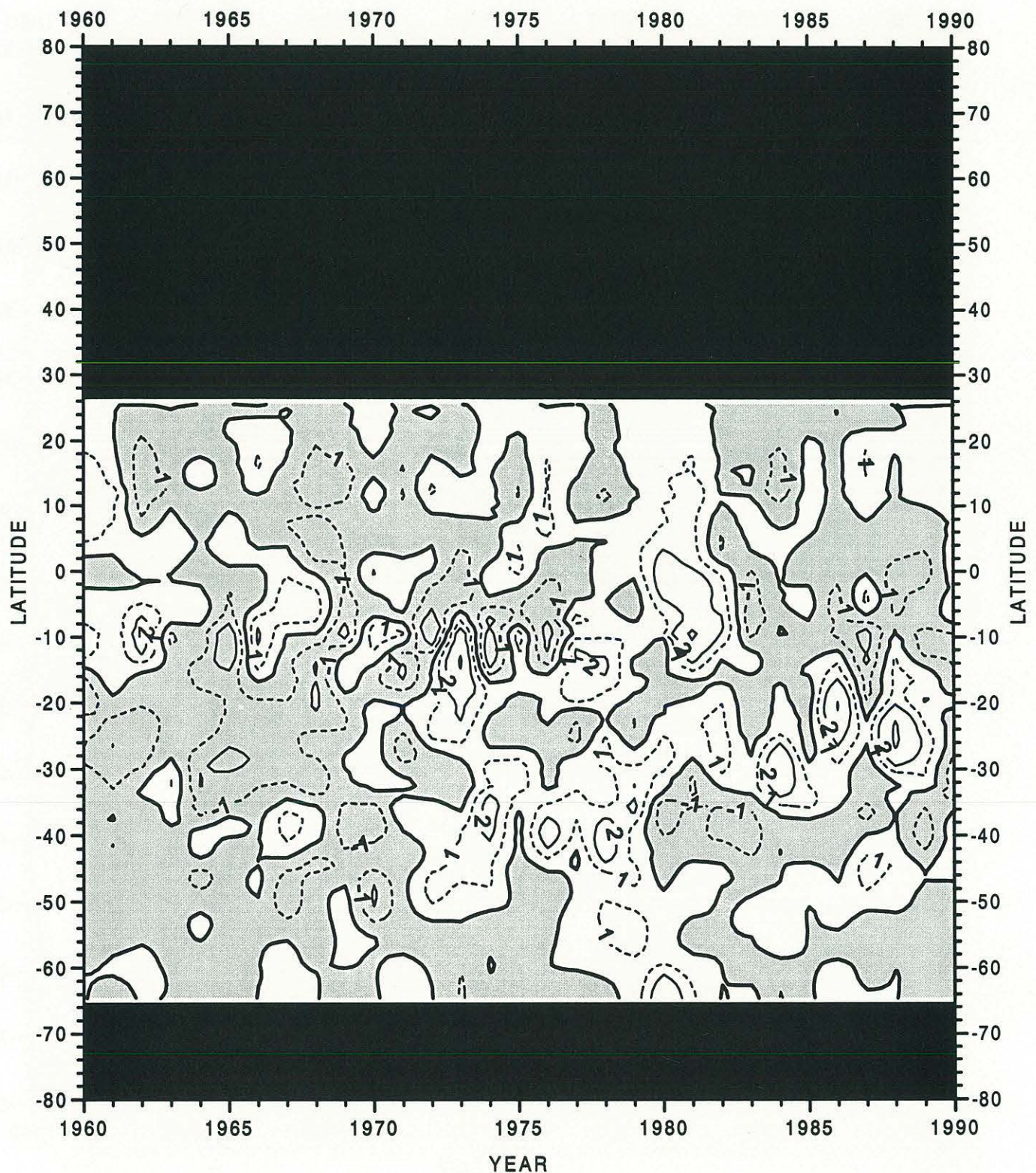


Fig. G4 Zonally integrated heat storage (10^{20} J) integrated through 275 meters depth for the Indian Ocean

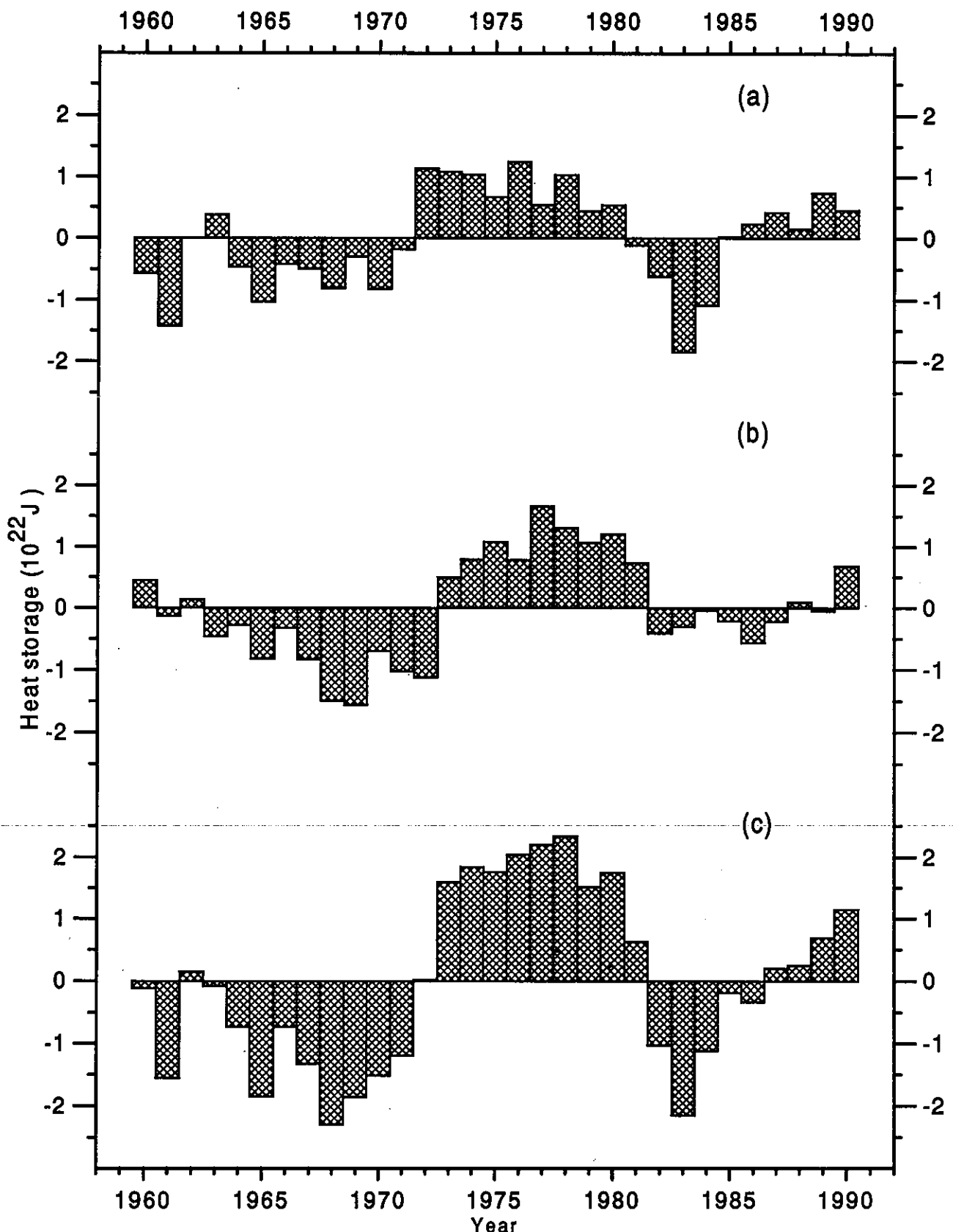


Fig. G5 Heat storage (10^{22} J) integrated through 275 meters depth for
 (a) the Southern and (b) the Northern Hemispheres, and (c) the World Ocean

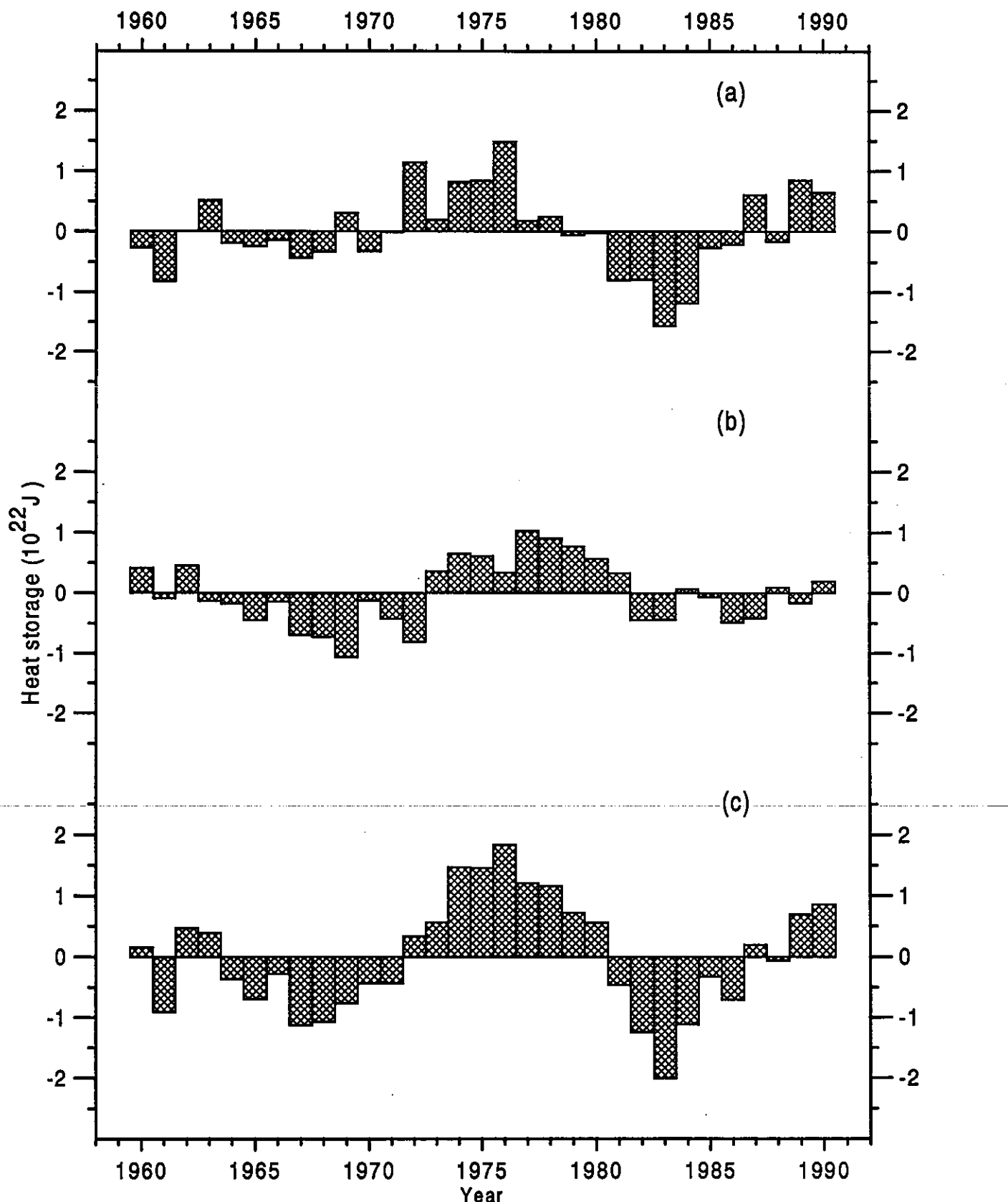


Fig. G6 Heat storage (10^{22} J) integrated through 275 meters depth
for (a) the South Pacific, (b) the North Pacific, and (c) the Pacific Ocean

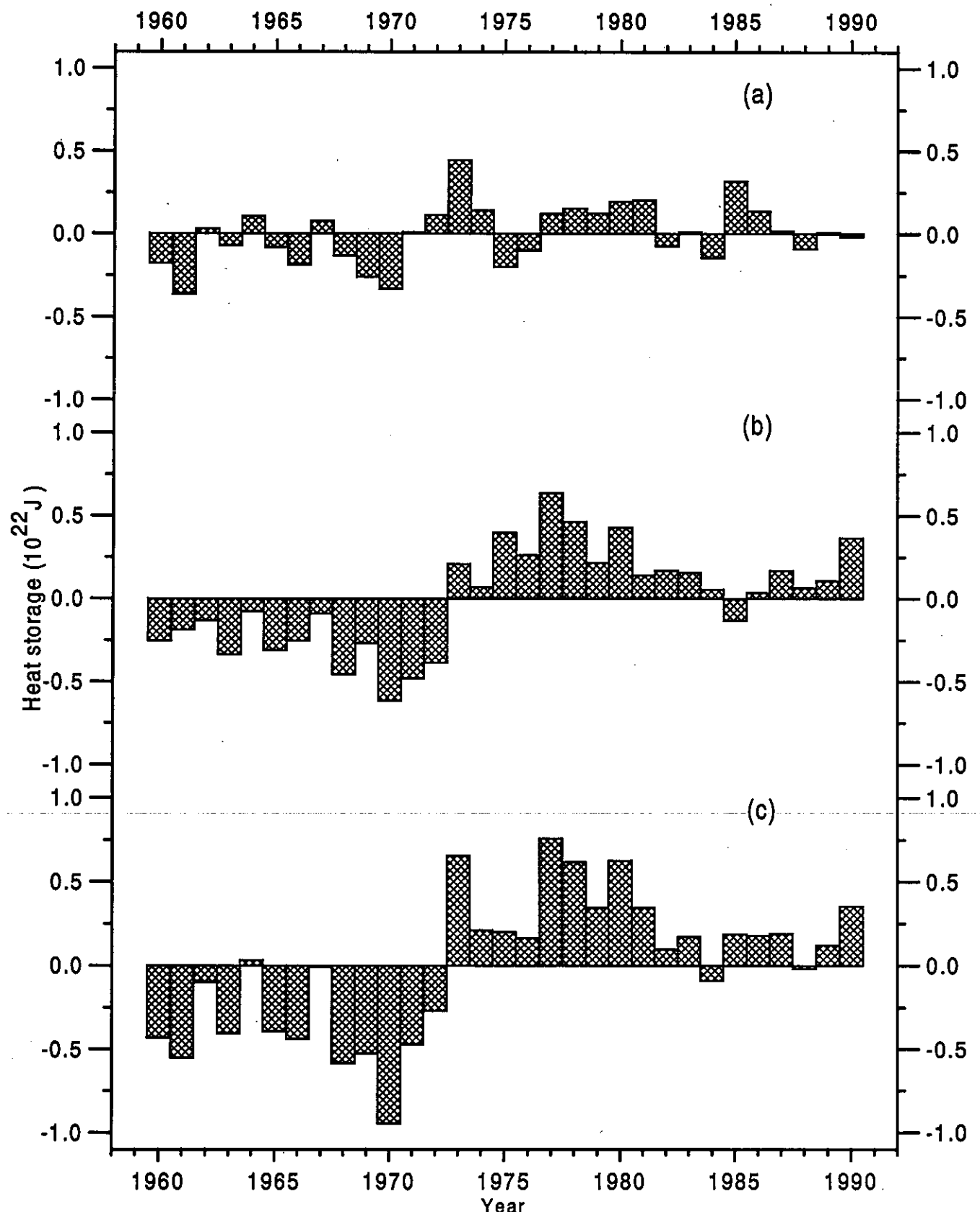


Fig. G7 Heat storage (10^{22} J) integrated through 275 meters depth
for (a) the South Atlantic, (b) the North Atlantic, and (c) the Atlantic Ocean

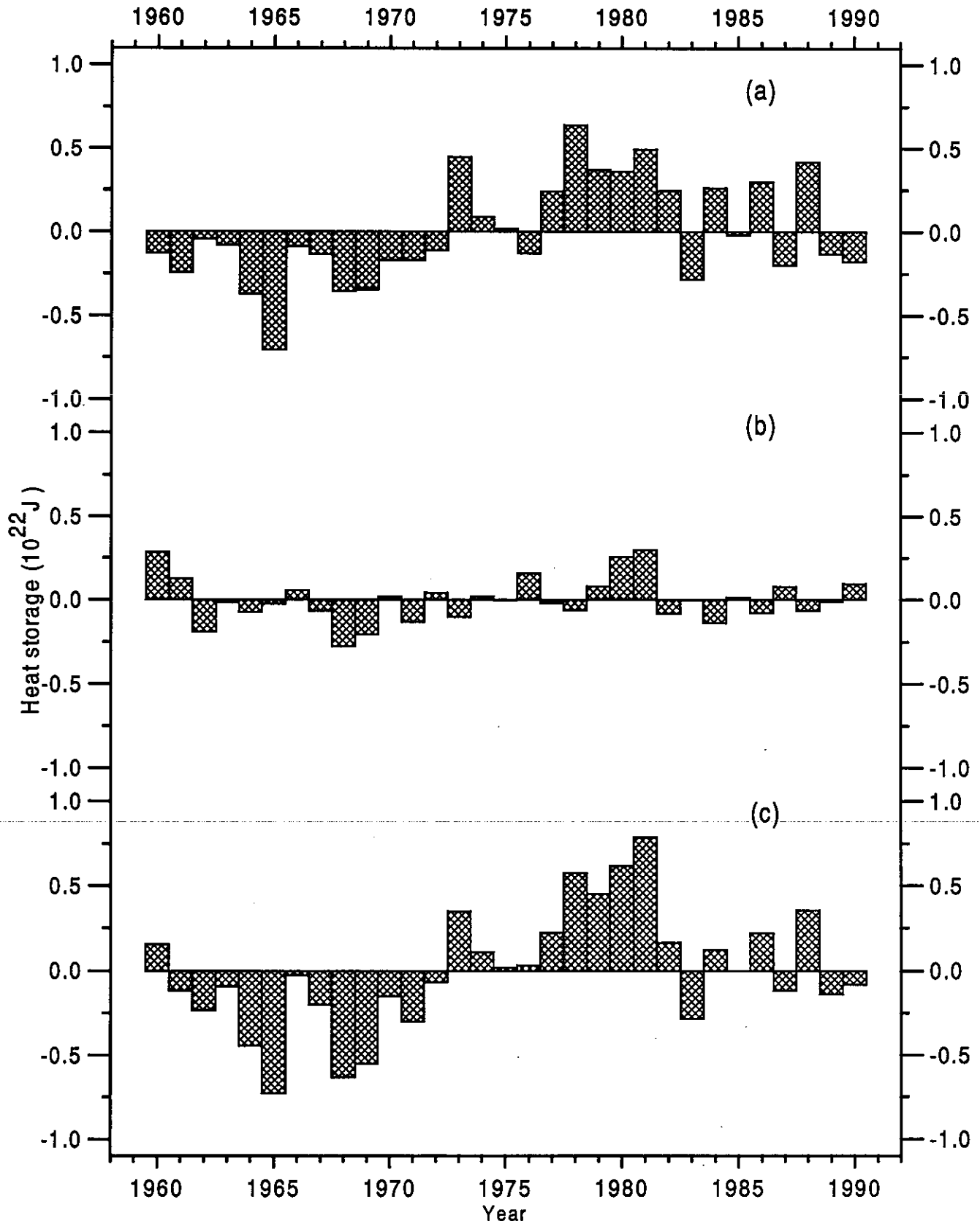


Fig. G8 Heat storage (10^{22} J) integrated through 275 meters depth
for (a) the South Indian, (b) the North Indian, and (c) the Indian Ocean

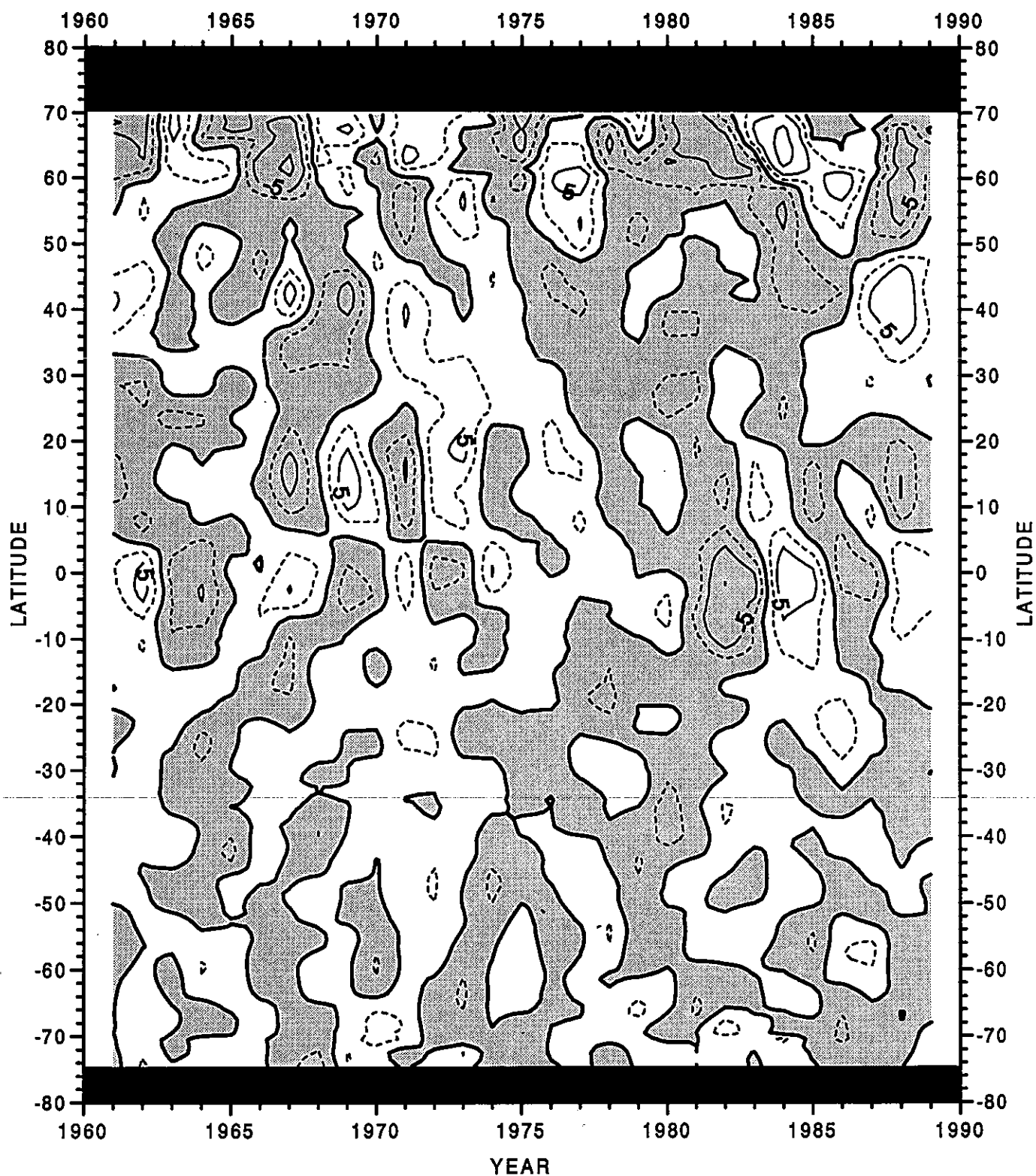


Fig. G9 Zonally averaged rate of heat storage ($\text{W} \cdot \text{M}^{-2}$) integrated through 275 meters depth for the World Ocean

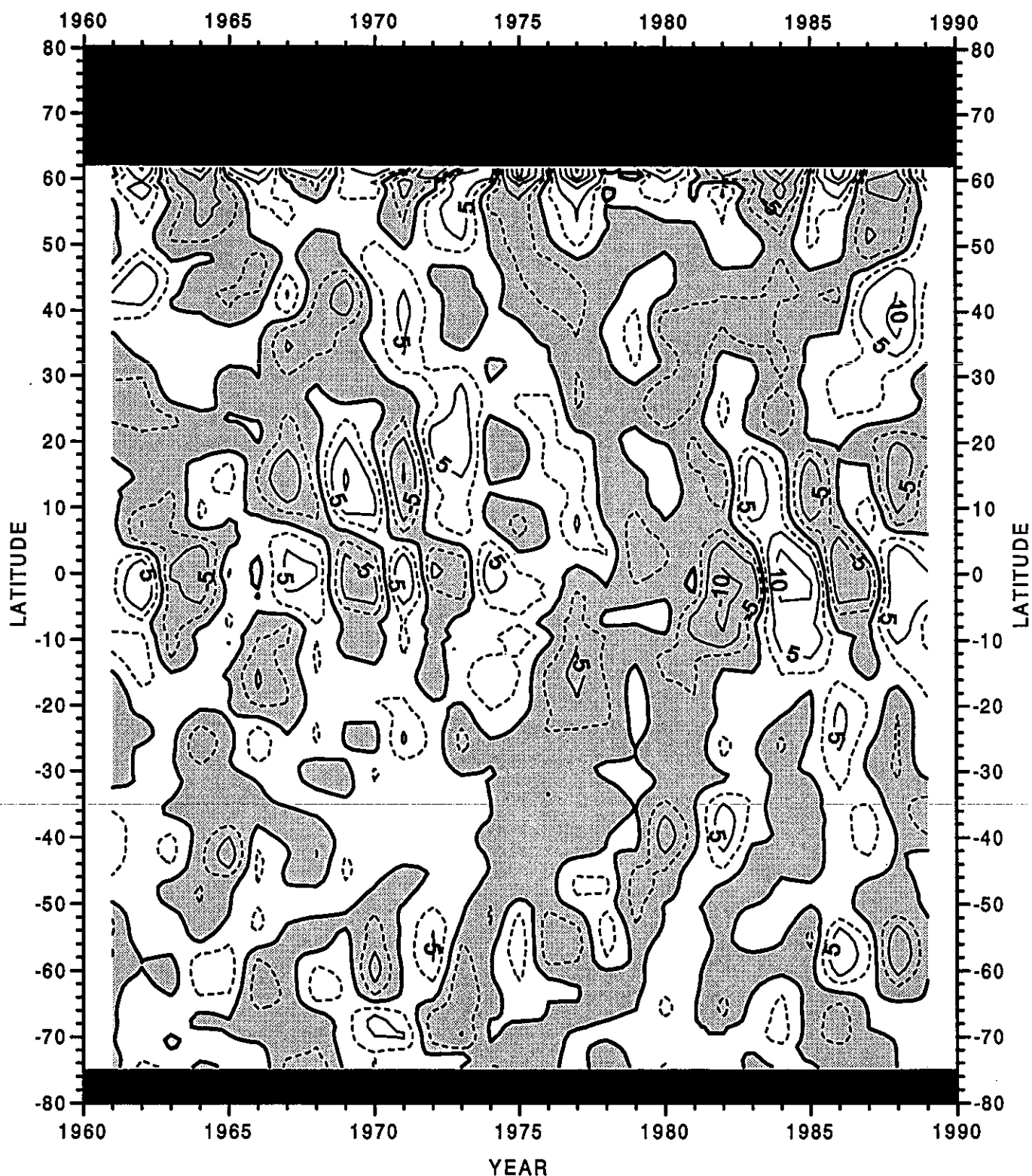


Fig. G10 Zonally averaged rate of heat storage ($\text{W} \cdot \text{M}^{-2}$) integrated through 275 meters depth for the Pacific Ocean

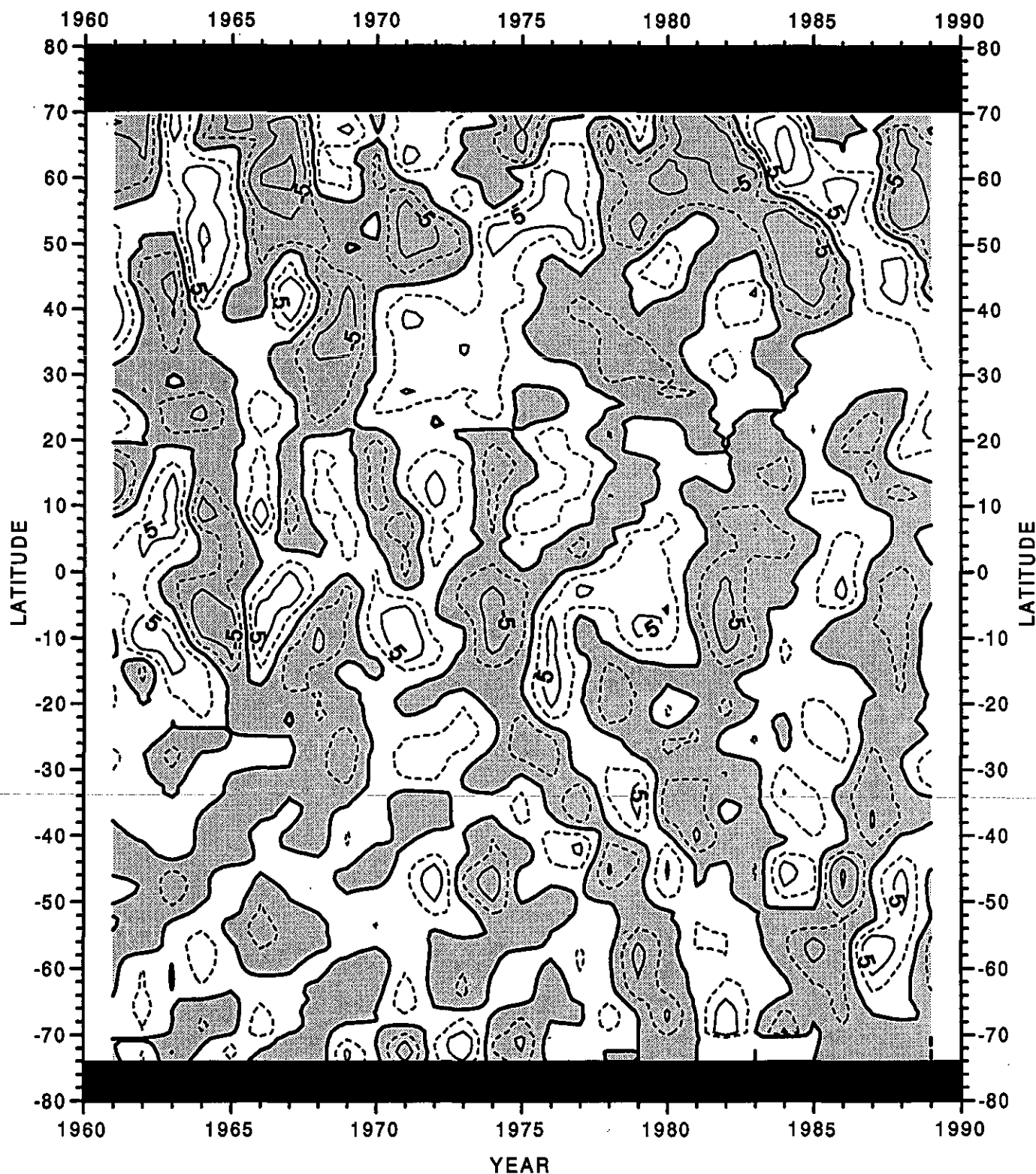


Fig. G11 Zonally averaged rate of heat storage ($\text{W} \cdot \text{m}^{-2}$) integrated through 275 meters depth for the Atlantic Ocean

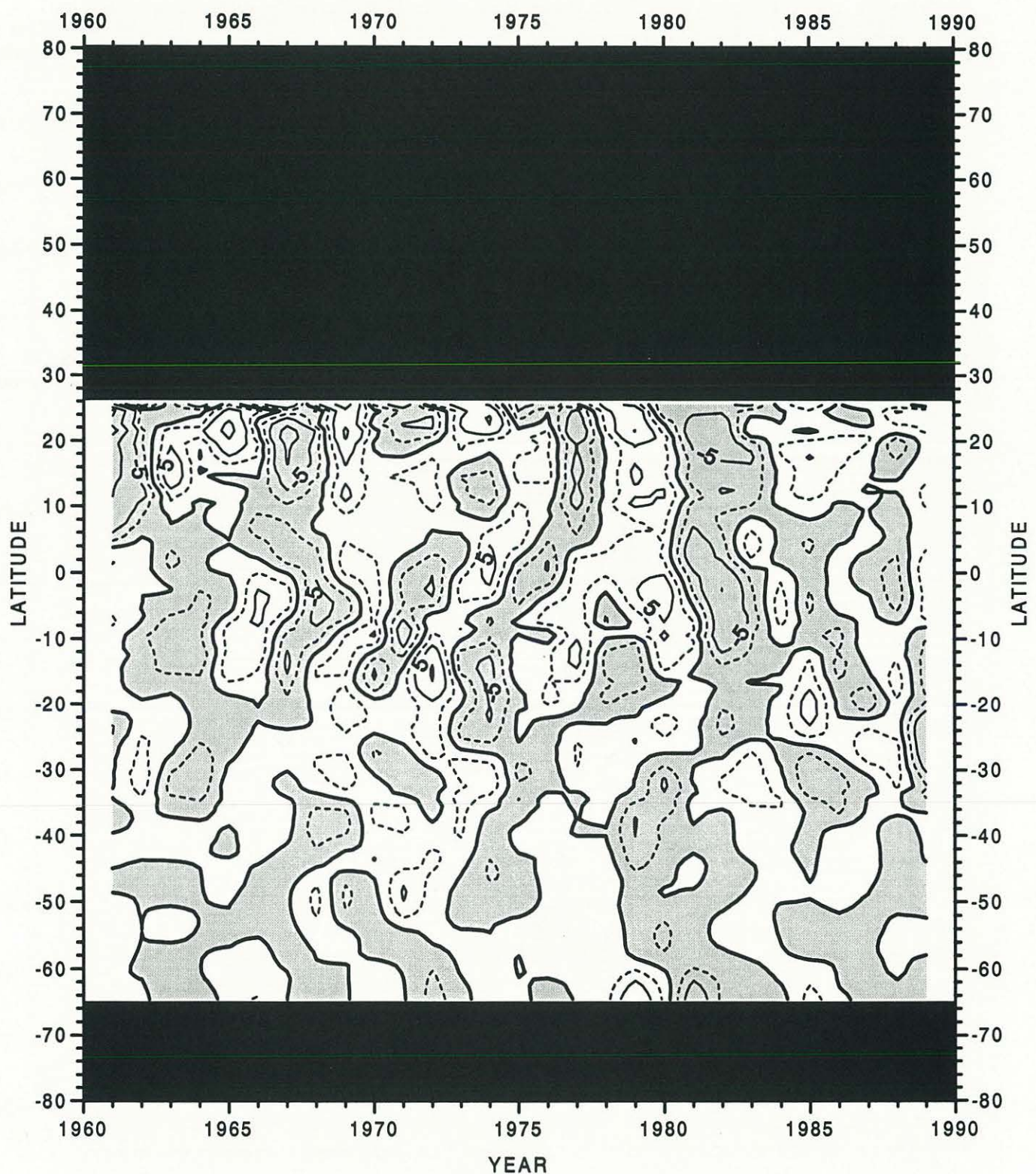


Fig. G12 Zonally averaged rate of heat storage ($\text{W} \cdot \text{m}^{-2}$) integrated through 275 meters depth for the Indian Ocean

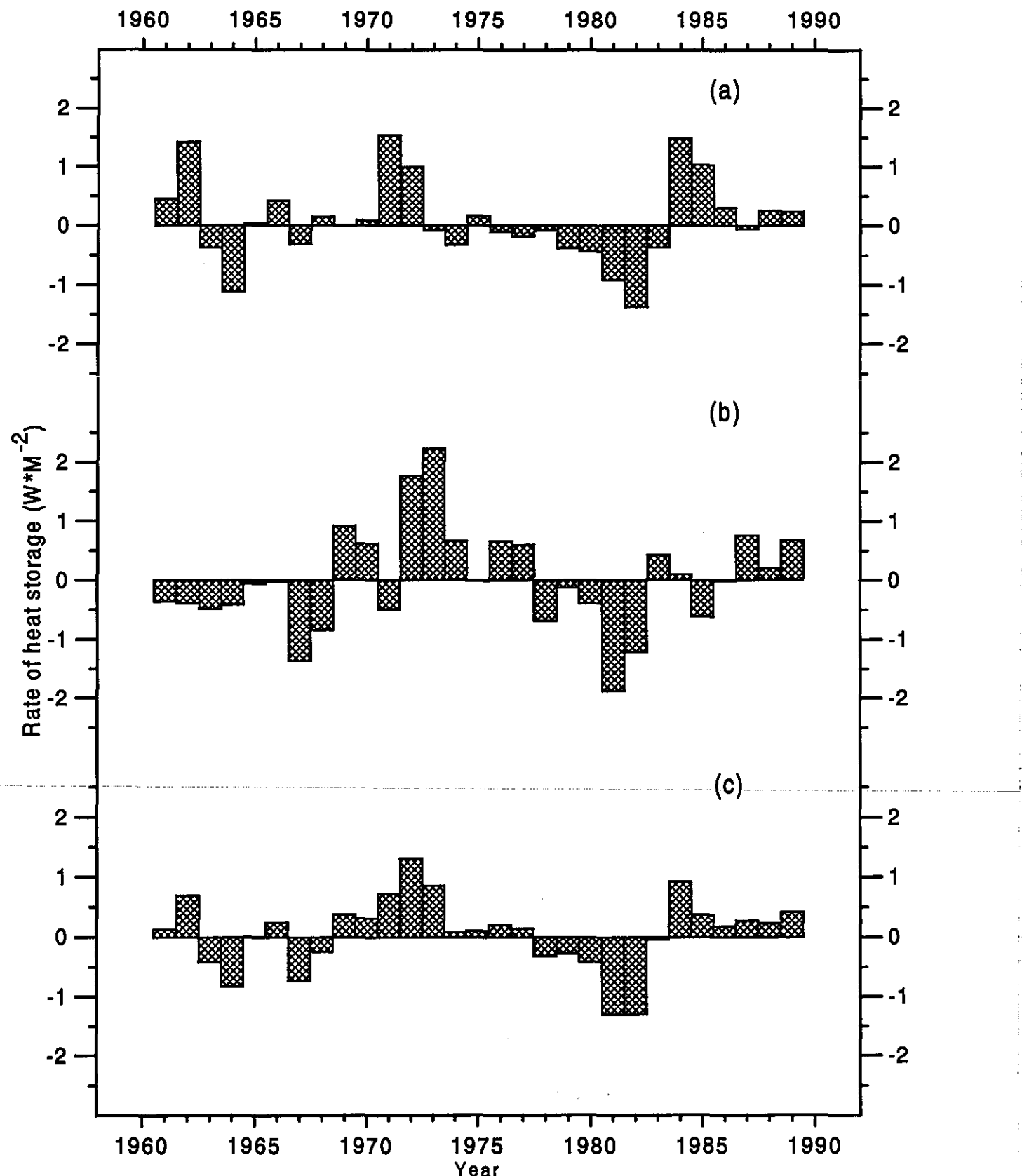


Fig. G13 Rate of heat storage ($\text{W} \cdot \text{M}^{-2}$) integrated through 275 m depth
for (a) the Southern and (b) Northern Hemispheres, and (c) the World Ocean

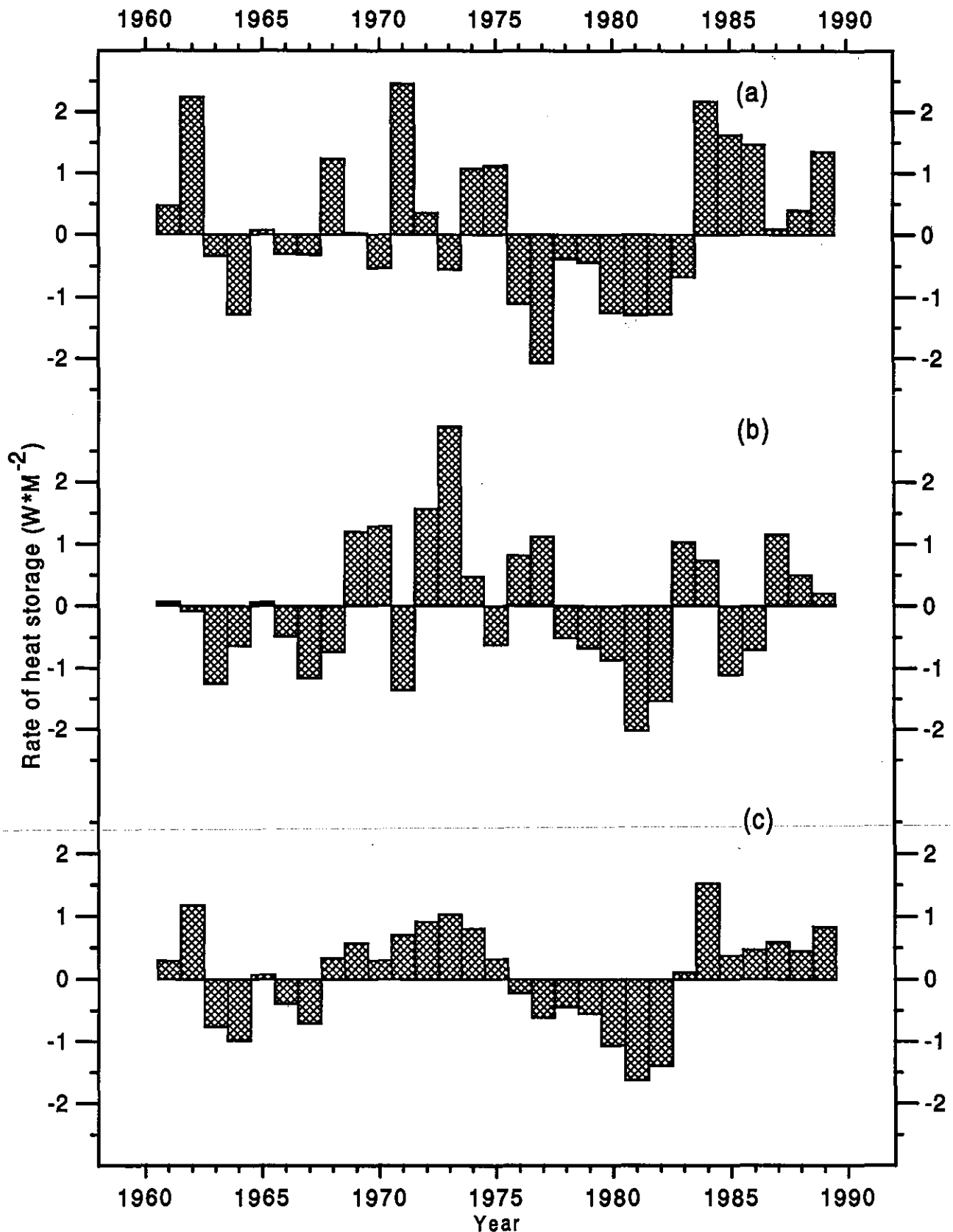


Fig. G14 Rate of heat storage ($\text{W} \cdot \text{M}^{-2}$) integrated through 275 m depth for (a) the South Pacific, (b) the North Pacific, and (c) the Pacific Ocean

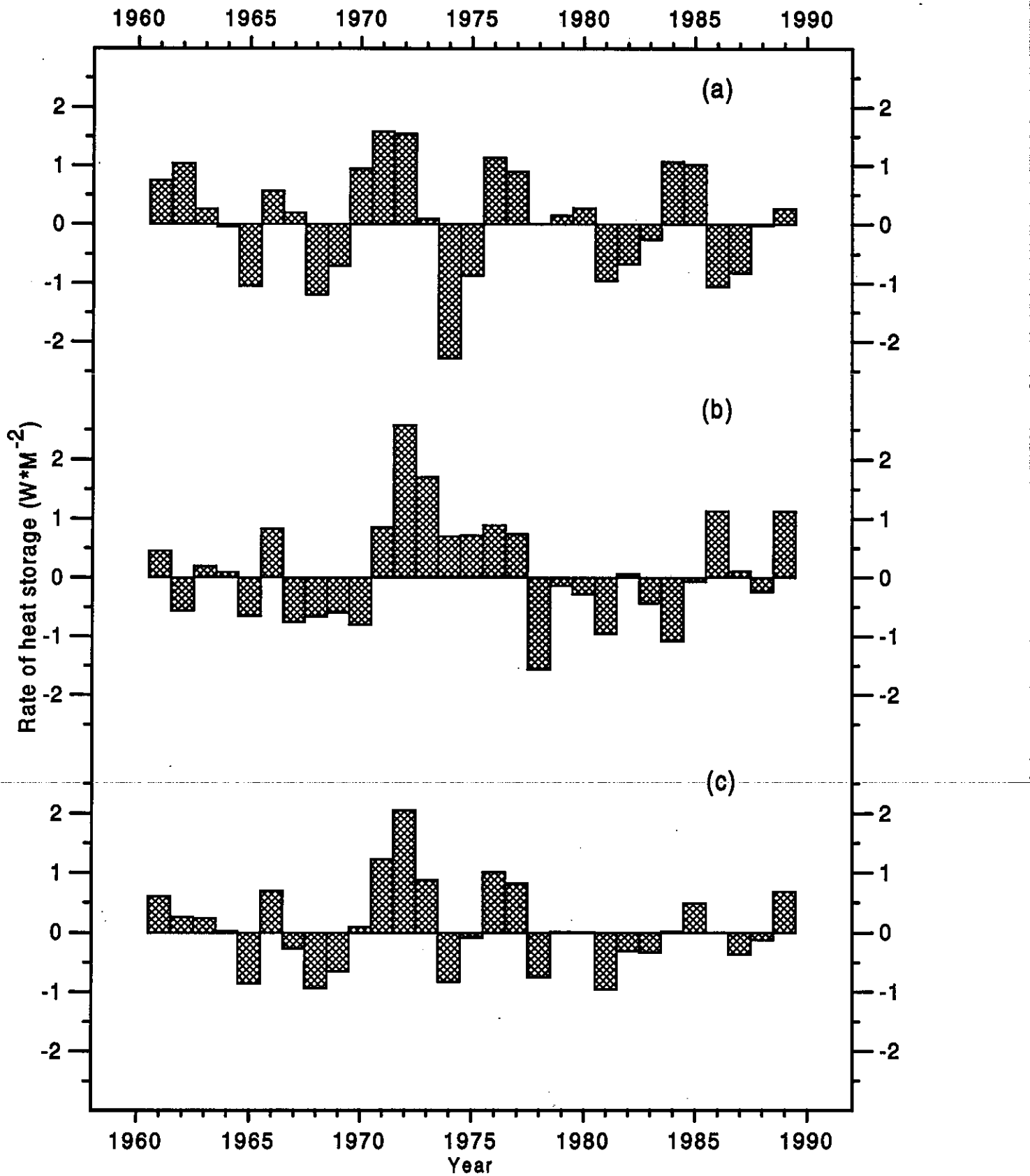


Fig. G15 Rate of heat storage ($\text{W} \cdot \text{M}^{-2}$) integrated through 275 m depth
for (a) the South Atlantic, (b) the North Atlantic, and (c) the Atlantic Ocean

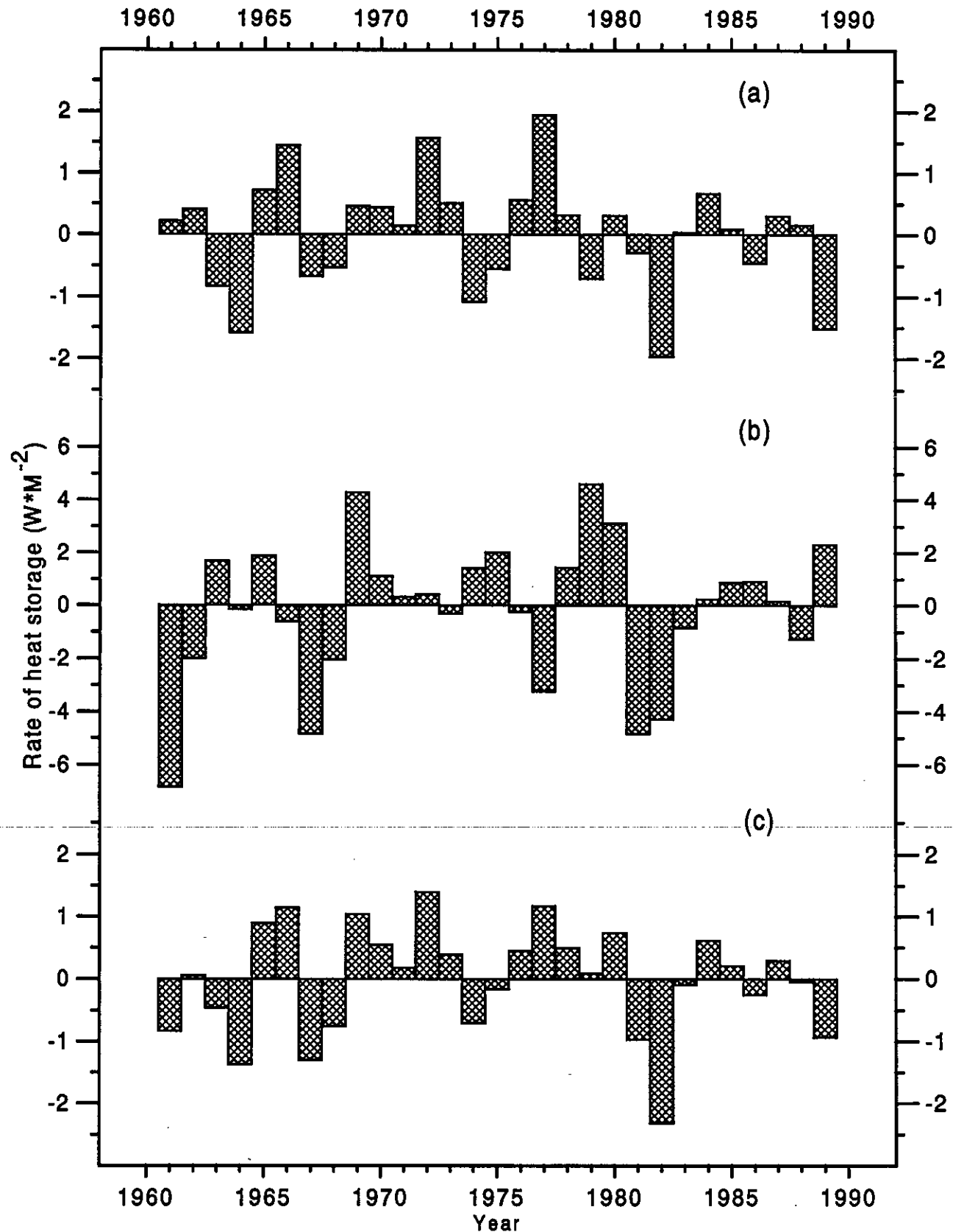


Fig. G16 Rate of heat storage (W^*M^{-2}) integrated through 275 m depth for (a) the South Indian, (b) the North Indian, and (c) the Indian Ocean

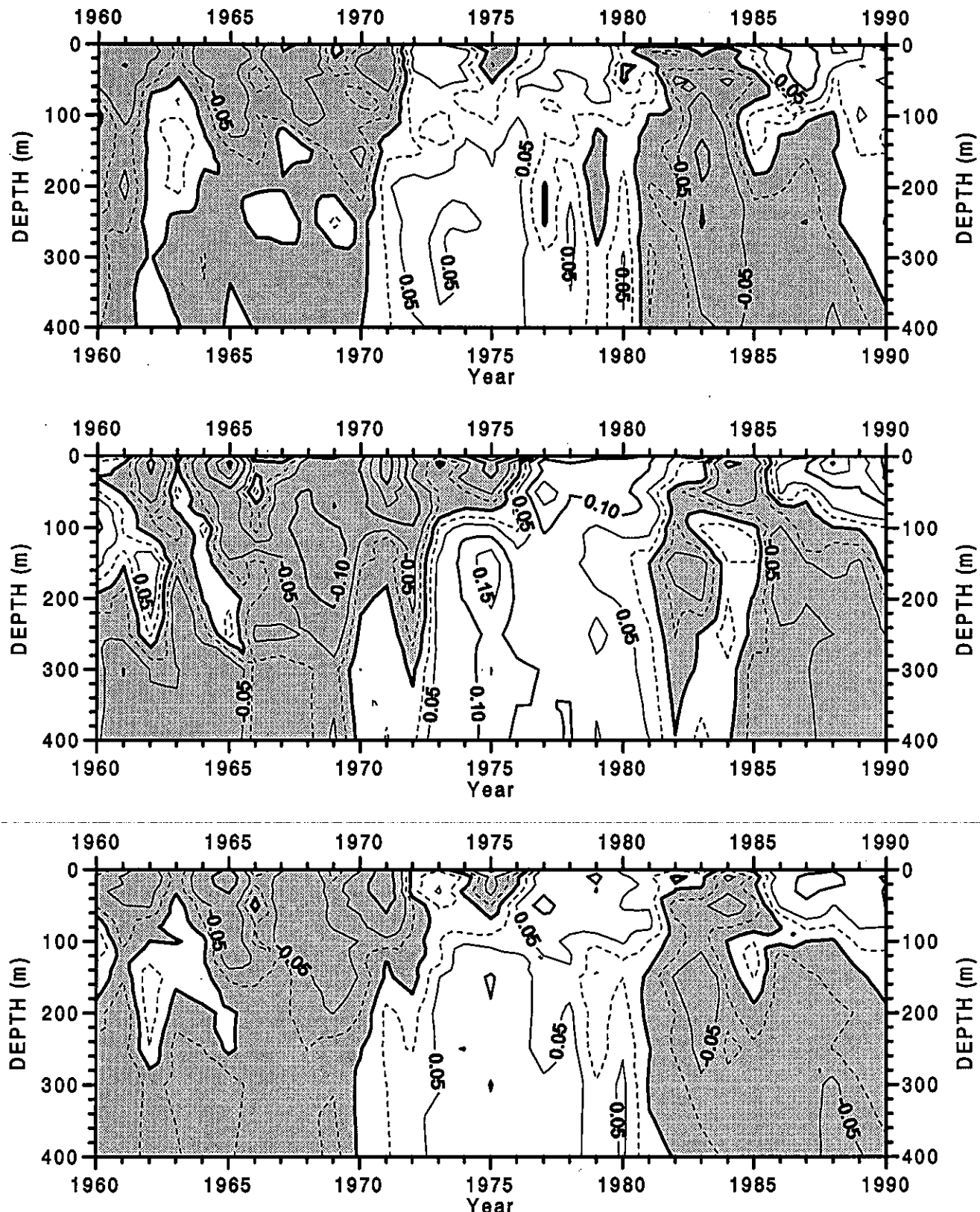


Fig. H1 Annual mean temperature anomaly ($^{\circ}\text{C}$) as a function of depth for the Southern (top) and the Northern (middle) Hemispheres, and the World Ocean (bottom)

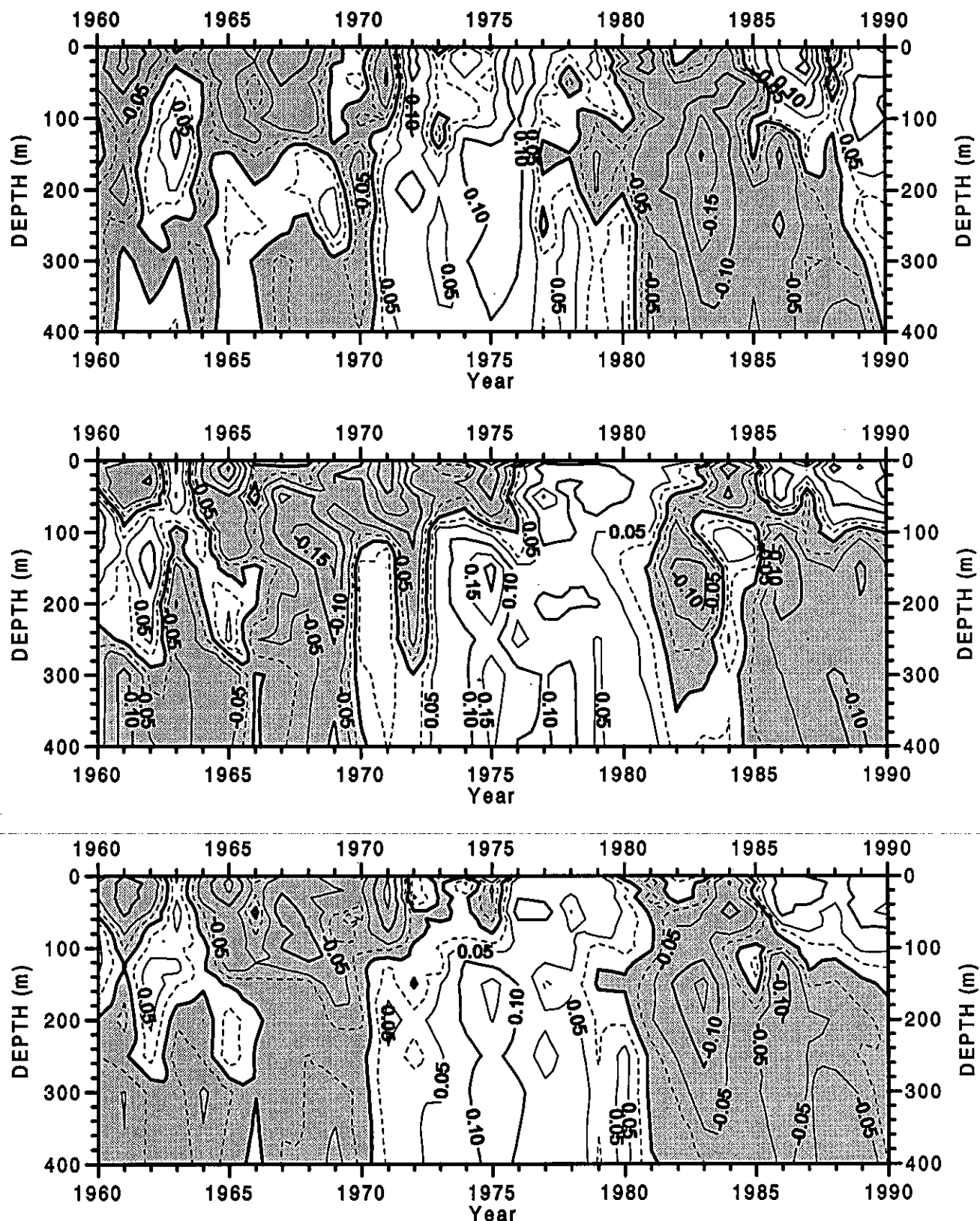


Fig. H2 Annual mean temperature anomaly ($^{\circ}\text{C}$) as a function of depth for the South Pacific (top), the North Pacific (middle), and the Pacific Ocean (bottom)

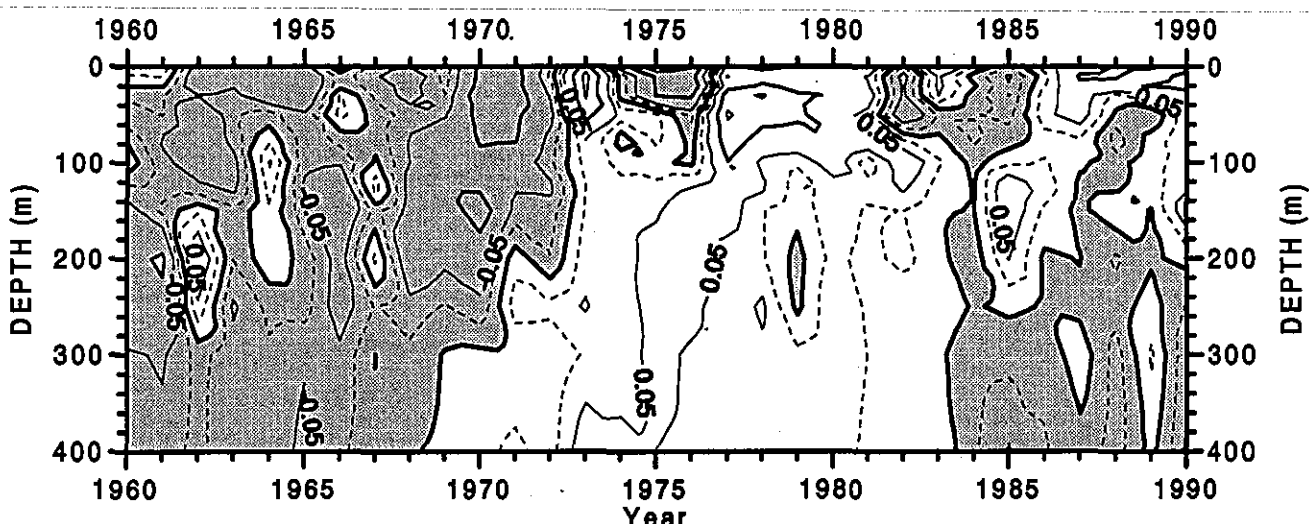
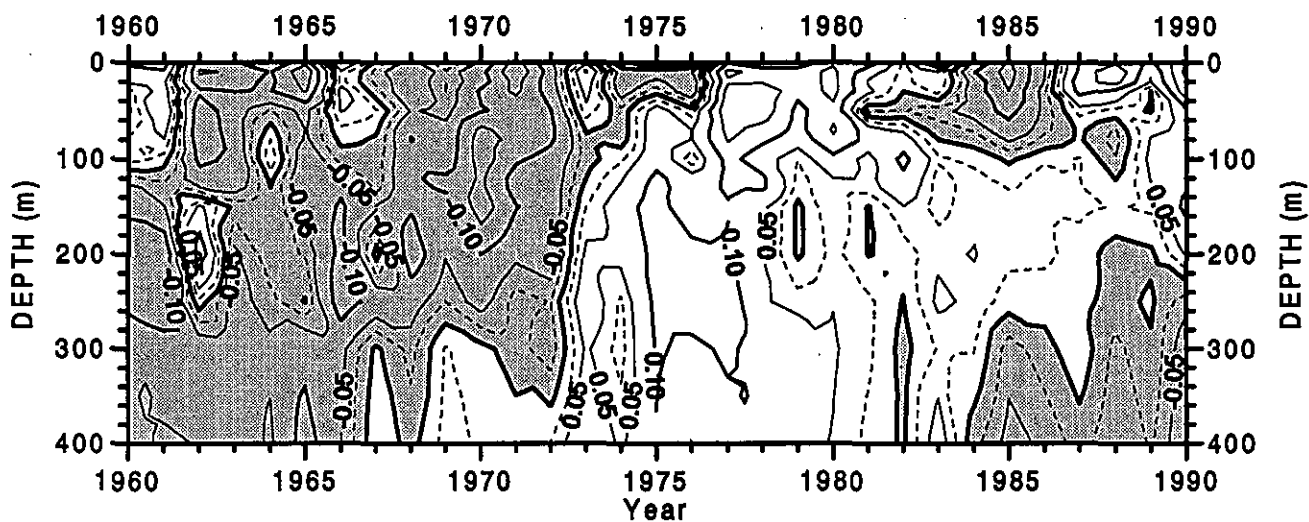
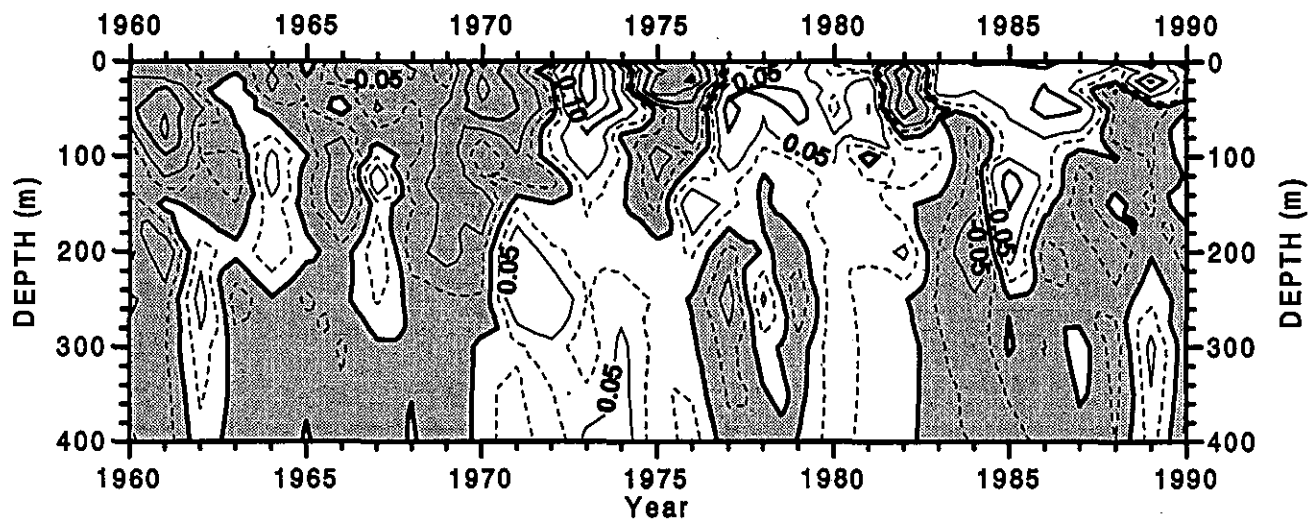


Fig. H3 Annual mean temperature anomaly ($^{\circ}\text{C}$) as a function of depth for the South Atlantic (top), the North Atlantic (middle), and the Atlantic Ocean (bottom)

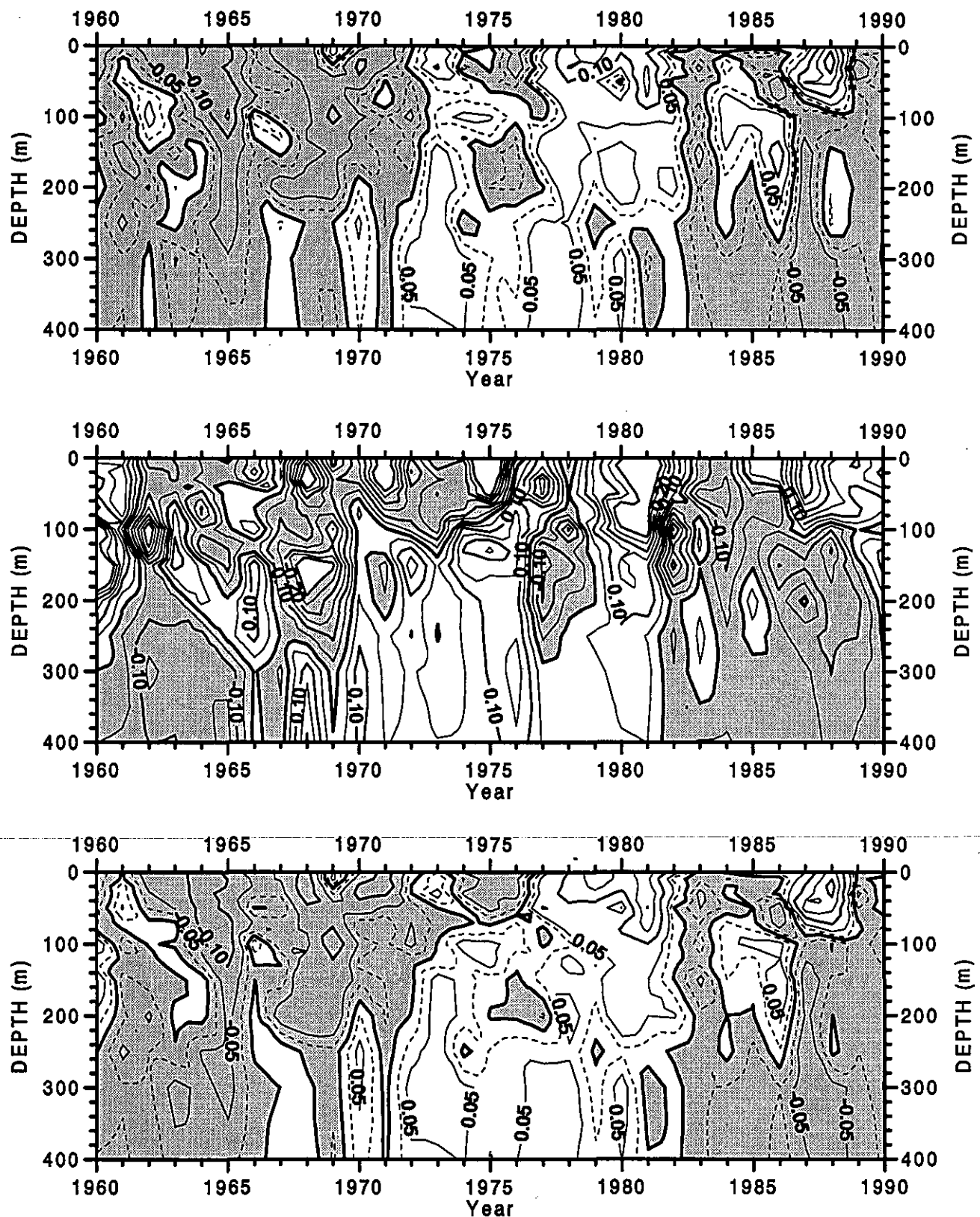


Fig. H4 Annual mean temperature anomaly ($^{\circ}\text{C}$) as a function of depth for the South Indian (top), the North Indian (middle), and the Indian Ocean (bottom)

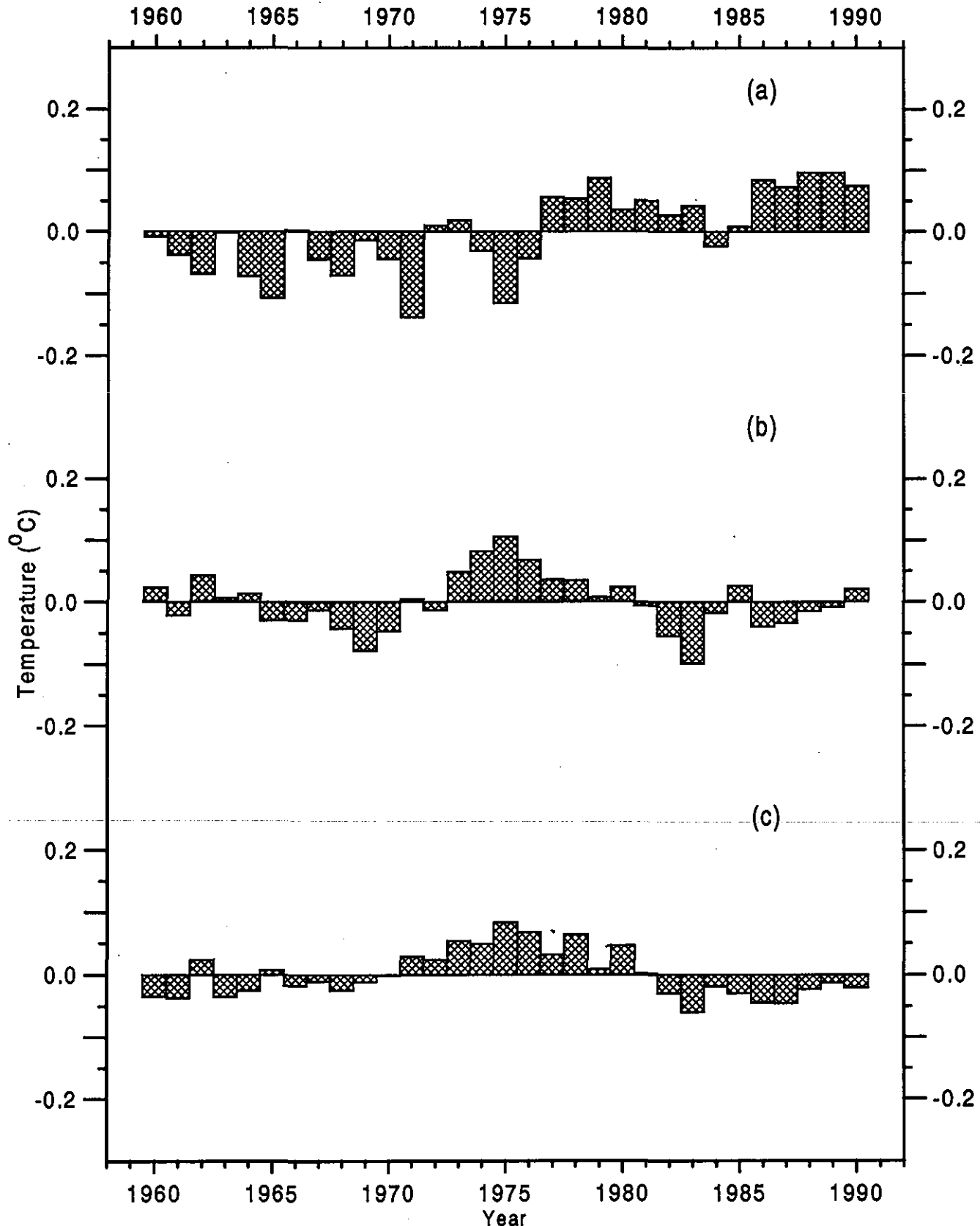


Fig. H5 Annual mean temperature deviations ($^{\circ}\text{C}$) from the 1960-90 mean for the World Ocean at (a) the surface, (b) 150 m depth, and (c) 250 m depth

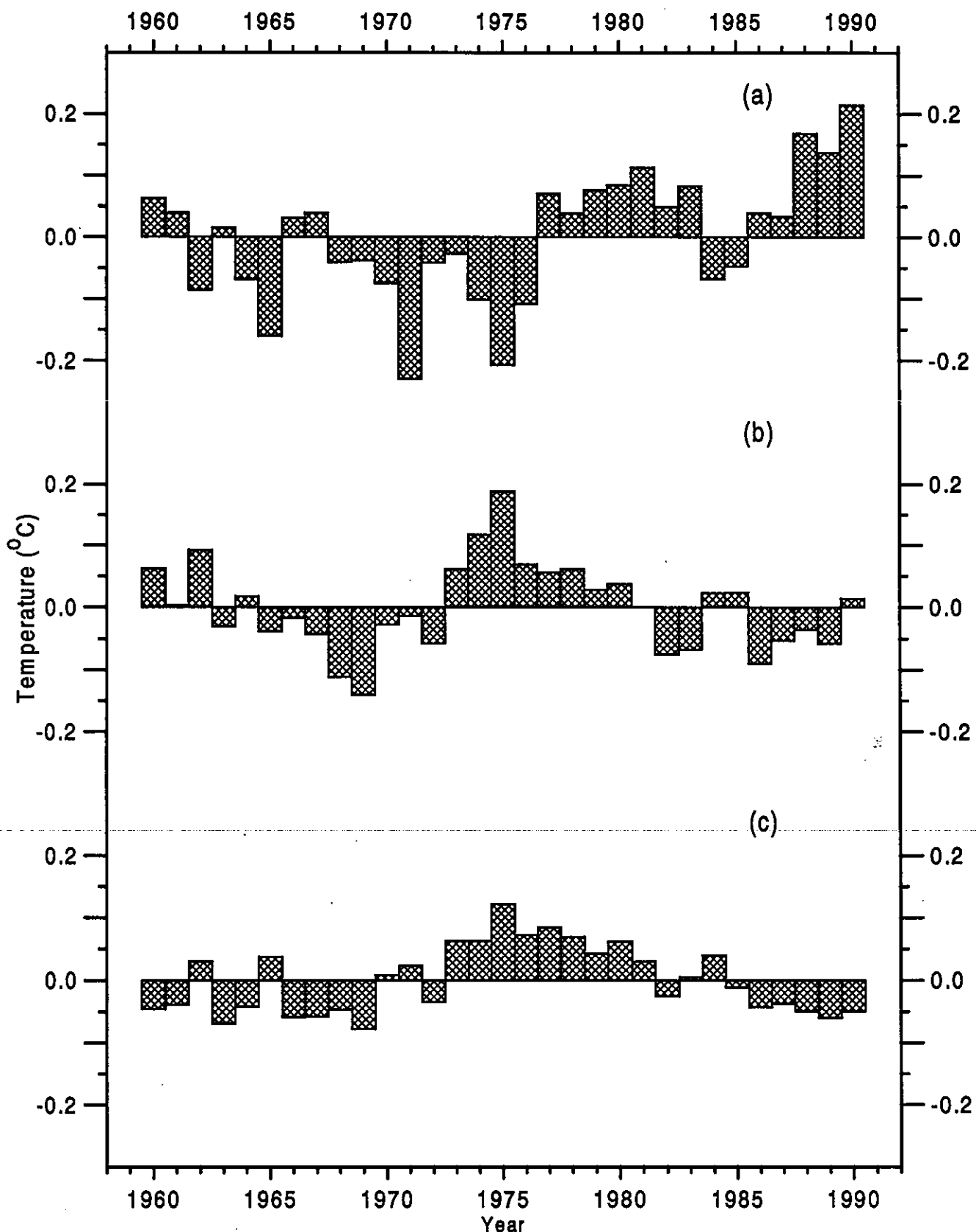


Fig. H6 Annual mean temperature deviations ($^{\circ}\text{C}$) from the 1960-90 mean for the Northern Hemisphere at (a) the surface, (b) 150 m depth, and (c) 250 m depth

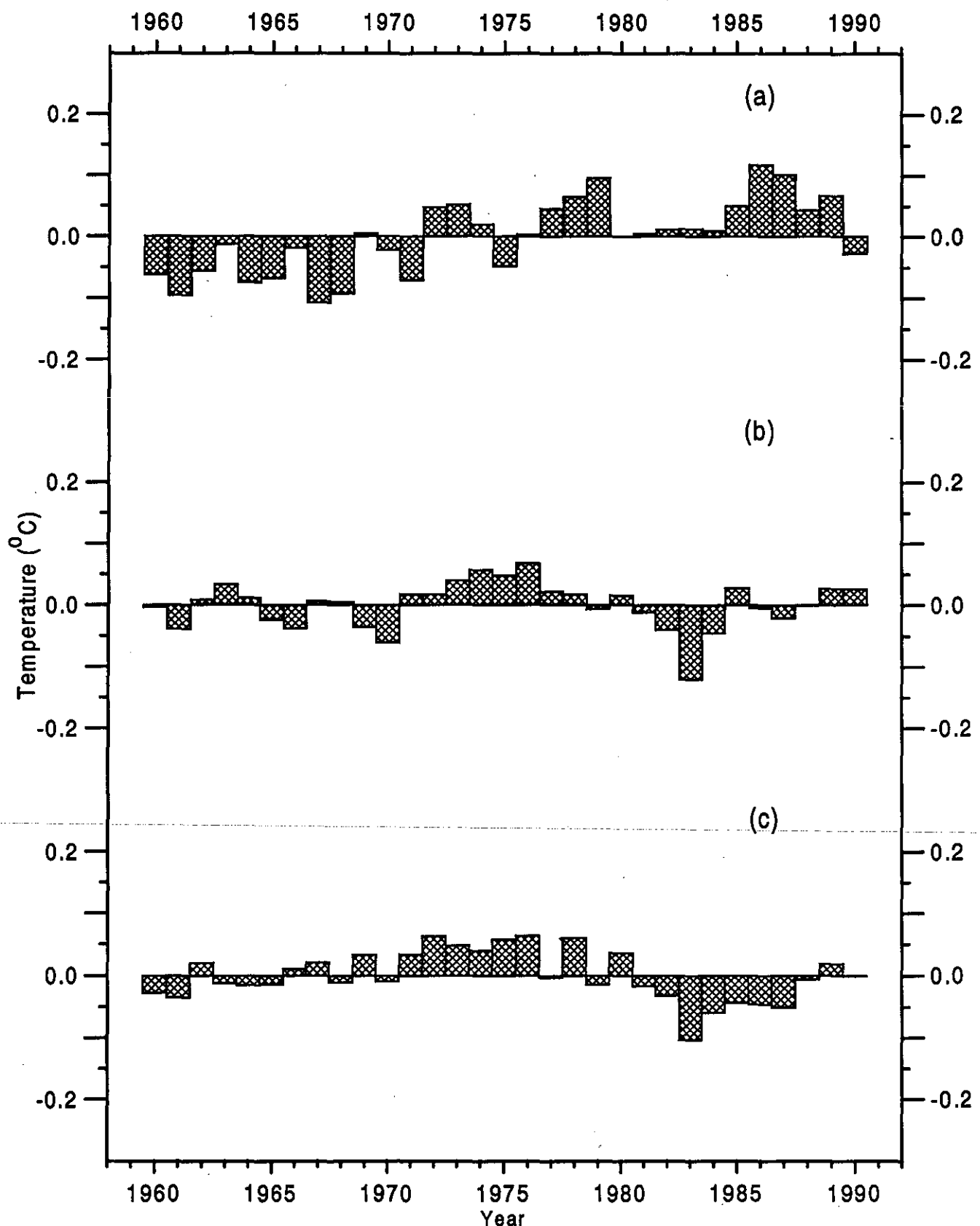


Fig. H7 Annual mean temperature deviations ($^{\circ}\text{C}$) from the 1960-90 mean for the Southern Hemisphere at (a) the surface, (b) 150 m depth, and (c) 250 m depth

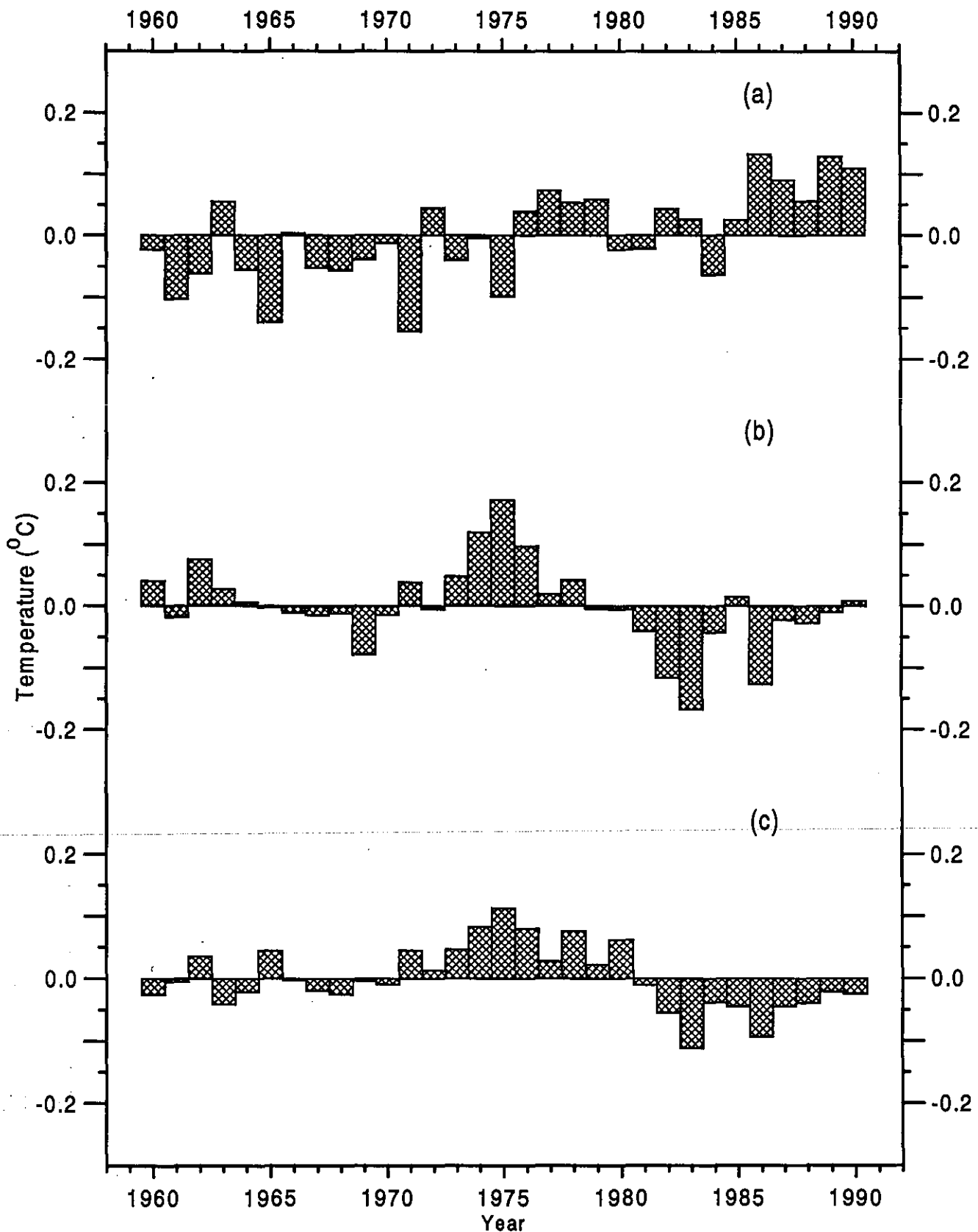


Fig. H8 Annual mean temperature deviations ($^{\circ}\text{C}$) from the 1960-90 mean for the Pacific Ocean at (a) the surface, (b) 150 m depth, and (c) 250 m depth

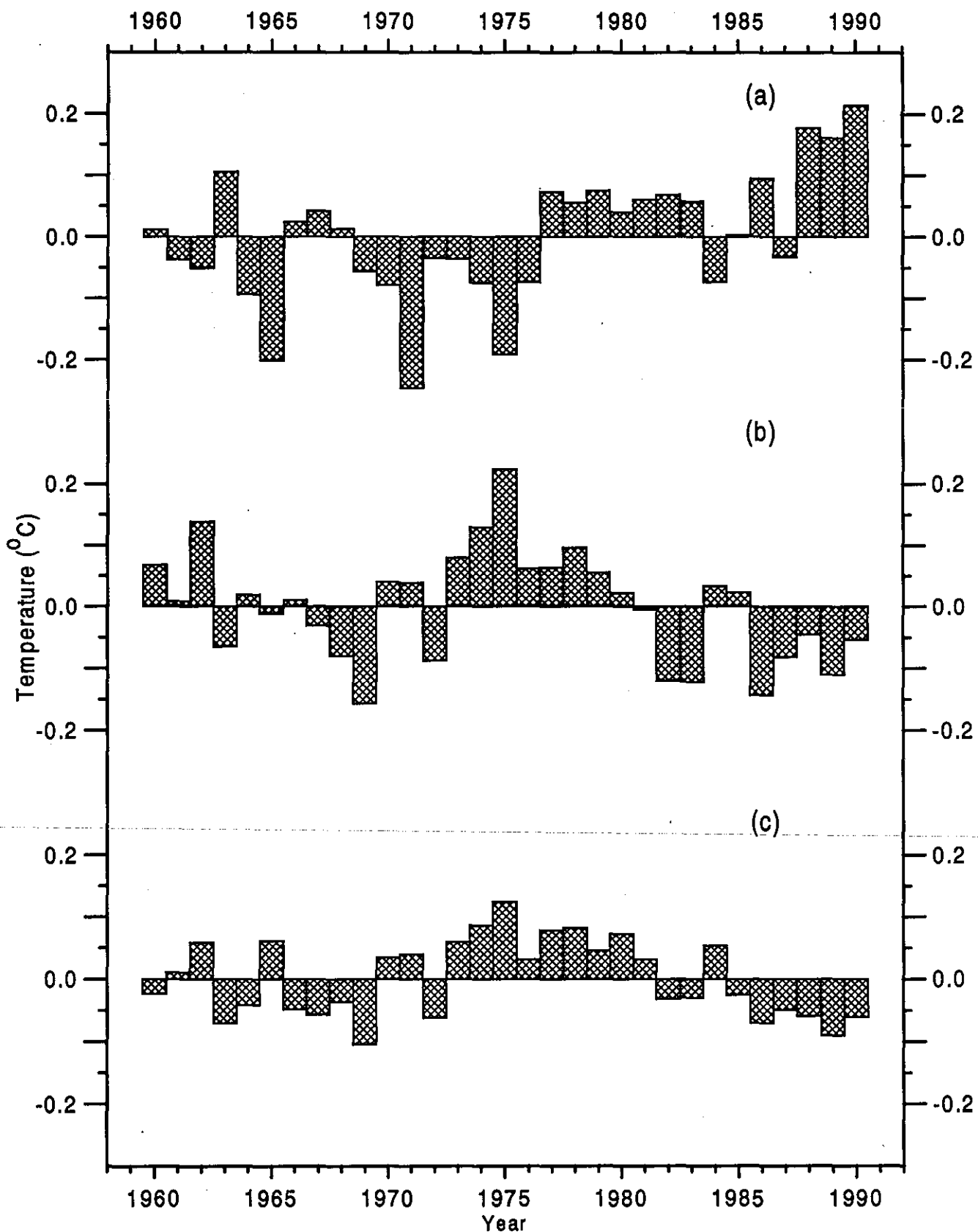


Fig. H9 Annual mean temperature deviations ($^{\circ}\text{C}$) from the 1960-90 mean for the North Pacific at (a) the surface, (b) 150 m depth, and (c) 250 m depth

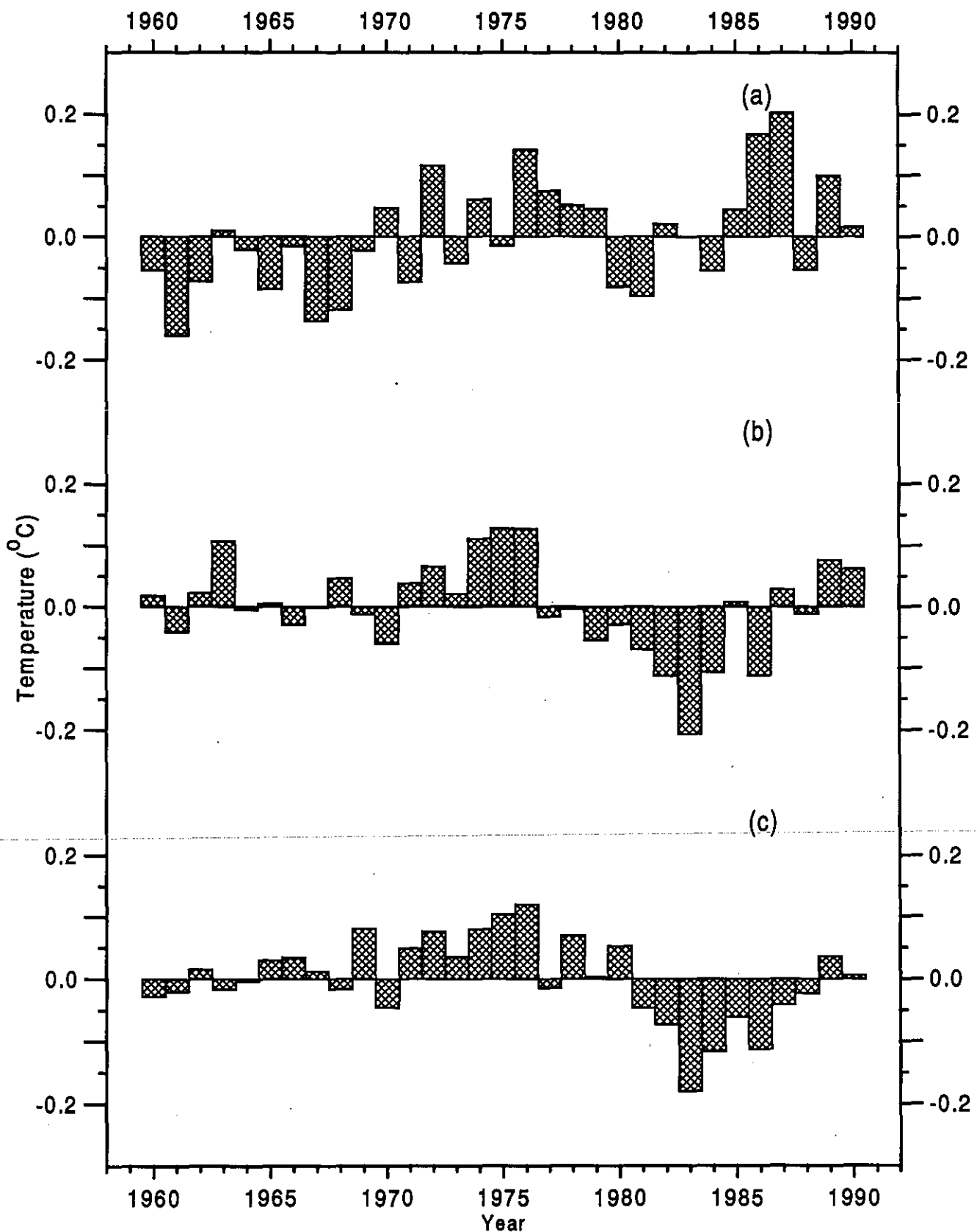


Fig. H10 Annual mean temperature deviations ($^{\circ}\text{C}$) from the 1960-90 mean for the South Pacific at (a) the surface, (b) 150 m depth, and (c) 250 m depth

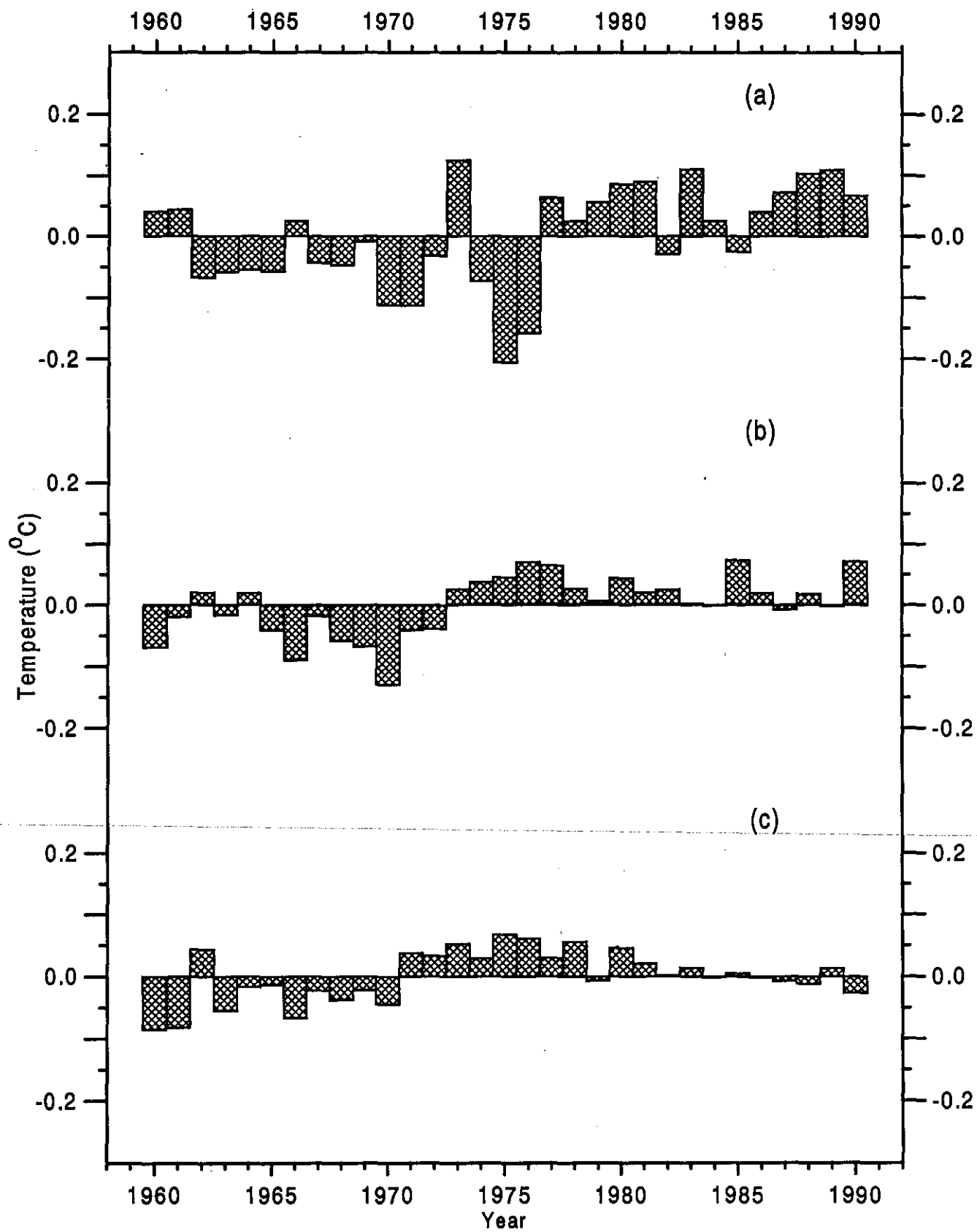


Fig. H11 Annual mean temperature deviations ($^{\circ}\text{C}$) from the 1960-90 mean for the Atlantic Ocean at (a) the surface, (b) 150 m depth, and (c) 250 m depth

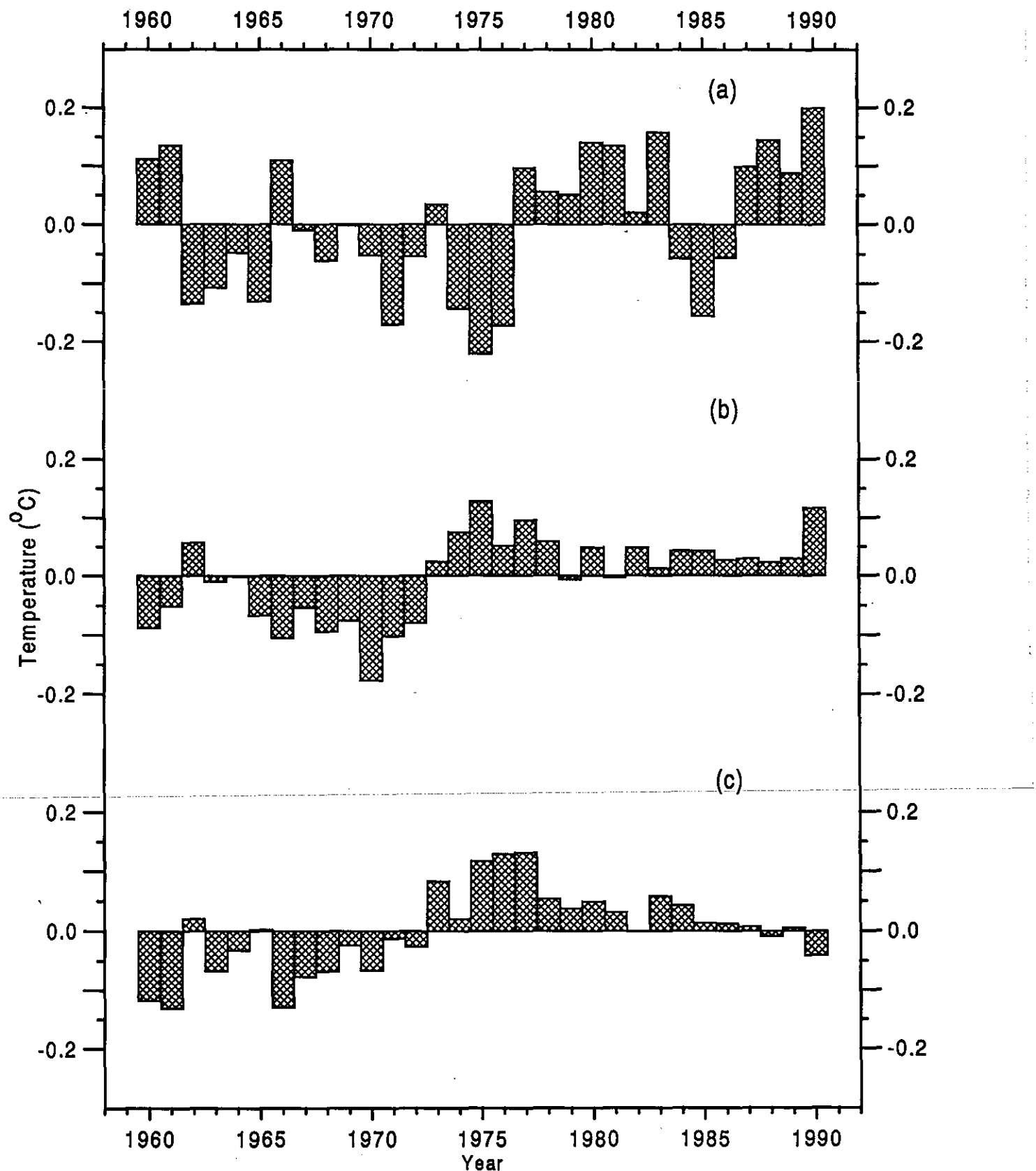


Fig. H12 Annual mean temperature deviations ($^{\circ}\text{C}$) from the 1960-90 mean for the North Atlantic at (a) the surface, (b) 150 m depth, and (c) 250 m depth

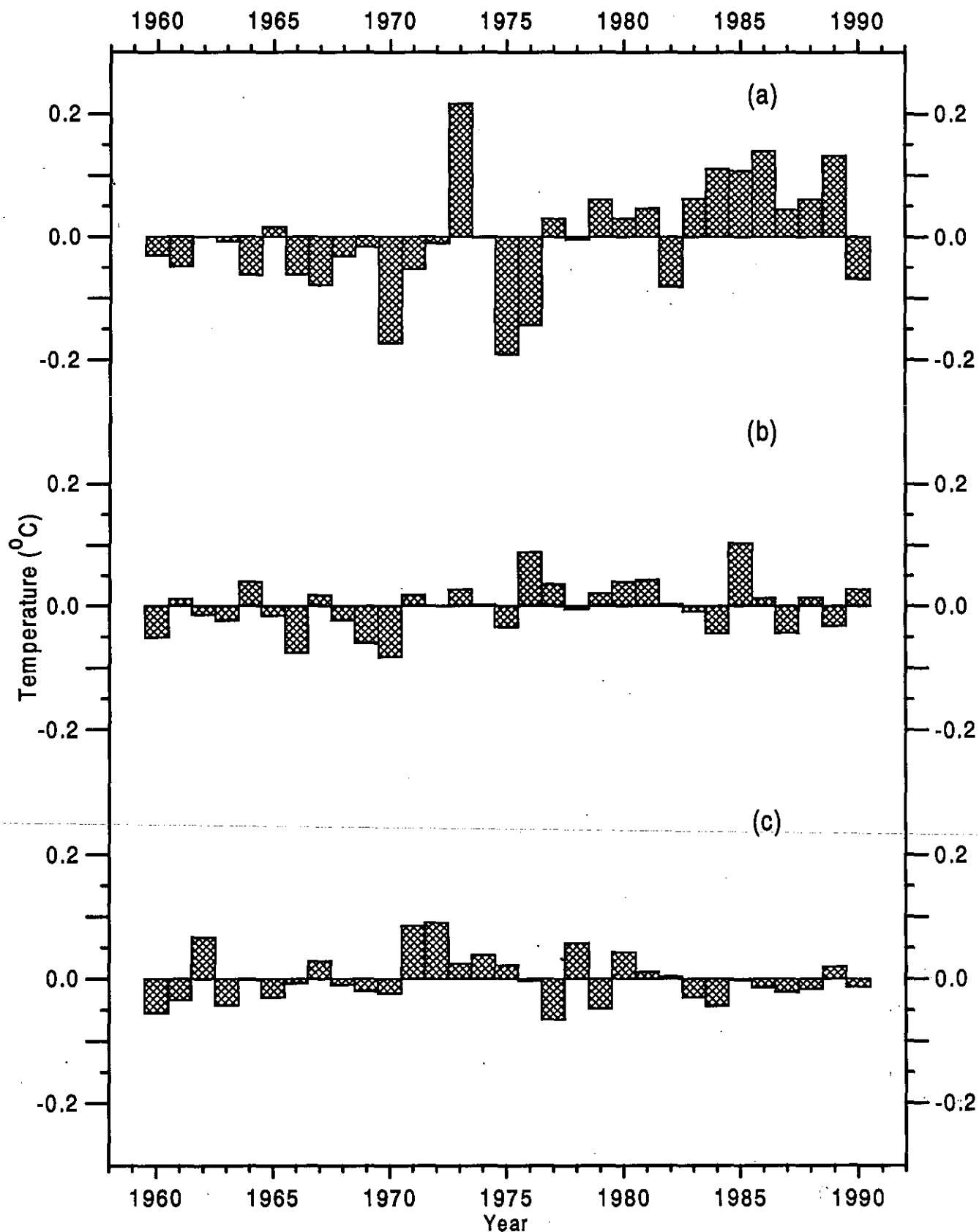


Fig. H13 Annual mean temperature deviations ($^{\circ}\text{C}$) from the 1960-90 mean for the South Atlantic at (a) the surface, (b) 150 m depth, and (c) 250 m depth

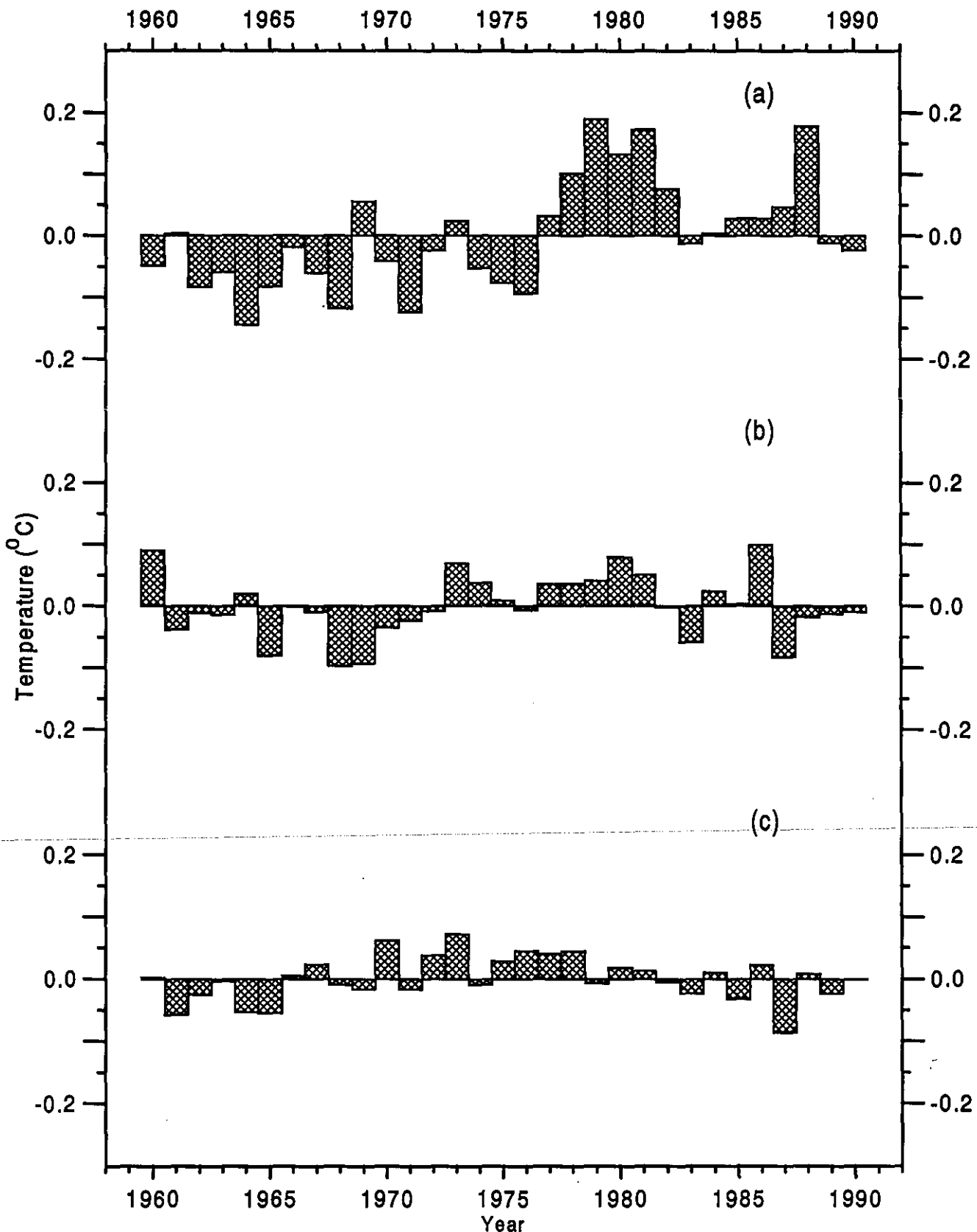


Fig. H14 Annual mean temperature deviations ($^{\circ}\text{C}$) from the 1960-90 mean for the Indian Ocean at (a) the surface, (b) 150 m depth, and (c) 250 m depth

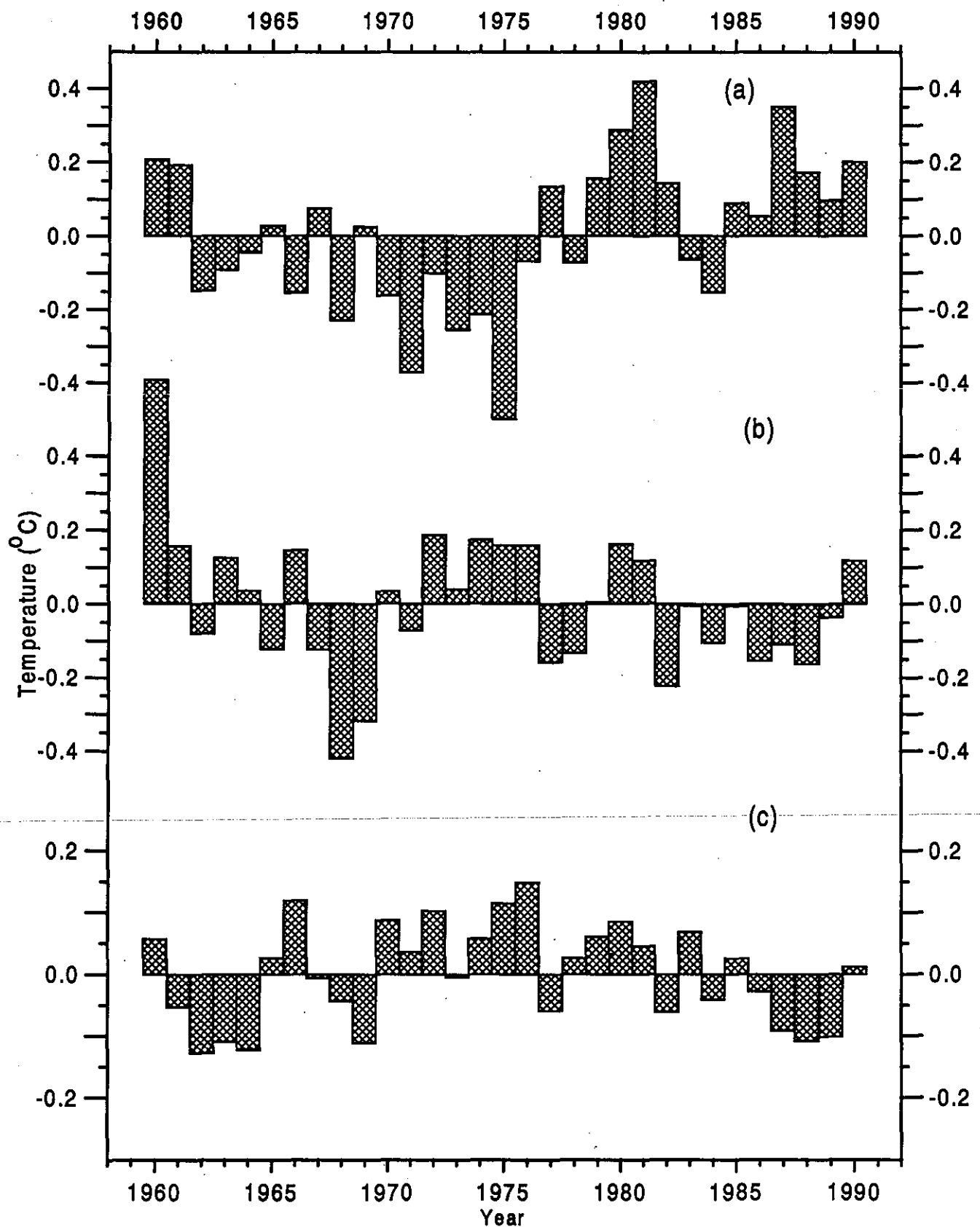


Fig. H15 Annual mean temperature deviations ($^{\circ}\text{C}$) from the 1960-90 mean for the North Indian at (a) the surface, (b) 150 m depth, and (c) 250 m depth

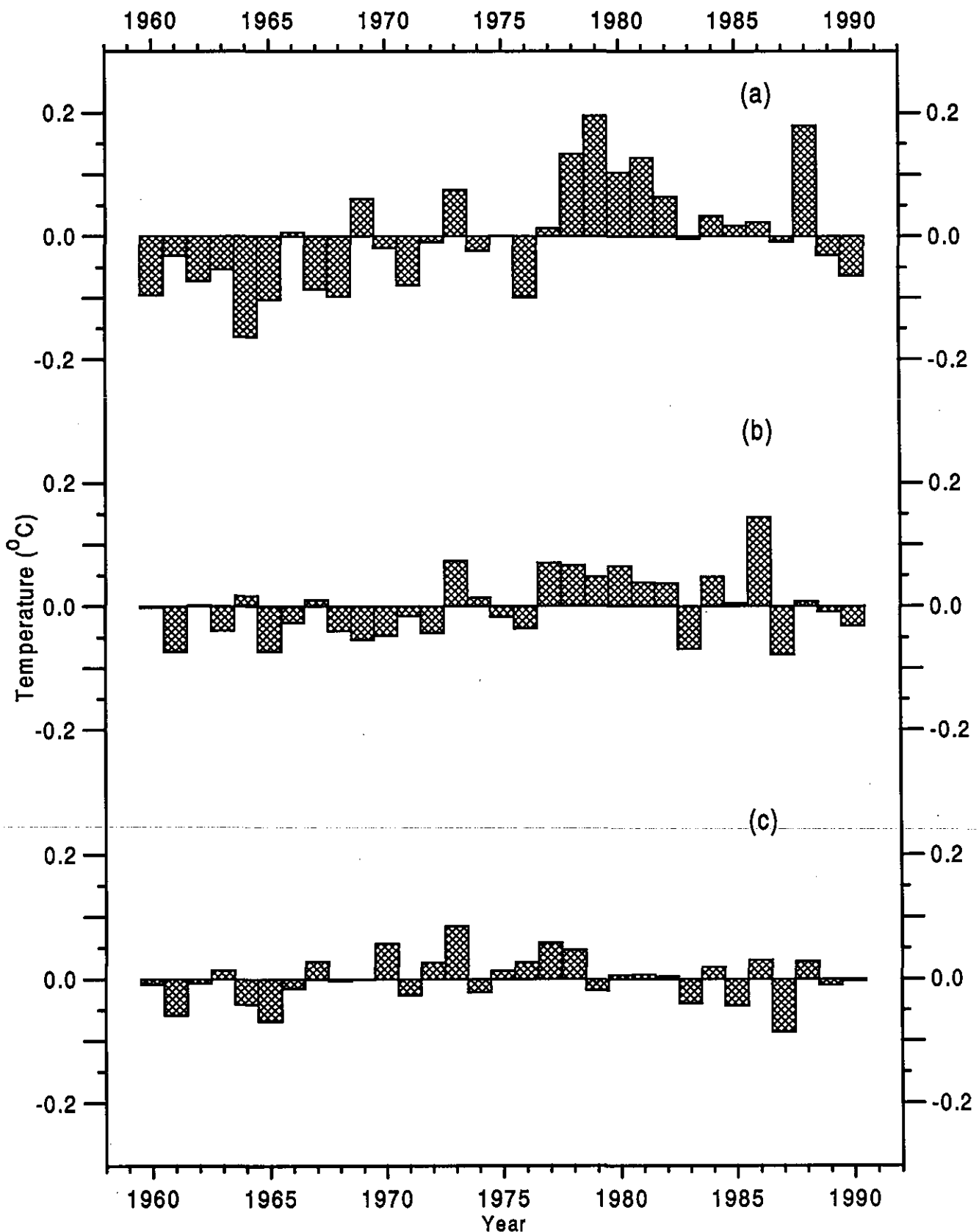


Fig. H16 Annual mean temperature deviations ($^{\circ}\text{C}$) from the 1960-90 mean for the South Indian at (a) the surface, (b) 150 m depth, and (c) 250 m depth

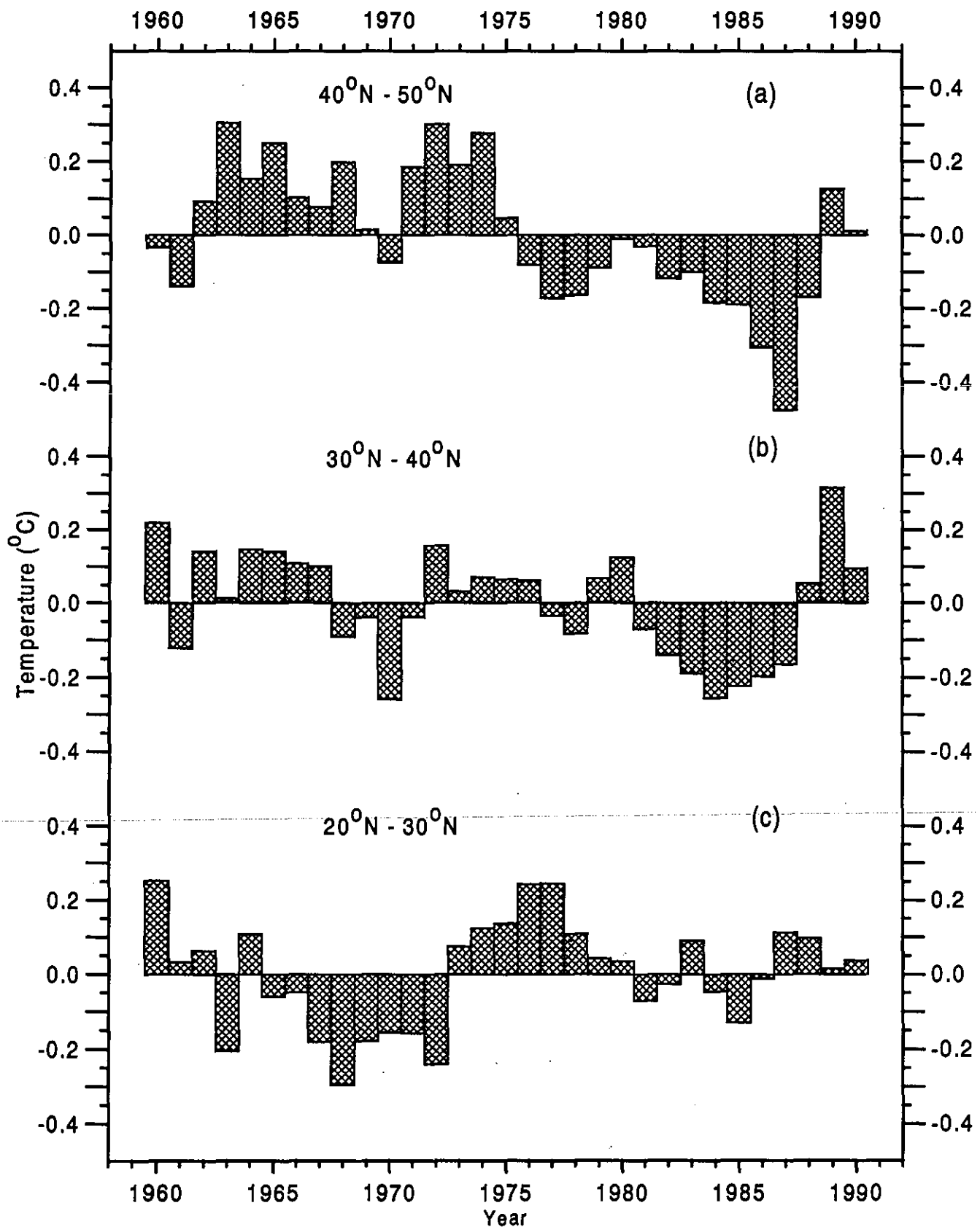


Fig.H17 Zonally averaged annual mean temperature deviations ($^{\circ}\text{C}$) from the 1960-90 mean in the North Pacific at 125 m depth:

(a) $40^{\circ}\text{N}-50^{\circ}\text{N}$, (b) $30^{\circ}\text{N}-40^{\circ}\text{N}$, and (c) $20^{\circ}\text{N}-30^{\circ}\text{N}$

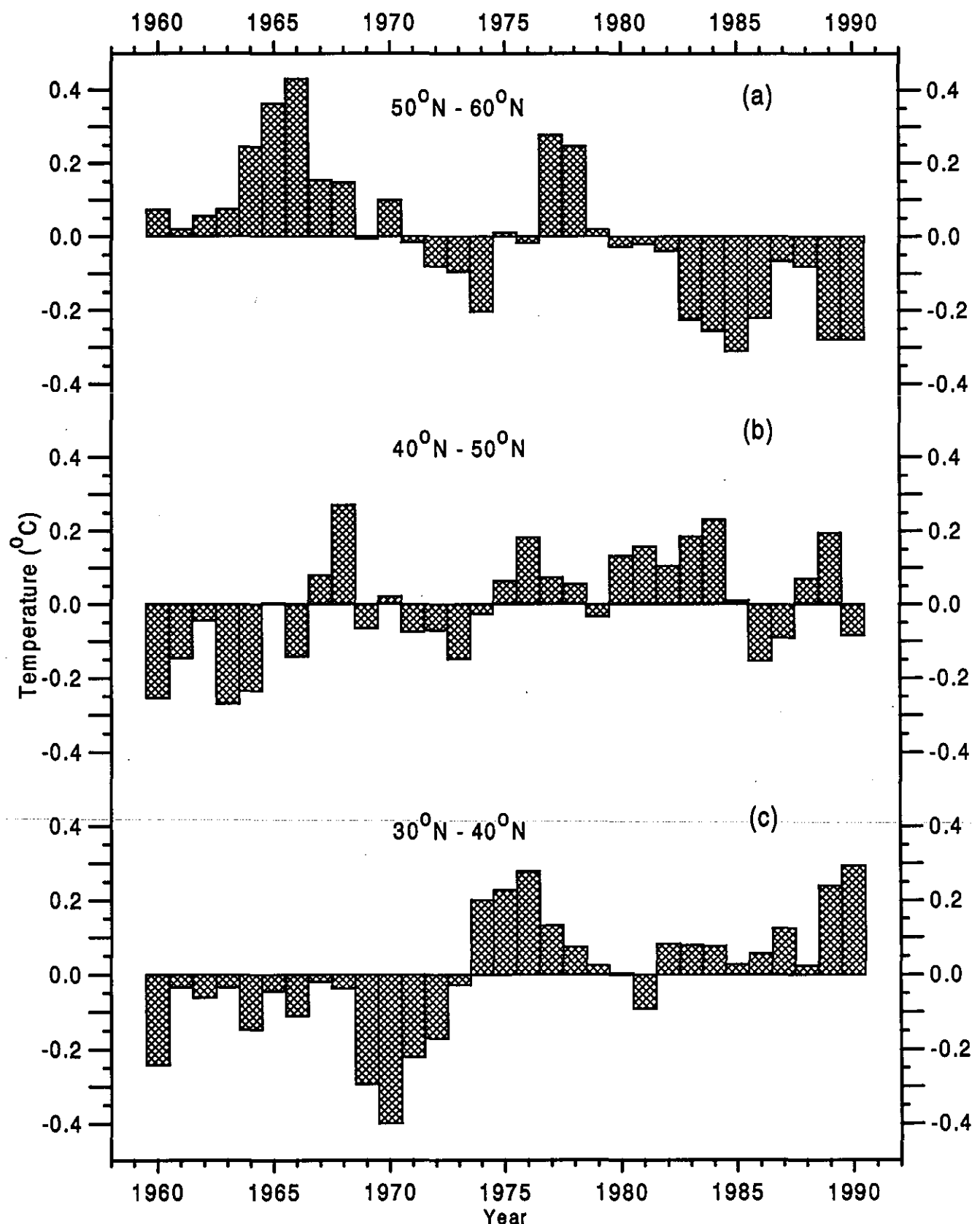


Fig.H18 Zonally averaged annual mean temperature deviations ($^{\circ}\text{C}$) from the 1960-90 mean in the North Atlantic at 125 m depth:

(a) $50^{\circ}\text{N}-60^{\circ}\text{N}$, (b) $40^{\circ}\text{N}-50^{\circ}\text{N}$, and (c) $30^{\circ}\text{N}-40^{\circ}\text{N}$

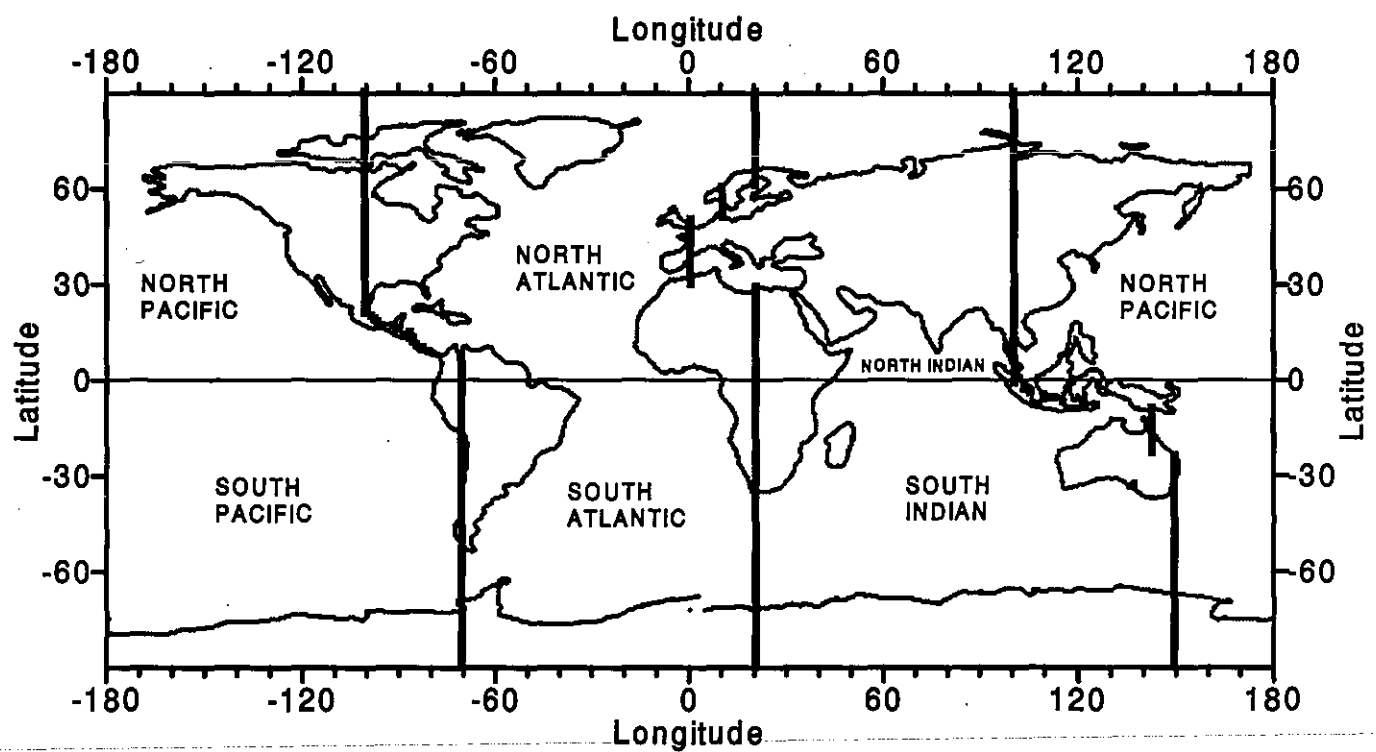


Fig. H19 Division of the World Ocean into individual basins